

**Optical coherence tomography of the human crystalline lens
and its application to the structural assessment of cataract in
the Down syndrome eye.**

Aman-Deep S. Mahil BSc (Hons), MCOptom

School of Biomedical Sciences

Faculty of Life and Health Sciences of the University of Ulster

PhD Thesis in Optometry and Vision Science

July 2018

I confirm that the word count of this thesis is less than 100 000

Table of Contents

Acknowledgements	I
Abstract	II
Abbreviations	III
List of Figures	V
List of Tables.....	VIII

Chapter One

Introduction.....	1
1.1 The Human Crystalline Lens and Cataract	1
1.1.1 Anatomy and Physiology of the Crystalline Lens	1
1.1.2 Refractive Index and Transparency of the Crystalline Lens	3
1.1.3 Cataract and its Development	3
1.1.4 Prevalence of Cataract	4
1.1.5 Clinical Grading of Cataract	8
1.1.5.1 Oxford Clinical Cataract Classification and Grading System.....	8
1.1.5.2 The Wilmer Cataract Grading System.....	9
1.1.5.3 The Wisconsin Cataract Grading System.....	10
1.1.5.4 The Lens Opacities Classification System III.....	10
1.1.6 The Advent of OCT – Potential for objective grading of cataract?	13
1.2 Alzheimer’s Disease	16
1.2.1 Pathophysiology of Alzheimer’s Disease	16
1.2.2 Biomarkers in Alzheimer’s Disease	19
1.2.3 The Eye as a Biomarker for Alzheimer’s Disease	20
1.2.3.1 Beta-amyloid and the Retina	20
1.2.3.2 A β and the Crystalline Lens	21
1.3 Down Syndrome	25
1.3.1 General Overview of Down Syndrome	25
1.3.2 Genetics of Down Syndrome	25
1.3.3 Epidemiology of Down Syndrome.....	26
1.3.4 Physical Characteristics of Down Syndrome	27
1.3.5 Health Characteristics of Down Syndrome.....	27
1.3.6 Cognitive Characteristics of Down Syndrome.....	29
1.3.6.1 Alzheimer’s Disease in Down Syndrome.....	30
1.4 Ophthalmic Characteristics of Down Syndrome.....	32
1.4.1 External Eye in Down Syndrome.....	32
1.4.2 Cornea in Down Syndrome	32
1.4.3 Iris in Down Syndrome	33
1.4.4 Crystalline Lens in Down Syndrome.....	34

1.4.4.1 Beta-Amyloid and Cataract in Down Syndrome.....	35
1.4.5 Retina in Down Syndrome.....	37
1.4.6 Strabismus in Down Syndrome.....	38
1.4.7 Nystagmus in Down Syndrome	38
1.5 Vision in Down Syndrome.....	39
1.5.1 Visual Function in Down Syndrome.....	39
1.5.2 Refractive Error in Down Syndrome.....	40
1.5.3 Accommodation in Down Syndrome	41
1.6 Summary of Introduction and Aims of this Thesis	43
Chapter 2: General Imaging Methods	44
2.1 Optical Coherence Tomography	44
2.1.1 History of Optical Coherence Tomography	44
2.1.2 Methods of Optical Coherence Tomography.....	45
2.1.2.1 Time Domain OCT	46
2.1.2.2 Fourier Domain OCT	47
2.1.3 Light Source Properties for Effective OCT Imaging.....	49
2.1.4 Recent Advances in OCT.....	51
2.1.5 OCT Methods to be Used in This Study.....	52
2.1.5.1 The Visante Anterior-Segment OCT.....	52
2.1.5.2 The Spectralis Posterior-Segment OCT.....	54
2.2 The Modification and Digitisation of a Slit-Lamp Photo-Biomicroscope for Imaging the Crystalline Lens	56
2.2.1 Introduction	56
2.2.2 Methods	57
2.2.2.1 Physical modification of the illumination system	58
2.2.2.2 Selection of a microcontroller, LED driver and overall system design	60
2.2.2.3 Integration of the microcontroller, digital camera and illumination system components.....	64
2.2.2.4 Final installation of the components.....	68
2.2.3 Results and Discussion	71
Chapter 3: Assessment of Lens Opacity and Cataract using OCT	73
3.1 Introduction	73
3.2 Sample Size Determination and Recruitment	73
3.2.1 Sample Size	73
3.2.2 Recruitment	74
3.3 Ethical Approval.....	74
3.4 Methods	75
3.4.1 Ophthalmic and Systemic History.....	75
3.4.2 Anterior Chamber Angle and Intraocular Pressure Assessment	75
3.4.2.1 Van Herick Angle Assessment	75
3.4.2.2 Intraocular Pressure Measurement	76
3.4.3 Visual Acuity.....	76
3.4.4 Contrast Sensitivity.....	77
3.4.5 C-Quant Retinal Straylight Assessment.....	78

3.4.6 Crystalline Lens Slit-lamp Imaging and LOCS III Grading	80
3.4.7 Visante Anterior Segment Imaging	83
3.4.7.1 Processing and Analysis of Visante Images	84
3.4.7.1.1 Image Processing of Visante Raw Sensor Data	84
3.4.7.1.2 Segmentation and Grading of Processed Visante Images	86
3.5 Results	90
3.5.1 Recruited Participants	90
3.5.2 Measures of Visual Function	91
3.5.2.1 Visual Acuity	91
3.5.2.2 Contrast Sensitivity	93
3.5.2.3 C-Quant Retinal Straylight	96
3.5.3 LOCS III Grading of Crystalline Lenses	99
3.5.3.1 LOCS III Nuclear Opalescence and Colour	99
3.5.3.2 LOCS III Cortical Grading	104
3.5.3.3 LOCS III Posterior Subcapsular Grading	107
3.5.3.4 Inter-Observer Agreement of LOCS III Grading	108
3.5.4 OCT Grading of Lens Opacity	111
3.5.4.1 OCT Nuclear Grading	111
3.5.4.1.2 Comparison of LOCS III Nuclear Grades and OCT	
PIRs	117
3.5.4.2 OCT Grading of Cortical Cataract	122
3.5.4.2.1 Comparisons of LOCS III Cortical Grades and OCT	
Cortical Measures	127
3.5.4.3 OCT Grading of Posterior Subcapsular Cataract	130
3.5.4.4 Repeatability of OCT Grading	131
3.6 Discussion	132
3.6.1 Participants and Success Rates	132
3.6.2 Visual Acuity	134
3.6.3 Contrast Sensitivity	134
3.6.4 Retinal Straylight	135
3.6.5 LOCS III Grading and its Interaction with Measures of	
Visual Function	136
3.6.6 Comparison of OCT and LOCS III Grading of Cataract	138
3.7 Conclusion	143

Chapter 4: Investigating Cataract and Retinal Structure in Down	
Syndrome	145
4.1 Introduction	145
4.2 Sample Size Determination and Recruitment	145
4.2.1 Sample Size	145
4.2.2 Recruitment	146
4.3 Ethical Approval	147
4.4 Methods	147
4.4.1 Ophthalmic and Systemic History	148
4.4.2 Visual Acuity	149
4.4.3 External Eye, Anterior Chamber and Intraocular	
Pressure Assessment	149
4.4.3.1 External Eye Assessment	149
4.4.3.2 Anterior Chamber Angle Assessment	150
4.4.3.3 Intraocular Pressure Measurement	150
4.4.4 Posterior-Segment Optical Coherence Tomography	151
4.4.5 Crystalline Lens Slit-Lamp Imaging and LOCS III Grading	154
4.4.6 Visante Anterior Segment Imaging and Grading	155

Chapter 5: Cataract in Down Syndrome	157
5.1 Introduction.....	157
5.2 Results	157
5.2.1 Recruited Participants	157
5.2.2 Visual Acuity Assessment.....	158
5.2.3 LOCS III Grading of Crystalline Lenses in Down Syndrome.....	161
5.2.3.1 LOCS III Nuclear Opalescence and Colour	161
5.2.3.2 LOCS III Cortical Grading.....	167
5.2.3.3 LOCS III Posterior Subcapsular Grading	169
5.2.4 OCT Grading of Lens Opacity in Down Syndrome.....	171
5.2.4.1 OCT Nuclear Grading.....	171
5.2.4.1.2 Comparison of Nuclear PIR to LOCS III Nuclear Grades	173
5.2.4.2 OCT Cortical Grading in DS	175
5.2.4.2.1 Comparisons of Cortical PIR Measures to LOCS III C Grades	178
5.2.4.3 OCT Posterior Subcapsular Grading in DS.....	180
5.3 Discussion.....	181
5.3.1 Recruitment of Participants.....	181
5.3.2 Visual Acuity.....	181
5.3.3 Morphology of Lens Opacity in DS	182
5.3.3.1 Success Rates of Imaging the Lens in DS	182
5.3.3.2 General Morphology of Lens Opacity in DS.....	183
5.3.3.3 Morphology of Cataract in DS Compared to Previous Studies.....	186
5.3.3.4 Morphology of Cataract in DS Compared to Beta-Amyloid Studies	188
5.4 Conclusion.....	190
Chapter 6: Posterior Segment OCT in Down Syndrome	192
6.1 Introduction	192
6.2 B-Scans of the Macula in DS	192
6.3 Volume Scans of the Macula in DS	197
6.4 Retinal Nerve Fibre Layer Thickness in DS.....	198
6.5 Discussion.....	199
6.5.1 Success Rates.....	199
6.5.2 Macular Thickness in DS.....	199
6.5.3 Retinal Nerve Fibre Layer Thickness in DS	202
6.5.4 Retinal Structure in DS Compared to Studies in AD	203
6.6 Conclusion.....	204
Chapter 7: Thesis Summary and Future Work	205
7.1 Primary Outcomes.....	205
7.2 Limitations.....	206
7.3 Future Work.....	207
References	209
Appendix A-1 Arduino Source Code	231
Appendix A-2 PIS and Consent forms for Typically Developed Adults.....	235

Appendix A-3	Ethical Approval PIS and Consent forms for DS (Ulster).....	239
Appendix A-4	Ethical Approval, PIS and Consent forms for DS (Cardiff).....	251

Acknowledgements

I would like to express my sincerest gratitude to my supervisors, Dr Julie-Anne Little and Professor Kathryn J. Saunders, for their kindness, dedication, patience, and guidance throughout this study. I would also like to thank Mr Patrick Richardson for all our technical and clinical conversations along with his assistance and advice in modifying the slit-lamp.

My thanks go out to Drs Maggie Woodhouse and Flors Vinuela-Navarro for organising participants and providing me with the facilities to carry out research at the School of Optometry and Vision Sciences, Cardiff University. I would also like to thank all of the participants who took part in this research.

I would like to acknowledge the Department for Employment and Learning, Northern Ireland for funding this research and the Association for Research in Vision and Ophthalmology for providing a travel grant, allowing me to present at their annual meeting.

I would like to thank my sisters, Meena and Simi, and my brother-in-law Opi, for holding things down while I pursued this thesis and always providing encouragement. To my wife Anu, thank you for your unconditional support and always keeping me happy; you are truly my partner in life. Finally, my greatest gratitude is reserved for my parents who have always been there to support me in achieving my goals, thank you Mum and Dad.

Abstract

Down syndrome (DS) is the most common cause of intellectual disability in humans and is associated with intellectual and physical complications, including Alzheimer's disease (AD). Ophthalmic problems are common in DS often resulting in mild-moderate visual impairment. Cataract (reported prevalence 4-72%) has also been reported, but morphology and type are not well understood. Recently, researchers have described 'supranuclear' cataract in the eyes of typically developed adults with AD and those with DS, linking this with beta-amyloid ($A\beta$) peptide accumulation, pathognomonic of AD. However, this assertion seems precipitous, given the lack of characterisation of lens opacities in DS.

This study has established a method of objectively grading any morphology of cataract using Optical Coherence Tomography (OCT). In a cohort of 90 typically developed adults aged 50 years and older, this newly-developed method was validated by comparing its measures of lens opacity to the commonly used, slit-lamp based Lens Opacities Classification System III. OCT subsequently characterised the morphology of lens opacity in a group of individuals with DS aged 6-55 years. Lens opacities were common in DS (prevalence 77.8%). Their presence was unrelated to age or visual acuity. The most common presentation was dot-like opacities scattered throughout the crystalline lens cortex and, occasionally, nucleus. These opacities were not supranuclear and do not appear to be consistent with $A\beta$ accumulation. There was little evidence of early onset of age-related nuclear, cortical and posterior-subcapsular cataract types. Retinal structure was examined using posterior-segment OCT in DS. Increased macular and nerve fibre layer thickness was found, in opposition to the neural thinning found in AD.

In summary, this work has developed and validated a novel technique of assessing crystalline lens structure, provided original, detailed quantitative data on typical DS cataract morphology, and shown that the DS eye does not exhibit the characteristic features reported in AD.

Abbreviations

2D	Two-Dimensional
3D	Three-Dimensional
AD	Alzheimer's Disease
APOE	Apolipoprotein
APP	Amyloid Precursor Protein
AS-OCT	Anterior Segment OCT
Aβ	Amyloid-beta
BACE1	β -secretase
BDES	Beaver Dam Eye Study
C	Cortical (LOCS III)
CCD	Charged-coupled Device
CS	Contrast Sensitivity
CSF	Cerebrospinal Fluid
cSLO	Confocal Scanning Laser Ophthalmoscope
CT	Computed Tomography
D	Diopter
DC	Direct Current
DS	Down Syndrome
FD-OCT	Fourier-Domain Optical Coherence Tomography
GCL	Ganglion Cell Layer
I/O	Input/output
ID	Intellectual Disability
IOP	Intraocular Pressure
LED	Light Emitting Diode
LOCS III	Lens Opacities Classification Grading System III
log[s]	Straylight Parameter
logMAR	Logarithm of the Minimum Angle of Resolution
MRI	Magnetic Resonance Imaging
NC	Nuclear Colour (LOCS III)
NFT	Neurofibrillary tangles of tau
NO	Nuclear Opacification (LOCS III)
OCCCGS	Oxford Clinical Cataract Classification and Grading System
OCT	Optical Coherence Tomography
OCT-A	OCT Angiography
OHT	Ocular Hypertension
P	Posterior Subcapsular (LOCS III)
PA	Pixel Area
PAR	Pixel Area Ratio
PET	Positron Emission Tomography
PI	Pixel Intensity
PIR	Pixel Intensity Ratio
PSC	Posterior Subcapsular Cataract

PSEN1	Presenelin-1
PSEN2	Presenelin-2
PS-OCT	Posterior Segment OCT
RNFL	Retinal Nerve Fibre Layer
ROI	Region of Interest
SD-OCT	Spectral-Domain Optical Coherence Tomography
SLR	Single Lens Reflex
SS-OCT	Swept-Source Optical Coherence Tomography
TD-OCT	Time-Domain Optical Coherence Tomography
USB	Universal Serial Bus
VA	Visual Acuity
VEP	Visually Evoked Potential

List of Figures

Figure 1.1.1: Slit images of the crystalline lens.	2
Figure 1.1.2: The set of standard images used for grading in the LOCS III.	12
Figure 1.2.1 The processing of APP.	18
Figure 1.2.2 Stereoscopic slit-lamp images showing supranuclear cataract.....	22
Figure 1.4.1 Slit-lamp images showing supranuclear cataract.....	36
Figure 2.1.1 Schematic of a generic OCT device.....	46
Figure 2.1.2 Schematic of a TD-OCT device.....	47
Figure 2.1.3 Schematics of FD-OCT devices.....	48
Figure 2.1.4 The Visante AS-OCT.....	53
Figure 2.1.5 The Spectralis PS-OCT instrument.....	55
Figure 2.2.1 Nikon FS-3 Beamsplitter.....	57
Figure 2.2.2 Nikon FS-3 Illumination Tower	59
Figure 2.2.3 Flowcharts demonstrating the BuckBlock and Arduino control of the LED.....	63
Figure 2.2.4 A flowchart depicting how the Arduino was programmed to run the system.....	67
Figure 2.2.5 Modification of the Nikon FS-3	69
Figure 2.2.6 Electrical schematic for the entire slit-lamp system.....	70
Figure 2.2.7 Photographs of an optic section and retroillumination of the anterior crystalline lens	71
Figure 3.4.1 Image of the stimulus used by the C-Quant	79
Figure 3.4.2 Demonstration of the resizing of the processed original 512 x 512 raw detector data	85
Figure 3.4.3 Demonstration of contrast adjustment of the processed images.....	86
Figure 3.4.4 Demonstration of the masking process.....	87
Figure 3.5.1 Histogram of VA frequencies from all 156 eyes	91
Figure 3.5.2 Scatterplot showing the significant relation between VA and age	92
Figure 3.5.3 Histogram and Q-Q plot of CS frequencies from all 156 eyes.....	93
Figure 3.5.4 Scatterplot showing the significant relation between CS and age	94
Figure 3.5.5 Scatterplot showing the significant relation between CS and VA.....	95
Figure 3.5.6 Histogram and Q-Q plot of log[s] frequencies from all 132 eyes	96
Figure 3.5.7 Scatterplot showing the significant relation between log[s] and CS.....	97
Figure 3.5.8 Scatterplot showing the significant relation between log[s] and age.....	98
Figure 3.5.9 Scatterplot showing the significant relation between log[s] and CS.....	98

Figure 3.5.10 Histograms for total participant NO (left) and NC (right).....	99
Figure 3.5.11 Q-Q plots of observed NO (left) and NC (right).....	99
Figure 3.5.12 Optic section image of various stages of nuclear opacity	100
Figure 3.5.13 Histogram (left) and Q-Q (right) plots of the C distribution.....	104
Figure 3.5.14 Retroillumination images.....	104
Figure 3.5.15 Retroillumination images.....	107
Figure 3.5.16 Bland-Altman plot showing inter-observer agreement for LOCS III NO grades.....	108
Figure 3.5.17 Bland-Altman plot showing inter-observer agreement for LOCS III NC grades.....	109
Figure 3.5.18 Bland-Altman plot showing inter-observer agreement for LOCS III C grades.....	109
Figure 3.5.19 Bland-Altman plot showing inter-observer agreement for LOCS III P grades	110
Figure 3.5.20 Histogram with overlaid distribution curve and Q-Q plot.....	111
Figure 3.5.21 Histogram with overlaid distribution curve and Q-Q plot.....	112
Figure 3.5.22 High-resolution OCT of Lens	112
Figure 3.5.23 High-resolution OCT of Lens	112
Figure 3.5.24 Scatterplot showing the significant relation between HR nuclear PIR and NO....	118
Figure 3.5.25 Scatterplot showing the significant relation between LR nuclear PIR and NO	119
Figure 3.5.26 Scatterplot showing the significant relation between HR nuclear PIR and NC	119
Figure 3.5.27 Scatterplot showing the significant relation between LR nuclear PIR and NC.....	120
Figure 3.5.28 Histogram with overlaid distribution curve and Q-Q plot.....	122
Figure 3.5.29 Histogram with overlaid distribution curve and Q-Q plot.....	123
Figure 3.5.30 High-resolution OCT and retroillumination of cortical cataract.....	123
Figure 3.5.30 Scatterplot showing the significant relation between cortical PIR and PAR	125
Figure 3.5.31 Scatterplot showing the significant relation between cortical PIR and LOCS III C...	128
Figure 3.5.32 Scatterplot showing the significant relation between cortical PAR and LOCS III C.	128
Figure 3.5.33 Retroillumination of a PSC and corresponding OCT.....	130
Figure 3.5.34 Bland-Altman plot showing agreement between reggraded images for PIR.....	131
Figure 4.4.1 The ETDRS grid analysis conducted by the Spectralis OCT.....	152
Figure 4.4.2 The RNFL analysis conducted by the Spectralis OCT	153
Figure 4.4.3 A Spectralis line scan through the macula.....	153
Figure 5.2.1 Histogram and Q-Q Plot of VA frequencies from all 18 DS eyes.....	159
Figure 5.2.2 Histogram and Q-Q Plot of VA frequencies from all 33 DS eyes.....	159
Figure 5.2.3 Histogram and Q-Q Plot of combined VA frequencies from all DS eyes	159

Figure 5.2.4 Scatterplot showing the significant relation between VA and age	160
Figure 5.2.5 Histograms for total participant NO (left) and NC (right).....	162
Figure 5.2.6 Q-Q plots of participant NO (left) and NC (right)	162
Figure 5.2.7 Scatterplots showing the significant relation between NO and Age and VA	164
Figure 5.2.8 Scatterplots showing the significant relation between NC and Age (top) and VA ..	165
Figure 5.2.9 Optic sections of crystalline lenses.....	166
Figure 5.2.10 Histogram (left) and Q-Q (right) plots of the C distribution.....	167
Figure 5.2.11 Retroillumination images and optic sections of crystalline lenses in DS.....	168
Figure 5.2.12 Histogram (left) and Q-Q (right) plots of the P distribution	169
Figure 5.2.13 Scatterplots showing the relation between P and Age (left) and VA (right).....	170
Figure 5.2.14 Retroillumination images of crystalline lenses showing PSC in DS.....	170
Figure 5.2.15 Histogram and Q-Q plot describing the distribution of Nuclear PIR in DS	171
Figure 5.2.16 Scatterplots showing the relation between P and VA and Age.....	172
Figure 5.2.17 Scatterplots showing the relation between Nuclear PIR and LOCS III NO and NC	174
Figure 5.2.18 Histogram and Q-Q plot describing the distribution of Cortical Dot PIR	176
Figure 5.2.19 Histogram and Q-Q plot describing the distribution of Cortical Dot PAR.....	176
Figure 5.2.20 Histogram and Q-Q plot describing the distribution of number of cortical dots.	176
Figure 5.2.21 AS-OCT B-Scans showing cortical cataract and dot opacities in DS participants	177
Figure 5.2.22 Scatterplots showing the relation between Cortical Dot PIR and LOCS C.....	179
Figure 5.2.23 AS-OCT B-scans of the posterior crystalline lens showing PSC in DS.....	180
Figure 5.3.1 Diagrams of the crystalline lens showing the location of supranuclear (SN) opacities.	189
Figure 6.2.1 Histogram and Q-Q plot describing the distribution of age	193
Figure 6.2.2 Histogram and Q-Q plot describing the distribution of VA.....	193
Figure 6.2.3 Scatterplot of the relationship between foveal pit depth and age	195
Figure 6.2.4 Scatterplot of the relationship between foveal pit depth and VA.....	196

List of Tables

Table 1.4.1: Studies of Lens Opacity in DS	35
Table 3.5.1 Stratified age ranges for all participants	90
Table 3.5.2 Summary of the VA distributions' mean, range and indicators of normality	91
Table 3.5.3 Summary of the CS distributions' mean, range and indicators of normality.....	93
Table 3.5.4 Summary of the log[s] distributions' mean, range and indicators of normality	97
Table 3.5.5 Summary of Spearman's rank order correlation	100
Table 3.5.6 Summary of linear regression.....	101
Table 3.5.7 Multiple regression analyses	101
Table 3.5.8 Significant Spearman correlations	102
Table 3.5.9 Summary data for NO and NC when stratified by age group.....	103
Table 3.5.10 Significant Spearman correlations	105
Table 3.5.11 Summary of descriptive statistics.....	105
Table 3.5.12 Summary of descriptive statistics.....	107
Table 3.5.13 Summary of Spearman correlations	113
Table 3.5.14 Summary of linear regression analyses	113
Table 3.5.15 Multiple regression analyses	114
Table 3.5.16 Descriptive data for high-resolution nuclear PIR.....	114
Table 3.5.17 Descriptive data for low-resolution nuclear PIR	115
Table 3.5.18 Summary of Spearman's correlations.....	115
Table 3.5.19 Summary of linear regression analyses	116
Table 3.5.20 Summary of Spearman's correlations	117
Table 3.5.21 Summary of linear regression analyses	121
Table 3.5.22 Summary of multiple regression analyses	121
Table 3.5.23 Summary of linear regression analyses.....	124
Table 3.5.24 Multiple regression analyses of OCT Cortical PIR and PAR.....	125
Table 3.5.25 Summary of Spearman's correlations for both cortical PIR and PAR.....	127
Table 3.5.26 Summary of Linear regression for both cortical PIR and PAR	129
Table 5.2.1 Summary of VA distributions' mean, median, range for DS.....	158
Table 5.2.2 Summary of LOCS III NO and NC measures for Down Syndrome.....	161
Table 5.2.3 Summary of Spearman's rank order correlation	162
Table 5.2.4 Summary of linear regression.....	163

Table 5.2.5 Summary of descriptive statistics of C grades.....	167
Table 5.2.6 Summary of descriptive statistics of P grades and analysis of Normality.....	169
Table 5.2.7 The statistics correlation and regression analyses.....	171
Table 5.2.8 Summary of the correlations between Nuclear PIR and LOCS III grades.....	173
Table 5.2.9 Summary of the regression analyses between Nuclear PIR and LOCS III grades....	173
Table 5.2.10 Descriptive statistics for OCT measures of cortical opacity in Down syndrome...	175
Table 5.2.11 Summary of Spearman's correlation and linear regression analyses	179
Table 6.2.1 Descriptive statistics for age and VA in participants with DS.....	192
Table 6.2.2 Descriptive statistics for age in participants with DS	193
Table 6.2.3 Descriptive statistics for VA in participants with DS	194
Table 6.2.4 Descriptive statistics for minimum foveal thickness in participants with DS.....	194
Table 6.2.5 Descriptive statistics for foveal pit depth in participants with DS	194
Table 6.3.1 Summary of average retinal thickness values.....	197
Table 6.4.1 Summary of average RNFL thickness values	198
Table 6.5.1 Summary of average retinal thickness values.....	200
Table 6.5.2 Summary of average RNFL values in μm	202

Chapter 1: Introduction

This literature review initially provides a background on the development, prevalence, and current systems of assessing opacities of the crystalline lens known as cataract. This is followed on by descriptions of Alzheimer's disease and Down syndrome, and their interface in exploring the potential of the eye, including cataract, as a possible biomarker. The purpose and aims of this thesis will then be described in the context of this review.

1.1 The Human Crystalline Lens and Cataract

1.1.1 Anatomy and Physiology of the Crystalline Lens

The human crystalline lens is a transparent, biconvex refractive structure located in the posterior chamber of the eye, situated anterior to the vitreous chamber and posterior to the iris. Anteriorly, the lens is surrounded by aqueous humor and is attached to the ciliary body and muscle by zonules of Zinn. Contraction of the ciliary muscle causes a change in tension of the zonules and subsequent steepening in the curvature of, primarily, the anterior surface of the lens; this yields an increase in dioptric power and is known as accommodation. Accommodation allows an emmetropic eye to have a sharply focused image on the retina when objects are not at optical infinity. In its relaxed, unaccommodated state the lens still acts as a refractive medium, aiding the cornea in forming sharp images of distant objects on the retina (for the emmetropic eye). The dioptric power of the normal lens is approximately 15D; it has the ability to produce a further 15-16D of accommodation in early life that decreases to less than 2D after the age of 50 years due to presbyopia (Bron *et al.* 1997).

The crystalline lens consists of four main structures: the capsule, epithelium, cortex and nucleus (Figure 1.1.1). Apart from a single layer of cuboidal epithelial cells forming the epithelium, the other structures of the lens are composed primarily of fibre cells. The capsule is a protective basement membrane that surrounds the entire lens. The epithelium

only exists between the capsule and anterior cortex; it progresses from the central pole of the lens to the equator, a peripheral area that runs circumferentially at the midpoint of the lens. There is no epithelium running from the equator of the lens to the posterior pole because, during embryology, these cells become the primary fibres of the fetal nucleus. The epithelial cells located at the equator constantly produce new fibrils throughout life (Andley 2007). The apical portions of the new fibres progress anteriorly towards the anterior pole, whereas the basal portions progress backwards to the posterior pole. The new fibres are developed at the outermost layer of the cortex and form a suture where they meet at the poles (Augusteyn 2010). This constant production of new fibres results in a steepening of curvature and thickening of the crystalline lens throughout life (as seen in Figure 1). The axial sagittal width of the lens is approximately 3.5-4.0 mm at birth and slowly increases to 4.75-5.0mm in the elderly; in contrast, the equatorial diameter of 6.5 mm at birth increases to 9-10mm in the second decade and stays mostly constant thereafter (Bron *et al.* 1997).

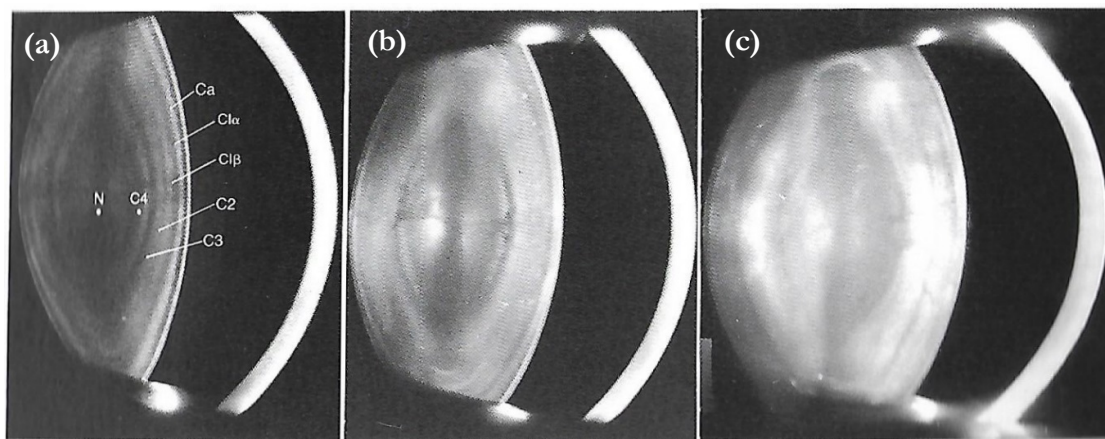


Figure 1.1.1: Slit images of the crystalline lens. (a) Layers of the lens at 20 years with Ca representing the capsule, C1 through C4 representing the cortex and N representing the nucleus. (b) The lens at 50 years. (c) The lens at 80 years. Image taken from Bron *et al.* (1997).

1.1.2 Refractive Index and Transparency of the Crystalline Lens

The refractive properties of the lens are primarily due to the presence of a water-soluble protein called crystallin, that resides in the cytosol of cortex and nucleus fibres. The crystallins account for 90% of the protein content in the lens (Sharma and Santhoshkumar 2009). The lens is said to have a 'gradient' refractive index due to the crystallin content in the fibres increasing from 15% in the outermost layer of the cortex to 70% in the nucleus, and then steadily decreasing again posteriorly (Remington 2012).

The lens maintains its transparency in many ways. Firstly, it is an avascular structure that receives its nutrients from the aqueous humor (Wormstone *et al.* 2006). The fibres in the cortex and nucleus have a very regular and tightly packed structure. They take on a hexagonal shape with their broad surfaces parallel to the vertical plane of the lens. This results in spacing that is smaller than the shortest wavelength of visible light. As a result, there is no scattering as light passes through the lens (Remington 2012). The cortex and nucleus fibres also maintain transparency due to a complete lack of organelles in the light path (Tholozan and Quinlan 2007). The organelles of the germinal epithelial cells that produce new fibres tend to reside in the periphery of the lens at the equator; this way they are behind the iris at normal pupil sizes where they cannot scatter light.

1.1.3 Cataract and its Development

The crystalline lens does not stay completely transparent throughout life. Often, certain areas within the crystalline lens lose their transparency to the point where they scatter light. This is generally caused by oxidative stress damaging the crystallin proteins in the cortex and nucleus; they then become insoluble, bind and clump together. Once the bound proteins become larger than the wavelength of visible light, they begin to scatter it; this occurrence is known as a cataract. The primary and most common cause of cataract is age: typically, above 50 years all human crystalline lenses will have some early cataractous

changes. There are three main types of age-related cataract, and these are classified according to their location: cortical cataract forms in the cortex (usually anteriorly), nuclear cataract forms in the nucleus, and posterior subcapsular cataract forms between the posterior capsule and cortex (Michael and Bron 2011). Cataract is the leading cause of blindness worldwide (Leske *et al.* 1997; Tan *et al.* 2011; Koo *et al.* 2013) but is amenable to treatment with surgery. This generally involves the creation of a hole in the anterior capsule and epithelium, and then breaking up and removing the entire cortex and nucleus (phacoemulsification). Subsequently, an artificial intraocular lens implant is suspended within the remaining capsule. Ocular biometry helps calculate an appropriately powered IOL implant to optimise vision.

There are other risk factors and causes of cataract; these include trauma or a congenital condition. Certain medications such as systemic steroids, environmental factors such as UV light exposure, lifestyle factors such as malnutrition, and smoking as well as systemic diseases such as diabetes, can all cause and/or accelerate the occurrence of cataract (Andley 2007).

1.1.4 Prevalence of Age-Related Cataract

Cataract is a multifactorial condition whose prevalence has been heavily studied throughout the world. Various large-scale studies have been conducted looking at factors causing vision loss and blindness in population-based cohorts. However, these studies often differ in their methodologies, definitions of cataract, grading systems used and age-ranges.

In developed nations, a variety of studies on the epidemiology of eye diseases causing visual impairment have been conducted. Of these, age-related cataract is often the most common cause. These studies all involve older populations but some have broader age

ranges than others. One of the earliest studies, the Framingham Eye Study (Kahn *et al.* 1977) conducted in Massachusetts, examined 2477 adults aged 52 to 85 years, and reported an increasing prevalence of cataract causing visual impairment (VA below 20/30) with increasing age; prevalence was: 5% in those aged 52-64 years, 18% in those aged 65-74 years and 46% in those aged 75-85 years.

One of the most well known studies of eye disease causing visual impairment in the US is the Beaver Dam Eye Study (BDES) (Klein *et al.* 1992). This study was conducted in the Wisconsin area and involved 4926 participants aged 43-84 years. The BDES measured cataract prevalence by morphology as well as employing a grading system to measure severity of opacification. The Wisconsin grading scale used was developed specifically for the study and involved five grades of increasing opacification (Klein *et al.* 1990). The prevalence of cataract in the BDES was determined to be 17.3% for nuclear cataract, 16.3% for cortical cataract and 6.0% for posterior subcapsular cataract (Klein *et al.* 1992).

A similar study to the BDES was conducted in an Australian population using a similar methodology. The Blue Mountains Eye Study carried out eye examinations on 3654 people aged 49-96 years who resided in a locality just outside of Sydney (Mitchell *et al.* 1997). The same Wisconsin grading scale for cataract that was used in the BDES was used to grade the severity of opacification. The presence of cataract was detected in the following amounts: nuclear in 53.3% of women and 49.7% of men; cortical cataract in 25.9% of women and 21.1% of men; posterior subcapsular in 6.2% of women and 6.5% of men. Although women showed a higher prevalence in all subgroups, this was only significantly higher for cortical cataract (Mitchell *et al.* 1997). The age-related increase in prevalence of cataract was also statistically significant.

A second large-scale study was carried out in the Australian state of Victoria. McCarty, Mukesh *et al.* (1999) used data from the Visual Impairment Study to estimate the prevalence of cataract in Australia. The cohort included 3271 urban residents, 403 nursing home residents and 1473 rural residents with ages ranging from 40 to 103 years old. The Wilmer system was used to grade opacification and cut-offs were set to define cataract independent of VA. Total age standardised prevalence of nuclear, cortical and posterior subcapsular cataract were 11.6%, 11.3% and 4.08% respectively (McCarty *et al.* 1999).

Studies have also been conducted in single geographic areas looking at race and cataract prevalence. One such is the Salisbury Eye Evaluation Project that took place in Maryland, USA (West *et al.* 1998). A cohort of 2520 people aged 65-84 years, of which 26.4% were African-American, were graded for presence of nuclear, cortical and posterior subcapsular cataract using the Wilmer grading scheme. The presence of lens opacity was solely used to define cataract and VA was not considered as a factor. The total prevalence of lens opacities was 66% for African-Americans and 55% for Whites in the cohort. (West *et al.* 1998). Cataract prevalence for African-Americans and Whites respectively was 33.5% and 50.7% for nuclear, 54.2% and 24.2% for cortical, and 5.5% and 13.0% for posterior subcapsular morphologies (West *et al.* 1998). African-American participants were 4 times more likely to have a cortical opacity while Caucasians were more likely to have nuclear or posterior subcapsular opacities (West *et al.* 1998).

The Baltimore Eye Survey examined visual impairment in a population of Caucasians and African-Americans in the Baltimore region of the USA (Rahmani *et al.* 1996). Out of a cohort of 5308 subjects aged 40 years and older who were initially assessed in community screenings, a total of 120 individuals with VAs between 20/40 and 20/200 were identified for subsequent detailed ophthalmic examinations to be carried out; in this group, 33% of the visual impairment was due to cataract. Stratified into age groups, 0% of visual

impairment in Whites under 65 years old was due to cataract whereas 27.1% was due to cataract in African-Americans under 65 years old. In Whites over 65 years old, 44% of visual impairment was due to cataract whereby 36.6% of visual impairment was due to cataract in African-Americans of this age range. The authors stated that this disparity was very likely due to Whites taking advantage of cataract surgery at a greater level compared to African-Americans (Rahmani *et al.* 1996).

Studies of visual impairment have also taken place in Europe. One such is the Rotterdam Study from the Netherlands (Klaver *et al.* 1998). This study involved 6775 subjects aged 55 years and higher. After using two different classification systems for blindness and visual impairment (World Health Organization and commonly used criteria in the United States), it was determined that 6% of blindness and 36% of visual impairment was caused by cataract. The prevalence of cataract causing visual impairment by stratified age group was: 18% in those aged 55 – 74; 26% in those aged 75 – 84; 42% in those aged 85 and higher (Klaver *et al.* 1998).

In the UK, a study of visual impairment was carried out in a North London population on 1547 individuals aged 65 years and higher (Reidy *et al.* 1998). Using a criterion of a VA of worse than 6/12, the prevalence of cataract causing visual impairment was determined to be 30%. Broken down into stratified age ranges cataract prevalence was: 16.3% in those aged 65-69; 24.4% in those aged 70-74; 41.5% in those aged 75-79; 58.5% in those aged 80-84; 70.6% in those aged 85-100 (Reidy *et al.* 1998).

While the above studies all have used slightly different methodologies, they demonstrate that cataract is a common age-related condition that occurs throughout the world. Different methods of clinically assessing the morphology of age-related cataract exist and are discussed below.

1.1.5 Clinical Grading of Cataract

While cataract could be considered to be a structural/anatomical problem, clinically it is often evaluated by its impact on vision and visual function. Thus, visual acuity is a common method to indicate the severity or impact of cataract in clinical practice. However, in considering cataract in terms of its structural nature, there have been many systems developed to quantify its severity. Perhaps the simplest method has been described by Mehra and Minassian (1988), who used an ophthalmoscope to visualise the red reflex through an undilated pupil and assigned a grade from 1 to 5 based upon the area of lenticular opacification seen. However, more sophisticated systems were required for epidemiological studies and a host of them have been developed that utilise the slit-lamp biomicroscope (Chylack *et al.* 1983; Sparrow *et al.* 1986; Chylack *et al.* 1988; West *et al.* 1988; Chylack *et al.* 1989; Taylor and West 1989; Klein *et al.* 1990; Chylack *et al.* 1993; Hall *et al.* 1999; Thylefors *et al.* 2002). These methods came about after the American Cooperative Cataract Research Group developed a system of describing cataractous changes in extracted crystalline lenses (Chylack *et al.* 1983).

Of these, there are a number of grading systems that have gone on to be used in subsequent research and epidemiological studies and are worth describing in further detail: these are the Oxford Clinical Cataract Grading System, the Wisconsin and Wilmer grading systems, and the Lens Opacities Classification Grading System III (LOCS III). The LOCS III is the a widely used and well-known method.

1.1.5.1 Oxford Clinical Cataract Classification and Grading System

The most comprehensive slit-lamp based grading system is the Oxford Clinical Cataract Classification and Grading System (OCCCGS) (Sparrow *et al.* 1986). In this system, 11 features of the lens are graded at the slit-lamp by comparison to a set of standard images and colour samples at scale ranging from zero to five in severity. These features are

categorised into two broad groups: cortical features and nuclear features. Cortical features include: Anterior subcapsular opacity: those opacities just posterior of the anterior capsule visible with either retro or focal-illumination; Posterior subcapsular opacity: opacities lying just anterior to the posterior capsule visible with either retro or focal-illumination; Cortical spoke (cuneiform) opacities: base out wedge-like opacities visible as shadows with retroillumination; Waterclefs: base out, wedge shaped features that are optically empty when seen by slit-beam illumination; Vacuoles: small, round cystic spaces that appear as diverging lenses and are found in the anterior or posterior cortex; Retro-dots: rounded features that are similar to vacuoles but are larger in size and behave as converging lenses that produce a reversed illumination pattern; Focal dots: grey to white punctate opacities lying in the peripheral cortex; Thickness of the anterior clear zone: a measure of the most anterior stratified layer of the cortex. Nuclear features include: Nuclear brunescence: the colour of the nucleus graded against Munsell colour scales; White nuclear scatter: the degree of opalescence in the anterior nucleus graded against Munsell neutral density scales. In the year 2000 the OCCCGS was modified and decimalized (Sparrow *et al.* 2000) to gain smaller scale intervals and increase accuracy (Bailey *et al.* 1991).

While the OCCCGS uniquely provides a grading system for many subtypes of cataract, it requires the use of numerous standard diagrams, images and colour scales. The system requires a high level of training and grading is time-intensive with experienced graders averaging five minutes to grade each cataract (Sparrow *et al.* 1986).

1.1.5.2 The Wilmer Cataract Grading System

The Wilmer system was created to allow live grading of cataract at the slit-lamp specifically for clinical and epidemiological studies of cataract (Taylor and West 1989). Observers are to compare optic sections of the nucleus to four standard images and then assign a grade of 0, 1, 2, 3 or 4 based upon whether what is seen is clearer or the same than the standard

image, without respect to brunescence. Cortical cataract is graded by obtaining retroillumination of the crystalline lens, and then assigning the same range of grades as the nuclear values but based upon estimation of the total circumference that the opacities cover; these correspond to no opacity, less than 1/8, less than 1/4, less than 1/2, or greater than 1/2 of the circumference for grades 0, 1, 2, 3, and 4 respectively. PSC opacities are simply measured for maximum horizontal and vertical length by adjusting the height of the slit beam; the height and width are then multiplied to obtain an area however, this does not represent true PSC as these opacities are usually irregular in shape (Taylor and West 1989).

1.1.5.3 The Wisconsin Cataract Grading System

The Wisconsin system was used in the Beaver Dam Eye Study and relies on slit-lamp photography. Optic sections of the nucleus and retroillumination images of the crystalline lens are captured and compared to a set of four standard photographs of cataract. In grading the nucleus, observers are to disregard colour and assign a value from 1 to 5 if images are gradable or 8 if this is not the case (Klein *et al.* 1990). As with the Wilmer system, grades are assigned based upon the observer's opinion as to whether the image they are grading is the same or clearer than the closest standard image. Unlike the Wilmer system, retroillumination images are graded for cortical or PSC by overlaying a grid of 9 equal sized areas to estimate the area of the lens that each opacity occupies (Klein *et al.* 1990).

1.1.5.4 The Lens Opacities Classification System III

A cataract grading system that has established itself is the Lens Opacities Classification System III (LOCS III) (Chylack *et al.* 1993). The LOCS III has evolved from a lineage of earlier systems. In 1988, the Lens Opacities Classification System described a simple method of grading cataract based upon black and white retro-illumination photos of

cortical and posterior subcapsular cataract, as well as a single colour slit-lamp photograph for the grading of nuclear colour and opalescence (Chylack *et al.* 1988). A second iteration of the system was then developed that used updated colour transparencies to grade cortical and posterior subcapsular cataract as well as nuclear colour and opalescence; this system was named the Lens Opacities Classification System II (LOCS II) (Chylack *et al.* 1989). While LOCS II was used in various clinical and epidemiological studies of cataract, it had limitations (Chylack *et al.* 1993). These included: a small scale for nuclear colour grading that was too coarse, unequal scaling systems, as well as underrepresentation of the early stages nuclear opalescence and posterior subcapsular opacification.

To address the above limitations of the LOCS II system, Chylack *et al.* (1993) updated it to the current LOCS III version. The grading system was decimalised as opposed to the previous integer based version, the scale for nuclear colour was expanded from three to six steps, the nuclear opalescence and posterior subcapsular cataract scales were expanded to represent earlier opacification, and objective bases for the selection of interval steps to grade cataract features were determined (Chylack *et al.* 1993).

The LOCS III system consists of three sets of standard images on a transparency; they are used to grade nuclear opacification (NO), nuclear colour (NC), cortical (C) and posterior subcapsular (P) opacification. NO and NC are each graded using six standard slit-beam images of increasing severity while C and P are each graded using five standard retro-illumination images of increasing severity. Grades of 0.1 to 6.9 are assigned to NO and NC and grades of 0.1 to 5.9 are assigned to C and P; 0.1 represents complete clarity, or zero opacification, while 6.9 or 5.9 represent the most severe cataract for their respective categories. Graders must use their intuition to imagine ten distinct levels of opacification between each standard image (Chylack *et al.* 1993). This tighter, decimalised grading system produced 95% tolerance limits of 0.7 for NO, 0.7 for NC, 0.5 for C and 1.0 for P

which significantly outperformed the LOCS II system (with 95% tolerance limits of 2.0 for each category) (Chylack *et al.* 1993). Figure 1.1.2 shows the standard images used for LOCS III grading.

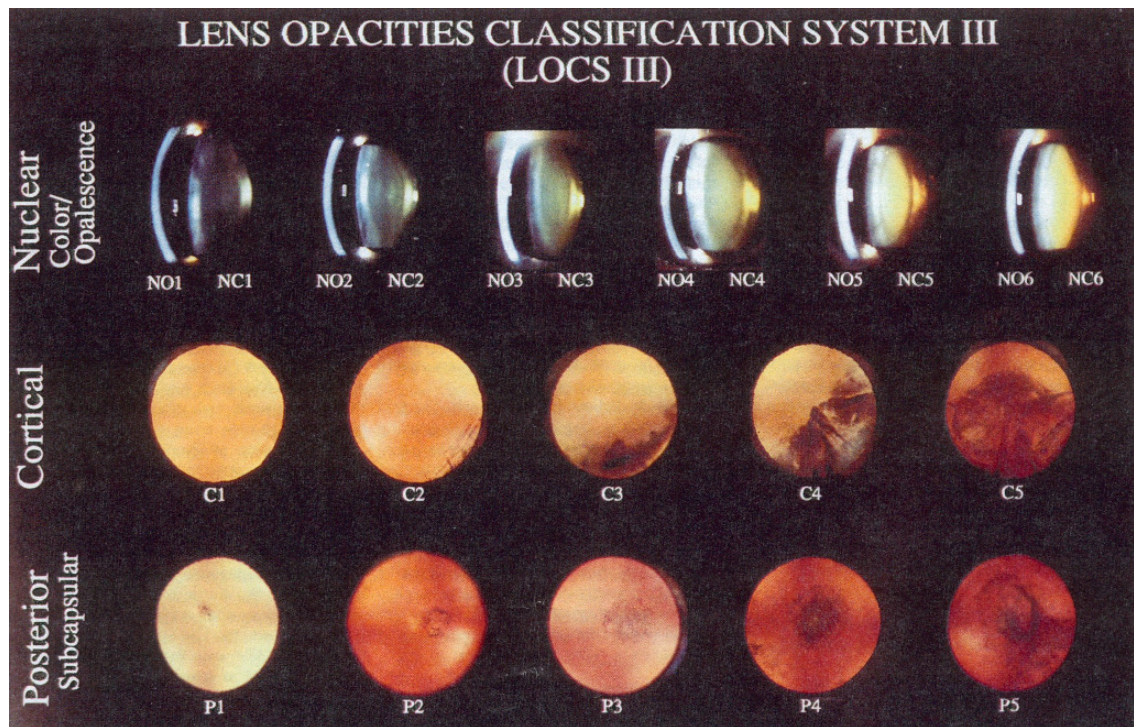


Figure 1.1.2: The set of standard images used for grading in the Lens Opacities Classification System III. Image taken from Chylack *et al.* (1993).

A unique aspect of the LOCS methods when compared to other slit-lamp based grading systems, is the ability to grade from photographs taken at the slit-lamp or by directly comparing the status of the lens to the standard images while at the slit-lamp. Karbassi *et al.* (1993) evaluated LOCS III photo-grading and grading at the slit-lamp. Two sets of participants ($n = 205$ eyes and 51 eyes respectively) were graded independently by two graders using both methods. The 95% tolerance limits for grading at the slit-lamp were slightly worse than photo-grading, ranging from 0.9 to 1.8 for the first set and 0.6 to 1.2 for the second set; the 95% tolerance levels for the first photo-graded set were 0.3 to 0.6 between observers and 0.6 to 0.8 for the same observer at two different sessions; the levels were similar for the second set of images (Karbassi *et al.* 1993).

While the LOCS III is a robust system for grading age-related cataract, it is, like all slit-lamp based systems, subjective. Changes to slit-lamp settings can have an influence on the appearance and therefore, grade assigned to cataract (Kirwan *et al.* 2003).

1.1.6 The Advent of OCT – Potential for objective grading of cataract?

In order to examine cataract in any area of the crystalline lens, it will be useful to have an objective method of grading severity and location using more modern imaging techniques. A potential method of doing so is that of using optical coherence tomography (OCT). OCT was developed and first described by Huang *et. al* (1991) and is a way of imaging transparent and semi-transparent biological tissues. In OCT, near infrared light is generated by a laser or superluminescent light emitting diode and then split into two separate beams: the reference arm (reflected by a mirror) and the measurement arm (reflected by ocular structures). Upon striking ocular tissues, incident light from the measurement arm is reflected and this is then recombined with the reflected reference arm to form an interference pattern. Through low coherence interferometry, A-Scan (axial) measurements of the targeted structures are formed. Joining a series of adjacent A-Scans creates B-Scan images, which can be thought of as 2D slices through the imaged area. OCT provides micron resolution cross-sectional images in a fast, non-invasive manner. In the eye, various layers of the cornea, crystalline lens and retina can be imaged. The ability of OCT to differentiate the layers within these structures is due to their different reflectivity profiles (Swanson *et al.* 1993).

The first use of OCT was in imaging the retina (Swanson *et al.* 1993). By providing high resolution cross-sectional images through the structure, its various layers can be examined. This has allowed visualisation of a tremendous amount of retinal pathology. For instance, conditions such as central serous retinopathy, other various maculopathies, neovascularisation and retinoschisis can all be detected, often before they are visible using

fundus biomicroscopy and standard fundus photography. There are also age-matched normalised databases that have been generated to provide standard values for measurements such as retinal nerve fibre layer thickness and neuro-retinal rim thickness. Other physical dimensions that are measured are optic nerve head size and cup-to-disc ratio. It is safe to say that OCT has revolutionised ophthalmic practice.

Aside from posterior segment imaging, OCT has also been found to be useful in imaging the anterior segment of the eye (Izatt *et al.* 1994). Manufacturers have developed OCT equipment specifically for imaging the anterior segment or have adapted their existing posterior segment OCT devices to add the facility. By using longer wavelengths of light than posterior segment OCT devices, dedicated anterior segment OCT devices have the ability to penetrate tissues more easily and provide a larger field of view.

While anterior segment OCT is primarily used to image the cornea and irido-corneal angle, there have been a few *in vivo* studies where cataract has been examined using the technique. Wong *et al.* (2009) used a Zeiss Visante Anterior Segment OCT to image and objectively grade nuclear cataract by measuring pixel intensity in 55 cataract patients. The authors found that the intensity grades correlated with LOCS III scores for nuclear colour and opalescence after performing Spearman analysis (Wong *et al.* 2009).

Two other studies have examined posterior-polar cataract using anterior segment OCT (Kymionis *et al.* 2014; Chan *et al.* 2014). Kymionis *et al.* (2014) used anterior segment OCT to preoperatively detect a capsular defect not visible with a slit-lamp in two of three patients who had posterior-polar cataract. Chan *et al.* (2014) assessed 37 eyes to develop a grading system for anterior segment OCT images of posterior-polar cataract based upon an observer's subjective opinion of the opacity's location when viewing a B-Scan; the

grading system was found to significantly detect risk for posterior capsular rupture during cataract surgery.

The most recent study of cataract grading with OCT has compared the CATALYS laser-assisted femtosecond surgery system with integrated spectral domain OCT, against LOCS III nuclear grading (Kim *et al.* 2016). Forty-seven eyes were imaged with the CATALYS system while patients were undergoing cataract surgery, and nuclear densities for each were calculated; a positive linear correlation was observed between the OCT grades and preoperative LOCS III nuclear opalescence scores (Kim *et al.* 2016). While this OCT system provides high resolution 3D scans of the entire lens, it is limited because it must come into physical contact with the eye through the use a liquid interface, and the scans are performed while patients are undergoing surgery.

The above studies show that there is very real potential for OCT to be a useful tool in the detection, localisation and measurement of cataract at any location in the crystalline lens and further work is warranted in this area.

1.2 Alzheimer's Disease

Dementia, a group of diseases caused by neurodegeneration and reduced cognitive functioning, is a condition affecting over 40 million adults over the age of 60 years worldwide; the number of those with the condition is predicted to double every 20 years to at least the year 2050 (Prince *et al.* 2013). Of all the forms of dementia, Alzheimer's disease (AD) is the most common (Scheltens *et al.* 2016). It is a disease that has been heavily researched but about which little is known and no cure available. The disease develops over decades including a lengthy preclinical stage. The hallmarks of AD are the cerebral deposition of amyloid-beta ($A\beta$) plaques and neurofibrillary tangles of tau (NFT). The classic signs of the disease are impaired memory and subsequent executive dysfunction however, impaired vision, language and executive problems can appear before memory impairment in atypical presentations (Scheltens *et al.* 2016). In the past, a diagnosis of AD was only possible based solely upon clinical symptoms. While definitive confirmation is still only possible after death and subsequent autopsy, the ability to detect the signs pathognomonic of AD through the use of magnetic resonance imaging (MRI), cerebrospinal fluid (CSF) biomarkers and positron emission tomography (PET) has become possible. Based upon these, the U.S. National Institute of Ageing has now devised suggested criteria for the preclinical, mild and full diagnoses of AD which is also preferred by the National Institute for Health Care and Excellence in the UK (Albert *et al.* 2011; Sperling *et al.* 2011; McKhann *et al.* 2011; NICE 2016). As current methods of assessing biomarkers for AD are invasive and expensive, the search for alternatives is underway.

1.2.1 Pathophysiology of Alzheimer's Disease

As mentioned above, the concrete diagnosis of AD requires both the presence of irregularly folded senile $A\beta$ plaques and NFTs of hyperphosphorylated tau protein in the brain. The leading causal theory of AD development is that of the Amyloid Cascade

Hypothesis (Hardy and Selkoe 2002; Karran *et al.* 2011). This theory, which has been established for over two decades, states that A β deposition in the brain is the first step in the development of AD (Hardy and Selkoe 2002; Normando *et al.* 2009; Karran *et al.* 2011). These deposits subsequently lead to synaptic and neuritic injury, oxidative stress/injury, NFTs and finally dementia (Hardy and Selkoe 2002). The genes involved in the production of A β are those that encode for the Amyloid Precursor Protein (APP), Presenelin-1 (PSEN1) and Presenelin-2 (PSEN2) proteins.

Beta-amyloid is a polypeptide consisting of 38 to 43 (commonly 38, 40 & 42) amino acid residues (Walsh and Selkoe 2007; Normando *et al.* 2009). A β derives from the APP whose gene exists on the 21st chromosome (Webb and Murphy 2012). Despite some uncertainty about the function of APP, it is hypothesized that it plays a role in processes such as neuronal survival, formation of synapses, and dendritic integrity (De Strooper and Annaert 2000; Tyan *et al.* 2012). APP is initially cleaved into smaller proteins by either α -secretase or β -secretase (BACE1) enzymes; the latter is responsible for the formation of A β . Firstly, BACE1 cleaves the protein into soluble APP (s-APP β) and C99 membrane bound protein; C99 is then cleaved by γ -secretase to form A β (Walsh and Selkoe 2007; Normando *et al.* 2009; Karran *et al.* 2011). The specific amino acid length of A β depends on where C99 is cleaved. It is important to note that although A β production is normal (Haass *et al.* 1992; Seubert *et al.* 1992; Shoji *et al.* 1992), it is an overproduction of the polypeptide that leads to detrimental effects (Walsh and Selkoe 2007). It should also be noted that while all A β lengths are capable of binding to one another, A β 42 is the most damaging as it is more prone to forming oligomers, and subsequently senile plaques, in AD (Burdick *et al.* 1992; Jarrett *et al.* 1993; Walsh and Selkoe 2007). Figure 1.2.1 outlines the cleavage of APP to form A β .

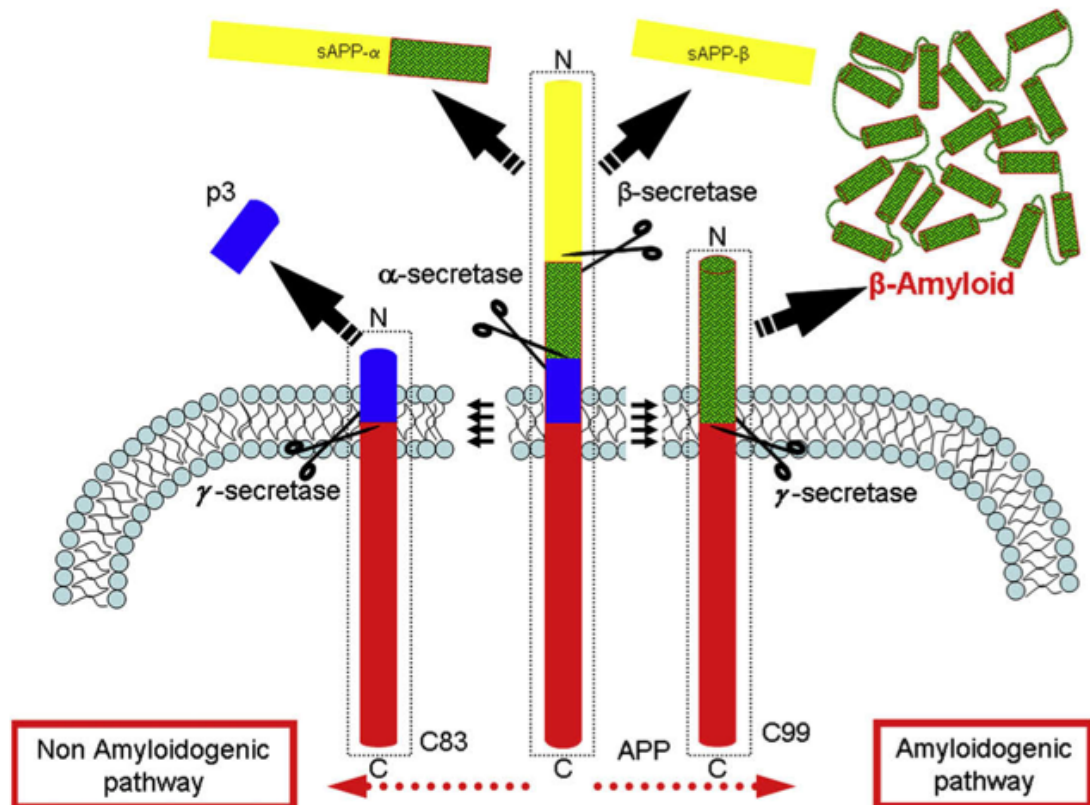


Figure 1.2.1 The processing of APP. The left side of the figure shows the non-amyloidogenic pathway where A β is not generated (APP cleaved by α -secretase). The right side shows the amyloidogenic pathway where A β is generated (APP cleaved by β -secretase). Image taken from Normando *et al.* (2009).

The genetics of AD are complex with over 20 genetic loci that have been associated with increased risk of developing the disease (Scheltens *et al.* 2016). The major genetic risk factor is for those homozygous with the E4 allele of Apolipoprotein (APOE4); lifetime risk is increased to 51% for males and 60% for females, whereas risk without reference to the APOE genotype at 85 years of age is only 11% in males and 14% in females (Genin *et al.* 2011). Those heterozygous for APOE4 and APOE3 have a risk of AD increase ranging from 20-30% (Genin *et al.* 2011). Amongst other effects, APOE4 reduces A β clearance from the brain and is broken down into neurotoxic fragments (Scheltens *et al.* 2016). In familial AD, that which occurs before the age of 65 years and with a hereditary link, mutations in APP, PSEN1 and PSEN2 are risk factors (Bertram and Tanzi 2008). PSEN1 and 2 are genes that encode the proteins at the catalytic centres of γ -secretase

enzymes and mutations, along with those in APP, are thought to increase production and aggregation as well as reduce clearance of A β (Bertram and Tanzi 2008; Scheltens *et al.* 2016).

1.2.2 Biomarkers in Alzheimer's Disease

Although a definitive diagnosis of AD can only be made post-mortem, there are various biomarkers that are currently used to aid in the diagnosis of the disease. These consist of bodily fluids as well as brain imaging. Cerebrospinal fluid can be extracted through a lumbar puncture and measured for A β 42, total tau and phosphorylated tau (Blennow *et al.* 2010; Scheltens *et al.* 2016). A β 42 levels represent cortical amyloid deposition, whereas total tau is a measure of the intensity of neurodegeneration, and phosphorylated tau correlates with NFTs (Blennow *et al.* 2010). CSF biomarkers are highly accurate with a sensitivity and specificity of 85-90% at mild AD stages, and can virtually exclude the diagnosis of AD when at normal levels in patients with mild cognitive impairment (Scheltens *et al.* 2016). Until recently, the measurement of CSF biomarkers varied across laboratories and therefore, normal values were not available. This has been rectified by the use of mass-spectrometry to determine validated and standardised values (Leinenbach *et al.* 2014).

Brain imaging using either computed tomography (CT) or magnetic resonance imaging (MRI) is commonly conducted at least once in dementia diagnosis to rule out other causes of cognitive impairment (Scheltens *et al.* 2016). These imaging technologies can also show diagnostic changes that help identify AD, including medial temporal atrophy in typical AD and parietal atrophy in those with posterior cortical atrophy, an atypical presentation of the disease (Frisoni *et al.* 2010; Lehmann *et al.* 2012). Positron emission tomography (PET) is also used to aid in the diagnosis of AD. Specifically, a radioactive tracer ^{18}F -fluorodeoxyglucose used with PET can assesses glucose uptake of neurons and glial cells

to measure synaptic dysfunction; this will signal AD if positive results are found in diagnostic areas of the brain and exclude dementia if results are negative (Scheltens *et al.* 2016; Yang *et al.* 2012).

1.2.3 The Eye as a Biomarker for Alzheimer's Disease

The above-mentioned methods of biomarker detection are invasive (CSF and PET) or expensive to perform and therefore, are not effective as tools for disease screening (Yang *et al.* 2012; Kerbage *et al.* 2014). The eye has been suggested as a site where AD biomarkers could possibly be measured in a non-invasive and simple manner. A variety of studies have been conducted to visualise A β in the retina and crystalline lens; these are discussed below.

1.2.3.1 A β and the Retina

As the retina is an extension of the central nervous system, various studies in both animals and humans have queried as to whether A β is detectable in this structure. Animal studies have mainly focused on the presence of A β in various layers of the retina. In a rat model of ocular hypertension (OHT), raised intraocular pressure (IOP) was associated with A β accumulation in retinal ganglion cells (McKinnon *et al.* 2002). Through similar research with rats, Guo *et al.* (2007) also noted increased A β deposition in the same area. Similar studies of AD and A β have also been conducted in mice. Ning *et al.* (2008) studied retinal degeneration in two transgenic mice strains that over-produced APP; A β was detected in the retinal nerve fibre layer (RNFL), ganglion cell layer (GCL) as well as the microvasculature of the retina and choriocapillaris. Another study in transgenic mice that overexpressed APP also found the presence of A β in the eye - specifically in the outer plexiform and inner nuclear layers of the retina (Perez *et al.* 2009). Building on the above study, Liu *et al.* (2009) investigated A β in the eyes of yet another mutant mouse model of AD; the polypeptide was detected in the optic nerve head, GCL, inner plexiform layer,

outer nuclear layer and photoreceptor outer segment. More recently, Ito *et al.* (2012) carried out a study investigating A β in the eye using non-human primates. The researchers induced monocular OHT, and subsequent glaucoma, in seven cynomolgus monkeys to study any associated deposition of A β 42 in the retina. After enucleation of the eyes and histological examination, A β 42 was found in the NFL, GCL and ONH of the eyes with induced glaucoma.

Results from studies that have been carried out in humans are not so clear compared to those achieved in animal models. Ho *et al.* (2014) conducted a post-mortem study examining 11 eyes using immunohistochemistry to detect the presence of AD biomarkers, and found no trace of A β in the retina. Similar research by another group also found no presence of A β in post-mortem AD retinas however, only two eyes were analysed in the study (Leger *et al.* 2011). A recent study, differing from the above two by analysing whole rather than partial retinal mounts, found the presence of A β plaques in the inner retinal layers of eight AD and five AD suspects (Koronyo-Hamaoui *et al.* 2011). Studies have also found subretinal A β plaques contained in drusen of AD eyes (Dentchev *et al.* 2003; Isas *et al.* 2010). The most recent post-mortem study examining A β presence in the AD retina found no traces in any of the 30 eyes analysed (Williams *et al.* 2017). The above summary demonstrates the complex nature of AD and much work needs to be done to determine whether the retina can be used as a biomarker for the disease.

1.2.3.2 A β and the Crystalline Lens

As outlined in section 1.1 the crystalline lens is subject to oxidation, protein aggregation and age-related changes leading to cataract. This has naturally led to the structure being investigated in relation to AD and A β accumulation. Studies conducted in humans, monkeys and rodents have shown the presence of A β in the lens. In an *in-vitro* study, Frederikse *et al.* (1996) exposed monkey, rodent and human lenses to oxidative stress in

the form of UV radiation and hydrogen peroxide. Immunohistochemical analysis revealed low baseline levels of A β that subsequently increased after exposure to oxidative stress (Frederikse *et al.* 1996); in human lenses, A β was detected in the cataractous cortical area of the lens although the authors failed to state how many lenses were analysed.

Spurred on by the findings of the above study Goldstein *et al.* (2003) conducted post-mortem examinations on nine crystalline lenses and brains from individuals diagnosed with AD, and compared the results to eight non-AD controls. After immunohistochemical analysis, the authors found similar concentrations of A β in the lenses as compared to the brain. By comparing an additional four lenses from AD donors to four control lenses, histology revealed that A β was exclusively located in the cytoplasm of deep cortical lens fibres. A surgical microscope was used to image all lenses and the authors found that deep cortical cataracts were consistently present in the AD lenses but not in those from control eyes. Goldstein *et al.* (2003) termed these cataracts ‘supranuclear’ and claimed them to be distinguishable from age-related cataract and therefore, pathognomonic of AD. The supranuclear area has been described as the interface between the deep cortical layers and superficial nucleus of the crystalline lens (Chylack *et al.* 1983). Figure 1.2.2 shows an example of the supranuclear opacities found by Goldstein *et al.* (2003).

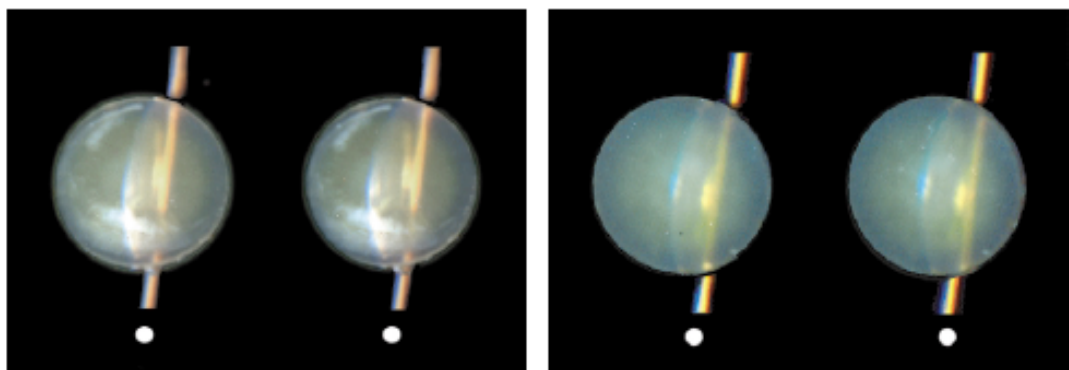


Figure 1.2.2 Stereoscopic slit-lamp images showing supranuclear cataract from an 80-year-old participant with AD (left) and a control lens from an 80-year-old participant showing no supranuclear cataract. Image taken from Goldstein *et al.* (2003).

Other authors report contradictory findings to the above study. Michael *et al.* (2013) used similar immunohistochemical techniques in a post-mortem study of 39 AD crystalline lenses and 15 controls, and failed to identify A β in any lens. The authors noted a limitation in their study was that many of the AD donors had been diagnosed by general practitioners instead of specialists and did not have their diagnosis confirmed post-mortem in contrast to Goldstein *et al.* (2003)'s protocol. The group also highlighted other variations in study protocol that may have led to differences in the results compared with those of Goldstein's group (Michael *et al.* 2013). To further their work, Michael's group used confocal Raman microspectroscopy on seven post-mortem lenses and matching hippocampal tissues from AD donors (Michael *et al.* 2014). Raman microspectroscopy is sensitive to the beta-sheets of A β fibrils and the authors detected fibrils in all the hippocampal tissues but none of the crystalline lenses (Michael *et al.* 2014). The researchers note that this technique is not definitive for the absence of A β but conclude that this evidence, combined with the findings from their previous study, demonstrates that A β is not present in the AD crystalline lens (Michael *et al.* 2014). One more study that failed to find A β in the AD lens was carried out by Ho *et al.* (2014). This group used similar immunostaining procedures to Goldstein *et al.* (2003) and Michael *et al.* (2013) on 11 AD donor lenses, six Parkinson's disease donor lenses and six controls, as well as corresponding brain tissues (Ho *et al.* 2014).

In contrast to the studies not supporting A β accumulation in the AD lens, Kerbage *et al.* (2014) developed a new technique to detect lens A β in-vivo, and claim to detect its presence in the supranuclear region of lenses in AD subjects. Aftobetin hydrochloride (AH) ointment was administered topically to the eyes of 20 probable AD subjects and 20 healthy volunteers. AH binds to A β and fluoresces when stimulated by light with a wavelength of 473nm (Kerbage *et al.* 2014). The team developed a Fluorescent Ligand Eye Scanning Device (FLESD) with a pulsed laser source peaking at 473nm to illuminate the

eye, and scan the supranuclear region of the crystalline lens (Kerbage *et al.* 2014). After excitation with light, fluorescent emission was recorded as a function of time delay (Kerbage *et al.* 2014). Upon analysis, the FLESD technique correctly predicted a clinical diagnosis of AD with 85% sensitivity and 95% specificity (Kerbage *et al.* 2014); positron emission tomography was also conducted on the brains of all subjects and it was determined that FLESD was the more accurate technique at predicting AD (Kerbage *et al.* 2014). It is noteworthy that this group, a private company, developed the technology and also conducted the research.

An in-vivo study conducted by Bei *et al.* (2015) again contradicts the findings obtained by the studies supporting supranuclear cataract associated with AD. In this novel study, the authors sought to determine whether cataract grade or lens opacity was related to the risk of AD in a pre-clinical population. Forty participants aged 45-years and over with no evidence of dementia and two with mild evidence of dementia took part in the study; the status of AD biomarkers was determined in each participant through PET and A β 42 CSF analysis (Bei *et al.* 2015). The participants then had their lenses graded using the LOCS III and densitometry measured with Scheimpflug imaging (Bei *et al.* 2015). Twenty-seven participants were negative for AD biomarkers and 15 were positive. There was no statistical significance between biomarker status, cataract or densitometry; furthermore the authors did not note any supranuclear cataract morphology (Bei *et al.* 2015).

As evidenced by the contradictory findings and small sample sizes of the above studies, it is obvious that further research is required to determine the exact interface between cataract, A β and AD. Despite this, a link between supranuclear cataract and Down Syndrome has been suggested (Moncaster *et al.* 2010). The following sections will outline Down Syndrome and why this link was made.

1.3 Down Syndrome

1.3.1 General Overview of Down Syndrome

Down Syndrome is the most common form of chromosomal abnormality and a leading cause of intellectual disability in humans. The condition was first described by John Langdon H. Down, a British physician, in 1866 however, it would be almost 100 years until Lejeune and colleagues used karyotyping to discover that DS is caused by the presence of an extra chromosome (Catalano 1990).

1.3.2 Genetics of Down Syndrome

It is now well known that DS is caused by a third full or partial copy of the 21st chromosome. It is a congenital condition for which there is no cure. There are three genetic sub-types of DS: I. Trisomy 21, II. Translocation and III. Mosaicism:

- I. In trisomy 21, all cells in the body contain an extra full copy of the 21st chromosome meaning there are a total of 47 chromosomes instead of the normal 46. During meiosis, non-disjunction of the 21st chromosome occurs resulting in an extra copy of the chromosome in the gamete. Trisomy 21 is the most common form of DS, occurring in 95% of cases (Selikowitz 2008; Bull 2011).
- II. Translocation occurs in 4% of DS cases (Selikowitz 2008; Bull 2011). In this form of DS all cells in the body have a partial extra copy of the 21st chromosome. In this form of DS, a Robertsonian translocation occurs between the long arms of chromosomes 21 and 13, 14, 15, 21 and 22. This can either happen in meiosis or can be inherited from a phenotypically normal parent with a balanced translocation.
- III. The Mosaicism form of DS occurs when some, but not all, cells in the body contain an extra copy of chromosome 21. This is the rarest form of DS, occurring in approximately 1% of cases (Selikowitz 2008; Bull 2011). Unlike the other two

forms of DS, mosaicism is caused after the egg is fertilised and during mitosis rather than meiosis. Mosaicism can occur during early cell division after the formation of a normal diploid zygote when a non-disjunction of chromosome 21 occurs, or can happen from a non-disjunction during mitosis of an embryo that was formed from a DS zygote; both of these occurrences will result in a mixture of normal diploid cells and cells with trisomy.

While the trisomy and translocation forms of DS affect individuals with the condition by the same degree, the form of mosaicism can have less of an effect on individuals due to the presence of normally developed cells mitigating developmental changes (Bull 2011).

1.3.3 Epidemiology of Down Syndrome

As previously mentioned, DS is the foremost genetic cause of intellectual disability in humans (Bell *et al.* 2003; Stoll *et al.* 2015). Recent estimates of the prevalence of DS in the United Kingdom have found rates of 6.6 and 6.3 per 10000 people respectively (Wu and Morris 2013; Alexander *et al.* 2016).

Various epidemiological studies on DS throughout the world have all found similar incidence levels of approximately 1 to 1.6 per 1000 live-births (Krivchenia *et al.* 1993; Olsen *et al.* 1996; Forrester and Merz 2002; Lai *et al.* 2002; Ménéki and Czeizel 2005; Tagliabue *et al.* 2007; Loane *et al.* 2013; Wu and Morris 2013). It should be noted that birth prevalence of DS would naturally occur at a higher rate, but prenatal screening and abortion have a mitigating effect on live-births (Loane *et al.* 2013; Alexander *et al.* 2016). For instance, Wu & Morris (2013) noted that although the instance of DS in England and Wales from 1989 to 2010 remained relatively constant at 1 per 1000 births, the expected live-birth rate should have been over 2 per 1000. An example of the expected live-birth rate can be seen in Ireland, where prenatal screening and termination are not conducted;

analysis of DS birth rates from 1981-1990 of four counties in Ireland showed an instance of over 1.8 per 1000 births (Johnson *et al.* 1996). Similarly, a retrospective study estimating the incidence of DS in Northern Ireland showed a minimum rate of approximately 1.7 in 1000 births (Devlin and Morrison 2004).

1.3.4 Physical Characteristics of Down Syndrome

There are many differences in physical appearance when comparing an individual with DS to a typically developed counterpart. These phenotypic features can be used by clinicians to suspect DS however, definitive diagnosis is determined by chromosome analysis (Roizen and Patterson 2003). Bull (2011) notes that those with DS commonly exhibit facial features such as a small brachycephalic head, small mouth and ears, a flat nasal bridge and excessive skin at the nape of the neck. The eyes take on a characteristic appearance which is described in section 1.4. Common features of the body include hypotonia, a single palmar crease and short fifth finger, and a deep plantar groove located between the first and second toes (Bull 2011). It should be noted that not all phenotypic features are present in every individual with DS.

1.3.5 Health Characteristics of Down Syndrome

There are a variety of systemic and general health conditions associated with DS that vary in prevalence and seriousness. Cardiac defects are common congenital malformations in DS with studies reporting a prevalence ranging from 26 to 50% (Selikowitz 1992; Kallen *et al.* 1996; Freeman *et al.* 1998; Roizen and Patterson 2003; Marder *et al.* 2015; Stoll *et al.* 2015). These cardiac problems are a major cause of death in the DS population (Marder *et al.* 2015). High prevalence of gastrointestinal disorders at levels greater than 70% are present as well as significant levels of obstructive sleep apnoea (30 to 50%) and epilepsy (12 to 46%) (Malt *et al.* 2013). Individuals with DS are at risk of higher levels of type 1 diabetes with a prevalence rate ranging from 1.0 to 10.6% (Anwar *et al.* 1998; Roizen and

Patterson 2003; Esbensen 2010). Cancer is also more common in DS including a higher incidence of leukaemia as well as, amongst others, increased rates of skin cancers, gastrointestinal cancers and brain tumours (Sullivan *et al.* 2007; Malt *et al.* 2013). Thyroid dysfunction, with hypothyroidism being most common, also has a higher incidence in people with DS (Roizen and Patterson 2003; Esbensen 2010; Malt *et al.* 2013). The immune system is thought to be deficient in DS causing increased susceptibility to infection in those with the condition (Kusters *et al.* 2009). Malt, Dahl *et al.* (2013) estimated the prevalence of this tendency of infection to be 100%.

There are high rates of sensory deficits in down syndrome including a prevalence of hearing loss ranging from 38-78% (Roizen and Patterson 2003; Malt *et al.* 2013) and a multitude of ophthalmic and vision deficits which will be detailed in later sections.

Life expectancy in those with DS has been steadily increasing from decade to decade. After analysing the mortality rates of 17897 people with DS living the USA, Yang *et al.* (2002) determined that the median age at death increased from 25 years in 1983 to 49 years in 1997; this amounted to an average increase of 1.7 years annually. An Australian study examining a cohort of 1332 people with DS who had registered with ID services from 1953 to 2000 showed that life expectancy had increased to 58.6 years with 25% of subjects living to the age of 62.9 years (Glasson *et al.* 2002). Four distinct age ranges, each with common causes for mortality, were revealed by the Australian study: prenatal, childhood and early adulthood (0-18 years), adulthood (18-40 years), and senescence (>40 years) (Bittles *et al.* 2007). While pneumonia and respiratory infection remained as the most common cause of death across the entire life span, a shift in comorbidities from congenital heart defects in childhood and early adulthood to coronary artery disease and failure of the cardiac renal or respiratory systems in senescence occurred (Bittles *et al.* 2007). With the relatively full lives those with DS now live, coupled with evidence suggesting accelerated

aging in the integumentary, immune, sensory, endocrine, musculoskeletal and neurological systems, the healthcare focus has shifted from maintaining quality of life to the management of treatable illness (Roth *et al.* 1996; Bittles *et al.* 2007; Zigman 2013).

1.3.6 Cognitive Characteristics of Down Syndrome

As DS is the most common genetic cause of intellectual disability, much has been studied regarding the cognitive development process in this population. A variety of traits have emerged that are phenotypic of the syndrome however, they occur in varying levels across individuals (Chapman and Hesketh 2000; Silverman 2007). In specific regard to intellectual disability (ID), the mean IQ in DS has been shown to be 50, with a wide range from 30-70 representing a large to borderline deficit (Vicari *et al.* 2005; Contestabile *et al.* 2010; Grieco *et al.* 2015). A decline is seen in both IQ and learning rate with age and cognitive testing shifts from assessing development to monitoring decline from middle-adulthood onwards (Patterson *et al.* 2013; Grieco *et al.* 2015). The ability to interpret visual rather than verbal information has been shown to be stronger in DS (Contestabile *et al.* 2010; Grieco *et al.* 2015). While non-verbal abilities continue to develop throughout childhood and into adolescence, the development of verbal ability tends to decline during the same period (Grieco *et al.* 2015). Studies have shown that syntactic development is impaired in DS from early childhood onwards (Silverman 2007).

Both short- and long-term memory problems are also characteristic of DS. Verbal short-term memory has been shown to be significantly reduced compared to visual-spatial short-term memory (Jarrold *et al.* 2009; Patterson *et al.* 2013). Individuals with DS display a disability in explicit long-term memory: that which requires conscious recollection (Jarrold *et al.* 2009). Vicari *et al.* (2005) showed that subjects with DS show much better long-term visual-spatial memory performance compared to visual-object memory performance.

In relation to cognitive characteristics, the anatomical properties of the brain are different in those with DS. Initially comparable in size to typically developing infants up to the age of six months, brain size becomes relatively smaller in DS thereafter (Nadel 2003). Nadel (2003) suggests that brain size does not affect intelligence and a smaller brain size may simply be due to allometry as individuals with DS are physically smaller. A more significant aspect of the brain in regard to intellectual disability is that certain areas are disproportionately smaller than typically developed peers when allometry is accounted for (Nadel 2003). Volumetric MRI studies in DS have shown that the hippocampus and cerebellum are the most disproportionately reduced in size, although multiple areas of the brain are also smaller, compared to typically developed controls (Beacher and Murphy 2006). The diminished hippocampal volume is constant from childhood to adulthood and may explain the various deficits in memory performance that occur in DS (Beacher and Murphy 2006). While the cerebellum is associated with motor function, a comprehensive understanding of its roles remains to be determined; the reduced volume of this structure in DS may explain the degraded motor, language, spatial and other higher cognitive functions present in this population (Beacher and Murphy 2006).

It is clear to see that many cognitive and brain changes are present in DS. Further unique sequelae to DS are the dementia and Alzheimer's like brain pathology that occur almost invariably. These are explained below.

1.3.6.1 Alzheimer's Disease in Down Syndrome

Coinciding with the above cognitive aspects that occur in DS, a high rate of AD also occurs in this population. As the gene for APP is located on chromosome 21, because of its triplication, those with DS produce more of the protein (Prasher 2006; Lee *et al.* 2017). Consequently, studies have detected the presence of senile A β plaques and NFT in the brain of DS adults aged 35 to 40 years and older (Wisniewski *et al.* 1985; Zana *et al.* 2007;

Lee *et al.* 2017). While AD neuropathology is detected in all individuals with DS by the age of 40 years, prevalence of dementia ranges from 8% in those aged 35-49, to 55% in those aged 50-59 and finally 75% in those above the age of 60 years (Zana *et al.* 2007). There are several other genes located on chromosome 21 that have also been suggested to play a role in the onset of AD in DS. Although the gene for APP is directly related to the accumulation of senile A β plaques, there are genes that contribute to the oxidative stress, hyperphosphorylation of tau and neuroinflammation that are also seen in AD (Prasher 2006; Zana *et al.* 2007; Hartley *et al.* 2015; Head *et al.* 2016; Lee *et al.* 2017).

While the above evidence shows the close relationship between DS and AD, the actual diagnosis of dementia in this population remains very difficult. The main challenge to diagnosis is the pre-existing intellectual disability masking initial symptoms as well as the inability to apply tests of cognitive ability and memory traditionally used in typically developed adults (Prasher 2006; Prasher *et al.* 2015; Lee *et al.* 2017). As AD diagnosis is complex in typically developed adults, the even greater difficulty in those with DS stresses the need for reliable biomarkers that would provide objective judgements on the presence of the disease. To this end, as explained in section 1.2.3.2 investigating cataract in AD, the crystalline lens has also been examined in DS as a potential site for A β accumulation. There are a variety of ophthalmic conditions, including cataract, that have been investigated in DS; these are summarised below.

1.4 Ophthalmic Characteristics of Down Syndrome

1.4.1 External Eye

There have been many findings in regard to the exterior eye in DS. Most notably is the upward and outward slanting of the palpebral fissure and associated smaller width of the palpebral aperture (Lowe 1949; Jaeger 1980; Catalano 1990). It has also been noted that individuals with DS have epicanthal folds at a higher prevalence than their typically developing peers (Catalano 1990; daCunha and Moreira 1996; Fong *et al.* 2013). Catalano (1990) stated that epicanthal folds in DS may differ structurally from typically developing individuals. There are fairly frequent reports of higher rates of blepharitis in DS (Jaeger 1980; Shapiro and France 1985; Catalano 1990; daCunha and Moreira 1996; Fong *et al.* 2013), which may be connected with atopic tendencies, and Catalano (1990) surmised that the blepharitis may be due to decreased ability to fight infection. Additionally, Filipello, Cascone *et al.* (1997) have concluded that the reduced density of conjunctival goblet cells found in individuals with DS may also increase susceptibility to anterior segment eye infections.

Specific to spectacle fitting, the above-mentioned facial features have been shown to require careful frame selection when dispensing eyewear to those with DS. Woodhouse *et al.* (1994) determined that DS children above the age of 14 years had a significantly smaller pupillary distance than controls; accounting for facial morphology, the following frame measurements were also different compared to controls: a smaller apical radius, larger splay angle, lower crest height and shorter front-to-bend (Woodhouse *et al.* 1994).

1.4.2 The Cornea

The cornea is the transparent and avascular primary refractive surface of the eye. It is comprised mostly of collagen whose fibrils are arranged in a highly ordered pattern. Until recently, the cornea was thought to consist of five distinct layers: the epithelium,

Bowman's layer, the stroma, Descemet's membrane and the endothelium; however, in 2013 Dua, Faraj *et al.* described a sixth layer resting between the stroma and Descemet's membrane. The cornea is a prolate ellipsoid in shape with an average central thickness of 530 microns and approximate anterior horizontal and vertical diameters of 12mm and 11mm respectively (Remington 2012). Compared to typical values, increased steepness in corneal curvature, a thinner cornea and higher levels of astigmatism have also been reported in the DS eye (Haugen, Hovding and Eide 2001; Evereklioglu *et al.* 2002; Vincent *et al.* 2005; Little, Woodhouse and Saunders 2009).

A higher prevalence of keratoconus, a disease that results in progressive thinning and steepening of the cornea, has been reported in DS (Cullen and Butler 1963; Jaeger 1980; Catalano 1990; Doyle *et al.* 1998; Woodhouse, Griffiths, *et al.* 2000). After this initial discovery, it was later found that corneal hydrops also exist at a higher rate in those DS individuals with keratoconus (Catalano, 1990). Catalano (1990) suggested that excessive eye rubbing, a risk factor for keratoconus, may also play a role in this population; it was also suggested that irritation from blepharitis can cause increased eye rubbing.

1.4.3 The Iris

There have been many reports of Brushfield spots which are defined as speckles of condensed collagen in the anterior iris stroma (Jaeger 1980; Catalano 1990). Jaeger (1980) reported a prevalence of these phenomena at 59% in DS compared to 10% in controls and noted a decreased likelihood of them occurring with increasing iris pigment. Berk *et al.* (1996) also noted less prevalence of these spots in darker coloured irides but found a lower overall prevalence of 36%. It has been noted in various studies that the presence of Brushfield spots is more prevalent in Caucasian DS populations compared to Asian populations (Liza-Sharmini *et al.* 2006; Fong *et al.* 2013).

1.4.4 The Crystalline Lens

In their study of young adults with DS, Haugen *et al.* (2001) noted decreased levels of crystalline lens thickness (3.27 ± 0.29 mm) and mean calculated lens power (17.70 ± 2.36 D) when compared to typically developed controls, whose values were 3.49 ± 0.20 mm and 19.48 ± 1.24 D respectively; the authors also found significantly higher axial density of the lens in their DS cohort.

Opacities of the crystalline lens have been reported at a prevalence ranging from 4-72% and at an earlier age in DS when compared to a typical population (Jaeger 1980; Catalano 1990; Hestnes *et al.* 1991; Berk *et al.* 1996; daCunha and Moreira 1996; Woodhouse, Griffiths, *et al.* 2000; Kim *et al.* 2002; Liza-Sharmini *et al.* 2006; Wong and Ho 1997; Fimiani *et al.* 2007; Krinsky-McHale *et al.* 2012; Fong *et al.* 2013) (Table 1.4.1). This wide range of reported values is conflicting and results from cursory and qualitative evaluation of lens opacities in this population. Perhaps as the range of serious sensory, neurologic, systemic and physical conditions is so great in DS, the study of cataract has been given less importance. It has also been reported that DS individuals are prone to congenital cataracts of a cerulean (blue-dot) type (Jaeger 1980; Catalano 1990; Fong *et al.* 2013). Although most studies on the ocular manifestations of DS have reported increased cataract prevalence, they do not often detail its type and location/severity. Furthermore, the definition of cataract varies by study with some only reporting cataracts when vision was affected and others reporting cataract as any opacification of the lens.

Authors	Date	Number of Participants	Age Range (Years)	Prevalence
Jaeger	1980	74	15-64	55%
Hestnes et al.	1991	30	21-72	50%
Berk et al.	1996	55	0.17-25	20%
daCunha et al.	1996	152	0.17-18	13%
Wong & Ho	1997	140	0.25-13	4%
Woodhouse et al.	2000	31	Mean 36.7+/- 11.25	23%
Kim et al.	2002	123	0.5-14	13%
Liza-Sharmini et al.	2006	60	0.08-17	13%
Fimiani et al.	2007	157	0.08-18	11%
Krinsky-McHale et al.	2012	455	30-80+	42%
Fong et al.	2013	91	30-56	73%

Table 1.4.1: Studies of Lens Opacity in DS.

1.4.4.1 Beta-Amyloid and Cataract in Down Syndrome

Due to the previously mentioned link between AD and DS, the blue-dot cataract type reported in DS, and the exploration of cataract as a potential biomarker for AD, the same group who detected the presence of A β in supranuclear lens opacities conducted a study in a cohort of DS subjects. Following on from their study in AD [(Goldstein *et al.* 2003)], Moncaster *et al.* (2010) obtained crystalline lenses from DS patients who underwent cataract surgery (n=3), post-mortem DS specimens (n=12), and post-mortem non-DS controls (n=34). Lenses were visually assessed for cataract using slit-lamp biomicroscopy and then underwent a battery of immunohistochemical analyses to detect the presence of

A β (Moncaster *et al.* 2010). Slit-lamp biomicroscopy revealed the supranuclear cataract phenotype in all surgical and post-mortem adult DS lenses; furthermore, the authors claim that the severity of supranuclear opacification increased with age (see figure 1.4.1); supranuclear cataract was not found in any control lens (Moncaster *et al.* 2010).

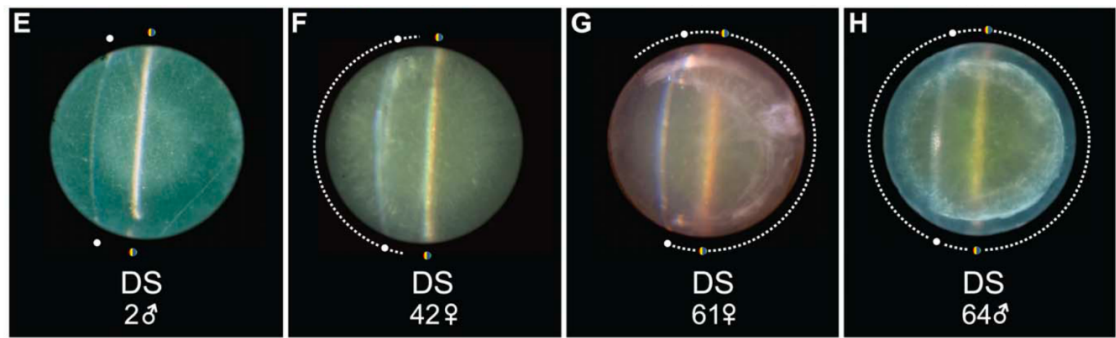


Figure 1.4.1 Slit-lamp images showing no cataract in a lens from a 2-year-old (E) and progressively worse supranuclear cataract in 42-year-old (F), 61-year-old (G) and 64-year-old (H) adults with DS. Images taken from Moncaster *et al.* (2010).

Amyloid histochemical analysis of the DS lenses showed positive Congo red staining and intense apple-green birefringence suggesting A β pathology; none of the control lenses were positive for staining (Moncaster *et al.* 2010). The amyloid pathology present in the histochemically stained lenses was co-localised with the supranuclear cataract in the deep cortical layers (Moncaster *et al.* 2010). Immunogold electron microscopy and mass spectrometry supported these findings in DS and control lenses (Moncaster *et al.* 2010). Moncaster *et al.* suggest that their data align with their previous findings of A β accumulation in the lens of AD participants and that supranuclear cataract may suggest the earliest signs of AD pathology. This is in contrast to the studies (mentioned in section 1.2.3.2) conducted by unrelated groups that refute these findings.

Although increased prevalence of cataract has been reported in DS individuals, as previously stated, little research has been conducted on its morphology and severity. The

conflicting evidence of the presence of A β in the crystalline lenses of those with AD and DS has not addressed this. The studies that are positive for the presence of A β in the crystalline lens report its existence in a specific supranuclear area (Kerbage et al. 2014, Goldstein et al. 2003, Moncaster et al. 2010), but it is unknown whether cataracts exist in this location in the DS eye in the absence of AD.

1.4.5 The Retina in Down Syndrome

The retina consists of light sensitive neural tissue lining the interior surface of the eye, its supporting structures and blood vessels. It is formed of ten distinct layers. Nerve fibres from the retina congregate at the optic nerve head, enter the brain through the optic nerve, are split through partial decussation at the optic chiasm, travel to the lateral geniculate nucleus and finally divide into optic radiations which proceed to the occipital cortex.

Adding to the battery of conditions reported in the DS eye, retinal changes have also been noted. The properties of the retina in DS have also had limited attention in the literature but include reports of increased vascularisation at the optic nerve head (Williams *et al.* 1973; Sherk and Williams 1979; Jaeger 1980; Berk *et al.* 1996; Kim *et al.* 2002), optic disk elevation (Al-Hemidan *et al.* 1999; Catalano and Simon 1990) and case reports of macular coloboma (Yamaguchi and Tamai 1990; Hayasaka and Hayasaka 2004). Recently, Stirn (2012) noted that, out of a cohort of 65 children with DS, 16.9% had retinal vessel abnormalities, 9.2% had a hypoplastic fovea and 6.1% had optic disc pallor.

Modern imaging techniques such as OCT have been seldom used to examine the retina in DS. Recently Laguna et al. (2013) investigated retinal thickness in five eyes from three individuals with DS and reported an increased thickness especially in the foveomacular region. Fong et. al. (2013) measured retinal nerve fibre layer thickness by scanning the optic nerve head with OCT in three DS eyes and found it to be normal. Most recently, O'Brien *et al.* (2015) performed macular OCT scans on 17 children with DS aged 6-16;

when compared to controls, the central subfield thickness as well as inner and outer retinal layer thickness were significantly greater in DS. Beyond these three aforementioned studies, there are no detailed analyses of retinal structure using OCT in the DS eye.

1.4.6 Strabismus in Down Syndrome

Strabismus, or heterotropia, is an involuntary misalignment of the visual axes of the two eyes when a person is fixating on an object. Deviations of the eyes can be medial (esotropias), lateral (exotropias) or vertical (hyper/hypotropias) in orientation. There are many reports of strabismus in DS with prevalence ranging from 19-42% (Jaeger 1980; Berk *et al.* 1996; daCunha and Moreira 1996; Haugen and Hovding 2001; Cregg *et al.* 2003; Liza-Sharmini *et al.* 2006; Yurdakul *et al.* 2006; Fimiani *et al.* 2007; Kim and Hwang 2009; Ljubic *et al.* 2011; Krinsky-McHale *et al.* 2012; Fong *et al.* 2013). All studies agree that esotropia is more common than exotropia and vertical deviations in those with DS; Kim and Hwang (2009) had an unusually high prevalence of exotropia in their cohort at 10.5% however, this was still well below the prevalence of esotropia (22.1%). In contrast to typically developing children, Cregg *et al.* (2003) as well as Kim and Hwang (2009) did not find strabismus to be related to refractive error.

1.4.7 Nystagmus in Down Syndrome

Nystagmus is an involuntary pendular or oscillating movement of the eyes that often results in reduced vision. It has also been shown that the prevalence of nystagmus is increased in DS with values ranging from 6% to over 33% (Jaeger 1980; Berk *et al.* 1996; daCunha and Moreira 1996; Liza-Sharmini *et al.* 2006; Fimiani *et al.* 2007; Kim and Hwang 2009; Ljubic *et al.* 2011; Krinsky-McHale *et al.* 2012; Fong *et al.* 2013). Wagner *et al.* (1990) characterised nystagmus in 188 DS participants, found a 29.8% prevalence and noted that a fine rapid horizontal nystagmus was most common.

1.5 Vision in Down Syndrome

1.5.1 Visual Function in Down Syndrome

Aside from the many ophthalmic features of DS, there are many differences in visual function. Studies have been carried out to analyse visual acuity, refractive error and amblyopia in this population. Of the studies of visual acuity in DS, they have all found reduced VA levels in those with DS when compared to controls. Courage et al. (1994) evaluated visual acuity using Teller acuity cards in children with DS aged two months to 18 years and found it to be reduced compared to age matched controls; this reduction was still present when ocular abnormalities were accounted for. Woodhouse et al. (1996) found reduced VA in a cohort of 53 children with DS and found that although normal visual development occurred before the age of two years, it was reduced from then on; the authors surmised that the reduction in VA in DS could very well be due to physiological changes in the visual cortex. In a study examining amblyopia, Tsiaras et al. (1999) examined visual acuity in 68 children with DS aged between five and 19 years; 47% of these participants had VAs between 20/30 to 20/40 while 31% and 24% had less than 20/50 in one or both eyes respectively. In a study designed to determine whether the reduced VA detected in DS was due to cognitive or behavioural deficits masking true levels, John et al. (2004) utilised visually evoked potential (VEP) to measure visual function; it was found that DS subjects exhibited poorer measures of VEP acuity than those obtained with behavioural techniques. This finding provides additional confirmation that a physiological deficit contributes to reduced VA in the DS population and that poor visual performance cannot be attributed solely to attentional and motivation issues in DS.

While the above studies demonstrate a true reduction of visual acuity in DS compared to age matched controls, they did not clarify whether the differing optics of the eye in DS play a role in this. To test this, Little et al. (2007) used grating resolution acuity and interferometric acuity analyses to measure VA in a cohort with DS. The authors found a

larger difference in grating acuity compared to interferometric acuity in those with DS when compared to age-matched controls. This suggests that the optics of the eye in DS do not wholly account for but do play a large role in the reduced VA that is found in this population. To add further confirmation of the sensory deficit that contributes to VA reduction in DS, Little *et al.* (2009) measured Vernier acuity in 25 children with DS and found it to be reduced by a factor of 2.7 when compared to 65 age-matched controls. Reduced Vernier acuity was also found in a small study ($n=5$) of Adult participants with DS (Krinsky-McHale *et al.* 2014).

Another important measure of visual function is contrast sensitivity. In contrast to the above studies of VA, there have been few studies of CS in DS populations. Courage *et al.* (1997) first assessed contrast sensitivity in children with DS and found it to be reduced compared to age-matched normals; furthermore, the reduction increased with increasing spatial frequency. There was also little improvement in CS with age. In a more thorough assessment of CS, John *et al.* (2004) assessed CS with behavioural and VEP tests. This study demonstrated reduced CS in both VEP and behavioural measures for the DS group of participants when compared to controls; the deficit remained after ocular abnormalities were accounted for. Finally, Krinsky-McHale *et al.* (2014) measured spatiotemporal CS in seven adults with DS and found a generalised reduction when compared to younger and older adults without intellectual disability. These studies of CS in DS all suggest a sensory component to the reduced visual function observed in DS.

1.5.2 Refractive Error in Down Syndrome

Like the differences in visual function that are present in DS, there are many reports of increased refractive error (Shapiro and France 1985; Caputo *et al.* 1989; Hestnes *et al.* 1991; Berk *et al.* 1996; daCunha and Moreira 1996; Woodhouse *et al.* 1997; Haugen, Hovding and Lundstrom 2001; Kim *et al.* 2002; Cregg *et al.* 2003; Liza-Sharmini *et al.* 2006; Fimiani *et al.*

2007; Kim and Hwang 2009; Ljubic *et al.* 2011; Fong *et al.* 2013). While most studies report a higher prevalence of hyperopia, there are some reports of similar prevalences of myopia and hyperopia (Shapiro and France 1985; Caputo *et al.* 1989; Liza-Sharmini *et al.* 2006; Kim and Hwang 2009). Interestingly, Fong *et al.* (2013) reported a higher incidence of myopia (59.3%) compared to hyperopia (30.2%) in a cohort of individuals with DS aged 30 years and older; this contrasts with most studies that have been conducted in younger populations. All studies also report high prevalence of astigmatism. The varying prevalence between studies may be due to the different criteria used to define refractive error, varying age-ranges between cohorts as well as differing techniques used to measure refractive error.

1.5.3 Accommodation in Down Syndrome

There have been various reports of reduced accommodative ability in DS. Woodhouse and colleagues used modified Nott retinoscopy as an objective technique of assessing accommodation in a group of 24 children with DS and found it to be significantly reduced compared to controls (Woodhouse *et al.* 1993). Following on from this, Woodhouse *et al.* (2000) found a similarly large level of under-accommodation in a group of 77 children with DS with a mean reduction of at least 50% at all testing distances when compared to controls; increasing under-accommodation with increasing age was also found to be significant. The authors did not determine the aetiology of under-accommodation in DS but postulated that it may be due to a sensory or motor deficit. Following on from the previous study, it was discovered that under-accommodation was present in DS regardless of refractive status however, increasing under-accommodation occurred with increasing hyperopia (Cregg *et al.* 2001); interestingly, spectacle correction of hyperopia did not improve accommodation. In a later study, it was found that bifocal spectacles improved accommodative responses in DS (Stewart *et al.* 2005). Surprisingly, the reduced lag of

accommodation remained when the participants viewed objects through the distance portion of their bifocal spectacles.

To try and understand the aetiology behind the lag in accommodation that occurs in DS, Doyle *et al.* (2016) recently examined the near triad using a photorefractometer system in a cohort of 24 children with DS and 75 controls. Participants with DS had a significantly lower mean accommodative response to accommodative demand; however, they demonstrated a very similar mean vergence response compared with typically developing controls. There was a significant difference in pupillary response to accommodative demand at 5D between the DS and control groups with controls showing greater constriction but baseline diameters were similar between groups. These data add additional support to the assertion made previously that the under-accommodation found in DS is affected by physiological or neurological components.

1.6 Summary of Introduction and Aims of Thesis

The above literature review has shown the complexity of AD, its relation to DS and the need for simple non-invasive biomarkers for its diagnosis. While supranuclear cataract has been suggested as a site for A β accumulation, there is conflicting evidence that precludes it as a definitive biomarker for AD. This is further weakened by the presumption of supranuclear cataract being characteristic of DS. While the above literature review discusses the numerous ophthalmic and visual sequelae that occur in DS, and shows that many have been studied in detail, there is a specific paucity of comprehensive analyses of lens opacity, with widely varying and vague reports of its morphology and presence in the population. This is most likely due to current methods of cataract grading being only applicable to age-related forms of the condition, as well as their unsuitability for use in those with intellectual disability. There is a need to undertake a detailed structural analysis of cataract in DS, but this requires an objective method of examining and quantifying opacity at any location within the crystalline lens.

The aim of this thesis is to profile, for the first time, presence, severity type and location of cataract in the DS eye. In order to accomplish this, an objective method of imaging and quantifying opacity within any location of the crystalline lens will be developed using *in-vivo* anterior-segment optical coherence tomography in typically developed adults and validated against the slit-lamp based LOCS III. By then applying this new technique to a cohort of children and adults with DS, a detailed structural profile of cataract can be obtained. Finally, as an adjunct to the above, posterior-segment optical coherence tomography will be used to gain further insight into retinal structure in those with DS.

Chapter 2: General Imaging Methods

The following chapter discusses two techniques used to image the eye throughout this thesis. Firstly, the development and current state of optical coherence tomography will be outlined and followed on by the specific instruments used in this study. Secondly, a method developed to modify a slit-lamp biomicroscope that was used for the traditional assessment and grading of cataract will be described.

2.1 Optical Coherence Tomography

Optical coherence tomography is a non-invasive and non-contact *in-vivo* medical imaging technique that can be thought of as analogous to B-scan ultrasound. Instead of using acoustics to image transparent and near-transparent biological tissue, OCT creates tomograms through the measurement of backscattered light produced from a coherent, broadband light source. These cross-sectional images are micron resolution and quick to obtain. As a result, OCT has evolved to become the standard of care in diagnosis and management of many ocular diseases. The following sections will outline this technology and its current use in the ophthalmic and vision sciences.

2.1.1 History of Optical Coherence Tomography

The origins of this technique came about through the development of femtosecond optics and its application to compute *ex-vivo* A-scan measurements of a bovine eye through analysing optical echo (Fujimoto and Swanson 2016). A team of researchers from the Massachusetts Institute of Technology (MIT) then, as a means of reducing cost and simplifying manufacturing, replaced femtosecond optics with interferometry based on earlier studies by other groups using the technique to image biological tissue (Fercher *et al.* 1988; Fujimoto and Swanson 2016). Ongoing work led to the first published B-Scans of the *ex-vivo* eye and coronary artery (Huang *et al.* 1991). It was then that this technology

became officially coined as Optical Coherence Tomography. At this point, the technology was slow, taking minutes to complete a scan and therefore, not yet feasible as an *in-vivo* technique (Huang *et al.* 1991). OCT was then refined by the MIT team using fibre optics and other sophisticated techniques to derive a slit-lamp based imaging system capable of capturing *in-vivo* images (Fujimoto and Swanson 2016). This faster system produced the first reports of *in-vivo* retinal and anterior segment images (Swanson *et al.* 1993; Izatt *et al.* 1994). Following this, a series of studies were conducted to image and characterise many retinal diseases over the mid to late 1990s (for a review see Fujimoto and Swanson 2016). Eventually, the spinoff company formed by MIT was purchased by Humphrey Zeiss and the first commercial OCT instrument was released in 1996. After some time, OCT has evolved to become critical in the management of many retinal and anterior segment ophthalmic conditions. There are a variety of manufacturers producing instruments and the technology has continued to improve in resolution and scan acquisition time. The following sections will outline the development of OCT technology and its clinical use.

2.1.2 Methods of Optical Coherence Tomography

All versions of OCT make use of an interferometer and low coherence light source. The interferometer splits the beam of light into a reference arm, which is reflected by a mirror, and a sample arm, which is focussed through the tissue structure to be imaged. Transparent and semi-transparent tissues can cause backscatter from the sample arm and when this is recombined with the reference arm through the interferometer, an interference pattern forms; processing the signal of the interference pattern from a detector yields a one-dimensional A-scan of the tissue. Using an optical system to focus and move the sample arm laterally, a transverse series of A-scans is taken to form a two-dimensional B-scan of the desired ocular structure. More recently, OCT instruments have gained the facility to combine multiple adjacent B-scans to form three-dimensional images of tissue structures. See the figure below for a schematic of a basic OCT system (figure

2.1.1).

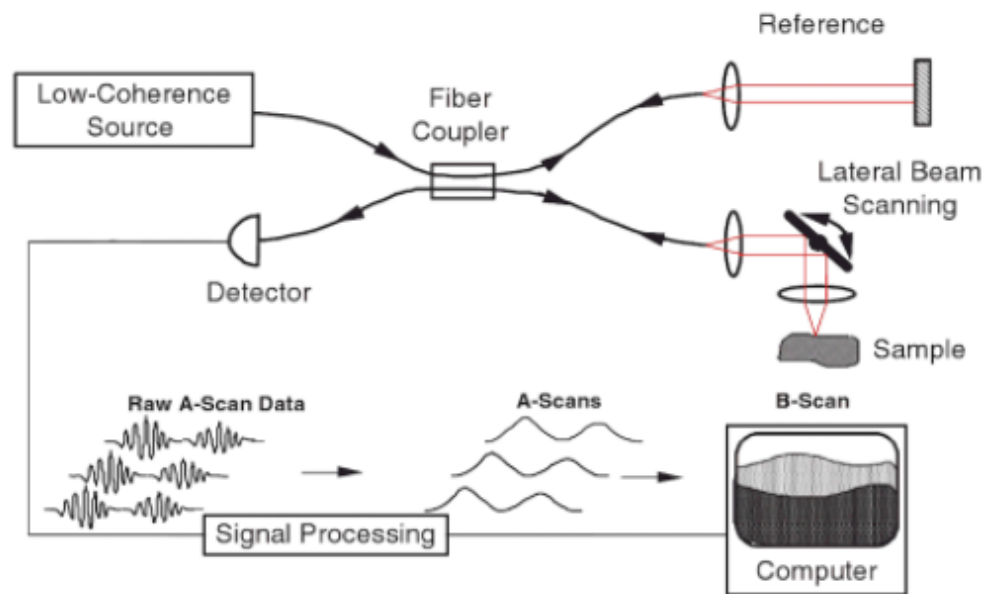


Figure 2.1.1 Schematic of a generic OCT device. Image taken from Drexler and Fujimoto (2008)

OCT technology has undergone a series of design evolutions with each producing significant improvements in resolution and scan times. These can be divided into two classes of instrument: Time Domain OCT (TD-OCT) and Fourier Domain OCT (FD-OCT). FD-OCT can be further classified into Spectral Domain OCT (SD-OCT) and Swept Source (SS-OCT) subgroups.

2.1.2.1 Time Domain OCT

The first instances of OCT were of the time domain type. TD-OCT generally makes use of a Michelson interferometer and a broadband light source. As mentioned previously, the light is split into reference and sample arms. In TD-OCT, the reference arm is reflected by a mirror that moves axially, whereas the sample arm is moved laterally and focused through imaged tissue by an optical system. Back reflected sample arm light from various scattering areas of the imaged tissue is recombined with the reference arm; an interference

pattern is generated when the reflected sample arm matches a specific axial location of the reference mirror; this provides the depth information for A-scans. A photodetector then sends this interference data to be analysed and processed by a computer. The scanning speed of 'TD-OCT' instruments is limited by the maximum oscillating speed of the reference mirror (Gabriele et al. 2010). Figure 2.1.2 shows the basic design of a 'TD-OCT' instrument.

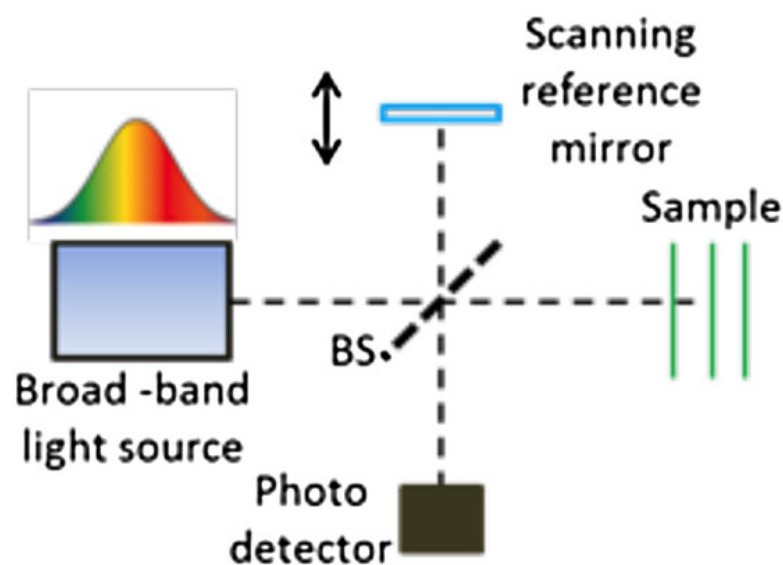


Figure 2.1.2 Schematic of a 'TD-OCT' device showing the oscillating scanning reference mirror. Image adapted from Drexler *et al.* (2014)

2.1.2.2 Fourier Domain OCT

FD-OCT was developed after 'TD-OCT' as a means of improving resolution and scan speed. FD-OCT differs from 'TD-OCT' in that there is no mechanical movement of the reference mirror. The first FD-OCTs were of spectral domain design and swept source technology then followed.

SD-OCT again makes use of a broadband light source and interferometer however a CCD camera and spectrometer take the place of the photodetector that is used in 'TD-OCT'. All depth information is extracted simultaneously by separating the spectrum of the back reflected sample and reference arms using a diffraction grating and then processing the

various spectral interference patterns (Gabriele *et al.* 2010; Drexler and Fujimoto 2008). SS-OCT differs from SD-OCT in that it uses a narrow width laser light source that can sweep at high-speed across multiple wavelengths. A photo-diode then detects the interference signal produced by the two optical arms as the light source sweeps across its various frequencies over time (Gabriele *et al.* 2010; Drexler *et al.* 2014). In both forms of FD-OCT, A-scans are generated through Fourier analysis of the signal from either the CCD camera or photo-detector. It is important to note that the acquisition time of SD-OCT is limited by the CCD camera's speed whereas the wavelength-tuning speed of the laser is the determining factor in SS-OCT (Drexler *et al.* 2014). Figure 2.1.3 demonstrates a schematic of SD-OCT and SS-OCT systems. As TD-OCT acquires A-scans sequentially through the sample tissue depth via mechanical movement of the reference mirror, the acquisition speed is much slower than FD-OCT where all depths are imaged simultaneously (Kiernan *et al.* 2010). This means FD-OCT systems are less susceptible to motion artifacts making them more useful in subjects with unsteady fixation.

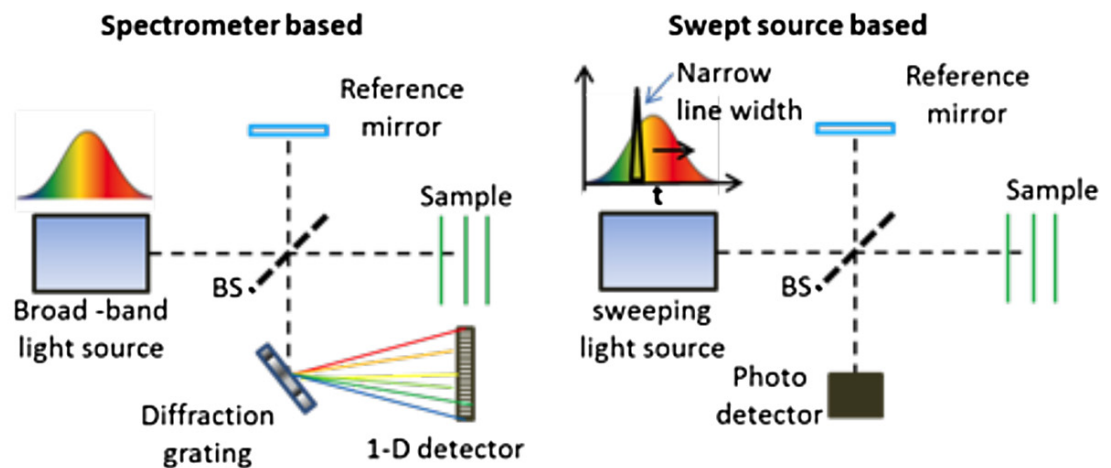


Figure 2.1.3 Schematics of FD-OCT devices. The left schematic shows a typical SD-OCT system while the right schematic outlines a SS-OCT. Image adapted from Drexler *et al.* (2014)

2.1.3 Light Source Properties for Effective OCT Imaging

The wavelength, bandwidth and intensity of light used in the design of various OCT instruments are all dependent on intended use. Most commercial OCTs designed for retinal imaging make use of light source centre wavelengths in the 800nm range (Wolfgang Drexler and Fujimoto 2008; Gabriele *et al.* 2010). Typical bandwidths have been approximately 25nm in magnitude (Gabriele *et al.* 2010). Axial resolution is dependent on bandwidth; more specifically, the coherence length of the light source in relation to the optical path length of the sample arm is inversely proportional to axial resolution (Drexler *et al.* 2014). Theoretical axial resolutions of 1 μ m are possible with \sim 800nm wavelengths however, to achieve this, wide bandwidths of 280nm are required making manufacture of the instruments impractical (Drexler 2004). For light sources with another common wavelength of \sim 1300nm, bandwidths are needed to be even wider to achieve similar axial resolutions; for instance, a 180nm bandwidth centred at 800nm would achieve a resolution on 1.6 μ m but this would drop to 4.1 μ m if the centre wavelength was 1300nm (Drexler 2004). It is important to note that these resolutions are theoretical and the dispersion of light within, as well as its scattering and absorption by, the imaged tissue all have detrimental effects.

Transverse resolution and depth of focus are dependent on an OCT instrument's imaging optics and numerical aperture size rather than light source. Altering the optics to improve transverse resolution decreases depth of focus and therefore, these two properties must be balanced in the design of OCT instruments (Drexler *et al.* 2014).

Imaging depth of various OCT instruments depends on whether they are of a TD or FD design. In TD-OCT, depth is dependent on the reference arm travel range whereas the light source centre wavelength and spectral resolution are the important factors in FD-OCT (Drexler *et al.* 2014). The properties of imaged tissues also have effects on imaging

depth. For instance, due to the melanin content of the retinal pigment epithelium having high scattering and absorption properties, many $\sim 800\text{nm}$ OCTs have poor penetration past this layer (Wolfgang Drexler and Fujimoto 2008). Along with melanin, haemoglobin content causes most biological tissues to absorb in the visible and near-infrared wavelength range (Drexler 2004). While absorption has a detrimental effect on imaging depth, the scattering properties of imaged tissues play an even greater role in affecting this property. At 800 to 1800nm wavelengths, which includes those used in OCT, increased scattering from tissue becomes the prominent limiting factor of imaging depth (Drexler 2004). Because longer wavelengths of light are scattered less, studies have shown that OCT imaging depths of one to two millimetres in most biological tissues are possible at optimal centre wavelengths ranging from 1300 to 1500nm (Drexler 2004). This is not the case for the retina where, due to water absorption from the ocular media, the ideal centre wavelengths are between 750 and 850nm or $\sim 1060\text{nm}$ (Drexler *et al.* 2014). As soft tissue is comprised of 50 to 90% water, wavelengths greater than 1800nm as well as circa 1430nm are inefficient for OCT imaging due to strong water absorption at these values (Drexler *et al.* 2014).

Specific to posterior segment imaging of the eye with OCT, light scatter due to cataract can have a detrimental effect on imaging (van Velthoven *et al.* 2006). As a means of improving image quality, Povazay *et al.* (2007) found that a device operating at a centre wavelength of 1050nm was significantly better at imaging the retina through cataract when compared to a 800nm instrument. Esmacelpour *et al.* (2010) also compared a 1060nm OCT to a commercial 800nm instrument in obtaining choroidal scans of eyes with moderate to severe cataract; the authors found that reduced signal strength occurred in 65% of 800nm images in comparison to only 10% of 1060nm scans. Although useful in eyes with cataract, it is important to note that the increased centre wavelength results in a decrease in axial resolution (Esmacelpour *et al.* 2010).

2.1.4 Recent Advances in OCT

Since the advent of FD-OCT, continued development of the technology has led to even greater utility. Namely, these have been in the form of OCT angiography (OCT-A) and whole-eye OCT. Blood flow in the eye has been measured using either doppler shift or speckle variance techniques to interpret OCT scans of vasculature (Gao *et al.* 2016). OCT-A commonly uses speckle variance as a means of imaging retinal and choroidal microvasculature (Gao *et al.* 2016); the technique relies on a series of B-Scans acquired in quick succession which are then analysed by removing the static overlap of tomographs to detect the motion of cells within blood vessels (Wang *et al.* 2007; Gao *et al.* 2016). This *in-vivo* and non-invasive method of angiography holds many advantages over traditional intravenous fluorescein and indocyanine green modalities in the assessment and management of age-related macular degeneration and diabetic retinopathy, with its primary disadvantage being the inability to measure stationary blood leakage and flow over a time course (Gao *et al.* 2016; Cicinelli *et al.* 2017).

Lately, efforts have been made to image the entire eye proceeding from the anterior chamber through to the retina and choroid. There are various methods that have been employed to carry out this whole-eye OCT imaging technique including combining two SD-OCT systems, creating customized systems by integrating three separate reference arms, and also using two separate beams of light from a single source that are orthogonally polarized (Kim *et al.* 2016; Grulkowski *et al.* 2018). Most recently, a whole-eye OCT system has been developed using swept-source illumination and a tuneable lens allowing variable focal distances to facilitate simultaneous imaging of the cornea, crystalline lens and retina (Grulkowski *et al.* 2018). While whole-eye OCT systems are, unlike OCT-A, not commercially available, their continued development will eventually supplement or replace current systems for assessing ocular biometry as well as methods of imaging the entire globe, including ultrasound, CT and MRI, which are necessary in the management of

conditions such as penetrating foreign bodies and tumours.

2.1.5 OCT Methods to be Used in This Study

This study will seek to image the crystalline lens and retina using two separate OCT systems: the Visante anterior-segment OCT (AS-OCT) (Carl Zeiss Meditec, Germany) and the Spectralis posterior-segment OCT (PS-OCT) (Heidelberg Engineering, Germany). The following subsections will outline the specifications of each instrument.

2.1.5.1 The Visante Anterior-Segment OCT

The Visante by Carl Zeiss Meditec was the first anterior segment OCT device to be made commercially available. The instrument is of the time-domain modality and uses a superluminescent diode as a light source with its wavelength centred at 1310nm. The Visante AS-OCT is capable of performing B-scans at resolutions of 18 μ m axially and 60 μ m transversely at a frequency of 2000 A-scans per second (Carl Zeiss Meditec n.d.). While the instrument has been designed to image the cornea and anterior chamber where automated segmentation and calliper tools are available for analysis, a ‘Raw Image Mode’ exists for imaging in their absence. This raw image mode has been shown to effectively capture B-scans of the crystalline lens (Richdale *et al.* 2008; Lehman *et al.* 2009; Wong *et al.* 2009; Doyle *et al.* 2013; Richdale *et al.* 2013; Chan *et al.* 2014; Kymionis *et al.* 2014). There are two options for capturing B-scans in raw image mode: low-resolution consisting of 256 A-scans with a length of 16mm and tissue depth of 6mm, and high-resolution consisting of 512 A-scans across a 10mm length with a tissue depth of 3mm (Carl Zeiss Meditec n.d.). This thesis used the Visante’s raw image modes to capture B-scans of the crystalline lens in all participants; development of custom software enabling the processing, subsequent segmentation and analysis of opacification of the instrument’s raw sensor data is described in Chapter 3. Figure 2.1.4 shows the Visante OCT.



Figure 2.1.4 The Visante AS-OCT instrument showing its height adjustable table and moveable chin and head rests.

2.1.5.2 The Spectralis Posterior-Segment OCT

A Spectralis (Heidelberg Engineering, Germany) instrument was used in this study to carry out PS-OCT imaging on all participants with DS. This instrument consists of a SD-OCT coupled with a confocal scanning laser ophthalmoscope (cSLO). The cSLO allows en-face imaging of the fundus in order to cross reference the location of captured posterior-segment tomographs. The Spectralis SD-OCT makes use of a superluminescent diode as a light source with a centre wavelength of 870nm. The Fourier-domain modality of the Spectralis allows high speed acquisition times with 40000 A-scans per second and excellent resolutions up to 3.9 μ m axially and 6 μ m laterally (Heidelberg Engineering 2013). As the light source wavelength is shorter than that of the Visante AS-OCT, the Spectralis PS-OCT is only able to obtain a scanning depth of 1.9mm in tissue. Through its TruTrack technology, the Heidelberg instrument tracks eye movement in real-time thereby avoiding motion artifact and allowing repositioning of the scan to the exact anatomical position on the retina should participants blink or move during imaging; this feature is helpful in imaging paediatric populations and those with intellectual disability. Figure 2.1.5 shows the Heidelberg Spectralis instrument.

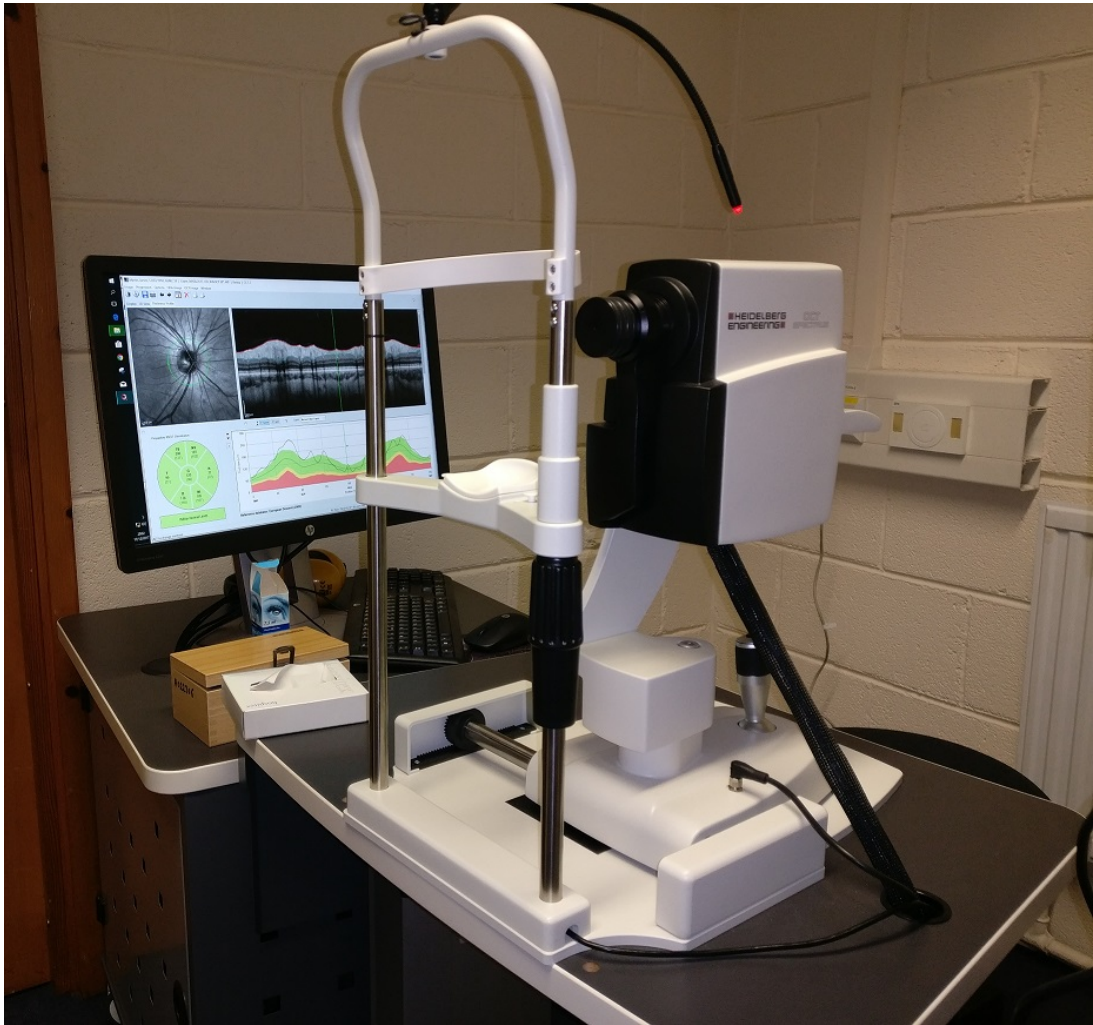


Figure 2.1.5 The Spectralis PS-OCT instrument sitting on its height adjustable table with a fixed forehead and moveable chin rest.

2.2 The Modification and Digitisation of a Slit-Lamp Photo-Biomicroscope for Imaging the Crystalline Lens

2.2.1 Introduction

Slit-lamp biomicroscopy is a pivotal tool in ophthalmic practice. A slit-lamp is an upright visible light biomicroscope with an adjustable slit-beam that can be varied for width, height, intensity, and angle of illumination to the objectives; the instrument provides three-dimensional cross-sections of the anterior eye structures and, with the use of a condensing lens, a stereoscopic view of the retina. Although recent developments in ophthalmic imaging technology such as OCT can provide important information for the treatment and management of ocular disease, slit-lamp biomicroscopy and photography are, comparatively, simple and cost-effective methods of viewing and documenting anterior segment pathology. Slit-lamp biomicroscopy is the primary technique used to diagnose and monitor cataract, including grading with the LOCS III (Chylack *et al.* 1993). In this thesis, the LOCS III method was used to grade cataract as a validation method for the development of crystalline lens opacity assessment with OCT. This required the need for a slit-lamp photo-biomicroscope capable of capturing images of high quality and resolution. While most slit-lamp biomicroscopes are well made, often consumables such as light bulbs fail and, occasionally, replacements have become obsolete rendering the instruments useless. Furthermore, replacing older analog slit-lamps that were capable of photography with modern digital versions is an expensive proposition. The following chapter discusses the modification and digitisation of an analogue Nikon FS-3 slit-lamp photo-biomicroscope (Tokyo, Japan) used for crystalline lens imaging and LOCS III grading in this study.

The Vision Science Research Laboratory at Ulster University was in possession of a Nikon FS-3 slit-lamp, which included a Nikon 35mm single lens reflex (SLR) film camera connected to a beamsplitter, xenon flashtube and flash controller, thereby facilitating

analog ophthalmic photography. Due to the high-quality optics of the slit-lamp, it was an ideal instrument for photographing the crystalline lens and performing LOCS III grading however, the xenon flashtube had failed and replacements were no longer available from the manufacturer or third parties. Successful digitisation of this slit-lamp was achieved by replacing the incandescent illumination and xenon flash sources with a single high-powered LED array, and using an Arduino microcontroller to interface with it, a new digital SLR camera and the existing slit-lamp controls/beamsplitter.

2.2.2 Methods

The existing system setup was comprised of, in brief: a beamsplitter containing a mirror connected to a solenoid in front of the right eyepiece that, when actuated, diverted 100% of the light downwards, through lens system and another mirror, to focus light onto the film of a 35mm camera mounted below the eyepieces (see figure 2.2.1). The entire process of capturing a photograph was automated by pressing a trigger on top of the joystick: the beamsplitter's solenoid-mirror momentarily actuated, the camera shutter fired, its hot shoe then triggered the flash controller, which subsequently fired the xenon flash tube for the correct exposure. This design provided high image quality to go along with the superb optics of the slit-lamp.

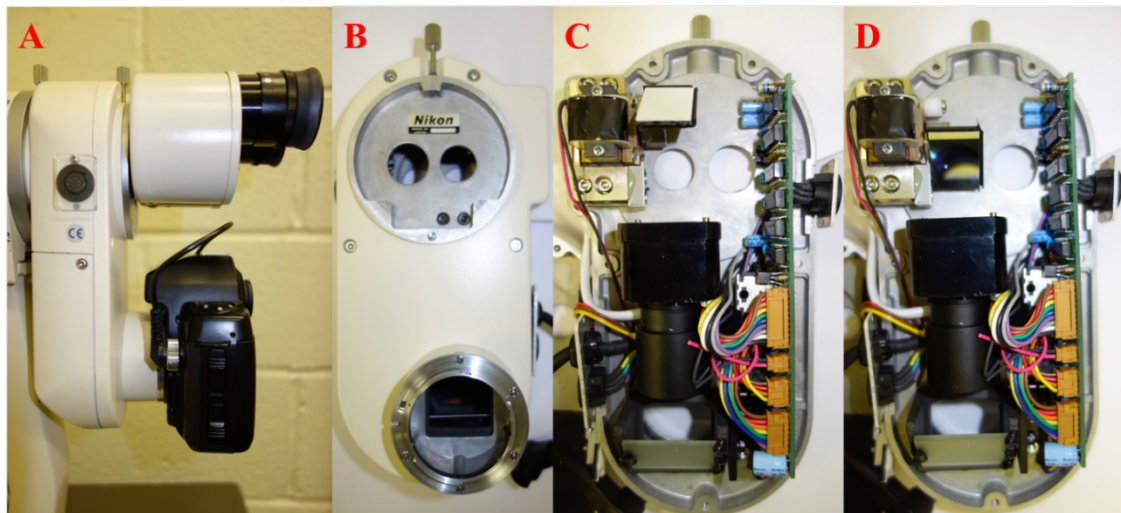


Figure 2.2.1 **A.** Beamsplitter attached to slit-lamp between objective and eyepieces with original film camera mounted. **B.** Unmounted beamsplitter attachment showing the camera mount. **C.** Inside view of the beamsplitter with solenoid/mirror (upper left-hand side) in the up position. **D.** Mirror in the down position covering the right eyepiece and diverting light through the lens/mirror system to the camera mount.

The methods to investigate and develop a digitised photographic system were undertaken in four parts. 2.2.2.1: Physical modification of the illumination system. 2.2.2.2: Selection of a microcontroller, LED driver and overall system design. 2.2.2.3: Integration of the microcontroller, digital camera and illumination system components with the slit-lamp's existing trigger and beamsplitter. 2.2.2.4: Final installation of the components.

Prior to commencement of the study, the choice of digital camera had to be considered. The mount on the FS-3 slit-lamp's beamsplitter was the same as a Nikon F-mount; thus, current Nikon digital SLR cameras fit this without any modification and a Nikon D3300 digital SLR camera was purchased for this task. The D3300 was mounted onto the beamsplitter without any issue and did not interfere with the eyepieces.

2.2.2.1 Physical modification of the illumination system

The Nikon FS-3 was designed with a dual system of illumination: a dimmable incandescent bulb for use by the practitioner, and the previously mentioned xenon flashtube that fired

for an instant when a photograph was taken. The incandescent bulb sat atop of a condensing lens that focused its element to a point at the centre of the xenon flashtube located below. This created a single compact conjugate source for both bulbs. As the flashtube was no longer available, it was decided that a high-powered LED would be used to replace both it and the incandescent bulb. The metal housing for the incandescent bulb was physically modified to allow a XLamp XHP70 LED array (Cree, Inc., Durham, USA), affixed to a fan cooled copper heatsink, to be mounted on top at the plane where the element of the incandescent bulb would have been; this allowed the optics of the slit lamp to remain unchanged (see figure 2.2.2). The fused xenon flash tube was removed from the slit lamp and the holes where it previously resided were plugged with rubber fittings.

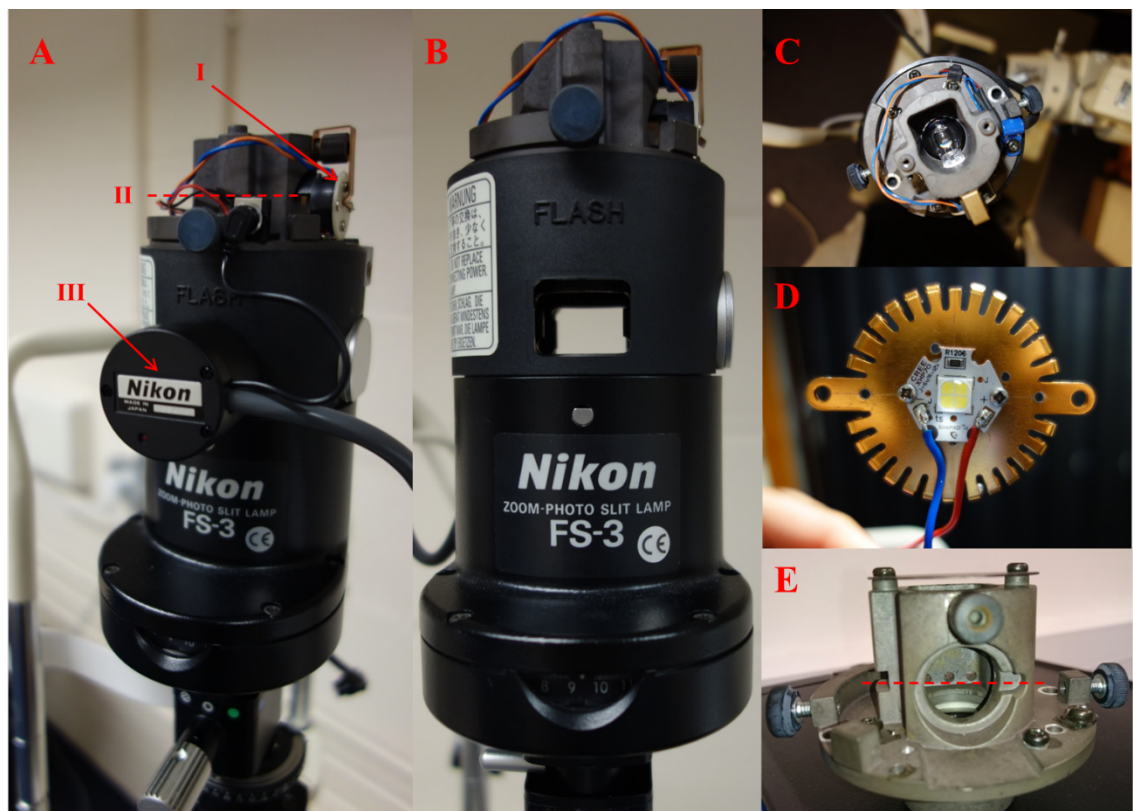


Figure 2.2.2 **A.** Illumination tower showing: (I) Incandescent bulb in its mount; (II) location where mount was cut in order to allow the LED/heatsink combination to rest in the correct location; (III) Xenon flashtube. **B.** Xenon flashtube removed showing holes that were plugged with rubber fittings. **C.** Transverse view of illumination tower showing the incandescent bulb mounted above its condensing lens. **D.** LED array mounted to the copper heatsink and fan casing. **E.** The incandescent bulb mount removed from the illumination tower. The dashed line shows where it was cut in order for the assembly in D to be mounted.

The decision to use a XHP70 LED array was made upon studying Nikon's original specifications for the FS-3 slit lamp. Nikon specified the power of the xenon flash to be 500Ws. The XHP70 was selected to be powered by a maximum of 15V DC at 2100mA. This would provide a package that was physically small enough to fit above the condensing lens while, when fired at full power for 1/60s, delivering a similar brightness to the xenon flash fired at 1/1000s through a 0.2mm optic section. Compared to the film speed of the original camera, the ISO speed of the D3300 would also be increased to exhibit similar exposure levels; this was acceptable due to the low noise generated by modern digital camera sensors. 1/60s was considered an acceptable maximum flash speed as it was felt that saccades or blink reflexes would cause minimal motion blur during photographic capture.

2.2.2.2 Selection of a microcontroller, LED driver and overall system design

An Arduino microcontroller is an open source hardware device that can be programmed using the open source *Processing* computer language. The devices are inexpensive, available in many configurations and consist of analog and digital pins that can be assigned input or output (I/O) functions. Depending on the Arduino model, the I/O pins operate at either 5V or 3.3V (common logic levels for digital devices) and then interface with other electronic components, including sensors and actuators. The Arduino runs two sets of code: an initial portion that runs once to assign variables and defines the roles of I/O pins when the device is first turned on, and a second code that runs continuously in a loop until the device is switched off. This second portion of the code comprises a collection of tasks that the Arduino is to perform. The code is written in a compiler that is freely available and then uploaded to the Arduino via USB.

An Arduino Pro Mini device operating at 5V and 16MHz was chosen to act as the main control unit for this study. This device had enough I/O pins to interface with an LED

driver optocoupler (to initiate maximum LED brightness during photograph capture and then return control to an analog potentiometer), solid state relay (acting as a failsafe and to turn the LED off during the remainder of the exposure during short flash intervals), slit-lamp joystick trigger (to initiate the process of shutter release on the camera), beamsplitter solenoid, as well as to control the D3300's remote shutter release (to start the photograph) and receive the hot shoe signal (to initiate maximum brightness of the LED, i.e. the flash). These processes are described in more detail below.

In order to power and drive the XHP70 LED at the required levels, a BuckBlock A009-D-V-2100 LED driver (LEDdynamics, Inc., Randolph, USA) and 30V 2.17A DC power supply (generic) were purchased. This combination was capable of driving the XHP70 at the maximum output during a brief flash period (maximum 1/60s) without damaging the LED or driver. As an analog method of controlling and limiting the LED's brightness to standard slit-lamp levels during normal, non-photographic use of the instrument, a 210 Ω resistor and 1k Ω linear potentiometer were connected in series with the BuckBlock's dimming circuit. An optocoupler was also wired in series with the BuckBlock's dimming circuit to be controlled by the Arduino microprocessor; this would act as a switch to initiate an open dimming circuit, causing the BuckBlock to enter a default mode of running the LED at full brightness and therefore act as the flash during photography.

In the above configuration, if the Arduino device failed, the LED would stay on at full brightness due to the design of the BuckBlock. This could potentially cause damaging levels of brightness if a patient was sitting at the slit-lamp when it occurred, and would definitely cause failure of the LED if power was not interrupted swiftly. To prevent this from happening, an AQY410EH photoMOS normally closed solid state relay (Panasonic Corp., Osaka, Japan) was wired in parallel with the dim circuit; this acted as a failsafe by shorting the BuckBlock's dimming circuit and causing the LED to turn off if the Arduino

microprocessor failed (see figure 2.2.3 for flowcharts depicting the above scenarios). This failsafe, combined with the resistor and potentiometer described above, ensured that the intensity of light emitted by the LED would be safe for exposure to the eye and adnexa. The photoMOS was also used to turn the LED off for the remainder of the exposure at shorter than 1/60s flash times, such as when photographing the eye during diffuse illumination; this method of controlling exposure eliminated the need to change shutter speeds on the D3300 camera and therefore, it could be simply left set at 1/60s. The Arduino was programmed with predefined, user selectable flash times, which are explained in more detail below and shown in figure 2.2.4.

The original FS-3 flash controller consisted of a large, heavy (approximately 9.6kg) apparatus, and this was used to receive the trigger signal from the slit-lamp's joystick, trigger the remote shutter release on the 35mm SLR camera and then fire the xenon flashtube after receiving a signal from the SLR's hot shoe. The control box also contained controls to set the flash brightness either manually or automatically. The manual brightness control consisted of 9 levels that were selected by pushing up/down buttons. In order to imitate this, the Arduino microprocessor was programmed with 9 brightness levels, each increasing the time that the LED was at maximum brightness, which could be selected using a momentary up/down toggle switch. These brightness levels allowed correct exposure at different slit widths and heights during photography. I/O pins on the Arduino were available to receive input from the switch and the device was programmed to show the flash level on a 16x2 backlit LCD display.

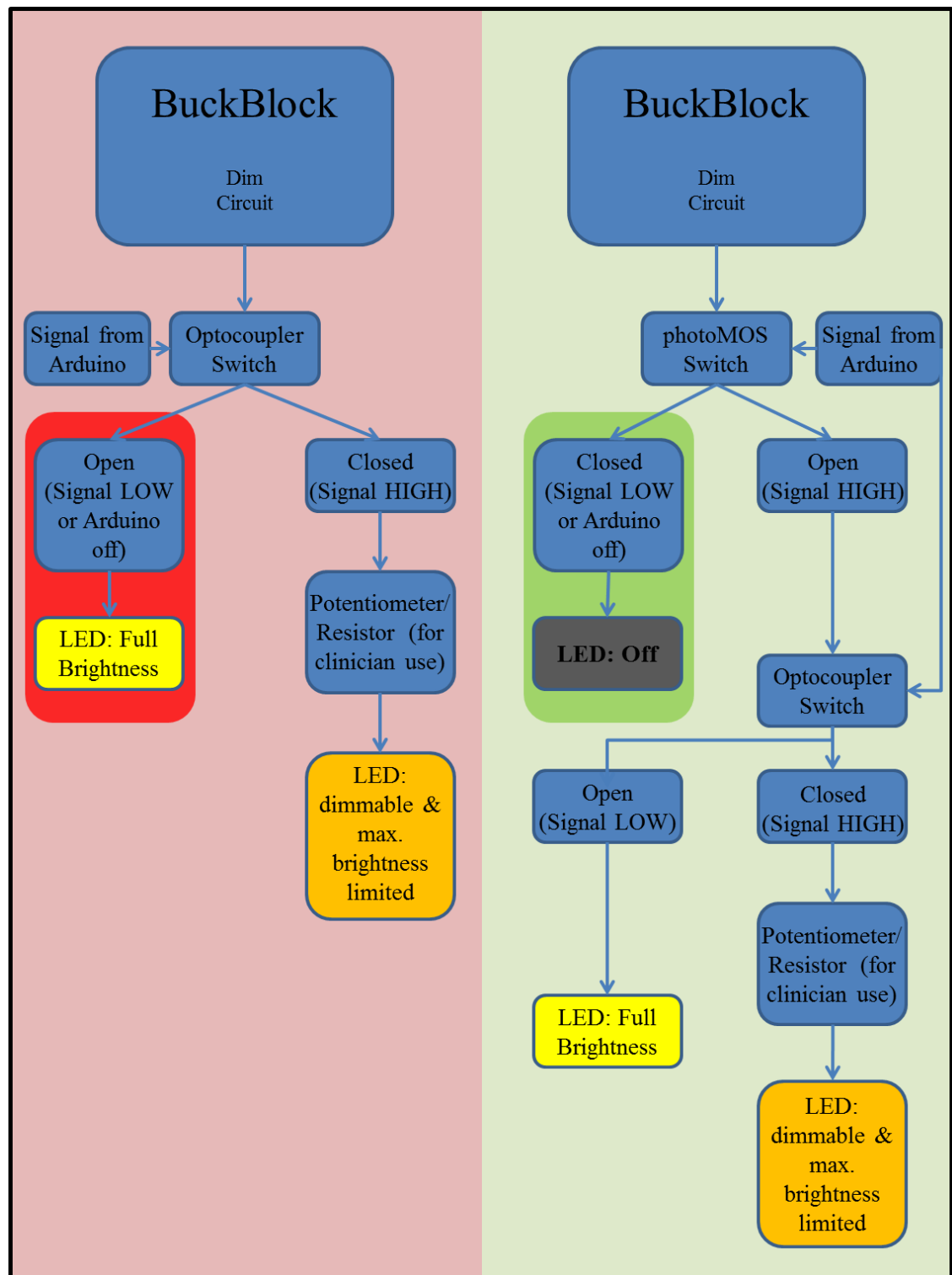


Figure 2.2.3 Flowcharts demonstrating the BuckBlock and Arduino control of the LED array's brightness. The chart on the left shows the undesired scenario where the LED defaults to full brightness if the signal is lost from the Arduino (highlighted). The chart on the right shows the failsafe and post-flash control scenario (highlighted) after the addition of a photoMOS solid state relay.

2.2.2.3 Integration of the microcontroller, digital camera and illumination system components with the slit-lamp's existing trigger and beamsplitter

In order to control the D3300's shutter with the Arduino microprocessor, a generic male 2.5mm to DC-2 shutter release cable was obtained. As the Nikon DSLR's shutter was triggered by creating a short between the focus, shutter and ground pins on the shutter release cable, an optocoupler controlled by the Arduino was used for this purpose. The corresponding shutter and focus terminals on a female 2.5mm audio connector were permanently shorted together and then connected to the ground pin through the optocoupler. When the Arduino microprocessor sent a HIGH signal to the optocoupler, the circuit would close causing the D3300's shutter to fire. The optocoupler eliminated any chance of damaging the camera's circuitry as it electrically isolated it from the Arduino. The shutter and focus pins of the shutter release cable were permanently shorted because the shutter would not activate unless both were grounded at the same time.

The existing trigger located in the joystick of the slit lamp was used to initiate the shutter release on the camera. One digital pin on the Arduino was programmed as an input with its internal pullup resistor activated, forcing its value to stay HIGH at 5V. This was then connected to a terminal on the joystick trigger while its other terminal was connected to the common ground. When the joystick trigger was pushed, this digital input pin would be grounded and its value would drop to LOW from HIGH. The Arduino microprocessor was programmed to set the output pin controlling the shutter optocoupler to HIGH when this occurred. As a result, the above-mentioned shutter release pins on the camera would be shorted, causing a photograph to be taken.

In terms of simplicity, it would have been convenient to program the LED to flash at maximum brightness by using the same signal from the slit lamp's joystick button as a trigger. Theoretically, the camera shutter and flash would fire at the same time. This was

attempted by programming the Arduino microprocessor to, upon the joystick button being pressed, change the value of its pin controlling the optocoupler on the BuckBlock's dimming circuit from HIGH to LOW for the user selected time period (causing it to enter its default mode of full brightness and creating a flash). In actuality, there was a variable delay that occurred within the camera between it receiving the signal from the remote shutter release and its subsequent opening of the shutter curtain. Consequently, in most cases, the flash fired before the photograph was taken. To rectify this situation, the camera's hot shoe was utilised to synchronise the shutter release and LED flash. A hot shoe adapter with one of its terminals connected to a pin on the Arduino and the other to the common ground was used for this purpose. The Arduino's pin was defined as a digital input with its internal pullup resistor activated. The configuration worked in a similar way to the shutter release signal from the joystick triggering the Arduino. When the camera opened its shutter curtain, it synchronised a temporary short between the central pin and ground rail of its hot shoe; this caused the value of the Arduino's hot shoe input pin to drop to LOW from HIGH. Upon this occurring, in order to create the flash, the Arduino was programmed to change the signal feeding the optocoupler on the BuckBlock's dimming circuit from HIGH to LOW for the time specified by the user selected flash brightness level.

The final step to this project was developing a method to control the solenoid-mirror fixture in the beamsplitter. The mirror was required to, in a synchronised fashion, divert incident light to the camera before a photograph was taken and then return to its original position in order to restore the view through the slit-lamp's right eyepiece. It was determined that 10V DC was adequate to activate the solenoid. In order to control the polarity so that the solenoid could be moved down and then back up, an H-bridge integrated circuit was utilised. The H-bridge was digitally controlled with two of the Arduino's output pins. Upon receiving the trigger signal from the slit-lamp's joystick

button, the Arduino was programmed to move the solenoid to the down position and then delay for 500ms before firing the camera's shutter. This delay allowed any vibration of the mirror to dissipate before the photograph was captured. Another delay for 500ms was initiated before the Arduino instructed the H-Bridge to move the solenoid back to the up position (see figure 2.2.4 for a flowchart depicting the Arduino's process of controlling the system).

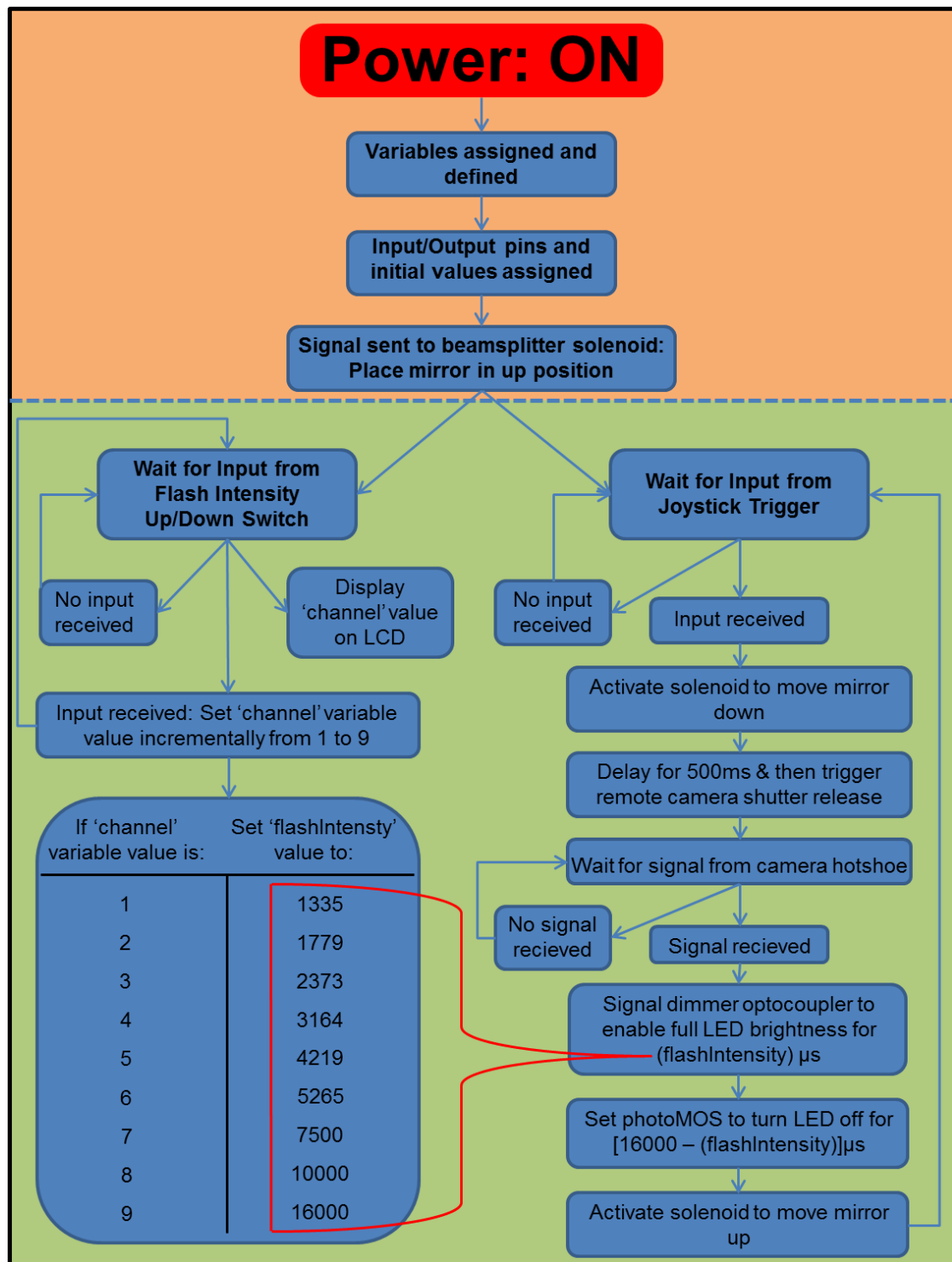


Figure 2.2.4 A flowchart depicting how the Arduino was programmed to run the system. The shaded top portion (demarcated by the dashed line) runs only once when the Arduino is turned on and the bottom shaded portion runs in a continuous loop until the Arduino is turned off.

2.2.2.4 Final installation of the components

Due to their compact sizes, the BuckBlock, flash intensity adjustment switch, 16x2 backlit LCD display and Arduino, with associated circuitry, were able to be installed under the slit-lamp table in the original incandescent bulb's power supply housing. The 30V DC 2.17A power supply was mounted to the slit-lamp table and connected to the original switch of the power supply unit. This power supply was sufficient enough to provide electricity to the LED, heat sink fan, beamsplitter solenoid and Arduino microprocessor. Connections were made from the power switch directly to the BuckBlock and to voltage regulators for the Arduino, H-Bridge and heatsink fan. The values of these voltage regulators were 6V, 10V and 12V respectively. The Arduino, H-Bridge, optocouplers, LCD display, flash intensity switch, various resistors, capacitors and voltage regulators were all soldered in the appropriate configuration to a stripboard. Removable connections were made between the stripboard and camera shutter release cable, hot shoe adapter, slit-lamp joystick trigger and BuckBlock dim circuit. Wires for the dim circuit potentiometer, LED, heatsink fan, shutter release cable, hot shoe cable, joystick trigger and beamsplitter solenoid were all run from the new control box, through the base of the slit-lamp and exited out of the existing slit-lamp ports. The potentiometer was mounted in the slit-lamp's original rheostat location and the voltage regulator for the heat sink fan was soldered to a small piece of stripboard and mounted to the top of the illumination system cover. Detachable connections were then made to the heat sink fan, and holes were drilled into the illumination housing cover to increase ventilation. The LED wire was connected with detachable connections to the BuckBlock LED circuit and XHP70 LED array. Finally, the new control box was mounted in its original position under slit-lamp table. Figure 2.2.5 gives a visual depiction of the above installation while figure 2.2.6 provides an electrical schematic for the entire design. The source code for the Arduino is provided in appendix A-1.

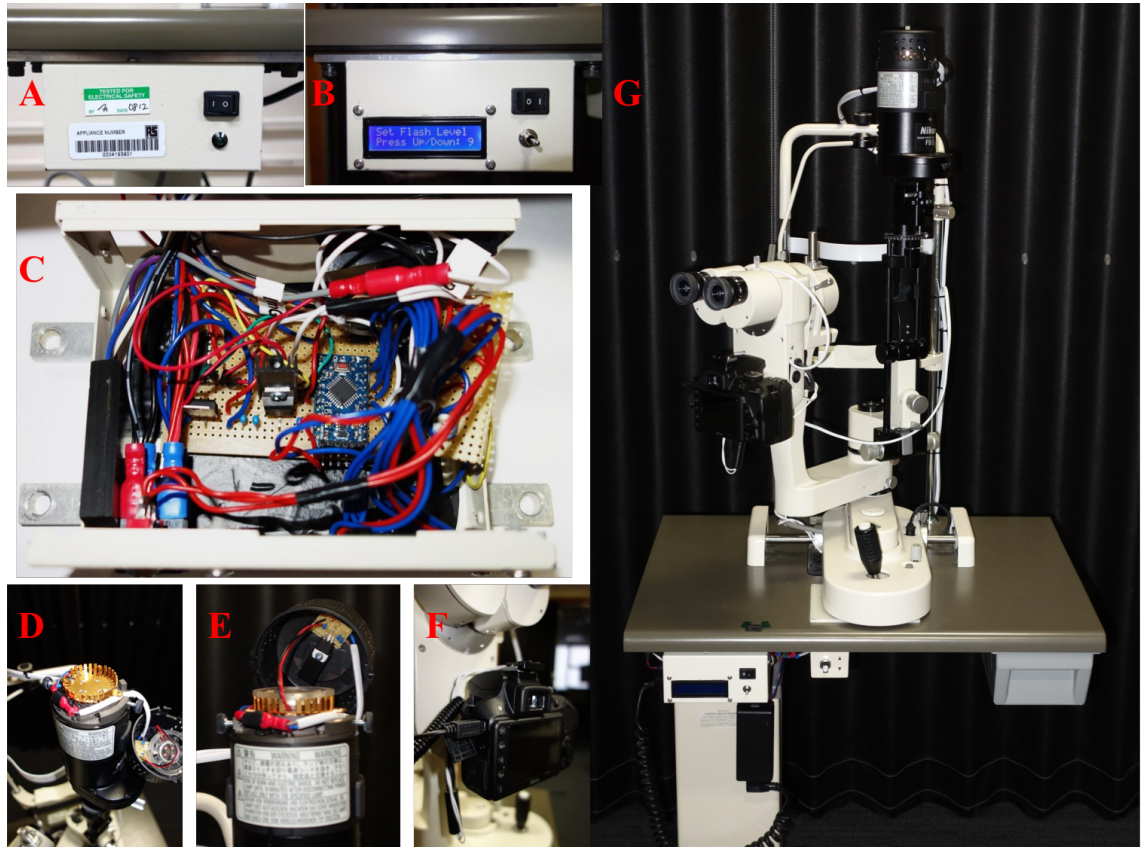
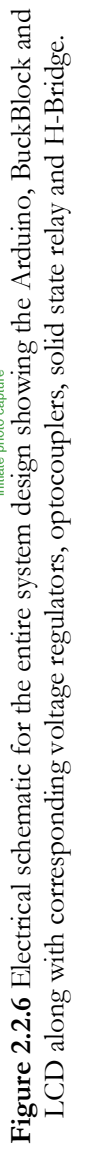


Figure 2.2.5 **A.** The original power supply housing for the incandescent bulb. **B.** The modified power supply housing with the 16x2 LCD display and the flash intensity up/down switch mounted below the power switch. **C.** The interior of the housing showing the BuckBlock LED driver (bottom left), DC power supply connections to the power switch (to the right of the BuckBlock) and Arduino with associated circuitry soldered to a stripboard. **D.** The LED/fan housing mounted to the modified bulb housing. **E.** The fan mounted to the LED/housing and its voltage regulator mounted to the illumination cover. **F.** The D3300 digital camera mounted to the beamsplitter with the hot shoe adapter and shutter release cable connected. **G.** The entire modified system showing all integrated wiring and the AC to DC power supply mounted below the Arduino/BuckBlock housing.



2.2.3 Results and Discussion

The modified photographic slit-lamp has been running for approximately two years, captured over 5000 photographs without failure and can be used with the same ease and fluency as its original analog state. The D3300 camera provides high resolution photographs (figure 2.2.7) and is also able to record high definition video. Furthermore, its HDMI out connection can be connected to an external display to show a live image. While this slit-lamp was modified strictly for photography, the beamsplitter's solenoid-mirror was manually moved into the down position to verify these video capabilities. A permanent fix for video capture would be to connect an additional switch to the Arduino and add the appropriate code that would, upon it being pressed, lower the solenoid to allow video capture; the button would be pressed again to re-raise the solenoid.

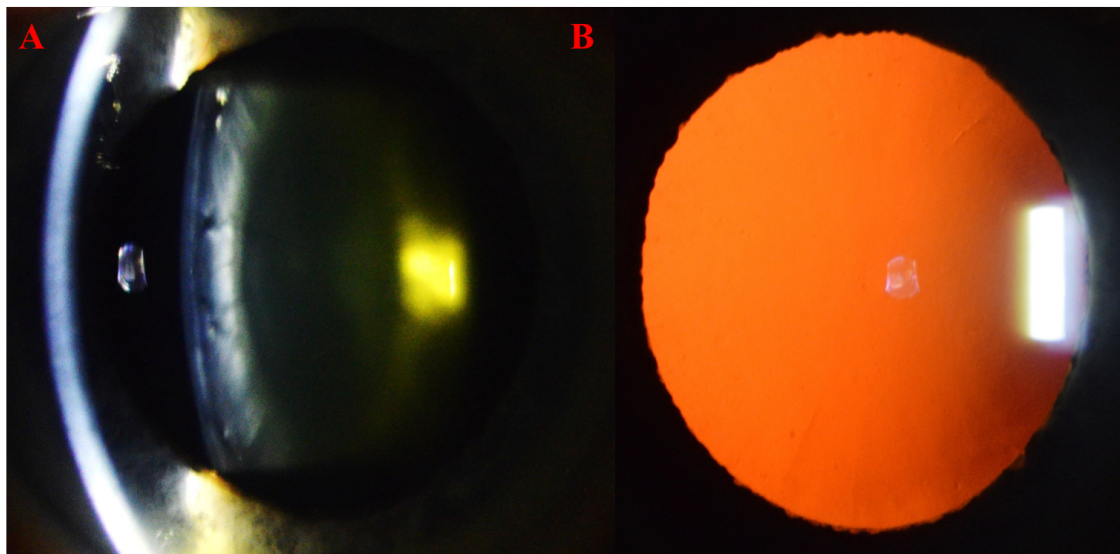


Figure 2.2.7 Photographs of (A) an optic section and (B) retroillumination of the anterior crystalline lens taken with the modified slit lamp

There are significant possibilities to customise the set-up described in this Chapter. Instead of the Pro Mini, Arduino microprocessors with an increased number of I/O pins can be used to add more functions to the slit-lamp system. For instance, Krohn & Kjersem (2012; 2013) described a method of photographing intraocular tumours with an

expensive Haag-Streit slit lamp; an additional LED could be added to the system described in this chapter to perform the same function.

As the use of an Arduino microprocessor allows all of the existing slit-lamp electronics to be bypassed, the methods that were used to modify this Nikon slit lamp can be easily adapted to microscopes produced by other manufacturers. Making things even simpler, slit-lamps that use optical beamsplitters for their camera attachments do not require the use of an H-Bridge and additional source code to control the mirror-solenoid combination. Depending on their design, this system can be added to slit-lamps that do not have photographic attachments. Additionally, as the method of remote shutter release and hot shoe control is fairly standardised across the photographic industry, the same principles described in this paper should be able to be applied to non-Nikon digital cameras. It should also be noted that as the Nikon D3300 used in this project contains an APS-C sized sensor, the photographs are taken with a 1.5X crop factor compared to the original 35mm film camera. This can be avoided by using a digital camera with a full frame sensor in place of the D3300.

The primary purpose of this project was to digitise a high-quality analog photographic slit-lamp system for which replacement parts had become unavailable and that was required by the researcher for LOCS III grading. While this was achieved, the methods described above will be useful for other research laboratories and clinical settings to upgrade and utilise effectively obsolete instrumentation at a low cost; the entire spend for this project came in at under £450. The modifications described in this chapter can easily be replicated, customised and adapted by those with a basic knowledge of computer programming and electronics.

Chapter 3: Assessment of Lens Opacity and Cataract using OCT

3.1 Introduction

As mentioned in Chapter 1, there are a lack of grading systems available to assess the severity and morphology of lens opacities and cataract that are not of the age-related type. Furthermore, the slit-lamp based systems that are most commonly used, such as LOCS III, are subjective and susceptible to variations in microscope settings. This study sought to develop a method to objectively measure lens opacity and cataract using anterior segment OCT with the Visante AS-OCT (Carl Zeiss Meditec, Germany). This chapter outlines the *in-vivo* imaging and analysis of crystalline lenses from a group of adults for opacification using AS-OCT and makes a comparison to LOCS III grading. To investigate functional correlates of media opacities, measures of visual function were also evaluated including habitual visual acuity, contrast sensitivity and retinal straylight. The following sections will outline the recruitment, data collection and analysis for these measures.

3.2 Sample Size Determination and Recruitment

3.2.1 Sample Size

This study sought to recruit 90 typically developed adult participants aged 50 years and higher, both with and without cataract. Participants were stratified by age providing a broad cross-section of natural age-related lens opacification. The stratified age ranges were:

- 30 Participants aged 50-60 years
- 30 Participants aged 60-70 years
- 30 Participants aged 70 years and older.

3.2.2 Recruitment

Three avenues were taken to recruit participants for this study. Participants were primarily recruited from the Ulster University Optometry Clinic and through emails circulated University-wide to staff and students. Other participants were recruited from the local community via retirement organisations (including the University of the 3rd age (U3A), and through word-of-mouth from participants to their families and friends.

Eligible clinic patients were approached after attending for their routine eye examinations about participation in the study. They were given Participant Information Sheets (PIS) (see appendix A-2) outlining the study and time to consider participating. If they decided to participate, an appointment was scheduled after a short series of screening questions were asked to ensure eligibility criteria were met. Emails sent to university staff and students were approved by the Faculty of Life and Health Sciences and then distributed to staff- and student-wide email lists by Information Technology Services. Those who responded were provided with the PIS and questioned as to whether they met eligibility criteria. The initial questioning to confirm eligibility consisted of open ended questions querying the presence of any eye disease or a history of any medical treatment or surgery to the eyes; appointments were made if appropriate. PIS forms were also distributed to members via a confidential email list of the Causeway U3A and interested participants were screened and scheduled as described above.

3.3. Ethical Approval

Ethical approval was received from the Ulster University Research Ethics Committee (UUREC) prior to the start of the study. Research was carried out in accordance with the Declaration of Helsinki.

3.4 Methods

The following procedures and assessments were conducted at the Vision Science Research Laboratory, Ulster University. Participants were seen on one occasion for approximately one hour. Upon attendance, participants were asked to complete and sign a consent form (See Appendix A-2), which was also signed by the researcher. The study was carried out on both eyes of the participant unless they specifically requested only one eye to be assessed, or if an eye did not meet inclusion criteria such as the presence of a heterotropia, corneal opacity or coloboma.

3.4.1 Ophthalmic and Systemic History

A brief review of participants' prior ophthalmic and systemic histories was undertaken to ensure that they met inclusion criteria and that there was no increased risk to pharmacologic pupil dilation. Participants were questioned on past ocular pathology, medical and surgical treatment, and spectacle wear. Questions were also asked about systemic health, medications and allergies including any past adverse reactions to eye drops. Exclusion criteria included narrow anterior chamber angles or glaucoma, the presence of corneal or lenticular pathology (apart from cataract) that would affect imaging, and pseudophakia or aphakia.

3.4.2 Anterior Chamber Angle and Intraocular Pressure Assessment

As participants' pupils were to be dilated with tropicamide 1% to enable crystalline lens imaging, the appropriate clinical checks were made prior to instillation. These included Van Herick angle assessment and intraocular pressure (IOP) measurement.

3.4.2.1 Van Herick Angle Assessment

There is an increased risk of pharmacologic pupil dilation causing acute angle closure glaucoma in those with physiologically narrow angles. Thus, the anterior chamber angle

was evaluated, using the Van Herick technique, prior to the installation of tropicamide 1%. Participants were seated at a slit-lamp biomicroscope. The slit width was set to an optic section, and the illumination was angled at 60 degrees temporal to the objective lenses for temporal angle measurement, and nasally for nasal angle measurement. Additionally, for nasal angle measurement, the entire objective and illumination system was rotated temporally by approximately 45 degrees and participants were asked to fixate between the objective lenses to enable an optic section of the cornea at the limbus. For temporal angle measurement, participants were asked to fixate straight ahead at the researcher's ear and the corneal optic section was focused at the limbus. The Van Herick technique estimates anterior chamber angle depth by comparing the width of the shadow between the posterior cornea and iris to the width of the corneal optic section at the limbus. Those with a grade 1 angle or less (width of shadow less than $\frac{1}{4}$ of cornea) were excluded from the study. After the Van Herick assessment, participants' anterior eyes were examined with the slit-lamp to ensure no contraindications to pupil dilation as well as to examine the cornea and lens for any pathology that would warrant exclusion from the study.

3.4.2.2 Intraocular Pressure Measurement

Again, to mitigate the risk of acute angle closure, pre- and one-hour-post-dilation IOPs were measured in each participant. Either a Pulsair (Keeler Ltd., U.K.) or ICare (Icare, Finland) tonometer were used for this purpose. Participants were asked to fixate on a target straight ahead and either three (Pulsair) or five (Icare) readings were taken of each eye as per manufacturer requirements to obtain accurate IOP measurements. A sharp rise in IOP after pupil dilation would indicate angle closure and require medical treatment. Participants were given an information sheet outlining the signs and symptoms of angle closure with instructions on the appropriate course of action to be taken should it occur after their appointment.

3.4.3 Visual Acuity

Distance visual acuity (VA) was measured monocularly with participants' habitual correction in place. A logMAR visual acuity chart was used in opposition to traditional Snellen notation due to its ability to provide per letter scoring, constant logarithmic progression of letter size per line and equal number of optotypes per row (Bailey and Lovie-Kitchin 2013). This system of measuring VA has been widely used across research and clinical trials due to its reliability and accuracy (Lovie-Kitchin 1989; Ferris and Bailey 1996; Bailey and Lovie-Kitchin 2013).

VA was measured under normal room illumination using a Bailey-Lovie logMAR chart (University of California, USA). Participants were seated 3m from the chart and asked to read from the top line downwards until they could no longer read any letter on a line correctly; participants were also asked to guess at the letters on the line below this to ensure the limit of their VA was met. When both eyes were included in the study, participants' right eyes were always measured first. VA was calculated using by-letter scoring. A value of 0.02 log units was used for each letter read correctly and then a 0.3 log unit correction factor was added to the final VA to account for the 3m chart distance. Participants were asked to read lines backwards or out of order if memorisation of the letters was suspected. Participants wore their habitual spectacle prescription and were questioned about the adequacy/age of correction. In the rare case that the researcher was not confident that the participant was wearing an up to date spectacle prescription, a pinhole test was carried out to ensure no drastic improvement in VA.

3.4.4 Contrast Sensitivity

To provide a further measure of participants' functional vision, their contrast sensitivity (CS) was assessed. Low spatial frequency CS has been shown to be largely unrelated to high spatial frequency VA, and often represents more of a real-world measurement of

visual function; it is considered to be a useful test in those symptomatically affected by cataract but who still achieve normal levels of VA (Elliott 1993; Richman *et al.* 2013).

A Pelli-Robson chart was used to assess monocular CS in participants. Assessment was carried out at a 1m distance, under adequate illumination of 60 – 120 cd/m² and ensuring no specular reflection from the chart (Elliott 2007). Participants were asked to read the chart from the top down as far they could while occluding their fellow eye; in cases where both eyes were included in the study, the right eye was always measures first. When the participant met their threshold, the next triplet of letters were pointed out and they were given 20 seconds to ensure nothing more could be seen. A log value of 0.15 was awarded for each triplet where two letters were read correctly while ignoring the first triplet (as it has a value of 0.00 log units).

3.4.5 C-Quant Retinal Straylight Assessment

The Commission Internationale de l'Eclairage includes retinal straylight as a significant contributor in the definition of disability glare (Van den Berg *et al.* 2013). Retinal straylight is intraocular light scattering caused by the ocular media that results in a veiling luminance on the retina; this forward scatter reduces image contrast (Mainster and Turner 2012). Various studies have demonstrated that retinal straylight increases with age and also due to cataract (Van Den Berg *et al.* 2007; Van Der Meulen *et al.* 2012; Michael *et al.* 2009; Van den Berg *et al.* 2013). Straylight measures have been shown to be unrelated to visual acuity (Van Den Berg *et al.* 2007; Van Der Meulen *et al.* 2012). In a study of 2422 people, retinal straylight was found to be more strongly related to LOCS III score than either contrast sensitivity or visual acuity (Michael *et al.* 2009).

Retinal straylight was measured in participants using a C-Quant Straylight Meter (Oculus GmbH, Germany). The C-Quant measures retinal straylight using the psychophysical

method of compensation comparison, which was first described in 2003 (Franssen *et al.* 2006; Van den Berg *et al.* 2013). The instrument implements an annulus as a straylight source with an average angular value of 7 degrees, surrounding a central dark test field consisting of a circle divided vertically into two halves (see figure 3.4.1). A flickering of the annulus will cause forward scatter and subsequent veiling luminance onto the retinal image of the central target. Over a series of approximately 20 short duration trials, the randomly selected right or left test field is flickered with additional compensation light and exactly out of phase with the straylight source. The test field without compensation will be seen by the observer to be flickering in phase with the straylight source during the test. By adjusting the compensation light added to the randomly chosen test field, it can appear to stop flickering or flicker less. The C-Quant utilizes a two-alternative forced choice method where the participant must choose which test field appears to be flickering more strongly. As a result, a straylight parameter known as $\log(s)$ can be calculated. Two reliability measures are also calculated: the standard deviation of $\log(s)$ known as E_{sd} and a quality factor known as Q ; $\log(s)$ is considered to be reliable when $E_{sd} < 0.08$ and $Q > 1$.

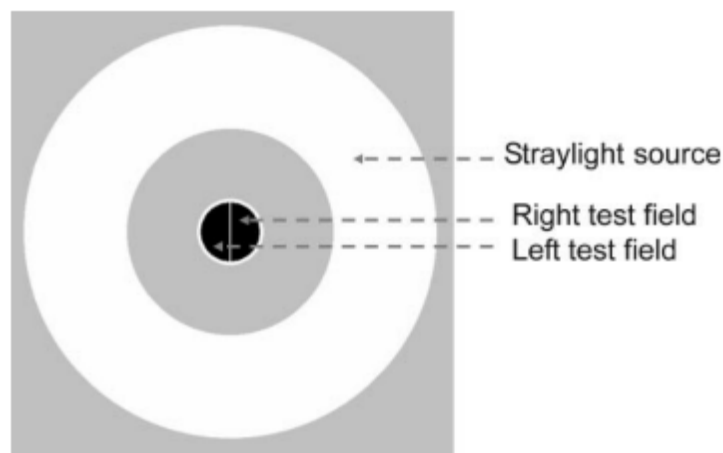


Figure 3.4.1 Image of the stimulus used by the C-Quant showing the straylight source and central test fields. Image taken from Franssen *et al.* (2006)

The C-Quant apparatus sits on a desktop and consists of a tube-like body with an eyepiece. The base of the instrument contains two buttons situated on the left- and right-hand sides, that participants push to select which test field they observe to be flickering more strongly. The instrument is connected to a computer that runs the stimulus control and analysis software.

The test was conducted monocularly using an eyepatch to occlude the eye not being assessed. Again, if both eyes were included in the study the right eye was measured first. The default range setting of E was used in all participants. To start, the participant was seated in front of the instrument and asked to place their eye close to the eyepiece but not firmly against it. They were instructed to fixate only on the central test fields and ignore the outside flickering ring. Participants were then told that a short series of flickering lights would be presented, and to use their first impulse to select which test field they observed to be flickering more strongly by pressing the corresponding button on the base of the instrument in a two-alternative forced choice paradigm. They were informed that it was normal for the determination to become very difficult and to use intuition to decide when this occurred. If the value of log (s) was determined not to be reliable based upon the Esd and Q metrics, the participant was given another chance to complete the test after increasing the range setting of the instrument to the highest level of F.

3.4.6 Crystalline Lens Slit-lamp Imaging and LOCS III Grading

After the above standard optometric and straylight measurements were completed, participants' pupils were dilated with tropicamide 1%. To ensure maximum pupil dilation, a period of at least 20 minutes elapsed before imaging was carried out. The modified Nikon FS-3 slit-lamp described in Chapter 2 was used to image nuclear, cortical and posterior subcapsular opacities in all participants. The following camera and slit-lamp settings were used for all images:

1. Camera Settings:

- a. ISO sensitivity: 6400
- b. Flash Intensity: Level #9 (1/60s of LED at full brightness)
- c. Shutter Speed: 1/60s

2. Slit-Lamp Settings:

- a. For imaging the Nucleus:
 - i. Slit width: 0.2mm
 - ii. Slit height: Extended over pupillary margins
 - iii. Angle of illumination: Exactly 45 degrees to objective lenses
 - iv. Filter: None
- b. For Imaging Cortical and PSC opacities:
 - i. Slit width: Variable, usually between 3-5mm
 - ii. Slit height: Variable – enough to provide adequate retroillumination
 - iii. Angle of illumination: 3-5 degrees to objective lenses
 - iv. Filter: None

As indicated by the above settings, optic sections of the lens focused at the nucleus centre were captured for nuclear grading and retroillumination images were captured for grading cortical and PSC opacities. The slit-lamp was focused at the planes of the pupil and posterior capsule for retroillumination images.

During imaging, the participant was seated at the slit-lamp with their chin and forehead placed against their respective rests. The chin rest was adjusted vertically to align the participant's lateral canthus against the corresponding marker on the slit-lamp. The participant was asked to fixate straight ahead just past the researcher's ear, and told they would experience very brief flashes of light as the photographs were taken. The optic section and retroillumination images of the crystalline lenses were then captured. All

images were captured with the room lights switched off. Multiple images were captured for each eye and the best quality image was then used for grading.

LOCS III grading of all captured images was conducted at a single computer terminal with constant monitor settings for brightness, contrast and colour. A transparency of the standard LOCS III images was illuminated with a lightbox; any areas of the light box that were not covered by the transparency were masked off to prevent light leakage. The lightbox was placed beside the computer monitor, and for every photographed eye, grades were assigned for each measure of opacity in accordance with the LOCS III instructions (Chylack *et al.* 1993).

Images were first graded for nuclear opalescence (NO) and nuclear colour (NC) by opening the nuclear optic section images on the computer workstation and making direct comparisons to the six standard LOCS III images. A grade between 0.1 (representing complete nuclear transparency) and 6.9 was assigned for each of NO and NC. Care was taken to grade NO based strictly by examining the hazy quality of the nucleus without respect to its brunescence. For NC evaluation, the haziness of the nucleus was ignored and a grade was assigned based upon the brunescence reflected off of the posterior capsule.

The retroillumination photographs were used to analyse cortical (C) opacification. Again, these images were viewed on the computer workstation and grades were obtained by making a direct comparison to the set of standard LOCS III C images at the lightbox. As per instructions, the researcher considered all areas of opacification solely as an aggregate to determine a value for P ranging from 0.1 to 5.9.

For grading PSC opacities, only the retroillumination photographs that were captured with the slit-lamp focused at the posterior plane of the capsule were used. In the same manner as above, grades ranging from 0.1 to 5.9 were assigned based upon direct comparison of the photograph to the P set of standard LOCS III images illuminated by the lightbox. Once more, care was taken to grade P by considering all areas of opacification as an aggregate. As per the LOCS III instructions, the opacity was only considered to be a true PSC if it extended into the central 3mm of the pupil.

3.4.7 Visante Anterior Segment Imaging

Directly after slit-lamp imaging, AS-OCT scans of participants' crystalline lenses were captured using the Visante instrument. Participants were asked to sit at the instrument with their chin placed on the chin rest and forehead placed against the forehead rest. They were then instructed to look at the centre of the instrument's internal fixation target. Using the video monitor and chin/forehead rest controls of the Visante, the participant's eye was aligned to perform a scan through the centre of the cornea/crystalline lens. The presence of the corneal reflex, which is an optical artifact that causes a vertical line to appear through the image, was visualised to ensure central alignment (Zeiss Visante User Manual [no date]). As this corneal reflex would make analysis of image opacification difficult, attempts were always made to save images just as it disappeared. B-scans across the 90-degree axis of the lenses were taken to mimic that of the slit-lamp optic section used during lens slit-lamp photography however, if sufficient quality scans were not attainable due to the participants' eyelids or other factors, 180-degree B-scans were taken instead. If there was the presence of non-nuclear cataract, the alignment of B-scans was adjusted to image through these opacities. Attempts were made to acquire both high- and low-resolution scans using the Raw Image mode of the Visante. As previously mentioned, because the high-resolution mode consists of 512 A-scans but with only a 3mm imaging depth, separate images of the anterior and posterior half of the lens were taken.

3.4.7.1 Processing and Analysis of Visante Images

Raw detector data were exported for all scans using the Visante Image Exporter software (Carl Zeiss Meditec, Germany). This sensor data was then processed, segmented and analysed for opacity with MATLAB (MathWorks Inc., USA) using customised, bespoke software. These processes are outlined below.

3.4.7.1.1 Image Processing of Visante Raw Sensor Data

Although Carl Zeiss Meditec do not provide information about the format or encoding properties of the raw files, scans were successfully opened after a period of trial and error by the author. An estimation of the encoding was determined from the high-resolution raw file sizes of 1mb, meaning they contained 8388608 bits of information. Knowing that the maximum resolution of the Visante was 512 A-scans, the vertical resolution of the detector was assumed to also be 512 pixels in size. Therefore, the total number of pixels was assumed to be 262144 (512 x 512). Dividing 8388608 by 262144 results in 32, which suggests the bit depth of the detector. The raw data was then successfully read into MATLAB in the form of a 512 x 512 matrix with 32-bit signed integer precision. To convert the images to the original aspect ratio used by the Visante, the matrix was then resized to 512x1280 resolution using the `imresize()` function and bicubic interpolation as described by Kao *et al.* (2011). The resized matrix was subsequently converted to a grayscale intensity image using the `mat2gray` function. See Figure 3.4.2 to see the original and resized images.

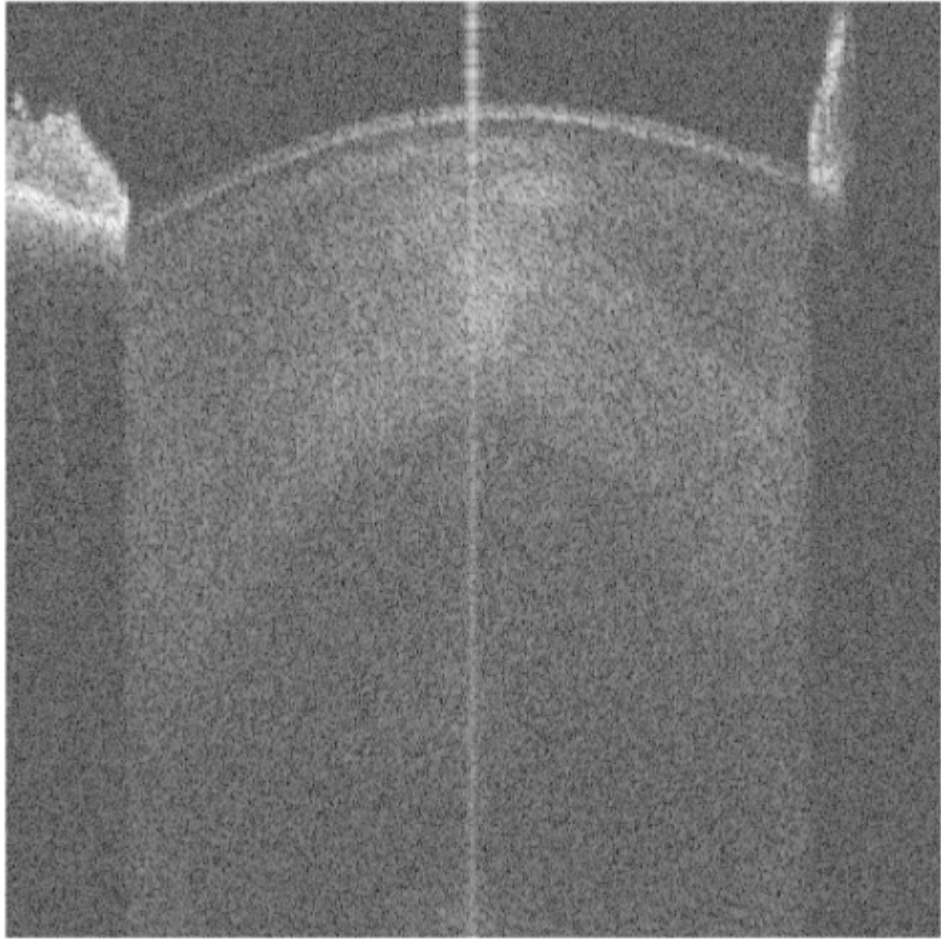
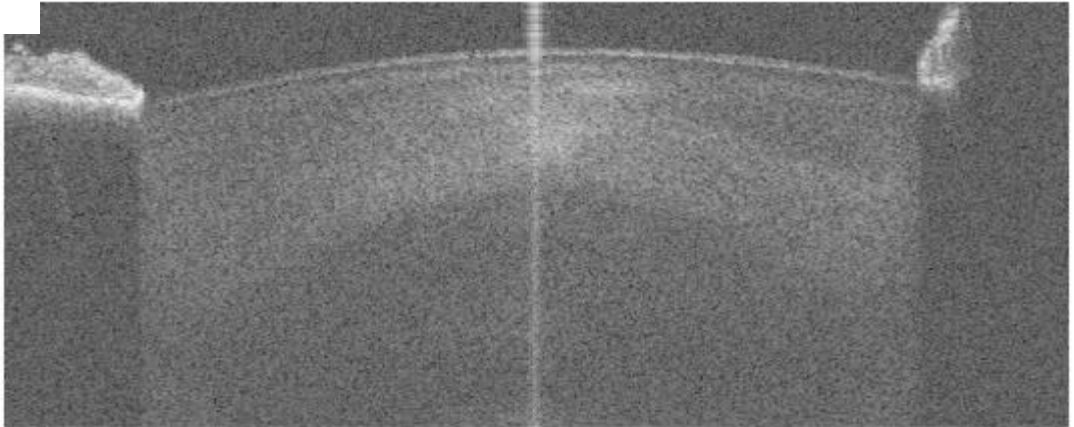
A**B**

Figure 3.4.2 Demonstration of the resizing of the processed original 512 x 512 raw detector data (A) to the 512 x 1280 aspect ratio (B). The vertical line through the centre of the images is the 'corneal' reflex.

The newly formed grayscale images were processed to increase contrast, which facilitated manual segmentation. The limits of contrast of each image were determined using the `stretchlim()` function. The `imadjust()` function was used in conjunction with these limits of contrast to map the intensity values to the final version of the image that was to be manually segmented and graded for cataract. Figure 3.4.3 demonstrates this process.

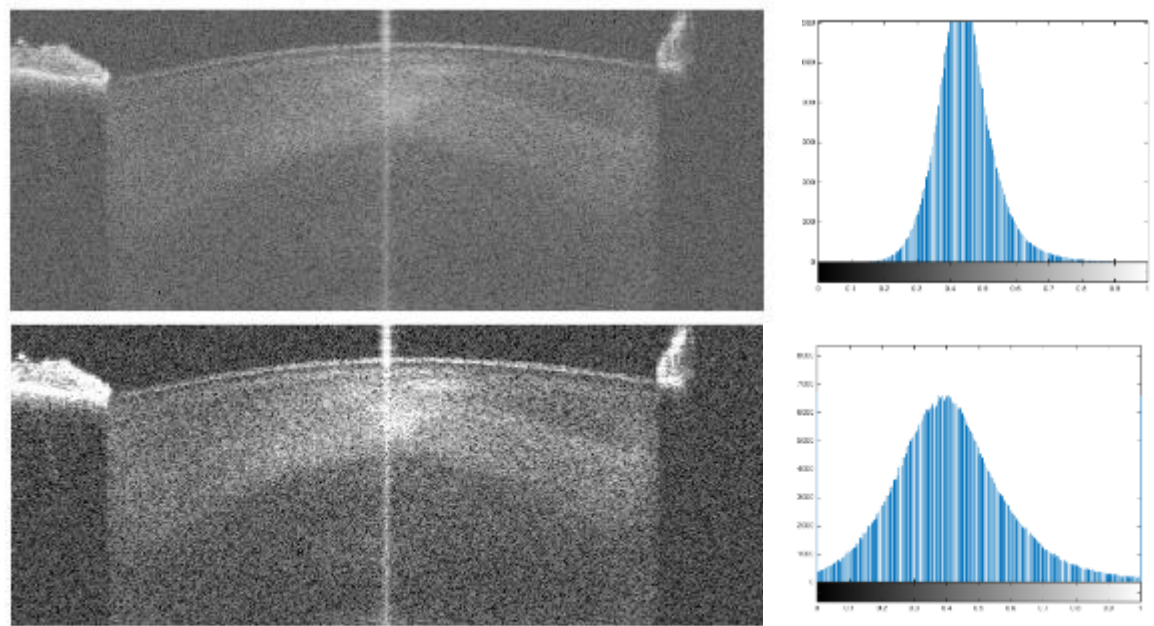


Figure 3.4.3 Demonstration of contrast adjustment of the processed images. The top image represents the unadjusted state, and the bottom image shows the change after applying the `imadjust()` function with the limits of contrast as a constraint. Histograms showing the pixel distributions are displayed to the right of each image.

3.4.7.1.2 Segmentation and Grading of Processed Visante Images

Once the image had been processed as above, the software displayed it using the `imshow()` function in order for manual segmentation to be carried out. The `impoly()` function was used so that the area to be graded, such as the nucleus or cortical opacity, could be manually outlined by the researcher; to do this, the mouse was used to control the cursor and click points along the border of the area to be graded. By connecting the first and last points, a region of interest (ROI) object was created. The `createmask()` function was then used on the ROI object to define a binary mask of the area of the lens to be graded. The

binary mask object was of a logical class so zero values in areas outside of the ROI would not influence measurements taken inside of it. The mean pixel intensity (PI) of the selected ROI was calculated by using the `mean()` function after finding the product of the grayscale image and binary mask. As each pixel represents an intensity, the mean PI provides a measure of overall opacification in the region of interest. The value of pixels range between zero and one, with zero representing black (or zero intensity) and one representing white (or maximum intensity). Figure 3.4.4 demonstrates the masking process.

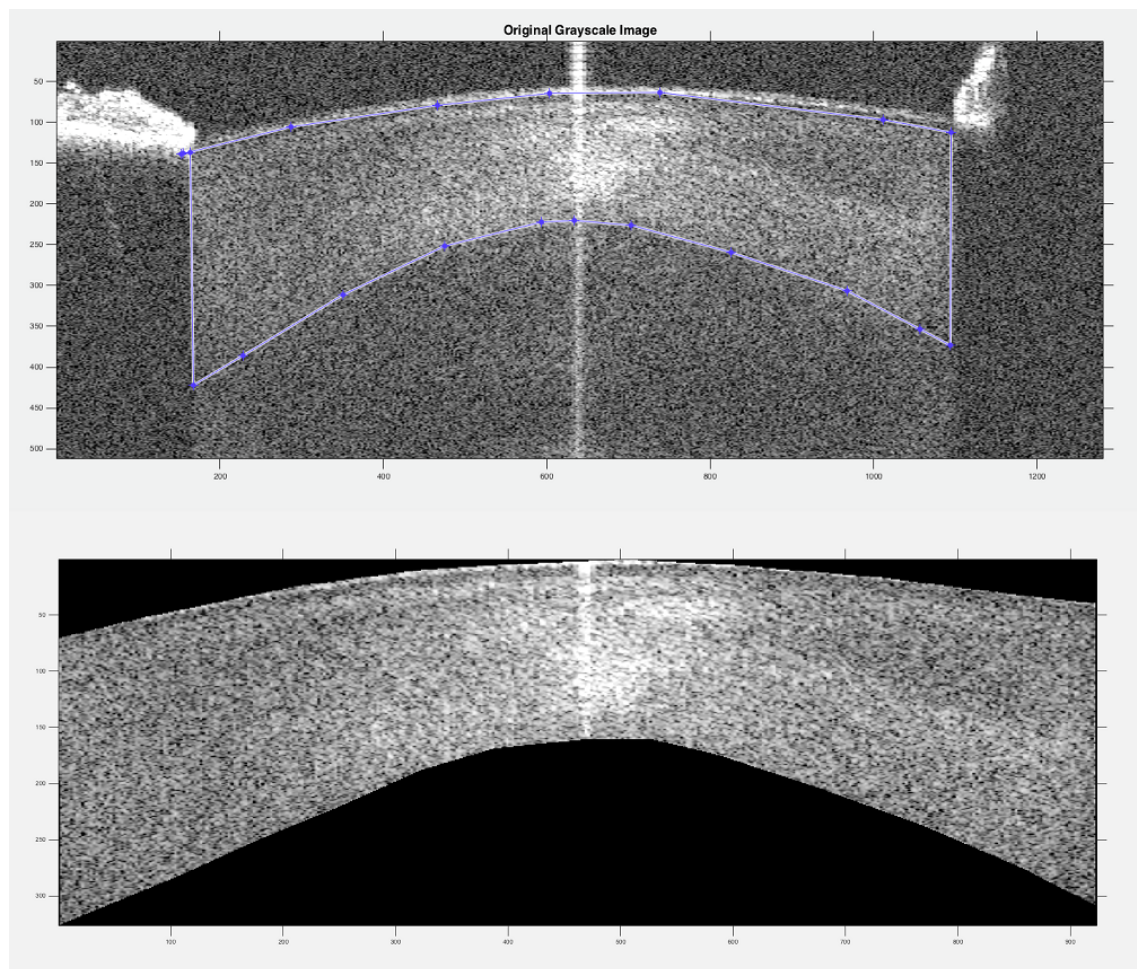


Figure 3.4.4 Demonstration of the masking process. The cortex was selected to be segmented by clicking the mouse along its border and connecting the first and last points(top image). The bottom image shows the segmented cortex.

Various techniques were used to calculate a grade of age-related opacity depending on its type. For high resolution images, nuclear opacification was determined by segmenting the nucleus from the anterior and posterior images of each half of the lens. A portion of the aqueous humor was also segmented from these same images respectively. The mean PI values of the aqueous represented background intensity levels that were unrelated to lenticular opacification. A mean nuclear pixel intensity ratio (PIR) was calculated by averaging the ratios taken between the anterior nucleus mean PI divided by anterior aqueous mean PI and the posterior nucleus mean PI divided by posterior aqueous mean PI. This final PIR represented the grade for nuclear opacity. The process of grading for low resolution images was easier as the entire crystalline lens was contained in the same image. The entire nucleus was segmented and a PIR was calculated from the mean nucleus and anterior aqueous PIs. Although, as mentioned previously, attempts were made to acquire AS-OCT scans of the lens just as the corneal reflex disappeared, this was not possible in all cases. In these instances, the corneal reflex was not included in calculations by taking care to avoid it during image segmentation.

Cortical lens opacities were graded in a similar way to the above. As a baseline, the entire anterior or posterior cortex was segmented depending on the location of the opacity. The software then provided the entire cortex mean PI. Due to the focal aspect of cortical opacities, it was also useful to know the area of the cortex. The software calculated this by applying the `bwarea()` function to the ROI mask of the cortex and providing a pixel area (PA). Any cortical opacities were then segmented using the same process. The cortical opacity PIR was calculated by dividing the opacity PI by the cortex PI. A pixel area ratio (PAR) was also calculated by dividing the opacity PA by the cortex PA. If multiple B-scans had been taken to image through opacities at different locations, the opacity PIRs and PARs were summed to determine overall grades for cortical opacification.

Posterior subcapsular cataract was analysed and graded in a similar way to cortical cataract. B-scans of the entire posterior cortex were segmented taking care not to include the areas of posterior subcapsular opacification. The areas of PSC were then segmented separately from the original B-scans. The PIR and PAR was calculated from these segmentations. Again, if the PSC was imaged with multiple B-scans, summed PIR and PAR values were used as a grade for opacification.

3.5 Results

3.5.1 Recruited Participants

Through the course of this study, 92 participants were recruited. Two participants were excluded due to the presence of narrow anterior chamber angles contra-indicating dilation, leaving a total study cohort of 90 participants. While attempts were made to include both eyes, this was not possible in all cases. Thus, a total of 156 eyes were imaged and the excluded eyes were due to the presence of amblyopia, coloboma, pseudophakia, or participant request. Participant ages ranged from 50 to 84 years with a mean of 64.06 ± 9.97 years. Table 3.5.1 outlines number of eyes based upon the stratified age ranges.

Age Range (Years)	N Individuals (% Total)	N Eyes (% Total)	Gender	Median Age (IQR) Per eye
50-60	37 (41%)	56 (36%)	Male: 16 Female: 21	53.50 (6.26)
60-70	28 (31%)	51 (33%)	Male: 8 Female: 20	66.07 (6.52)
70+	25 (28%)	49 (31%)	Male: 10 Female: 15	77.11 (5.04)
Total	90 (100%)	156 (100%)	Male: 34 Female: 56	64.33 (17.72)

Table 3.5.1 Stratified age ranges for all participants showing the number of eyes, percentage of total, number of males and females, and mean age.

3.5.2 Measures of Visual Function

3.5.2.1 Visual Acuity

Monocular habitual visual acuity (VA) was obtained in 100% of imaged eyes. Mean VA for all eyes was 0.00 ± 0.14 (SD) logMAR with a range of -0.26 to 0.68 logMAR. VA for the entire group of eyes was not normally distributed (Shapiro-Wilk, $p < 0.001$) with a positive skew (1.236). Figure 3.5.1 shows the histogram and Q-Q plots for VA.

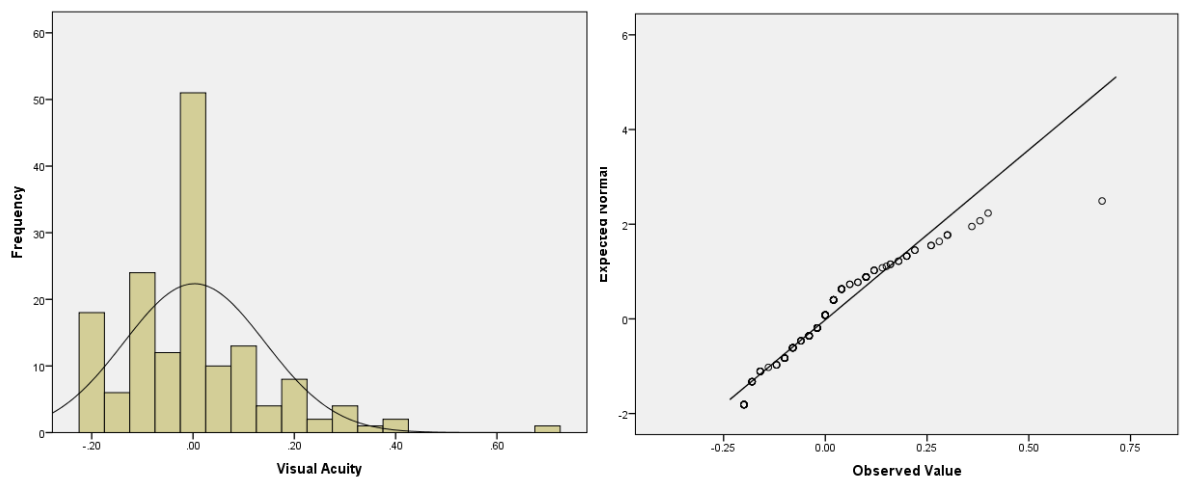


Figure 3.5.1 Histogram of VA frequencies from all 156 eyes showing positive skewness that still remains after removal of the outlier (0.68 logMAR).

For the stratified age ranges, VA was only normally distributed for the 60 to 70-year-old group (Shapiro-Wilk $p > 0.05$). Table 3.5.2 summarises VA in each age group.

Age Range (Years)	Mean VA (Std. Dev.)	Range (VA)	Shapiro-Wilk	Skewness	Kurtosis
50-60	-0.05 (0.12)	-0.20 to 0.38	$p < 0.001$	1.500	3.418
60-70	-0.01 (0.11)	-0.20 to 0.30	$p > 0.001$	0.340	0.524
70+	0.06 (0.16)	-0.20 to 0.68	$p < 0.001$	1.403	4.074
All Participant Eyes	0.00 (0.14)	-0.20 to 0.68	$p < 0.001$	1.236	3.446

Table 3.5.2 Summary of the VA distributions' mean, range and indicators of normality for all measured eyes.

Spearman rank order analysis was conducted comparing age and VA for all 85 left eyes to avoid any confounding from participants where both eyes were imaged. This showed a moderate correlation between decreasing VA and increasing age ($\rho=0.456$, $p<0.001$). Linear regression also showed a significant association between VA and age ($F_{(1,83)}=17.662$, $p<0.001$, $R^2=0.175$). Figure 3.5.2 demonstrates this relationship.

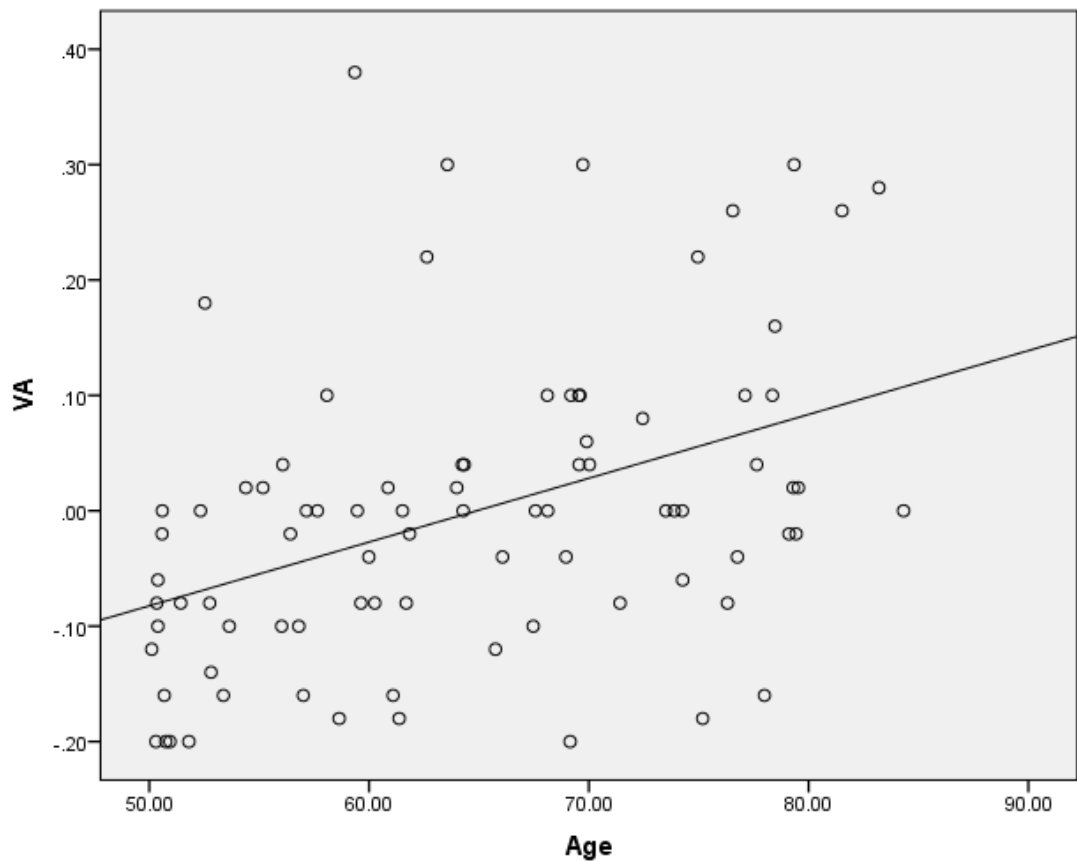


Figure 3.5.2 Scatterplot showing the significant relation between VA and age ($F_{(1, 83)} = 17.662$, $p < 0.001$, $R^2 = 0.175$).

3.5.2.2 Contrast Sensitivity

Contrast sensitivity (CS) measures were obtained in 100% of imaged eyes. Mean CS for all eyes was 1.85 ± 0.16 (SD) log units with values ranging from 1.20 to 1.95. CS data was not normally distributed (Shapiro-Wilk, $p < 0.001$) and heavily skewed to the left (-1.703). Figure 3.5.3 shows the histogram and Q-Q plots for CS.

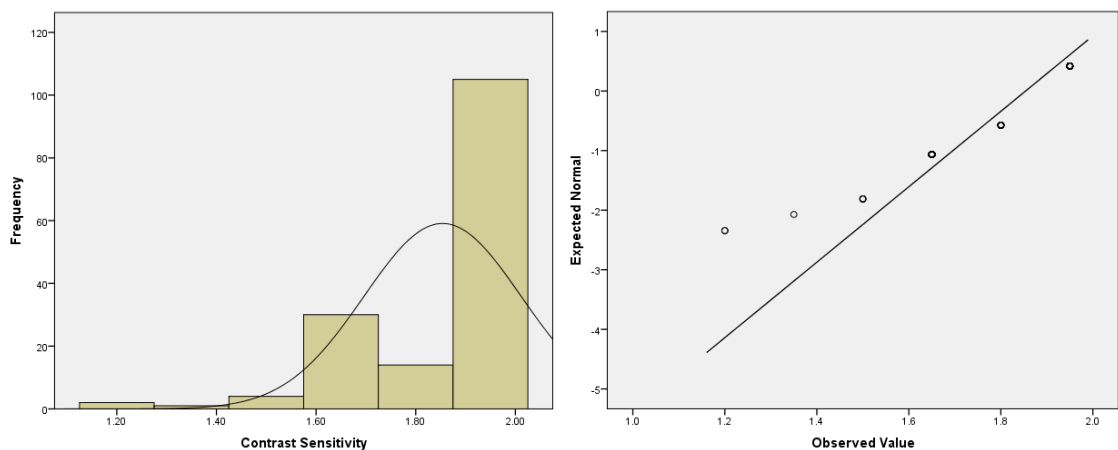


Figure 3.5.3 Histogram and Q-Q plot of CS frequencies from all 156 eyes showing negative skewness.

CS data were not normal for any of the age stratified groups. Table 3.5.3 summarises these values.

Age Range (Years)	Mean CS (Std. Dev.)	Range (CS)	Shapiro-Wilk	Skewness	Kurtosis
50-60	1.93 (0.07)	1.65 to 1.95	$p < 0.001$	-3.264	10.344
60-70	1.86 (0.13)	1.65 to 1.95	$p < 0.001$	-0.820	-1.181
70+	1.77 (0.21)	1.20 to 1.95	$p < 0.001$	-0.942	0.377
All Participant Eyes	1.85 (0.16)	1.20 to 1.95	$p < 0.001$	-1.703	2.903

Table 3.5.3 Summary of the CS distributions' mean, range and indicators of normality for all measured eyes.

Spearman's rank-order analysis showed that CS was moderately correlated with both age ($\rho = -0.418$, $p < 0.001$) and VA ($\rho = -0.493$, $p < 0.001$). Linear regression also showed significant associations between CS and both age ($F_{(1, 154)} = 38.996$, $p < 0.001$, $R^2 = 0.202$) and VA ($F_{(1, 154)} = 48.054$, $p < 0.001$, $R^2 = 0.238$). Figures 3.5.4 and 3.5.5 show the scatterplots for the regression analyses.

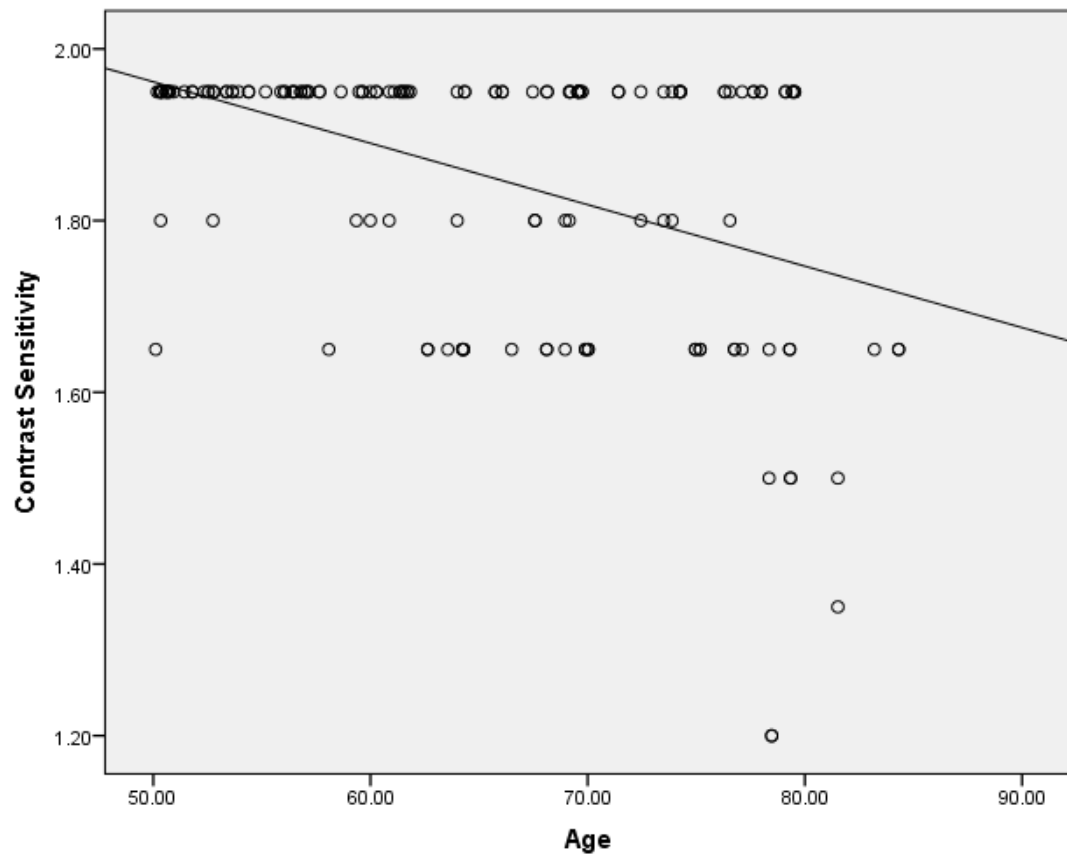


Figure 3.5.4 Scatterplot showing the significant relation between CS and age ($F_{(1, 154)} = 38.996$, $p < 0.001$, $R^2 = 0.202$).

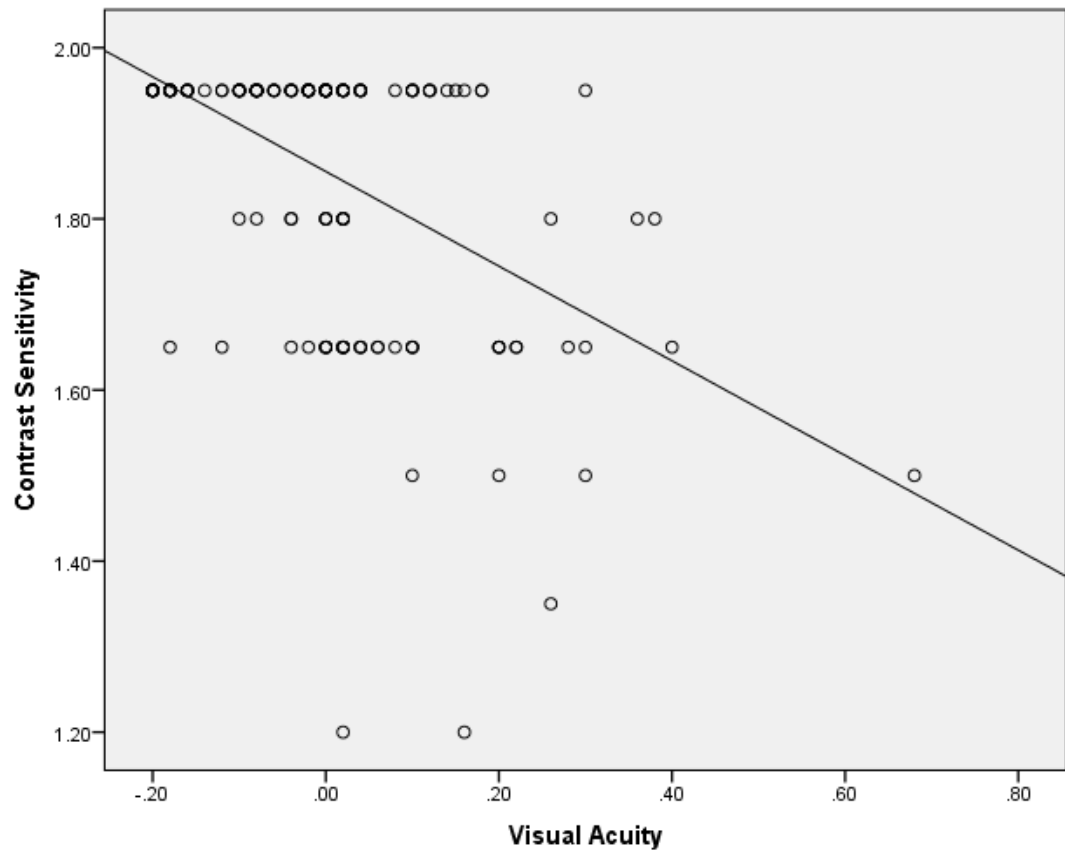


Figure 3.5.5 Scatterplot showing the significant relation between CS and VA ($F_{(1, 154)} = 48.054$, $p < 0.001$, $R^2 = 0.238$).

3.5.2.3 C-Quant Retinal Straylight

Straylight values were obtained in 132 (85%) of imaged eyes. Of the missing values for the 48 eyes, a software fault was responsible for eight (17%) and in all other cases, participants were unable to achieve results with valid reliability markers (Q and eSD) for either of their two attempts.

Mean log[s] values for the entire group of eyes were 1.20 ± 0.26 (SD) with a range of 0.68 to 2.34. Straylight values for all eyes were not normally distributed (Shapiro-Wilk, $p < 0.001$) and positively skewed (1.133). The histogram and Q-Q plots for log[s] are shown below in figure 3.5.6.

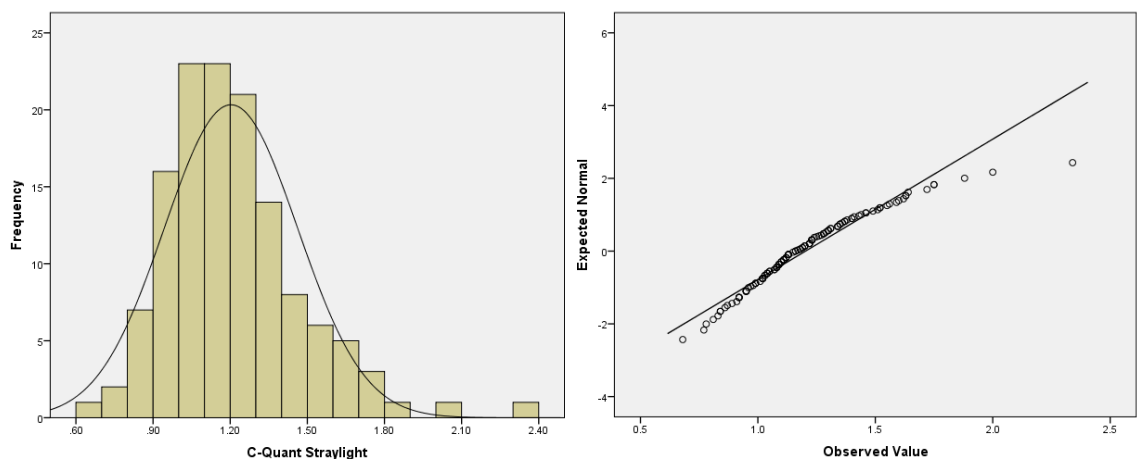


Figure 3.5.6 Histogram and Q-Q plot of log[s] frequencies from all 132 eyes showing negative skewness.

Log[s] data were normally distributed for both the 50 to 60-year-old and 70-year-old plus age groups (Shapiro-Wilk, $p > 0.05$) but not for those aged 60 to 70 years (Shapiro-Wilk, $p = 0.043$). Table 3.5.4 summarises the distributions and tests of normality for the above groups.

Age Range (Years)	Mean log[s] (Std. Dev.)	Range (log[s])	Shapiro-Wilk	Skewness	Kurtosis
50-60 (n = 52)	1.06 (0.15)	0.68 to 1.40	p = 0.934	-0.097	-0.066
60-70 (n = 41)	1.24 (0.24)	0.91 to 2.00	p = 0.043	0.866	1.302
70+ (n = 39)	1.34 (0.31)	0.77 to 2.34	p = 0.054	0.843	1.659
All Participant Eyes	1.20 (0.26)	0.68 to 2.34	p < 0.001	1.133	2.523

Table 3.5.4 Summary of the log[s] distributions' mean, range and indicators of normality for all measured eyes.

Spearman's rank order analyses for all eyes showed correlation between log[s] and both age ($\rho = 0.465$, $p < 0.001$) and CS ($\rho = -0.365$, $p < 0.001$) but not VA. Linear regression showed significant association between log[s] and CS ($F_{(1, 130)} = 26.398$, $p < 0.001$, $R^2 = 0.169$), age ($F_{(1, 130)} = 33.566$, $p < 0.001$, $R^2 = 0.205$) and VA, although very weakly for the latter ($F_{(1, 130)} = 4.291$, $p = 0.04$, $R^2 = 0.032$). The p-value for VA was also bordering on the result being of no significance. Figures 3.5.7, 3.5.8 and 3.5.9 show the scatterplots for these associations.

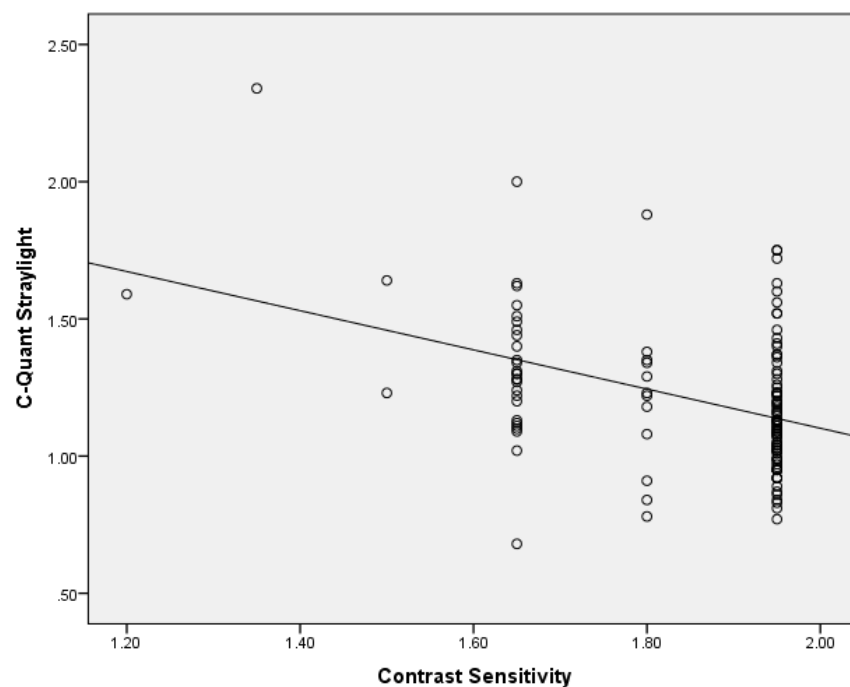


Figure 3.5.7 Scatterplot showing the significant relation between log[s] and CS ($F_{(1, 130)} = 26.398$, $p < 0.001$, $R^2 = 0.169$).

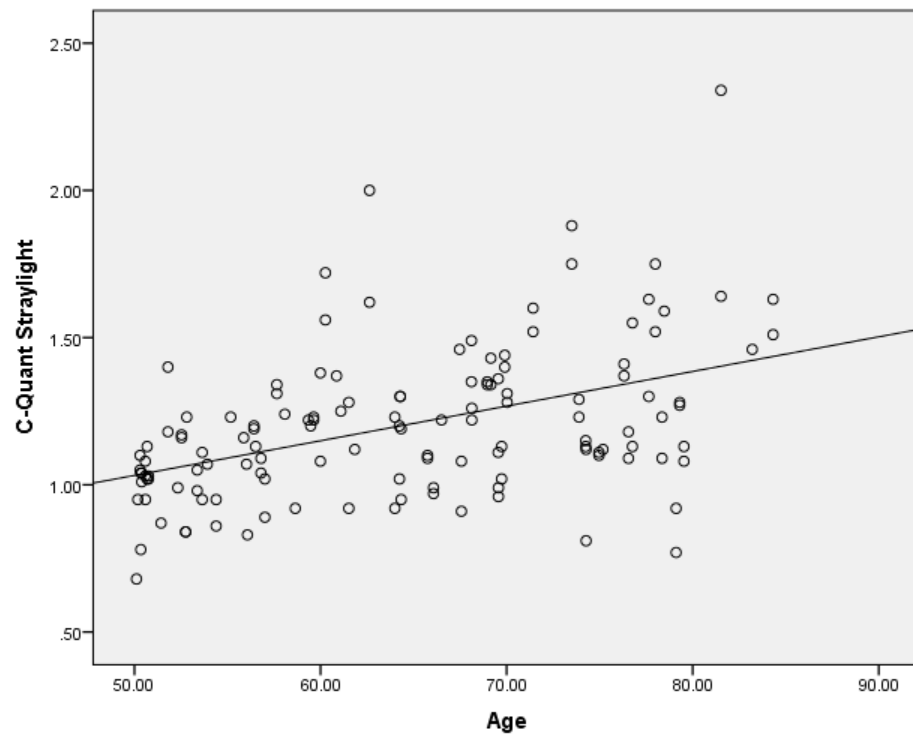


Figure 3.5.8 Scatterplot showing the significant relation between $\log[s]$ and age ($F_{(1, 130)} = 33.566$, $p < 0.001$, $R^2 = 0.205$).

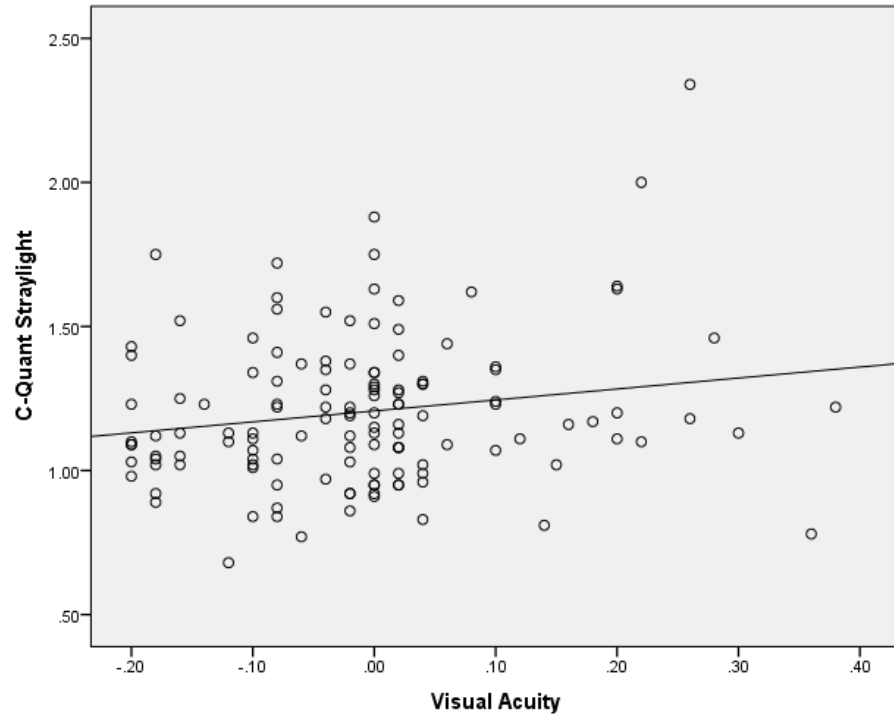


Figure 3.5.9 Scatterplot showing the significant relation between $\log[s]$ and CS ($F_{(1, 130)} = 4.291$, $p = 0.04$, $R^2 = 0.032$).

3.5.3 LOCS III Grading of Crystalline Lenses

Adequate pupil dilation and subsequent slit-lamp photography, with sufficient image quality to perform LOCS III grading, was successful in 100% (n=156) of eyes included in the cohort. The following subsections outline the results for nuclear, cortical and posterior subcapsular cataract.

3.5.3.1 LOCS III Nuclear Opalescence and Colour

Mean LOCS III NO for all eyes was 2.3 ± 0.8 (SD) with a range of 1.2 to 5.2. NC values ranged from 0.5 to 5.1 with a mean of 2.3 ± 0.8 (SD). Neither NO or NC were normally distributed (Shapiro-Wilk, $p < 0.001$). Figures 3.5.10 and 3.5.11 show the histograms and Q-Q plots for these distributions. Figure 3.5.12 shows images of various stages of nuclear opacity.

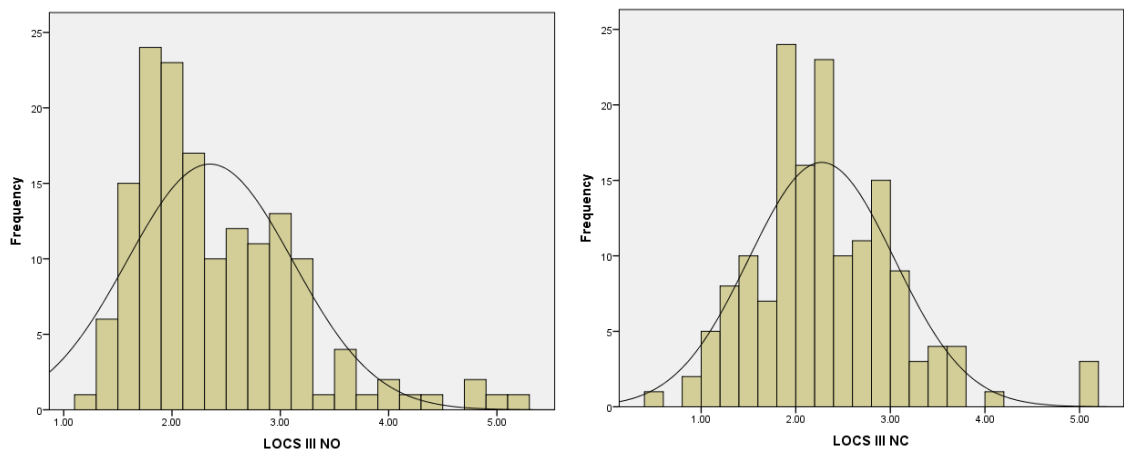


Figure 3.5.10 Histograms for total participant NO (left) and NC (right) with overlaid distribution curves.

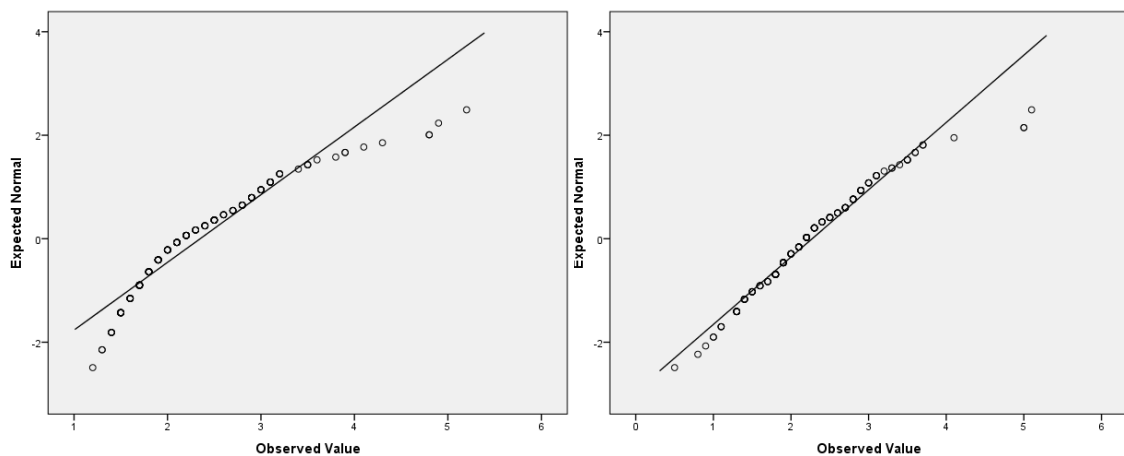


Figure 3.5.11 Q-Q plots of observed NO (left) and NC (right) values showing deviation from normality in both cases.

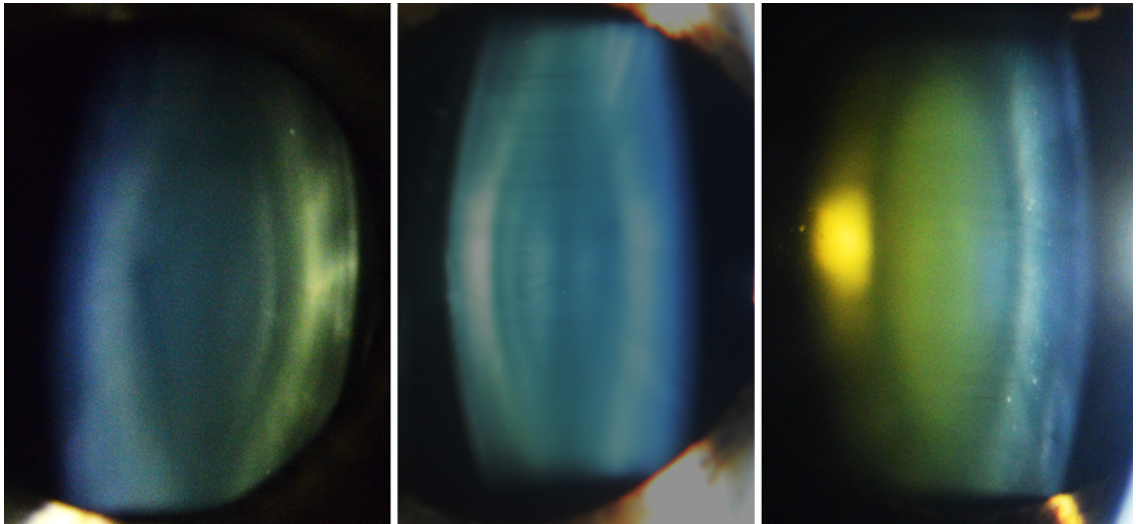


Figure 3.5.12 Optic section image of various stages of nuclear opacity. Respective LOCS III NO and NC grades for each image: Left: NO 1.2, NC 1.5; Centre: NO 1.9, NC 0.5; Right: NO 5.2, NC 4.1

According to Spearman's analyses for the entire group of participants, both NO and NC showed correlations with age and the three measures of visual function. Rho values and significances were very similar between both measures with age showing the strongest association. These data are summarised in table 3.5.5.

	NO		NC	
	Rho	Sig.	Rho	Sig.
Age	0.674	$p < 0.001$	0.724	$p < 0.001$
VA	0.417	$p < 0.001$	0.424	$p < 0.001$
CS	-0.366	$p < 0.001$	-0.479	$p < 0.001$
log[s]	0.257	$p = 0.003$	0.386	$p < 0.001$

Table 3.5.5 Summary of Spearman's rank order correlation between NO, NC and age as well as measures of visual function.

Linear regression also showed similar results to the above with moderate associations between the LOCS III nuclear measures to those of age and visual function. Again, values for the F-distributions, significances and R^2 values were all very similar between NO and NC. Table 3.5.6 shows this.

	NO			NC		
	F	Sig.	R ²	F	Sig.	R ²
Age	(1,154) = 129.364	p < 0.001	0.457	(1, 154) = 159.431	p < 0.001	0.509
VA	(1, 154) = 47.778	p < 0.001	0.237	(1, 154) = 49.939	p < 0.001	0.245
CS	(1, 154) = 64.363	p < 0.001	0.295	(1, 154) = 77.977	p < 0.001	0.336
log[s]	(1, 130) = 20.315	p < 0.001	0.135	(1, 130) = 35.897	p < 0.001	0.216

Table 3.5.6 Summary of linear regression between NO, NC and age as well as measures of visual function.

Although they were similar, all indicators for regression and correlation showed a higher association between NC and compared variables than for NO and the same compared measures.

Multiple linear regression was performed for both NO and NC with the three measures of visual function as predictors. Both models were significant (NO: $F_{(3, 128)} = 16.824$, $p < 0.001$, $R^2 = 0.283$; NC: $F_{(3, 128)} = 25.121$, $p < 0.001$, $R^2 = 0.371$). All measures of visual function showed significance as predictors in each model; table 3.5.7 summarises this data.

Model	Measures of Visual Function			
	Measure	Coefficient	t	p
NO $F_{(3, 128)}=16.824$, $p<0.001$, $R^2=0.283$	VA	0.259	3.115	=0.002
	CS	-0.222	-2.480	=0.014
	log[s]	0.230	2.801	=0.006
NC $F_{(3, 128)}=25.121$, $p<0.001$, $R^2=0.371$	VA	0.208	2.668	=0.009
	CS	0.288	-3.432	=0.001
	log[s]	0.310	4.025	<0.001

Table 3.5.7 Multiple regression analyses of LOCS III Nuclear grades vs measures of visual function.

When the data was sorted into stratified age ranges, the Shapiro-Wilk test showed that the 60 to 70-year-old group was normally distributed for both NO ($p = 0.129$) and NC ($p = 0.611$), while the 50 to 60-year-old group was normally distributed for NC only ($p =$

0.442); the 70-years and older group was not normally distributed for either LOCS III nuclear measure. Spearman correlation between the LOCS III nuclear measures and those of age and visual function varied between each stratified age group; these are summarised in the following table (3.5.8).

Age Range (Years)	Significant Correlations					
	Measure	NO		Measure	NC	
		Rho	p		Rho	p
50 - 60	VA	0.438	<0.001	None	N/A	N/A
60 - 70	Age	0.343	=0.014	CS	-0.336	=0.016
70+	VA	0.306	=0.032	VA	0.376	=0.008
	CS	-0.359	=0.011	CS	-0.534	<0.001

Table 3.5.8 Significant Spearman correlations between NO and NC compared to age and measures of visual function.

Linear regression also showed mixed associations between LOCS III nuclear measures compared to those of age and visual function. Associations grew stronger with each level of age range. Table 3.5.9 summarises this data.

LOCS Measure	Descriptive Statistics			Significant Linear Regression			
	Age Group (Years)	Mean (SD)	Range	Age	VA	CS	log[s]
NO	50 - 60	1.8 (0.34)	1.2 to 2.7	No	$F_{(1,54)}=12.83$ ($p=0.001$) ($R^2=0.192$)	No	No
	60 - 70	2.3 (0.50)	1.4 to 3.2	$F_{(1,49)}=8.12$ ($p=0.006$) ($R^2=0.142$)	No	No	$F_{(1,39)}=4.49$ ($p=0.041$) ($R^2=0.103$)
	70+	3.0 (0.84)	1.7 to 5.2	$F_{(1,47)}=5.64$ ($p=0.022$) ($R^2=0.107$)	$F_{(1,47)}=13.24$ ($p=0.001$) ($R^2=0.220$)	$F_{(1,47)}=19.09$ ($p<0.001$) ($R^2=0.289$)	$F_{(1,37)}=5.44$ ($p=0.025$) ($R^2=0.128$)
NC	50 - 60	1.7 (0.45)	0.5 to 2.5	No	No	No	No
	60 - 70	2.2 (0.47)	1.1 to 3.3	No	$F_{(1,49)}=4.64$ ($p=0.036$) ($R^2=0.086$)	$F_{(1,49)}=5.08$ ($p=0.029$) ($R^2=0.94$)	No
	70+	3.0 (0.72)	1.9 to 5.1	$F_{(1,47)}=5.17$ ($p=0.028$) ($R^2=0.099$)	$F_{(1,47)}=21.87$ ($p<0.001$) ($R^2=0.318$)	$F_{(1,47)}=26.93$ ($p<0.001$) ($R^2=0.364$)	$F_{(1,37)}=6.18$ ($p=0.018$) ($R^2=0.143$)

Table 3.5.9 Summary data for NO and NC when stratified by age group. Descriptive statistics show increasing means for increasing age groups and linear regression show a trend of increasing association to measures of visual function with age.

3.5.3.2 LOCS III Cortical Grading

Mean LOCS III C grades were 0.6 ± 0.8 (SD) with a range from 0.1 to 3.5. The vast majority of participants had no cortical cataract and therefore, were given grades of 0.1. Grades greater than 0.1 occurred in 49 (31%) of eyes; of these, 38 (24%) had grades above one and 18 (11%) had grades above 2.0. The distribution of C was not normal (Shapiro-Wilk, $p < 0.001$) and strongly skewed (1.663) due to the number of 0.1 grades assigned to participants with no cortical opacities. Figure 3.5.13 shows the histogram and Q-Q plots for C. Figure 3.5.14 shows slit lamp images of clear and significant cortical cataract.

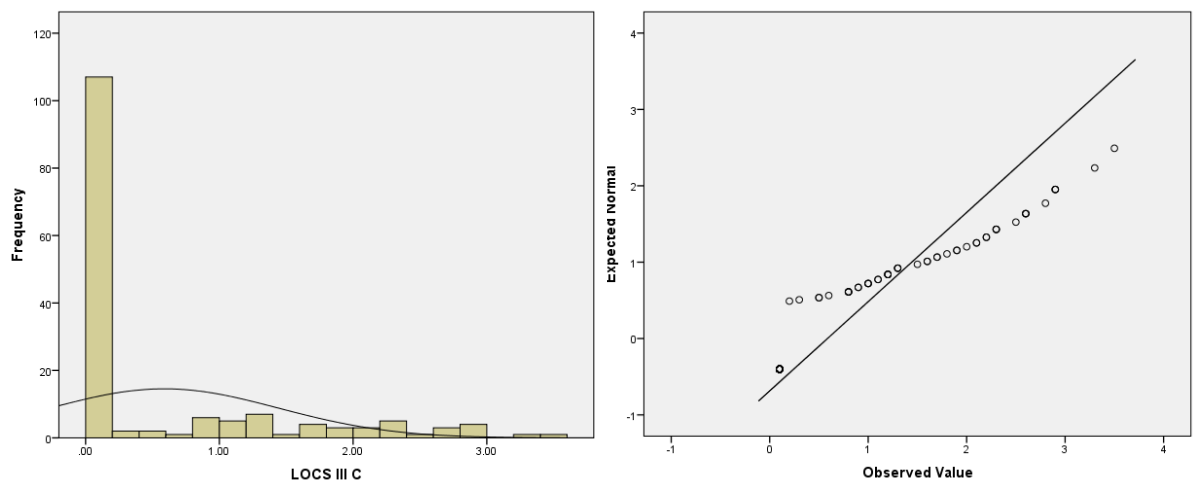


Figure 3.5.13 Histogram (left) and Q-Q (right) plots of the C distribution for all participants, showing a strong positive skewness.

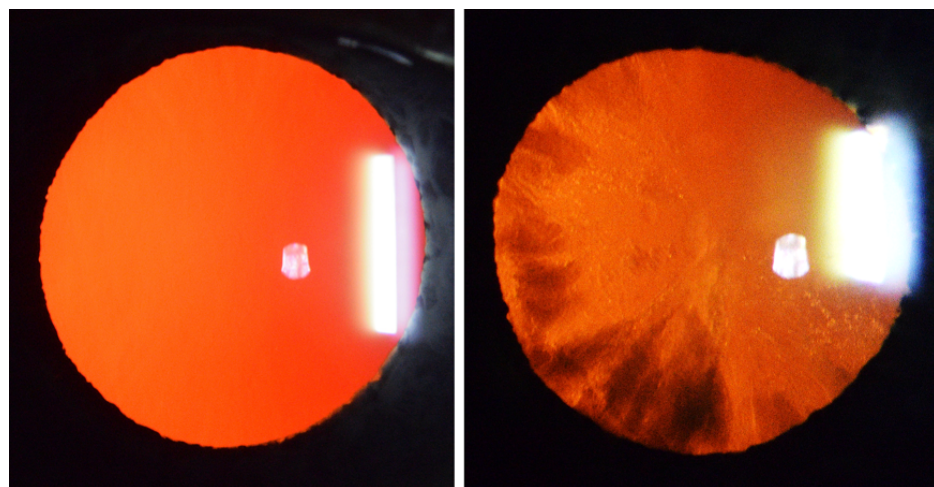


Figure 3.5.14 Retroillumination images showing a clear (left) lens with a LOCS III C grade of 0.1 and significant cortical opacity (right) with LOCS III C grade of 3.5.

Spearman's rank order analyses showed correlation between C and age as well as all measures of visual function as seen in table 3.5.10. Age showed the strongest correlation to C whereas VA and CS were moderately correlated and log[s] showed a weak correlation.

Measure	Spearman's Correlation to LOCS III C	
	Rho	Sig.
Age	0.509	$p < 0.001$
VA	0.256	$p = 0.001$
CS	0.270	$p = 0.001$
log[s]	0.179	$p = 0.040$

Table 3.5.10 Significant Spearman correlations for LOCS III C compared to age and measures of visual function.

Linear regression showed significant associations between C and age ($F_{(1, 154)} = 38.755$, $p < 0.001$, $R^2 = 0.201$), as well as weakly to both CS ($F_{(1, 154)} = 10.216$, $p = 0.002$, $R^2 = 0.062$) and log[s] ($F_{(1, 130)} = 5.386$, $p = 0.022$, $R^2 = 0.040$). A model of multiple regression comparing VA, CS and log[s] to C, showed no significance for any predictor.

When stratified by age, each group was not normally distributed (Shapiro-Wilk, $p < 0.001$) and heavily skewed to the right due to the paucity of upped LOCS III grades for C. Descriptive statistics for stratified age groups are displayed in table 3.5.11.

Age Range	Median	IQR	Range	Mean	Std. Dev.	Shapiro-Wilk
50 – 60 (n = 56)	0.1	0.0	0.1 to 2.6	0.2	0.4	$p < 0.001$
60 – 70 (n = 51)	0.1	0.7	0.1 to 2.9	0.5	0.8	$p < 0.001$
70+ (n = 49)	0.9	1.9	0.1 to 3.5	1.1	1.0	$p < 0.001$
Total (n = 156)	0.1	0.8	0.1 to 3.5	0.6	0.9	$p < 0.001$

Table 3.5.11 Summary of descriptive statistics for LOCS III C when stratified by age.

Spearman's rank order correlation showed an association between C and log[s] ($\rho = -0.310$, $p = 0.03$) in the 50 to 60-year old group and no other associations between the LOCS score and age or any measure of visual function in any other group. Similarly, linear regression between C and age as well as measures of visual function showed no association within any of the stratified age groups.

3.5.3.3 LOCS III Posterior Subcapsular Grading

Very low levels of posterior subcapsular opacification were present in this sample of participants. Only five participants had any sort of grade for P ranging from 0.2 to 2.2. Naturally, this sample was not normally distributed (Shapiro-Wilk, $p < 0.001$) with a heavy positive skew. Table 3.5.12 below outlines the descriptive statistics for LOCS III P grades. Figure 3.5.15 shows images of a clear lens and one with significant PSC. Due to the low presence of P grades, correlation and regression comparisons were not made between the measure and those of age and visual function as they would not yield adequate statistical power.

Age Range	Median	IQR	Range	Mean	Std. Dev.	Shapiro-Wilk
50 – 60 (n = 56)	No levels of P – all values 0.1					
60 – 70 (n = 51)	0.1	0.0	0.1 to 2.2	0.1	0.3	$p < 0.001$
70+ (n = 49)	0.1	0.1	0.1 to 1.9	0.2	0.4	$p < 0.001$
Total (n = 156)	0.1	0.0	0.1 to 2.2	0.1	0.3	$p < 0.001$

Table 3.5.12 Summary of descriptive statistics for LOCS III P when stratified by age.

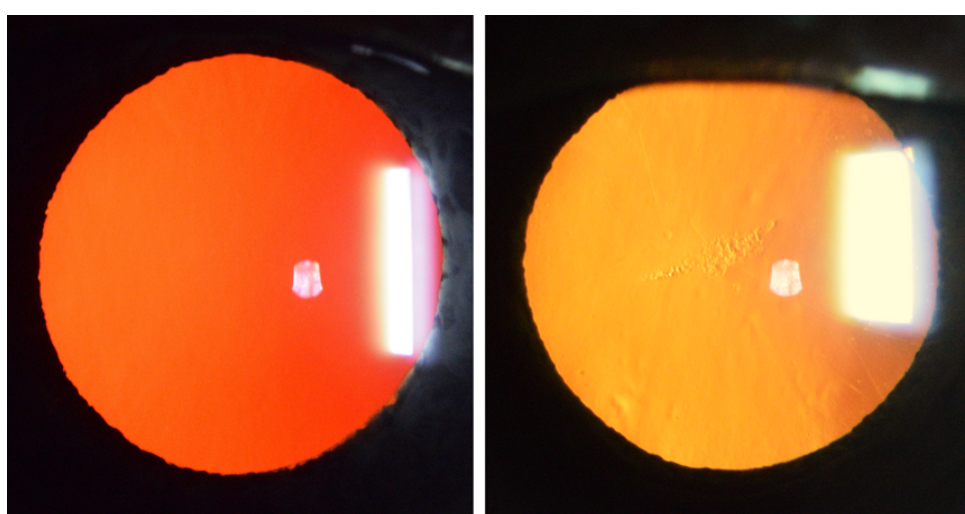


Figure 3.5.15 Retroillumination images showing a clear (left) lens with a LOCS III P grade of 0.1 and significant PSC opacity (right) with LOCS III P grade of 1.9.

3.5.3.4 Inter-Observer Agreement of LOCS III Grading

To verify the accuracy of LOCS III grading by the researcher (ASM), 23 eyes (15% of total) were chosen at random and graded by an experienced optometrist and researcher (JAL). Bland-Altman plots were made up for all four LOCS III measures which are shown in figures 3.5.16, 3.5.17, 3.5.18 and 3.5.19. Agreement between ASM and JAL was very good with less than a 0.1 LOCS III score of bias for all measures of opacification.

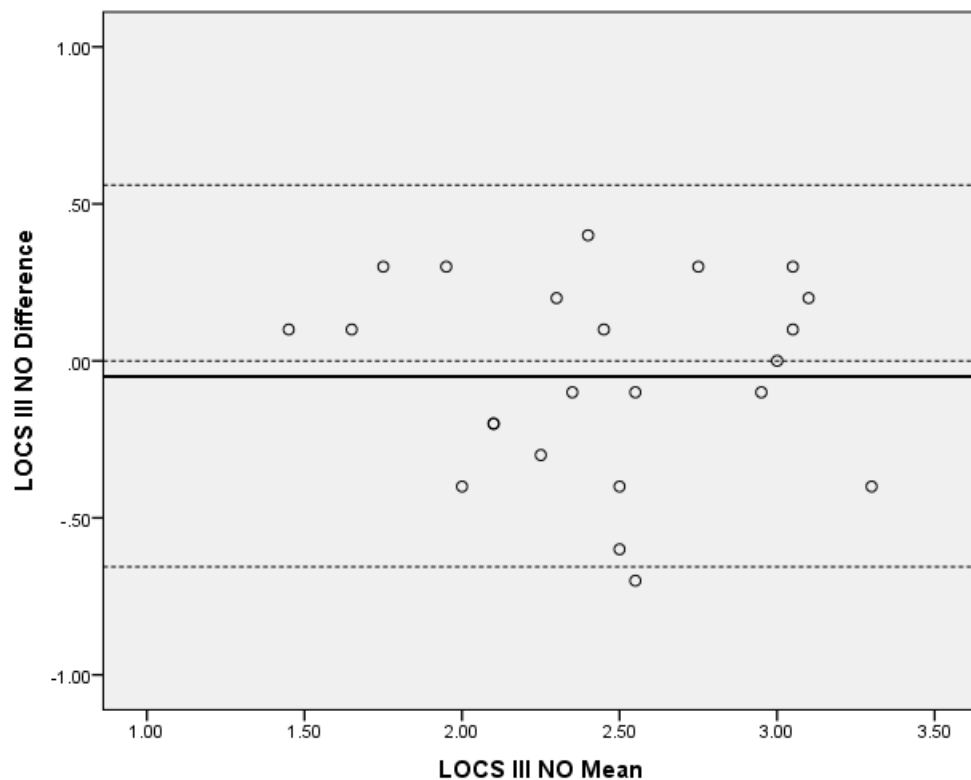


Figure 3.5.16 Bland-Altman plot showing inter-observer agreement for LOCS III NO grades.

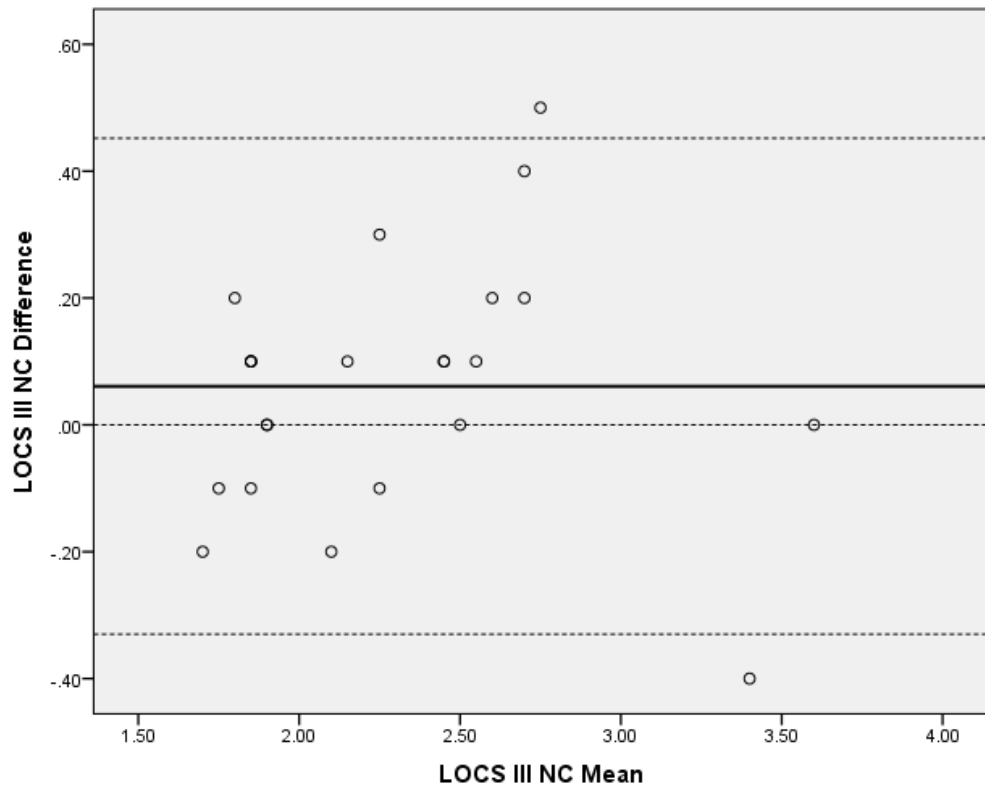


Figure 3.5.17 Bland-Altman plot showing inter-observer agreement for LOCS III NC grades.

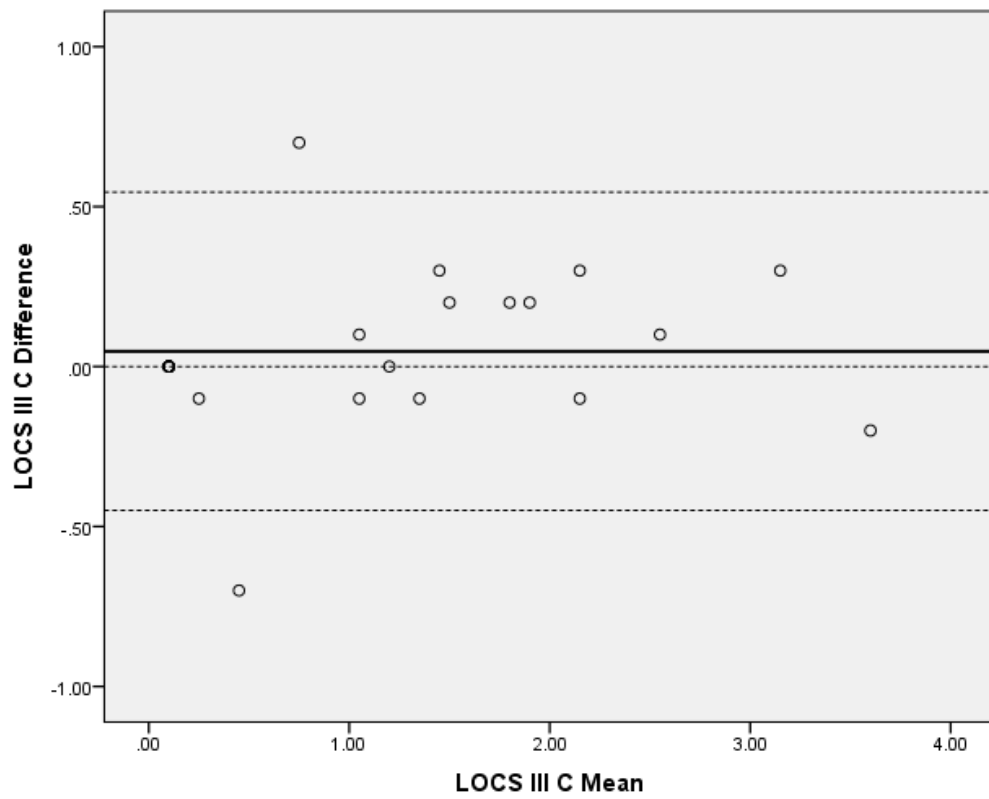


Figure 3.5.18 Bland-Altman plot showing inter-observer agreement for LOCS III C grades.

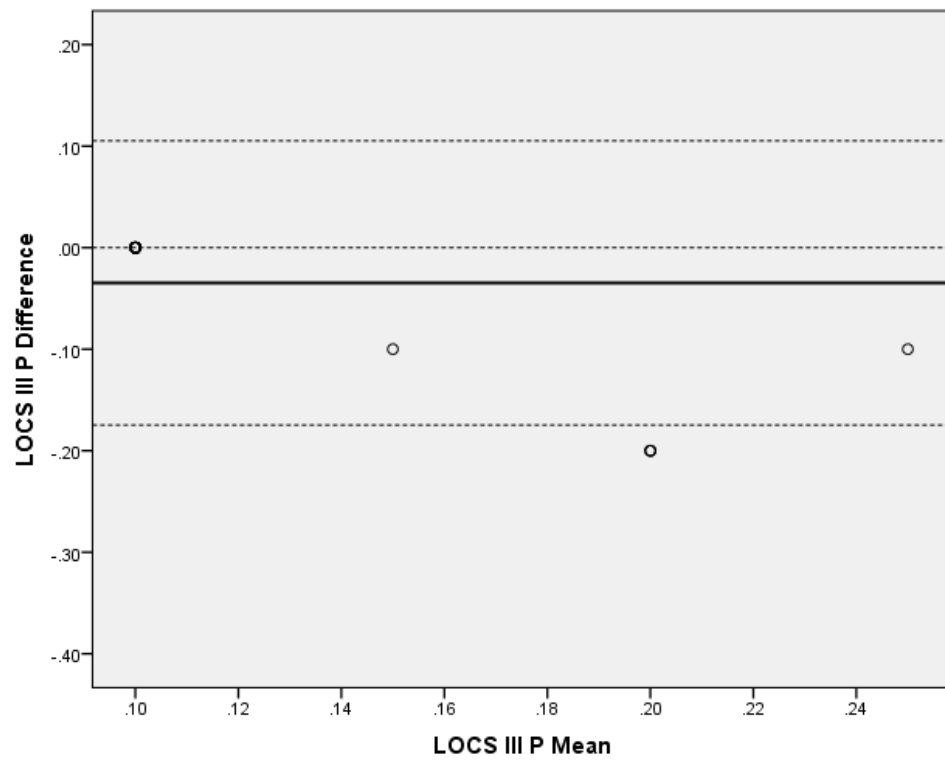


Figure 3.5.19 Bland-Altman plot showing inter-observer agreement for LOCS III P grades.

3.5.4 OCT Grading of Lens Opacity

3.5.4.1 OCT Nuclear Grading

Out of the 156 imaged eyes, both the anterior and posterior high-resolution OCT B-scans required for grading nuclear opacity were successfully captured in 129 (83%) eyes. A slightly higher success rate was achieved in imaging the lens with low-resolution scans (149 eyes, 96%) due to the easier participant alignment and faster acquisition times that resulted from the ability to image the entire crystalline lens at once in this mode.

For the entire group, median high resolution PIR was 1.282 ± 0.090 (IQR), and these were not normally distributed (Shapiro-Wilk, $p=0.037$). Similarly, values for low resolution PIR measures were not normally distributed (Shapiro-Wilk, $p < 0.001$) with a median of 1.102 ± 0.049 (IQR). Figures 3.5.20 and 3.5.21 show the histograms and Q-Q plots for high- and low-resolution PIRs respectively. Figure 3.5.22 and 3.5.23 show B-scans of crystalline lenses with low and significant nuclear opacification along with their corresponding slit lamp images.

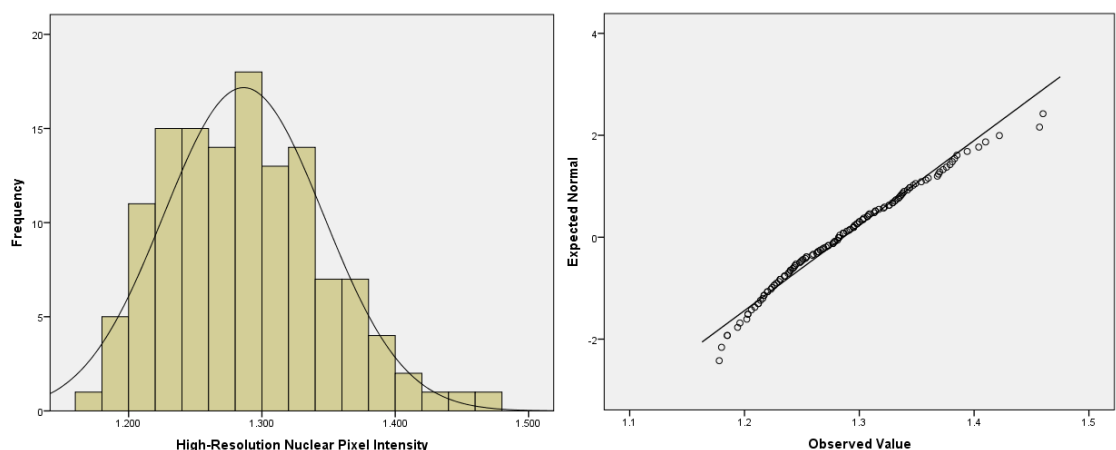


Figure 3.5.20 Histogram with overlaid distribution curve and Q-Q plot for total participant High-Resolution Nuclear PIR.

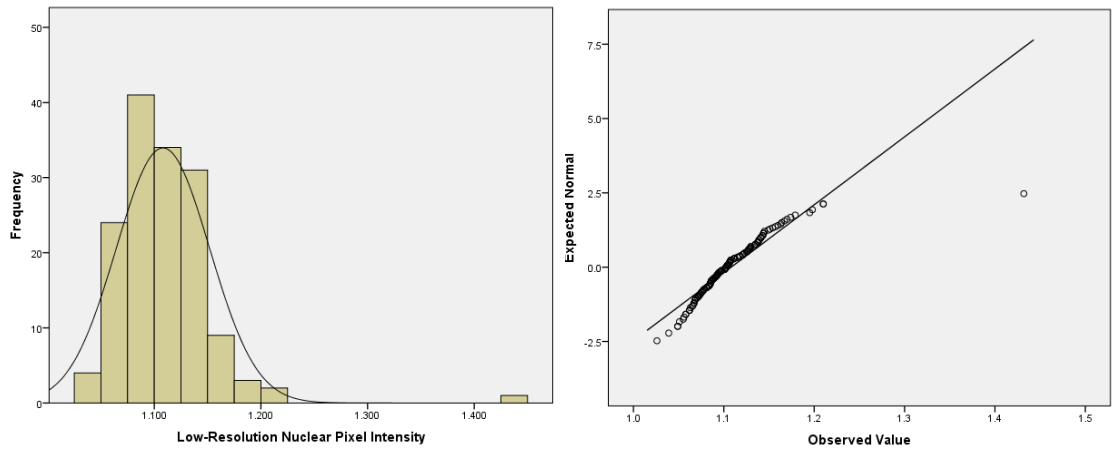


Figure 3.5.21 Histogram with overlaid distribution curve and Q-Q plot for total participant Low-Resolution Nuclear PIR.

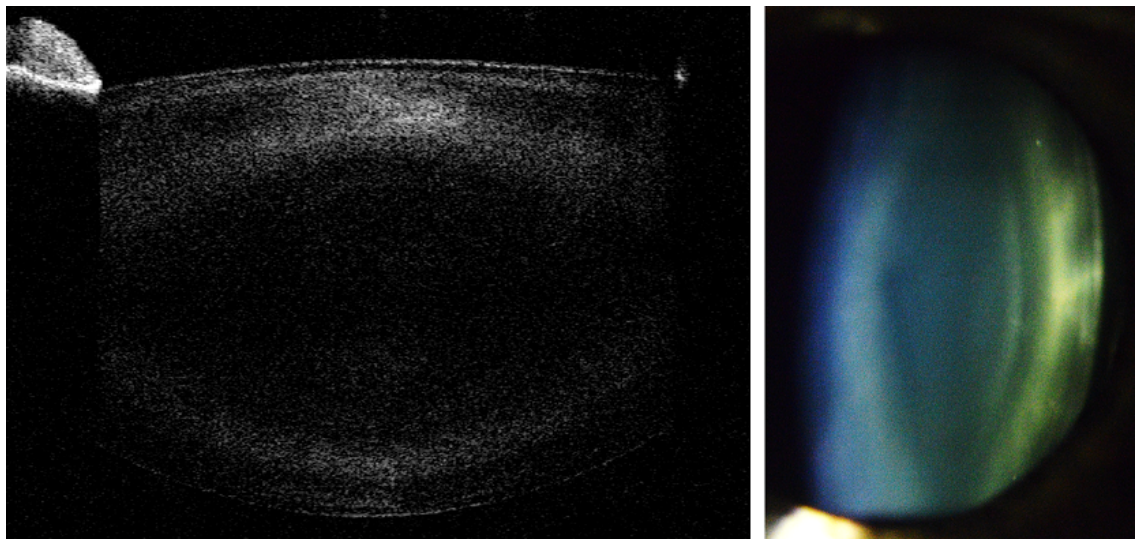


Figure 3.5.22 High-resolution OCT (left) with a Nuclear PIR grade of 1.185 and corresponding optic section (right) with LOCS III scores of 1.2 and 1.5 for NO and NC respectively.

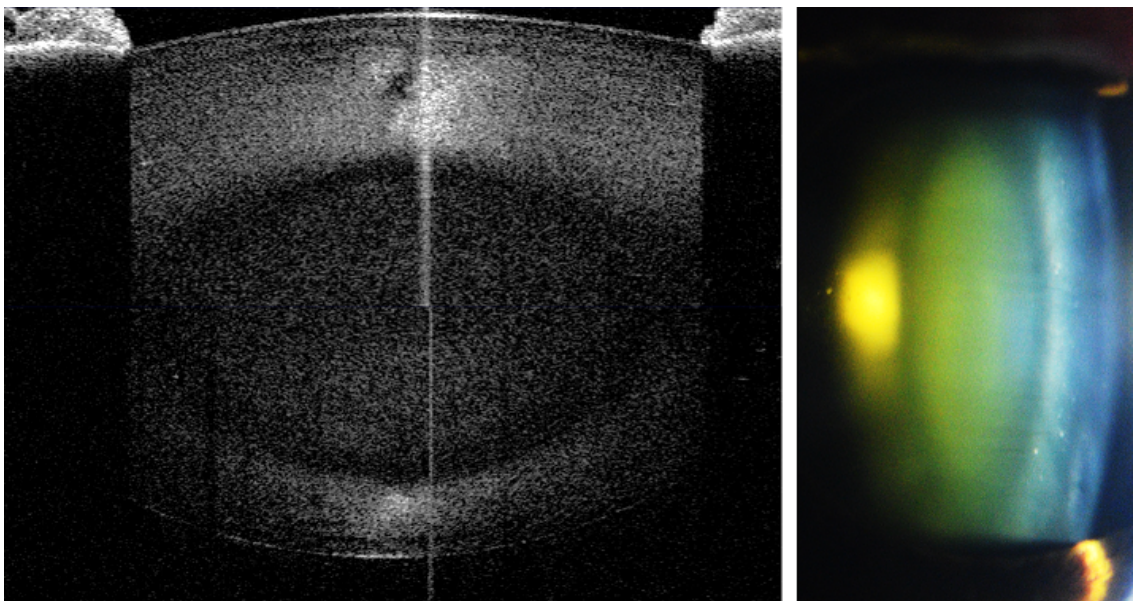


Figure 3.5.23 High-resolution OCT (left) with a Nuclear PIR grade of 1.457 and corresponding optic section (right) with LOCS III scores of 5.2 and 4.1 for NO and NC respectively.

Spearman's rank order analysis showed significant correlations between PIR and age as well as all measures of visual function for high-resolution images. Age showed the strongest correlation followed by log[s], CS and VA. For low-resolution images, PIR was correlated with age, VA, and CS although this was weaker for most measures compared to high-resolution PIRs. Table 3.5.13 summarizes the correlations for the entire group.

	High-resolution PIR		Low-resolution PIR	
	Rho	Sig.	Rho	Sig.
Age	0.621	$p < 0.001$	0.427	$p < 0.001$
VA	0.218	$p = 0.013$	0.219	$p = 0.007$
CS	-0.231	$p = 0.008$	No Correlation	n/a
log[s]	0.325	$p < 0.001$	0.193	$p = 0.029$

Table 3.5.13 Summary of Spearman correlations for both high and low-resolution nuclear PIR compared to age and measures of visual function.

Linear regression showed significant relations between high-resolution PIR values and measures of visual function and age. Again, age showed the strongest relation followed by CS, log[s], and VA. Age and measures of visual function were also linearly associated with low-resolution PIRs albeit at weaker levels. Table 3.5.14 outlines the regression analyses for both high- and low-resolution PIR values.

	High-Resolution PIR			Low-Resolution PIR		
	F	Sig.	R ²	F	Sig.	R ²
Age	(1,127) = 81.946	$p < 0.001$	0.392	(1, 147) = 28.031	$p < 0.001$	0.160
VA	(1, 127) = 7.111	$p = 0.009$	0.053	(1, 147) = 27.840	$p < 0.001$	0.159
CS	(1, 127) = 16.574	$p < 0.001$	0.115	(1, 147) = 13.470	$p < 0.001$	0.084
log[s]	(1, 110) = 13.584	$p < 0.001$	0.110	(1, 126) = 8.941	$p = 0.003$	0.066

Table 3.5.14 Summary of linear regression analyses for both high and low-resolution PIR compared to age and measures of visual function.

Significant models of multiple linear regression occurred for all three measures of visual function as predictors of high- ($F_{(3, 108)} = 5.596$, $p = 0.001$, $R^2 = 0.135$) and low-resolution

($F_{(3, 124)} = 4.026$, $p = 0.009$, $R^2 = 0.089$) PIRs. For both high- and low-resolution PIR models, only log[s] was a significant predictor while VA and CS were not (see table 3.5.15).

Model	Measures of Visual Function			
	Measure	Coefficient	t	p
High-resolution PIR $F_{(3, 108)}=5.596$, $p=0.001$, $R^2=0.135$	VA	0.024	0.243	0.808
	CS	-0.162	-1.494	0.138
	log[s]	0.256	2.569	0.012
Low-resolution PIR $F_{(3, 124)}=4.121$, $p=0.009$, $R^2=0.089$	VA	0.103	1.084	0.280
	CS	-0.084	-0.817	0.415
	log[s]	0.205	2.194	0.030

Table 3.5.15 Multiple regression analyses of OCT Nuclear PIRs vs measures of visual function.

When stratified by age, each group showed normal distributions for high-resolution PIRs. Capture rates in each group were good for high-resolution PIRs with 82.1% ($n = 46$), 88.2% ($n = 45$) and 77.6% ($n = 38$) of eyes successfully imaged in the 50 to 60, 60 to 70 and 70-years-and-older ranges respectively. Capture rates were higher for low-resolution scans in each age bracket when compared to their corresponding high-resolution scans at 92.9% ($n = 52$), 94.1% ($n = 48$) and 100% ($n = 49$) for 50 to 60, 60 to 70, and 70 years-and-older age ranges respectively. In contrast to the stratified high-resolution PIRs, only the distribution for the 60 – 70-year-old group was normal (Shapiro-Wilk, $p = 0.673$) for the low-resolution groups. The descriptive data is summarised in tables 3.5.16 and 3.5.17.

Age Range	Median	IQR	Range	Mean	Std. Dev.	Shapiro-Wilk
50 – 60 ($n = 46$)	1.239	0.055	1.178 to 1.354	1.246	0.042	$p = 0.140$
60 – 70 ($n = 45$)	1.286	0.068	1.180 to 1.369	1.286	0.044	$p = 0.748$
70+ ($n = 38$)	1.335	0.080	1.217 to 1.460	1.335	0.060	$p = 0.882$
Total ($n = 129$)	1.282	0.090	1.178 to 1.460	1.286	0.060	$p = 0.037$

Table 3.5.16 Descriptive data for high-resolution nuclear PIR when stratified by age.

Age Range	Median	IQR	Range	Mean	Std. Dev.	Shapiro-Wilk
50 – 60 (n = 52)	1.089	0.040	1.039 to 1.174	1.094	0.029	p = 0.020
60 – 70 (n = 48)	1.098	0.050	1.026 to 1.167	1.101	0.032	p = 0.673
70+ (n = 49)	1.123	0.040	1.058 to 1.432	1.131	0.057	p < 0.001
Total (n = 149)	1.102	0.049	1.026 to 1.432	1.108	0.044	p < 0.001

Table 3.5.17 Descriptive data for low-resolution nuclear PIR when stratified by age.

Spearman's correlations for high- and low-resolution PIRs compared to measures of visual function when grouped by age brackets showed variable results with no significant associations for high-resolution PIRs and only some for low-resolution measures; the data is summarised in table 3.5.18.

Age Range (Years)	Significant Correlations					
	Measure	High-resolution PIR		Measure	Low-resolution PIR	
		Rho	p		Rho	p
50 - 60	Age	Not sig.	=0.055	Age	Not sig.	=0.499
	VA	Not sig.	=0.605	VA	Not sig.	=0.226
	CS	Not sig.	=0.753	CS	Not sig.	=0.603
	Straylight	Not sig.	=0.072	Straylight	Not sig.	=0.112
60 - 70	Age	Not sig.	=0.405	Age	Not sig.	=0.164
	VA	Not sig.	=0.619	VA	Not sig.	=0.488
	CS	Not sig.	=0.862	CS	Not sig.	=0.774
	Straylight	Not sig.	=0.066	Straylight	-0.369	=0.019
70+	Age	Not sig.	=0.356	Age	0.318	=0.026
	VA	Not sig.	=0.766	VA	Not sig.	=0.392
	CS	Not sig.	=0.460	CS	Not sig.	=0.304
	Straylight	Not sig.	=0.221	Straylight	0.365	=0.022

Table 3.5.18 Summary of Spearman's correlations for both high and low-resolution nuclear PIR compared to age and measures of visual function when sorted into stratified age group.

Linear regression was performed comparing both high- and low-resolution PIRs to each measure of visual function and age. Again, results were variable with certain measures of visual function across age brackets showing significance depending on resolution or stratified age range. Table 3.5.19 outlines these results.

PIR Measure	Age Group (Years)	Significant Linear Regression			
		Age	VA	CS	log[s]
High-resolution	50 - 60	$F_{(1,44)}=4.807$ ($p=0.034$) ($R^2=0.098$)	No	No	No
	60 - 70	No	No	No	$F_{(1,35)}=4.903$ ($p=0.033$) ($R^2=0.123$)
	70+	No	No	No	No
Low-resolution	50 - 60	No	No	No	No
	60 - 70	No	No	No	$F_{(1,38)}=4.622$ ($p=0.038$) ($R^2=0.108$)
	70+	No	$F_{(1,47)}=16.260$ ($p<0.001$) ($R^2=0.257$)	$F_{(1,47)}=4.104$ ($p=0.048$) ($R^2=0.080$)	$F_{(1,37)}=4.637$ ($p=0.038$) ($R^2=0.111$)

Table 3.5.19 Summary of linear regression analyses for both high and low-resolution nuclear PIR compared to age and measures of visual function when sorted into stratified age group.

Multiple linear regressions with the three measures of visual function as predictors of either high- or low-resolution PIR showed no significance for any stratified age range.

3.5.4.1.2 Comparison of LOCS III Nuclear Grades and OCT PIRs

To determine the viability of OCT in grading nuclear cataract, comparisons were made between participants' LOCS III nuclear grades and PIR values. Spearman's analyses determined that both high and low-resolution PIRs were moderately-to-highly associated with NO and NC with high resolution PIRs showing a stronger trend. When stratified by age, the relationship still existed however, the overall association was weaker in all groups and in most cases, there were no associations between low resolution PIRs and NC. Table 3.5.20 summarises the correlations between PIRs and LOCS III nuclear grades.

	Age Range	High-resolution PIR	Low-resolution PIR
LOCS III NO	50 - 60	Rho = 0.420 p = 0.004	Rho = 0.325 p = 0.019
	60 - 70	Rho = 0.568 p < 0.001	Rho = 0.515 p < 0.001
	70+	Rho = 0.550 p < 0.001	Rho = 0.494 p < 0.001
	All ages	Rho = 0.671 p < 0.001	Rho = 0.542 p < 0.001
LOCS III NC	50 - 60	Rho = 0.429 p = 0.003	Not significant
	60 - 70	Rho = 0.296 p = 0.048	Not significant
	70+	Rho = 0.469 p = 0.003	Rho = 0.403 p = 0.004
	All ages	Rho = 0.633 p < 0.001	Rho = 0.409 p < 0.001

Table 3.5.20 Summary of Spearman's correlations for high and low-resolution nuclear PIR compared to LOCS III NO and NC. Data is stratified by age and compared in total.

Linear regression also showed moderate associations between PIR and LOCS III NO scores (high-resolution PIR: $F_{(1, 127)} = 128.54$, $p < 0.001$, $R^2 = 0.503$; low-resolution PIR: $F_{(1, 127)} = 104.263$, $p < 0.001$, $R^2 = 0.451$). Slightly weaker significant associations occurred for NC scores (high-resolution PIR: $F_{(1, 147)} = 75.435$, $p < 0.001$, $R^2 = 0.339$; low-resolution PIR: $F_{(1, 147)} = 56.816$, $p < 0.001$, $R^2 = 0.279$). Figures 3.5.24, 3.5.25, 3.5.26 and 3.5.27 show the scatterplots for the above-mentioned regressions.

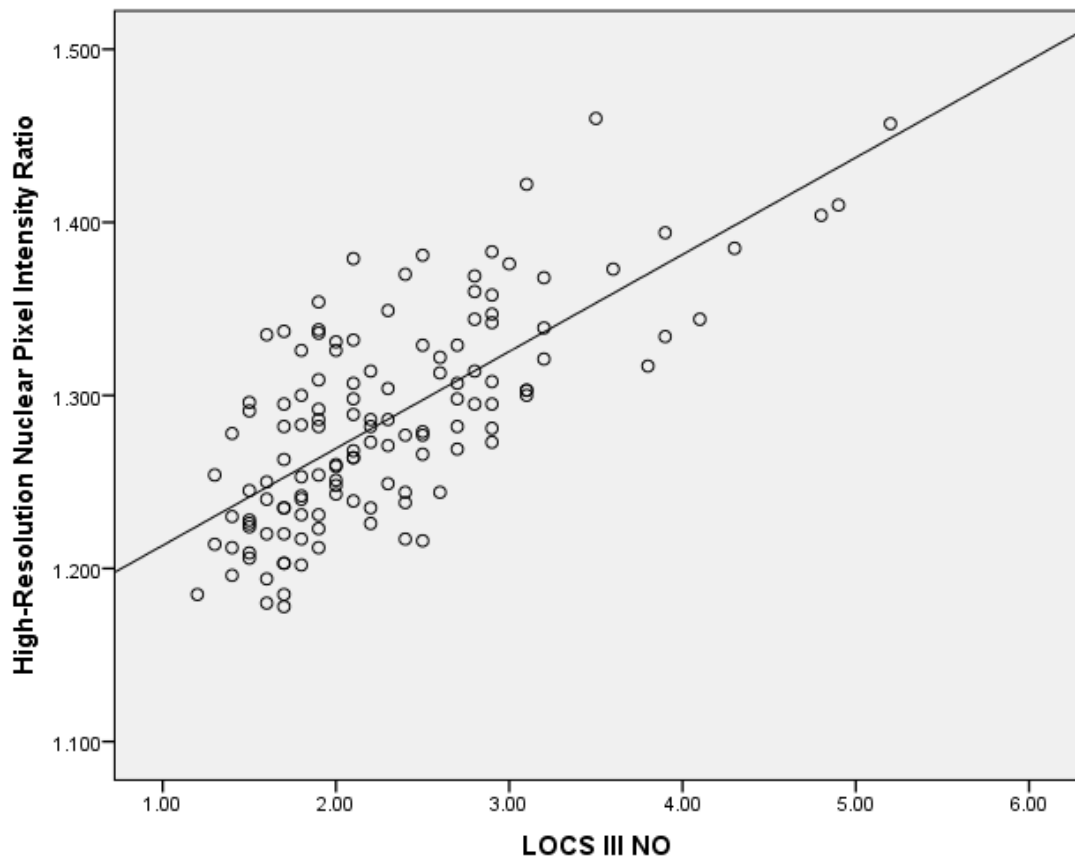


Figure 3.5.24 Scatterplot showing the significant relation between high-resolution nuclear PIR LOCS III NO ($F_{(1, 127)} = 128.54$, $p < 0.001$, $R^2 = 0.503$).

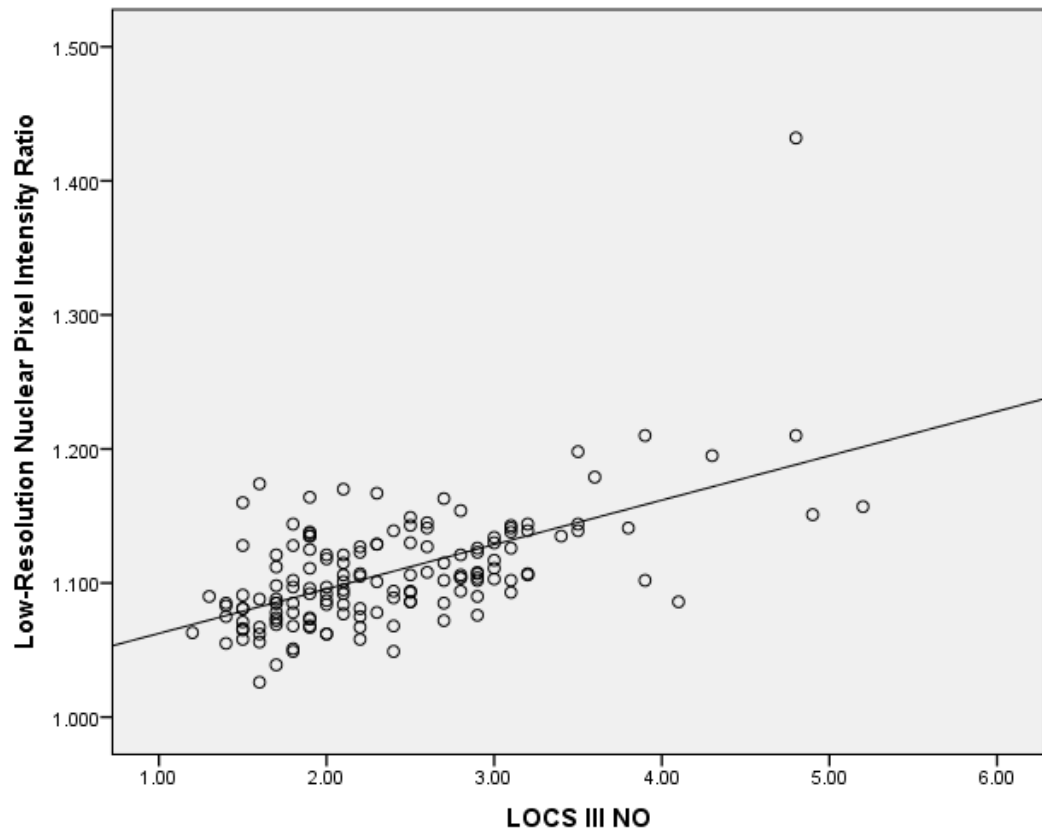


Figure 3.5.25 Scatterplot showing the significant relation between low-resolution nuclear PIR LOCS III NO ($F_{(1,127)} = 104.263$, $p < 0.001$, $R^2 = 0.451$).

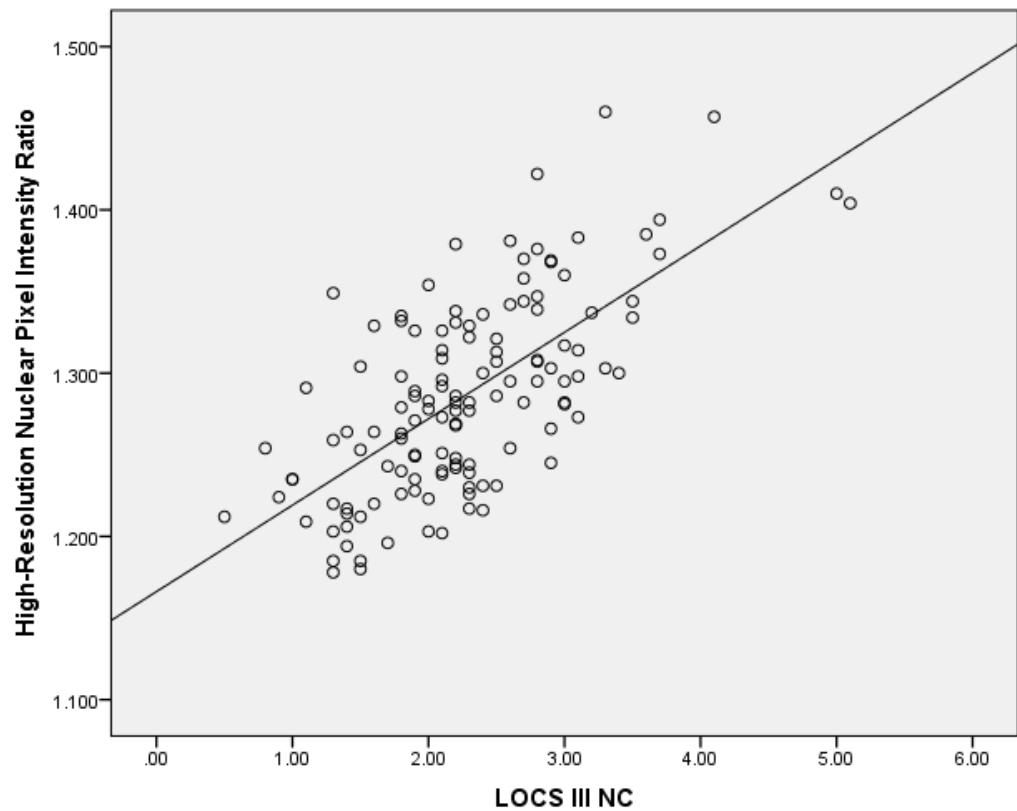


Figure 3.5.26 Scatterplot showing the significant relation between high-resolution nuclear PIR LOCS III NC ($F_{(1,147)} = 75.435$, $p < 0.001$, $R^2 = 0.339$).

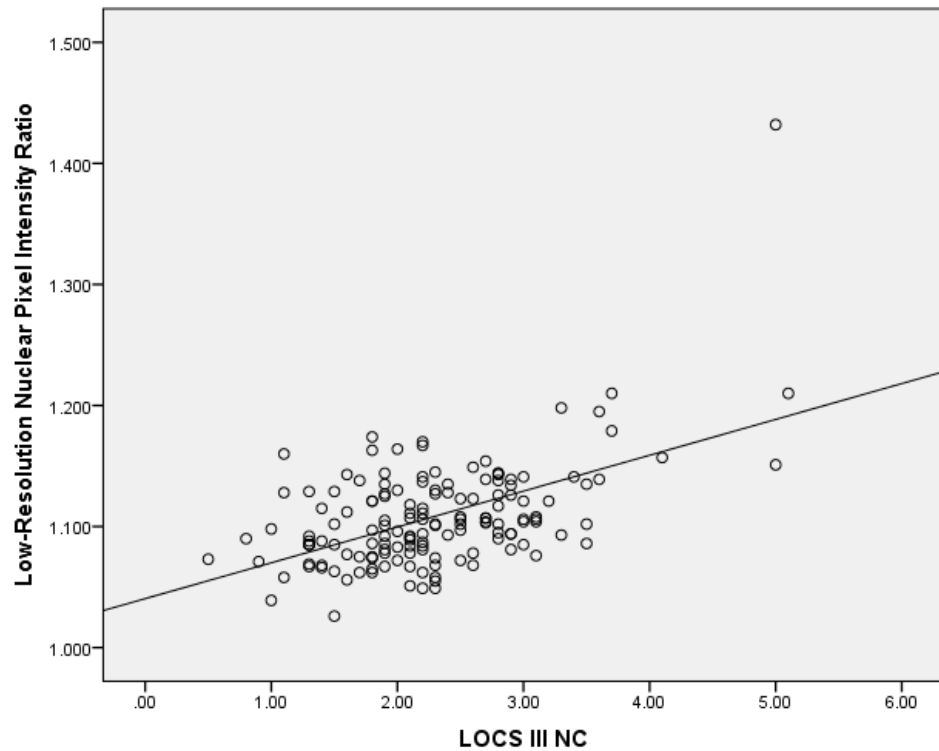


Figure 3.5.27 Scatterplot showing the significant relation between low-resolution nuclear PIR LOCS III NC ($F_{(1,147)} = 56.816$, $p < 0.001$, $R^2 = 0.279$).

The above linear regressions were also performed within each stratified age group. Associations were similar except NO showed no significant relation to low-resolution PIR for the 50 to 60-year-old group and NC was not related to low-resolution PIR in the 50 to 60 and 60 to 70-year-old groups. The significant associations were also weaker when stratified by age as compared to the entire group as a whole. Table 3.5.21 summarises the linear regressions for each age group.

Age-Range	Linear Regression			
	High-Resolution PIR vs. NO	High-Resolution PIR vs. NC	Low-Resolution PIR vs. NO	Low-Resolution PIR vs NC
50 - 60	$F_{(1,44)} = 9.363$ $p = 0.004$ $R^2 = 0.175$	$F_{(1,44)} = 8.256$ $p = 0.006$ $R^2 = 0.158$	Not significant	Not significant
60 - 70	$F_{(1,43)} = 24.662$ $p < 0.001$ $R^2 = 0.364$	$F_{(1,43)} = 5.804$ $p = 0.020$ $R^2 = 0.119$	$F_{(1,46)} = 14.268$ $p < 0.001$ $R^2 = 0.237$	Not significant
70+	$F_{(1,36)} = 18.746$ $p < 0.001$ $R^2 = 0.342$	$F_{(1,36)} = 14.559$ $p = 0.001$ $R^2 = 0.288$	$F_{(1,47)} = 20.273$ $p < 0.001$ $R^2 = 0.175$	$F_{(1,47)} = 26.589$ $p < 0.001$ $R^2 = 0.348$
All ages	$F_{(1,127)} = 128.54$ $p < 0.001$ $R^2 = 0.503$	$F_{(1,147)} = 75.435$ $p < 0.001$ $R^2 = 0.339$	$F_{(1,127)} = 104.263$ $p < 0.001$ $R^2 = 0.451$	$F_{(1,147)} = 56.816$ $p < 0.001$ $R^2 = 0.279$

Table 3.5.21 Summary of linear regression analyses for both high and low-resolution nuclear PIR compared to LOCS III NO and NC grades. Data is shown for each stratified age group and the total cohort.

A model of multiple linear regression with LOCS III NO and NC as predictors of PIR showed significant moderate relations for both high-resolution ($F_{(2,126)} = 71.472$, $p < 0.001$, $R^2 = 0.532$) and low-resolution ($F_{(2,146)} = 38.630$, $p < 0.001$, $R^2 = 0.346$). In contrast to the high-resolution model, NC was not significant as a coefficient for the low-resolution model. Values for the multiple regression are summarised in table 3.5.22.

Model	LOCS III Nuclear Measures			
	Measure	Coefficient	t	p
High-resolution PIR $F_{(2,126)}=71.472$, $p<0.001$, $R^2=0.532$	NO	0.479	4.658	<0.001
	NC	0.286	2.776	=0.006
Low-resolution PIR $F_{(3,128)}=25.121$, $p<0.001$, $R^2=0.371$	NO	0.460	3.876	<0.001

Table 3.5.22 Summary of multiple regression analyses for both high and low-resolution nuclear PIR with LOCS III NO and NC as predictors. Only the significant coefficients are displayed.

3.5.4.2 OCT Grading of Cortical Cataract

As previously mentioned, the presence of cortical cataract in the study population was low; a total of 26 participants had grades above 0.000 for cortical PIR and PAR OCT measures. None of the participants aged 50 to 60 years old received a value greater than 0.000 for either cortical PIR or PAR due to the fact that OCT imaging of the only participant who had significant cortical cataract was unsuccessful. Of those aged 60 to 70 years, only seven received cortical PIR and PAR scores greater than 0.000 and for those aged 70 years and older, 19 received grades above 0.000. As a result, the distributions for both cortical PIR and PAR were heavily skewed and not normal (Shapiro-Wilk, $p < 0.001$). The median value for PIR was 0.000 ± 0.000 (IQR) with a range of 0.000 to 1.338 and for PAR was 0.000 ± 0.000 (IQR) with a range of 0.000 to 0.808. Figures 3.5.28 and 3.5.29 show the histograms and Q-Q plots for the cortical PIR and PAR distributions. Figure 3.5.30 shows a B-scan through significant cortical cataract along with the corresponding slit lamp image.

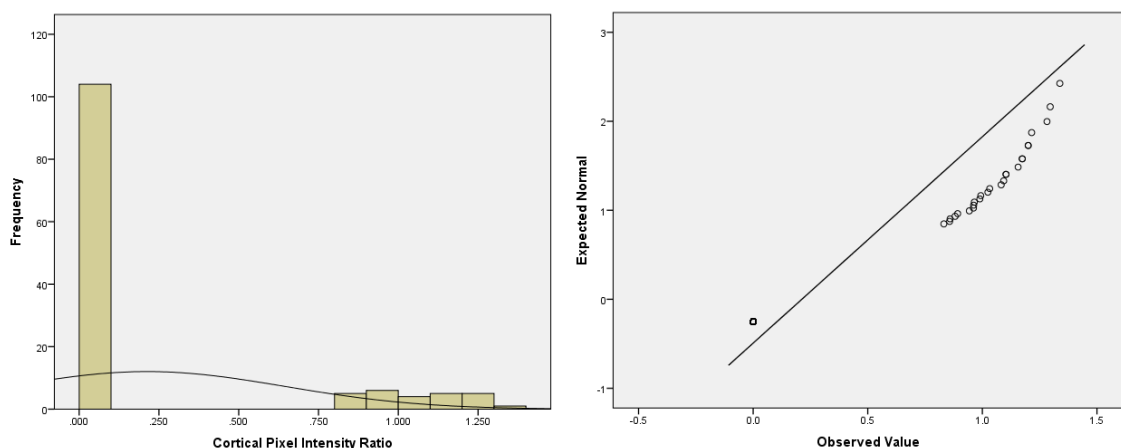


Figure 3.5.28 Histogram with overlaid distribution curve and Q-Q plot for total participant Cortical PIR.

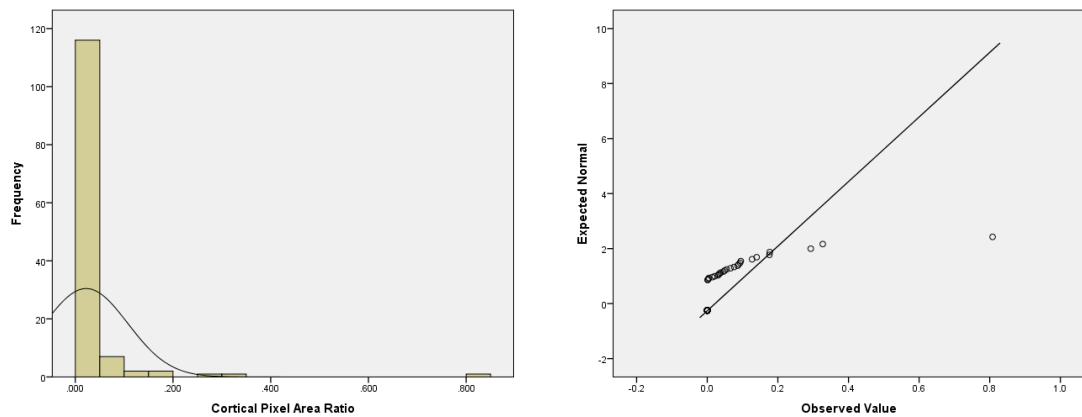


Figure 3.5.29 Histogram with overlaid distribution curve and Q-Q plot for total participant Cortical PAR.

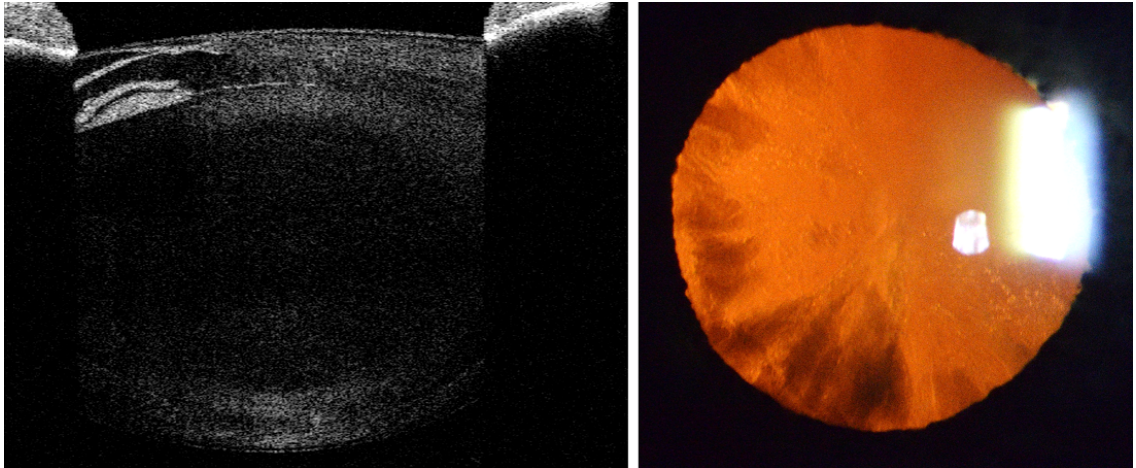


Figure 3.5.30 High-resolution OCT (left) with a cortical PIR grade of 1.156 and PAR of 0.808. The corresponding optic section is shown on the right with a LOCS III C grade of 3.5. The OCT B-scan was oriented at 57 degrees in order to image through the most significant area of cortical opacity.

Spearman's correlation analyses showed significant associations between age as well as visual acuity and contrast sensitivity to both cortical PIR and PAR. Age was moderately correlated (PIR: $\text{Rho} = 0.458$, $p < 0.001$; PAR: $\text{Rho} = 0.468$, $p < 0.001$) followed by VA (PIR: $\text{Rho} = 0.298$, $p = 0.001$; PAR: $\text{Rho} = 0.301$, $p < 0.001$) and CS (PIR: $\text{Rho} = -0.264$, $p = 0.002$; PAR: $\text{Rho} = -0.277$, $p = 0.001$). There was no significant correlation between either cortical measure and straylight.

Linear regression was performed comparing both cortical PIR and PAR to age and measures of visual function. Statistically weak significance was shown for certain measures; these are outlined in table 3.5.23.

	Cortical PIR			Cortical PAR		
	F	Sig.	R ²	F	Sig.	R ²
Age	(1,128) = 31.661	p < 0.001	0.198	(1, 128) = 6.516	p = 0.012	0.048
VA	(1, 128) = 6.119	p = 0.015	0.046	Not significant	N/A	N/A
CS	(1, 128) = 8,861	p < 0.003	0.065	Not significant	N/A	N/A
log[s]	Not significant	N/A	N/A	Not significant	N/A	N/A

Table 3.5.23 Summary of linear regression analyses for both cortical PIR and PIR compared to age and measures of visual function.

A Spearman correlation showed strong association between PIR and PAR values ($\rho = 0.983$, $p < 0.001$) however the relationship between the two measures was much weaker when linear regression was performed ($F_{(1, 128)} = 50.609$, $p < 0.001$ $R^2 = 0.283$). Figure 3.5.30 shows the scatterplot for cortical PIR vs PAR.

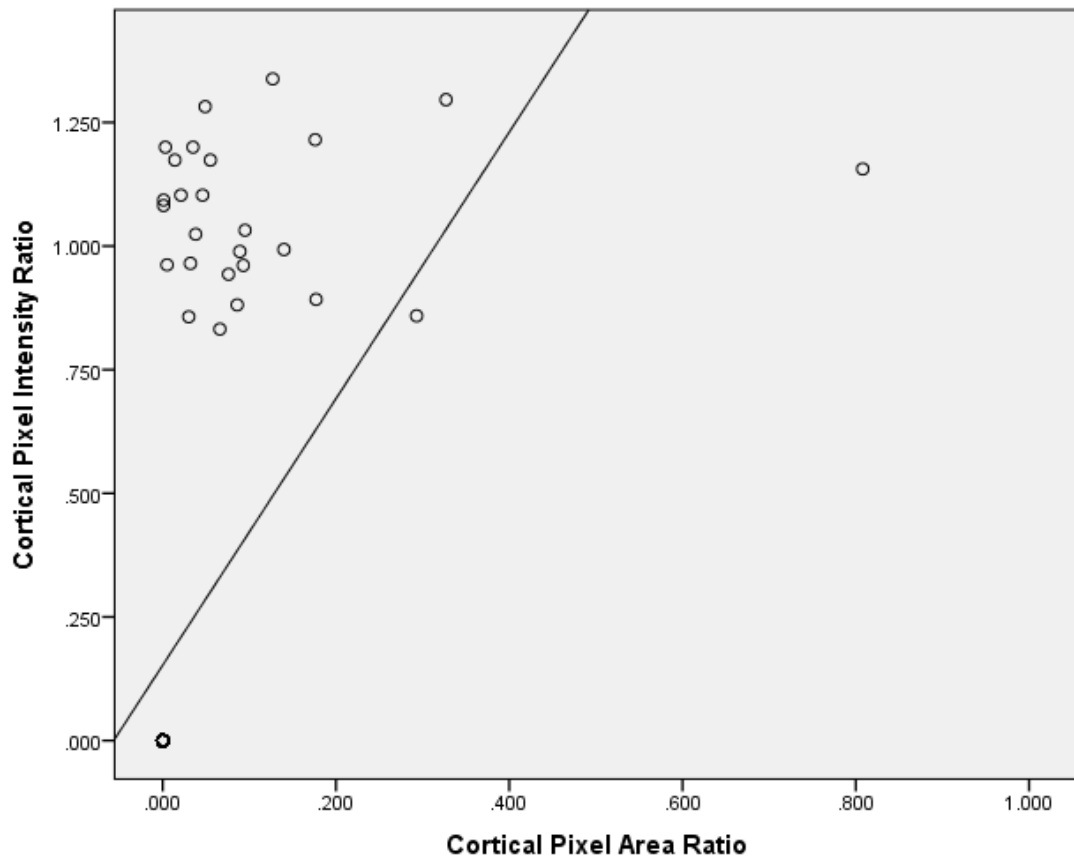


Figure 3.5.30 Scatterplot showing the significant relation between cortical PIR and PAR ($F_{(1, 128)} = 50.609$, $p < 0.001$, $R^2 = 0.283$). Note: the point at (0.000, 0.000) represents all of the multiple data points from B-scans where there were no cortical opacities present.

A model of multiple regression with VA, CS and log[s] as predictors of PAR showed significance, although with a very weak association ($F_{(3, 108)} = 2.795$, $p = 0.044$, $R^2 = 0.072$). CS was the only predictor that showed significance in this model. A significant but weak association was also shown with PIR as the dependent variable ($F_{(3, 108)} = 3.260$, $p < 0.024$, $R^2 = 0.083$). In contrast to PAR, CS was not a significant predictor. The regression model is summarised in table 3.5.24.

Model	Measures of Visual Function			
	Measure	Coefficient	t	p
Cortical PAR $F_{(3, 108)} = 2.795$, $p = 0.044$, $R^2 = 0.072$	VA	0.038	0.369	0.713
	CS	-0.240	-2.140	0.035
	log[s]	0.019	0.181	0.856
Cortical PIR $F_{(3, 108)} = 3.260$, $p = 0.024$, $R^2 = 0.083$	VA	0.099	0.957	0.341
	CS	-0.219	-1.960	0.053
	log[s]	0.023	0.223	0.824

Table 3.5.24 Multiple regression analyses of OCT Cortical PIR and PAR vs measures of visual function.

When stratified by age, there was no significant correlation or regression for age or any measure of visual function in any age-group to either cortical PIR or PAR.

3.5.4.2.1 Comparisons of LOCS III Cortical Grades and OCT Cortical Measures

As with the nuclear PIR comparison to LOCS III N grades conducted in section 3.5.4.1.2, cortical PIR and PAR measures were compared to LOCS III C grades. Spearman correlation showed strong associations between LOCS III C grades and both cortical PIR ($Rho = 0.799$, $p < 0.001$) and PAR ($Rho = 0.812$, $p < 0.001$). When stratified by age, strong correlations still existed in both the 60 to 70-year-old and 70-years-and-older age groups; correlation analyses were not possible in the 50 to 60-year-old group due to the cortical PAR and PIR grades being constant at 0.000. Table 3.5.25 summarises the correlations for each age group.

	Age Range	Cortical PIR	Cortical PAR
LOCS III C	50 - 60	N/A	N/A
	60 - 70	$Rho = 0.716$ $p < 0.001$	$Rho = 0.726$ $p < 0.001$
	70+	$Rho = 0.819$ $p < 0.001$	$Rho = 0.910$ $p < 0.001$
	All ages	$Rho = 0.799$ $p < 0.001$	$Rho = 0.812$ $p < 0.001$

Table 3.5.25 Summary of Spearman's correlations for both cortical PIR and PAR compared to LOCS III C. Data is stratified by age and compared in total.

Linear regression showed moderate to strong relations of LOCS III C grades to cortical PAR ($F_{(1, 128)} = 99.384$, $p < 0.001$, $R^2 = 0.437$) and PIR ($F_{(1, 128)} = 358.740$, $p < 0.001$, $R^2 = 0.737$) respectively. Figures 3.5.31 and 3.5.32 show the scatterplots for the regressions.

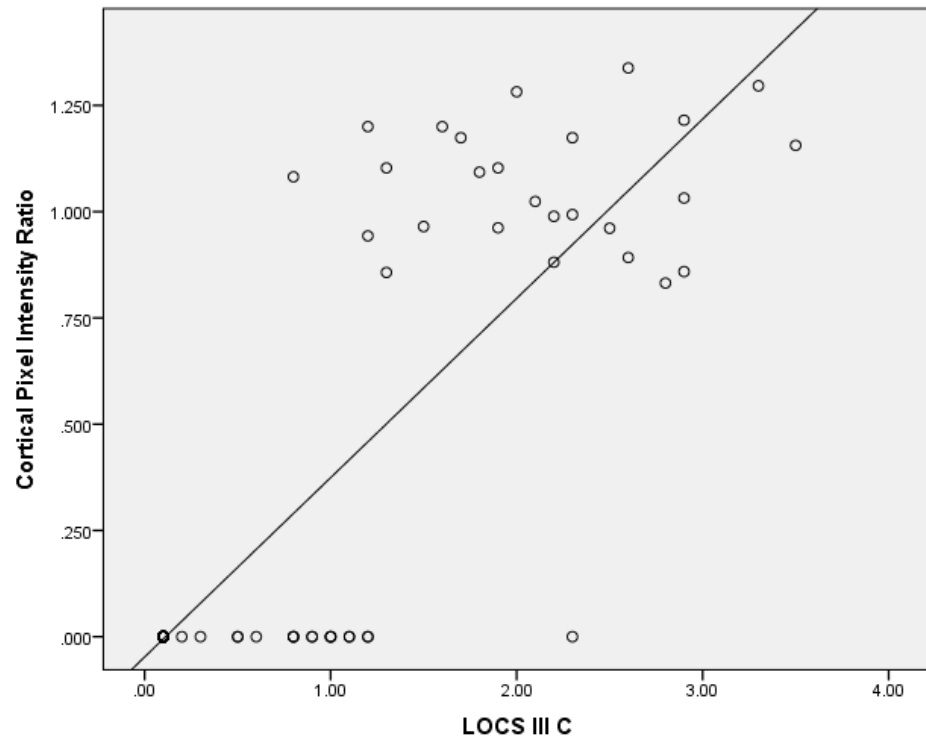


Figure 3.5.31 Scatterplot showing the significant relation between cortical PIR and LOCS III C ($F_{(1,128)} = 358.740$, $p < 0.001$, $R^2 = 0.737$).

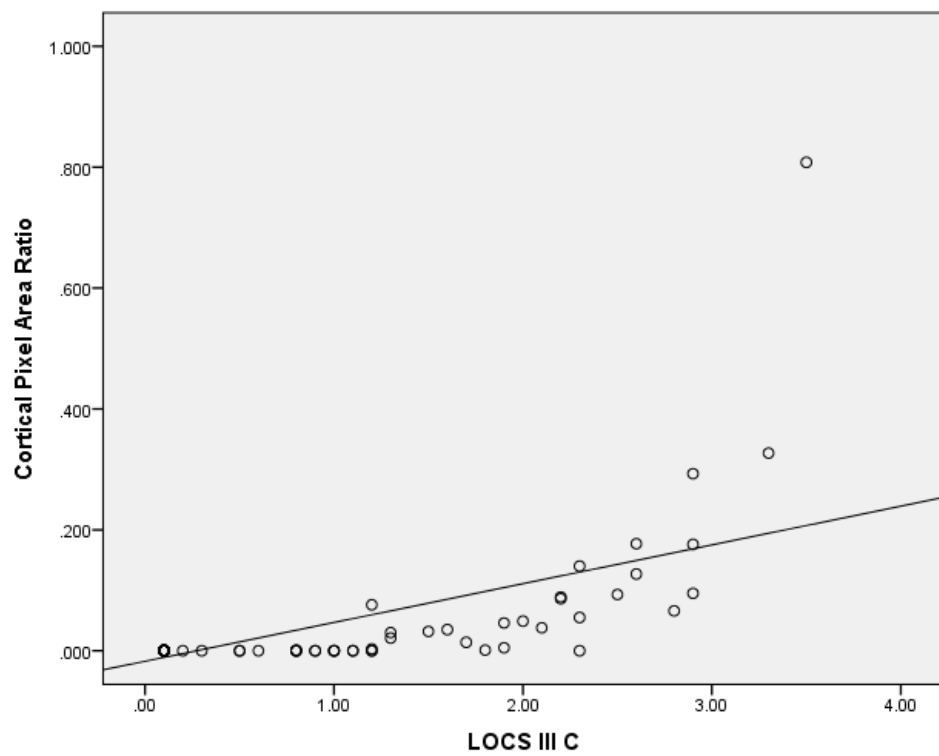


Figure 3.5.32 Scatterplot showing the significant relation between cortical PAR and LOCS III C ($F_{(1,128)} = 99.384$, $p < 0.001$, $R^2 = 0.437$).

The moderate to strong relation between LOCS III C and cortical OCT grades remained when stratified by age. In both the 60 to 70-year-old and 70-years-and-older groups PIR showed a stronger relation to LOCS III C than PAR. The data are summarised in table 3.5.26. Again, the regression was not performed for the group of those aged 50 to 60-years due to the constant value of 0.000 for all cortical PIR and PAR grades.

Age-Range	Linear Regression	
	Cortical PIR vs LOCS III C	Cortical PAR vs LOCS III C
50 - 60	N/A	N/A
60 - 70	$F_{(1,43)} = 70.124$ $p < 0.001$ $R^2 = 0.620$	$F_{(1,43)} = 42.019$ $p < 0.001$ $R^2 = 0.494$
70+	$F_{(1,37)} = 95.251$ $p < 0.001$ $R^2 = 0.720$	$F_{(1,36)} = 28.579$ $p < 0.001$ $R^2 = 0.436$
All ages	$F_{(1,128)} = 358.740$ $p < 0.001$ $R^2 = 0.737$	$F_{(1,128)} = 99.384$ $p < 0.001$ $R^2 = 0.437$

Table 3.5.26 Summary of Linear regression for both cortical PIR and PAR compared to LOCS III C. Data is stratified by age and compared in total.

3.5.4.3 OCT Grading of Posterior Subcapsular Cataract

Successful OCT imaging and grading of posterior-subcapsular opacification was only successful for one of the five participants who received LOCS III P scores over 0.1. The OCT image was graded for both PIR and PAR. The values for the left eye of participant number 51 were 1.267 and 0.132 for PIR and PAR respectively. Participant number 51's LOCS III P score was 1.2. Figure 3.5.33 shows the participant's SL retro-illumination and posterior high-resolution OCT images. Statistical analyses were not performed on OCT PSC measures as the lack of data would yield no statistical power.

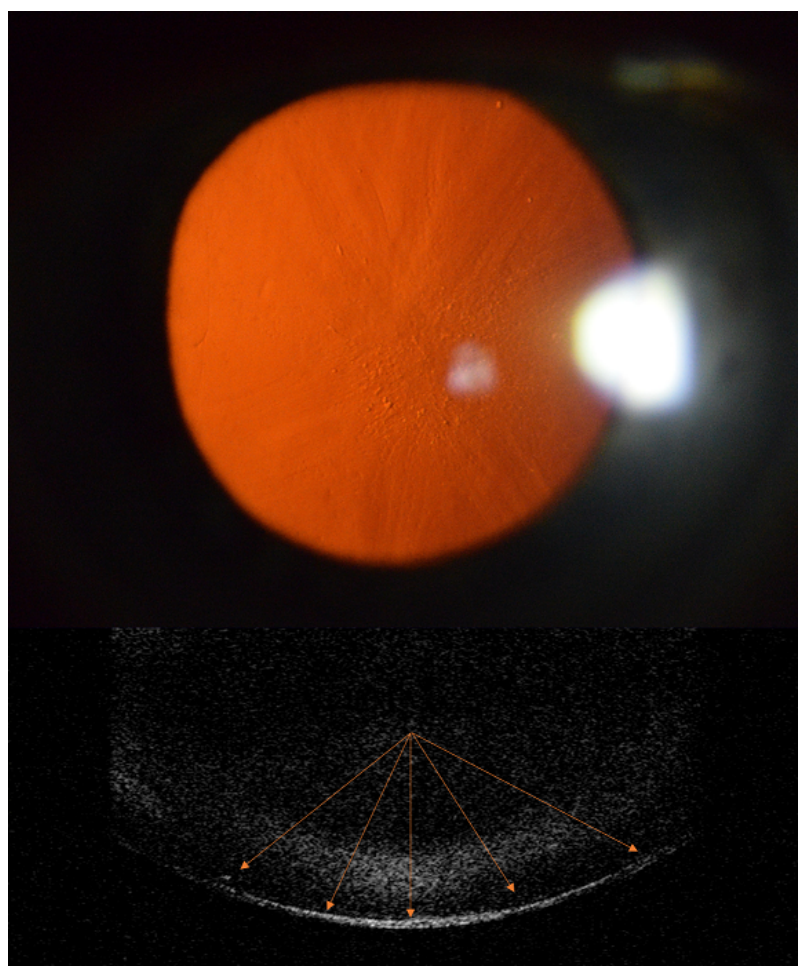


Figure 3.5.33 Retroillumination of a PSC is seen (top) with a LOCS III P grade of 1.2. The corresponding high-resolution OCT is shown below with a PSC PIR grade of 1.267 and PAR of 0.132; the orange arrows show the extent of the PSC.

3.5.4.4 Repeatability of OCT Grading

To assess the performance of OCT grading of lens opacity, 19 randomly chosen high-resolution B-scans (15% of imaged eyes) were regraded for PIR by the researcher (ASM). Figure 3.5.34 shows the Bland Altman plot for the original and regraded images. It can be seen that there was very high repeatability for OCT grading of opacification. Bias between the original and regraded B-scans was -0.00005.

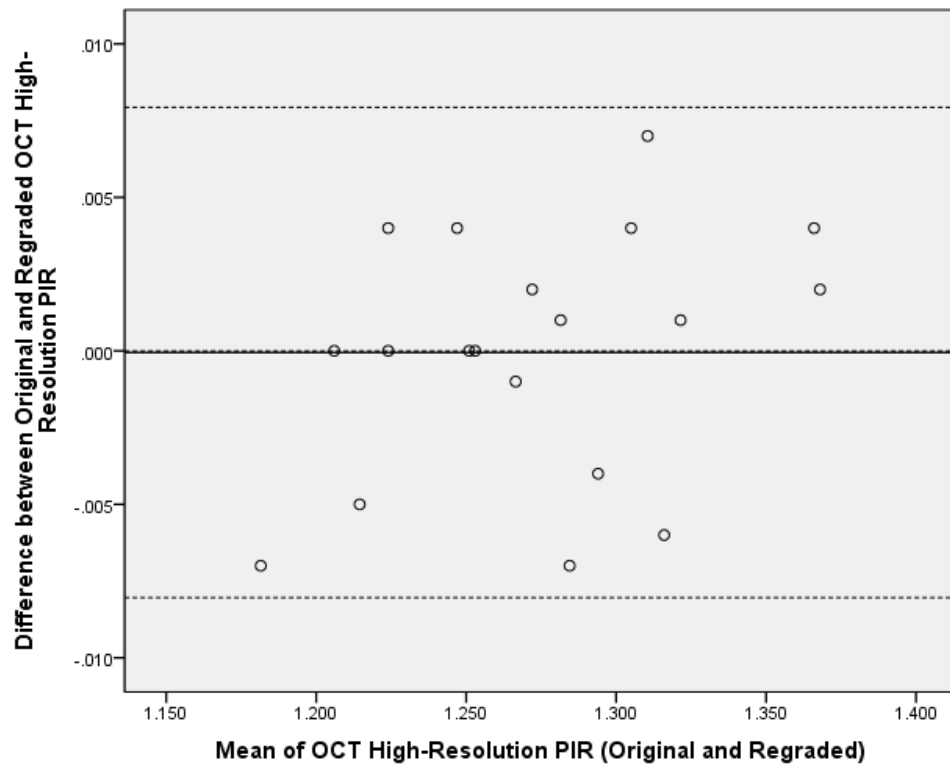


Figure 3.5.34 Bland-Altman plot showing agreement between regraded images for PIR.

3.6 Discussion

3.6.1 Participants and Success Rates

This study effectively recruited the desired sample size of 90 participants however, as mentioned in section 3.5.1, the stratified age groups did not contain 30 participants each. The numbers of participants were slightly higher in the lower age groups simply due to the demographics of the University Eye Clinic where most of the recruiting was conducted. The exclusion criteria also played a detrimental role due to the higher presence of ocular disease and pseudophakia with increasing age. Although this skewness occurred, the sample sizes were very similar across age groups when taking into account the numbers of eyes imaged with 36%, 33% and 31% of total eyes imaged in the 50 to 60, 60 to 70 and 70-years-and-older age groups respectively. This worked nicely for statistical analyses.

Success rates for obtaining measures of visual function were excellent across all participants apart from retinal straylight. Visual acuity and contrast sensitivity were measured in 100% of eyes. This was not the case for log[s], with only an 85% success rate. While VA and CS are easily and quickly performed clinical measures for which all participants were familiar, the C-Quant instrument was a new experience for all. Some participants found the C-Quant device and its requirement for multiple trial responses tedious and difficult to complete.

Slit-lamp imaging and LOCS III grading was also very successful in the study group with 100% of eyes imaged at the slit-lamp and graded. Imaging using the modified slit-lamp was quick to perform with photographs only taking slightly over 500ms to capture (from the press of the trigger). Multiple photographs could be taken in rapid succession to ensure gradable images were captured. Participants also found the process easy as imaging required minimal cooperation only requiring positioning into the head and chinrests with

fixation straight ahead. The slit-lamp objective and illumination systems also did not come into close contact with participants which added to their comfort.

The excellent capture rates that occurred in slit-lamp photography became slightly reduced upon imaging with the Visante AS-OCT. More specifically, while low-resolution OCT B-scan capture rate was high at 96%, this dropped to 83% with high-resolution scans. The ergonomics required during OCT imaging were much more awkward compared to SL imaging. Participants were required to place their chin and forehead on rests which continually moved in order to achieve correct alignment and focussing of the crystalline lens. The OCT instrument's exterior and lens system were also very close to each participant's face and eye respectively causing discomfort in some cases. Finally, participants were required to keep their body positioning still and eye fixated on the internal target without blinking while images were captured.

As the Visante AS-OCT is of the time-domain modality, image capture was much slower and therefore, more susceptible to image artefacts compared to more modern Fourier-domain technologies. Low-resolution B-Scan capture was more successful than high-resolution imaging due to the faster acquisition time (256 vs 512 A-Scans) and facility to image the entire lens at once. A major problem during high-resolution capture was acquiring adequate quality scans of the posterior lens; the limits of the focusing and penetration capabilities of the Visante AS-OCT were straddled to achieve this and therefore, caused difficulty in obtaining images. Also, difficulty in maintaining accurate alignment of the eye added to the lower success rate in capturing high-resolution images of the posterior lens. Due to this, any eye where a posterior high-resolution scan was not possible could not be graded. It should be noted that over 750 OCT images were taken through the study and as it progressed, the researcher's skill in obtaining gradable images increased greatly. In one case, successful imaging of a participant with cortical cataract

occurred however, a power failure caused the image files to become corrupted upon saving.

3.6.2 Visual Acuity

Participants' visual acuity measures corresponded well with those in the normal population. Elliot et al.'s (1995) data of logMAR VAs of those without ocular disease and stratified by age showed mean values of -0.10 (CI: 0.00 to -0.20) for those aged 50-59 years, -0.06 (CI: 0.04 to -0.16) for those aged 60 to 69 years and -0.02 (CI: 0.08 to -0.12) for those aged 70 and older. All of this study's median and mean values for each stratified age group fit within the appropriate range of the above-mentioned figures. As Elliott et al.'s study cohort consisted of those with optimal correction and the absence of ocular disease, this suggests that the participants in this study were of similar characteristics in regard to their refractive correction and ocular health status. As mentioned in Chapter 3, while habitual correction was used to determine VA and most participants had undergone recent eye exams based upon their histories, the researcher used a pinhole to determine whether an improvement occurred in the few cases where participants were unsure of their last refraction; there was no improvement of VA in any of these cases. The VA levels of participants suggests that most did not have a level of lens opacity that would affect high contrast vision.

3.6.3 Contrast Sensitivity

Most participants had good levels of contrast sensitivity across all age ranges as evidenced by the heavily skewed distribution. All median CS levels for each stratified age group were higher than 1.80 – a normal value for those aged 20 to 50 years of age (Elliott 2007). This suggests the low presence of significant cataract in the study cohort as it has been shown that large letter CS, like that of the Pelli-Robson chart, is often not affected by early cataract (Elliott and Situ 1998). It has also been shown that early nuclear cataract only

begins to affect CS at spatial frequencies above 12 CPD and early cortical/PSC have a greater effect on CS but only at spatial frequencies above 6 CPD (Chua *et al.* 2004); Pelli-Robson CS would not be effective in this participant group as its spatial frequency is 1 CPD and the majority of cataract in participants was nuclear, with only five having PSC. When stratified by age, mean and median CS levels remained within the normal range for each group. As expected, lower CS was correlated and related with increasing age (Elliott 2007; Mäntyjärvi and Laitinen 2001; Chua *et al.* 2004).

3.6.4 Retinal Straylight

As mentioned previously, the success rate with the C-Quant was not 100% as opposed to the other measures of visual function. This may have played a major factor in its statistical analysis relating to cataract, as many participants with the worst levels of LOCS III NO and NC did not obtain a reliable log[s] value. In fact, the eye with the highest NO and NC scores of 5.2 and 4.1 respectively (#41 LE) was unsuccessful in obtaining a log[s] value. Out of the 29 eyes with moderate NO levels of 3.0 and above, 7 (24%) were missing C-Quant data. The missing log[s] values for LOCS III C data were not as dramatic however, and as most cortical cataract was in the periphery of the lens, log[s] would most like not have been affected.

Log[s] and VA were quite independent from one another and this has been confirmed by previous work comparing the two measures (Gholami *et al.* 2017; Michael *et al.* 2009; Van Den Berg *et al.* 2007). Age was found to be related to log[s] thorough both correlation and linear regression analyses; this coincides with other studies comparing the two measures (Gholami *et al.* 2017; Van den Berg *et al.* 2013; Van Den Berg *et al.* 2007). Linear regression and correlation also showed that participants' log[s] increased with worsening CS, with very similar strengths of association between the measures as those found by Michael et al. (2009).

3.6.5 LOCS III Grading and its Interaction with Measures of Visual Function

The results and trends were interesting when comparing measures of visual function against LOCS III scores. Many of the results aligned with previous research comparing VA, CS and log[s] against LOCS III grades of cataract. Gholami et al. (2017) reviewed and performed statistical analysis on the combined results of five studies that compared log[s] to LOCS III grading as well as VA and CS in cataract populations. While the various definitions of cataract in each interpreted study differed from one another, early cataract LOCS values were defined as approximately 2.0 while more moderate cataract included levels of 3.0 or more (Gholami *et al.* 2017). The authors found increasing levels of log[s] with each of the age-related cataract types with PSC followed by cortical and then nuclear having the greatest to lowest effect respectively. In this study, nuclear cataract had the strongest relation to log[s] however, the presence of cortical and PSC opacities were very low. All three cataract types were very early in their stages in this study with NO and NC median values at just over 2.0 and both C and P median values being the lowest possible grade of 0.1. This is in contrast to the above study that selected participants specifically for cataract. Also, it should be noted that some of the studies reviewed by Gholami et al. (2017) did not dilate the pupil to perform LOCS III grading and so should be considered with caution as LOCS III requires adequate dilation in order to effectively grade opacity (Chylack *et al.* 1993).

A study included in the above mentioned review article conducted by Filgueira et al. (2016), looked at early nuclear (14 eyes with LOCS III NO1 and NO2) and PSC (20 eyes LOCS III P1 and P2) grades in a population aged 50 to 70 years, and compared the measures to VA, contrast threshold and log[s]. The authors found a much stronger correlation of log[s] to LOCS III NO scores compared to this study, but this is likely due to the selection of participants only with cataract by Filguiera et al. In contrast, the correlation between LOCS III grades and VA in Filgueira et al.'s paper was very similar to

this study. Although this study and the one conducted by Filgueira *et al.* confirm the link between increasing log[s] and decreasing VA with worsening LOCS III scores, the data from this study may provide a more reasonable account of the relation between the measures as the sample size is much larger.

Studies on a group of over 2000 European drivers have reported and compared the measurements of VA, CS, log[s] and grading of cataract using LOCS III in various ways (Michael *et al.* 2009; Nischler *et al.* 2010; Van Den Berg *et al.* 2007). As with this study, the above research on European drivers showed statistically significant relations between increasing LOCS score and increasing log[s] as well as worsening Pelli-Robson CS and VA (Michael *et al.* 2009; Nischler *et al.* 2010). These relations are all similar to this study's NO and NC relations to visual function however, they were not as strong in this study. Michael *et al.* (2009) also carried out multiple linear regression with VA, CS and log[s] as predictors of LOCS III scores and, like the results of this study for nuclear grades, found them all to be significant. It should be noted that, although the presence of cataract was low in this study, its results may be a better reflection of the real world for a few important reasons: the above research studies in Europe did not dilate participants' pupils prior to LOCS grading and the grading was also carried out by non-medical staff; the LOCS III N, C and P measures for each eye in these studies were also averaged together into a single number – a highly unorthodox practice (Van Den Berg *et al.* 2007; Michael *et al.* 2009). These discrepancies with LOCS III grading most likely caused an over-estimation of the severity of cataract and therefore, showed stronger relations to visual measures as compared to those in this study.

While the LOCS III scores for C in this study did correlate with all measures of visual function, they only showed significant relations to CS and log[s] upon linear regression, albeit very weakly; as the presence of cortical and PSC were very low in this study it seems

logical, based on the limited data available, that their LOCS III measures would be related in the same way to measures of visual function outlined in the above reviewed studies.

This study is unique in that it did not single out only LOCS III grades for eyes confirmed to have cataract and then compare them to measures of visual function. The results showed similarity to previous research but the more fastidious attention to the correct LOCS III protocol, coupled with the very good inter-observer repeatability in the grading of cataract by clinicians, may provide a more realistic view of the interaction between visual function and LOCS grading of cataract.

3.6.6 Comparison of OCT and LOCS III Grading of Cataract

Overall, this study demonstrates that OCT grading of cataract was very comparable to LOCS III grading. The correlations between nuclear PIR and age as well as measures of visual function were very similar to those between LOCS III nuclear grades and the measures, especially for high-resolution nuclear PIR. Linear regression again showed similarities between LOCS III nuclear grades and OCT nuclear PIRs and their relation to age, VA, CS and log[s]. The regressions showed a slightly weaker relation between PIR values and all variables compared to LOCS III nuclear grades however, this may be due to the missing data from the poorer imaging success rates that occurred with OCT. Things were different when comparing the multiple regression models of measures of visual function as predictors of nuclear opacity grades; while all predictors were significant for LOCS III NO and NC, only log[s] showed significance for high- and low-resolution PIRs; again this may be due to the missing data for PIR from those with higher levels of cataract but also could reflect the relationship between the scatter of light by the lens in disability glare (log[s]) and the imaging modality of OCT.

There were very good agreements between the measures of opacity when nuclear PIRs were directly compared to LOCS III nuclear grades. Moderate to borderline-strong correlations occurred between high-resolution and low-resolution PIRs when compared to LOCS III NO. The correlations were similar between high-resolution PIR and NC but this was not the case with low-resolution PIR and NC where overall, there was a moderate correlation but significance disappeared in the 50 to 60 and 60 to 70-year-old groups. In all cases high-resolution PIR showed a stronger correlation than low-resolution PIR to both NO and NC even though there were fewer images that were graded. This suggests that high-resolution imaging is more effective for cataract grading.

Linear regression showed a stronger trend between high-resolution PIR and LOCS III NO and NC grades compared to low-resolution PIR. This was even the case although there was less data in the high-resolution sample. The stronger relation between high-resolution PIR and LOCS III nuclear grades became more evident when data was stratified by age. Significant relations between high-resolution PIR and NO and NC remained for all age groups whereas low-resolution PIR lost significance compared to NO and NC for the 50 to 60-year-old age group and to NC for the 60 to 70-year-old group. To further confirm the stronger relationship between high-resolution PIR and LOCS III nuclear values, the models of multiple regression with NO and NC as predictors of either high-resolution or low-resolution PIRs showed a stronger relation to high-resolution scans with both NO and NC holding statistical significance as opposed to just NO for low-resolution scans.

This study found good agreement between nuclear PIR and LOCS III measures. There are many strengths compared to the previous two studies that have attempted to grade nuclear cataract with AS-OCT. In Wong et al.'s (2009) study, the 55 eyes were selected from a population of participants with known moderate to severe cataract; this will have biased the slightly stronger relation they found comparing PIR to NO and NC compared

to this study, where the severity of cataract was low. Wong et al. (2009) also seemed to have used an incorrect protocol for LOCS III assessment as their grades were on a 0.5 rather than 0.1 interval scale; this could exaggerate the correlations between PIR and LOCS III. Furthermore, unlike this study, raw sensor data was not used to determine pixel intensity by Wong et al (2009); the authors used commercial software to analyse the B-scans that were pre-processed by the Visante AS-OCT and captured using the instrument's corneal imaging mode. This study utilised a much more robust method by processing and analysing the Visante AS-OCT's raw sensor data using custom software to ensure as little as possible information was lost. An example of this is the lack of a correlation between VA and either OCT or LOCS III grades by Wong et al. (2009). This study had much lower LOCS III NO and NC grades compared to Wong et al. but correlation and regression found significant associations between VA and both PIR and LOCS III nuclear measures. It is most likely that the incorrect LOCS III grading scale was not sensitive enough to find any correlation by Wong et al (2009). Also, the possible loss of information in the methods used by Wong et al. for processing and analysis of the B-scans may have also contributed to the lack of correlation.

The methods in relation to LOCS III grading used by Kim et al. (2016) in their study assessing nuclear cataract with a surgical OCT system have also shown weakness compared to this study. Kim et al. (2016) graded cataract in 47 eyes with LOCS III NO scores above 3.0 however the researchers, similarly to Wong et al. (2009), erroneously used a 0.5 interval to assign grades, rather than the correct scale of 0.1. In their analysis of OCT images for nuclear opacification, the researchers did not appear to grade the anterior chamber to determine a background pixel intensity; this will most likely have affected their nuclear OCT grades as there is certain to be, at least slight, variation in background intensity between different images. Kim et al. (2016) did still find a significant correlation between their OCT measure of nuclear cataract and LOCS III NO scores. As described

above in relation to the study by Wong et al. (2009), the methods developed and utilized in this study also provide a much more convincing association between LOCS III and OCT based assessment of cataract as compared to those by Kim et al. (2016).

This study is the first to assess cortical cataract using OCT. While there was a low presence of cortical cataract in the study cohort, an effective and objective grading system through the use of PIR and PAR was developed. Both PIR and PAR were useful measures of cortical opacification based upon the morphology of cortical opacity; in some cases, the size of cortical opacity was large but low in intensity while in others, the exact opposite occurred. This is reflected in the correlation and regression analysis comparing cortical PIR and PAR; the measures were strongly correlated but moderately related under regression precisely because of this discrepancy between size and intensity of opacification in some cases.

Cortical PIR and PAR measures were very comparable to LOCS III C grades showing a moderate to strong association in both correlation and regression analyses. This is reinforced by the similar correlation and regression strengths between each measure of opacification and age, as well as measures of visual function; although PIR and PAR were not associated with straylight while LOCS III C was, this is most likely due to inadequate data obtained resulting from the lower success rates of OCT capture and acquisition of log[s] values. The two variations of measuring opacity with OCT also present a great strength compared to LOCS III grading as the latter technique requires the observer's subjective opinion of cortical area with specific disregard to darkness or colour when grading cortical or PSC opacities. There is a limitation to the OCT analysis of cortical opacity in this study as only single B-scans through the greatest position of cortical cataract could be imaged; this can be corrected in the future through the use of the much faster and higher-resolution SS-OCT technology in the form of rasterised volumetric scans of

the entire crystalline lens.

There are only two other studies examining non-nuclear cataract with OCT. Chan et al. (2014) imaged 37 eyes with significant posterior polar cataract requiring surgery and developed a grading system based upon the position of the opacity in regard to the posterior capsule. This was a rudimentary grading system that did not involve any objective analysis using software, but simply relied on the observer to estimate the position of the opacity when viewing the B-scan (Chan *et al.* 2014). In a small report, Kymionis et al. (2014) also imaged posterior polar cataract in three patients using a Visante OCT as a means of assessing capsule integrity. While Chan et al.'s and Kymionis et al.'s work focused on assessing posterior polar cataract in order to identify risk of capsule rupture during surgery, this study presents a much more robust method of assessing the morphology and severity of lens opacity objectively and could be used for this purpose as well. The fact that PSC, which is much subtler in appearance to polar cataract, was successfully imaged and graded with OCT in this study further supports this method as an effective means of assessing lens opacity.

3.7 Conclusion

This study set out to develop a robust and objective method of assessing lens opacity using AS-OCT. Through the development of customised software for processing, segmenting, and grading raw OCT sensor data, and a protocol for acquiring high quality B-scans of the crystalline lens, this has been achieved. OCT measures of PIR and PAR were comparable to LOCS grades for nuclear, cortical, and posterior-subcapsular opacity but the developed method of OCT analysis allows any area of the lens to be graded, enabling the assessment of non-age-related opacification. Furthermore, the high repeatability of this method reinforces its objectivity.

The major limitation of this study is the use of the time-domain modality of OCT acquisition. Even in its high-resolution mode, the Visante AS-OCT captures at a slow rate and inferior resolution compared to more modern Fourier-domain modalities. In High-resolution mode, the Visante AS-OCT only allowed capture of a single B-scan along one meridian of one-half of the crystalline lens at a time. As mentioned previously, more modern SS-OCT technology would allow high-speed rasterised volumetric scans of the entire lens; this would enable opacities to be segmented and graded in entirety as opposed to through one section of the lens containing the greatest level of opacity.

Overall, this study has demonstrated a method of imaging and grading lens opacity that is superior to the commonly used subjective methods. The Visante's high-resolution imaging of the crystalline lens and the subsequent analysis using the custom software, gives the ability to objectively assess opacity at any location within the crystalline lens. Further work is warranted in applying this modality using more modern OCT technology, and developing the software to shift from manual to automated segmentation and analysis. This will provide a complete tool for screening and monitoring the progression of cataract.

Finally, OCT imaging and analysis is applicable to both age-related and all other forms of lens opacity and, therefore, presents an ideal solution of monitoring the condition in disease, and as a tool to foresee and prevent complications during surgery.

Chapter 4: Investigating Cataract and Retinal Structure in Down Syndrome

4.1 Introduction

The following section will outline studies involving assessment of cataract in a Down Syndrome population and, as a corollary, the assessment of retinal structure in this same cohort using OCT. As mentioned in Chapter 1, there is a paucity of information surrounding the severity and morphology of cataract that exists in DS. Also, the disputed link between cataract and beta-amyloid requires the determination of the typical characteristics of lens opacity in DS. The method developed in Chapter 3 was used to assess lens opacity while the retina was imaged using the Spectralis OCT described in section 2.1.5.2. The imaging and assessment of these two structures will be discussed in chapters 5 and 6 while the methods are outlined below.

4.2 Sample Size Determination and Recruitment

4.2.1 Sample Size

The sample size was determined through a power calculation based on 90% power and 5% significance. A 59% prevalence of cataract in a DS population aged 40 years and over (Castane *et al.* 2004) against a 33% prevalence in a typically developed population aged 70 to 79 years (Reidy *et al.* 1998) was used in the calculation. Based on this, the sample size was determined to be 30 participants. The participant age range was selected to be from six to 60-years. The calculation is shown below:

$$n = \frac{1}{d^2} \left(z_{\alpha} \sqrt{\pi_0(1 - \pi_0)} + z_{\beta} \sqrt{\pi_1(1 - \pi_1)} \right)^2$$

$$\therefore n = \frac{1}{0.26^2} \left(1.6449 \sqrt{0.33 \times 0.67} + 1.2816 \sqrt{0.59 \times 0.41} \right)^2$$

$$\therefore n = 29.1$$

4.2.2 Recruitment

Participants were recruited from the paediatric and special needs clinic at Ulster University's optometry department which contains a cohort of children with DS. Those within the specified age range and who met eligibility criteria were identified through patient records; their parents or guardians were contacted via telephone to determine interest in participation. Appointments were set for participants to attend a one-hour appointment at the eye clinic at Ulster University; all parents and guardians were given a PIS and consent form to sign (see appendix A-3). Parents and guardians of participants with DS who were attending the eye clinic were also solicited for participation. In this case, PIS and consent forms were given directly to parents and guardians; in some cases they elected to participate in the study directly after the eye exam and in others, appointments were made for them to return at a later date.

Young adults and children with DS were also recruited from the Down's Syndrome Vision Research Unit at Cardiff University. This centre is the UK's largest research unit examining vision and the eye in DS. Potential participants who fit the eligibility criteria were identified from the cohort of over 250 and an information package was mailed to their parents and guardians inviting them to take part in the research. The information package consisted of a PIS and consent form (Appendix A-4) with contact details. Interested participants contacted the Eye Clinic at the Cardiff University School of Optometry and Vision Sciences to set up an appointment. The researcher attended the clinic at Cardiff University for a two-week period to carry out the study on participants.

Two other avenues were undertaken to recruit potential participants directly from the community. Firstly, the researcher along with his supervisor (JAL) attended a meeting at the Up and Downs: a community group of parents caring for children with DS. A general presentation on DS and vision was given to parents and then they were solicited for

participation in this study. PIS as well as consent forms were given out and any queries by parents were answered. Parents were then asked to book in for their children to attend an appointment at Ulster University's Eye Clinic.

Finally, adult participants were recruited from two Health and Social Care Northern Ireland (HSCNI) Northern Trust Day Centres: Millbrook in Ballymoney and Mountfern in Coleraine. The researcher liaised with the manager of each centre for an information package containing the various PISs and consent forms (Appendix A-3) to be sent out to the parents, guardians or participants directly, if they were able to consent for themselves. Participants were then booked via the day centre managers to visit the university Eye Clinic for participation in the study. Transportation to and from the clinic was arranged by the day centre.

4.3 Ethical Approval

Ethical approval was received from the UUREC, the Northern Health and Social Care Trust (NHST) and the Office for Research Ethics Committee Northern Ireland (ORECNI) (Appendix A-3). These approvals were for the recruiting of participants from Northern Ireland and with the Ulster University Vision Research Laboratory as the research site. For those participants seen at Cardiff University, an amendment was made for the blanket research ethics approval in place for the Down's Syndrome Research Unit (Appendix A-4). Research was carried out in accordance with the Declaration of Helsinki.

4.4 Methods

The following section will outline the procedures and assessments that were carried out on participants in Northern Ireland at the Vision Science Research Laboratory, Ulster University and in Wales at the Cardiff University School of Optometry and Vision

Sciences. Participants were seen on one occasion for approximately one hour. If participants were children, their parents or guardians were asked to sign a consent form on their behalf (Appendix A-3). If participants were adults who were unable to consent, an assent form was signed on their behalf by their parent or guardian (Appendix A-3); if they were adults able to consent, they were asked to sign a simplified consent form themselves (Appendix A-3). The researcher also signed all consent and assent forms. The study was conducted on both eyes unless either met any exclusion criteria:

- Undergone cataract surgery
- Nystagmus
- Ocular albinism
- Significant corneal or lenticular (apart from cataract) pathology adversely affecting imaging of the crystalline lens and retina

4.4.1 Ophthalmic and Systemic History

Parents or carers were questioned in regard to participants' ophthalmic and systemic histories on initial attendance for their appointment. This was to confirm adherence to the inclusion criteria and to ensure no increased risk to pharmacologic pupil dilation. Ophthalmic history included questions on spectacle wear, presence of pathology and any previous or current surgical or medical treatment to the eyes. Systemic history included questions on the presence of any general medical conditions, current medications and the presence of any allergies. The exclusion criteria for the study are mentioned above. Finally, the previous occurrence of any adverse reaction to pharmacologic pupil dilation was ascertained.

4.4.2 Visual Acuity

Following the assessment of participant history, an evaluation of visual acuity was undertaken. Distance VA was measured monocularly with participants' habitual correction in place. For those capable of reading letters and with sufficient intellectual capacity, VA was recorded in logMAR using the Keeler Crowded logMAR test; if this was not possible, the Crowded Kay Picture test was used. Both tests were carried out under normal room illumination at a distance of 3m. To determine the initial point of testing, the Keeler Crowded logMAR test uses a series of screening cards where four letters are presented in decreasing size in accordance with the logarithmic scale. The test was conducted using the crowded series of four letters at the smallest screening letter size identified by the participant. The Kay picture test consists of a booklet with each page containing a series of four pictures subtending a specific degree of visual angle; the pictures decrease in size logarithmically on each page. For either test, a habitual VA for each eye was determined using individual letter scoring. If participants were non-verbal, a matching card was provided enabling them to indicate pictures or letters using their fingers.

4.4.3 External Eye, Anterior Chamber and Intraocular Pressure Assessment

In order to determine the presence of any pathology that would preclude imaging and to assess the anterior chamber to ensure that it was safe to dilate the pupil with tropicamide 1%, the anterior eye was examined with a slit-lamp. Additionally, IOP was measured as another means of determining safe conditions for pupil dilation.

4.4.3.1 External Eye Assessment

The external eye of all participants was examined using a slit-lamp biomicroscope. Participants were asked to place their chin and head on the slit-lamp's rests and asked to fixate straight ahead. If participants' intellectual disability interfered with fixation, the

researcher used hand movements and verbal encouragement to capture their attention and obtain momentary views of the eye; this allowed a thorough assessment of the eye within a few minutes time. White light was used to examine the eye. The angle and width of the microscope's illumination was varied to accurately assess the external eye, with an emphasis on the cornea, iris and crystalline lens. If any pathology such as severe keratoconus or corneal opacities that would impair imaging were discovered, the eye was excluded from the study.

4.4.3.2 Anterior Chamber Angle Assessment

As described in Chapter 3, pharmacologic pupil dilation carries a risk of inducing acute angle closure glaucoma in those who are anatomically predisposed. The Van Herrick technique was used to determine whether the irido-corneal angle was sufficiently open to proceed with the instillation of tropicamide 1% eye drops. This was conducted during the external eye assessment and the technique used is described in Chapter 3. Any participant whose grade was 1 or less was excluded from the study. Angle estimation using the Van Herick technique requires accurate fixation for reliability and repeatability however, as this group consisted of members with intellectual disability where accurate fixation would not always be possible, the researcher used his judgement as a clinician as to whether the angle was sufficiently open to warrant pupil dilation.

4.4.3.3 Intraocular Pressure Measurement

To mitigate and detect any angle closure as an adverse reaction to tropicamide 1%, pre- and post-dilation IOPs were measured in all participants using the ICare (ICare, Finland) tonometer. The ICare tonometer did not require the use of any anaesthetic to numb the cornea and, in contrast to pneumatic non-contact tonometry, provided a nearly sensation free method of measuring IOP; this was ideal for participants with intellectual disability. As per manufacturer instructions, a total of five measurements were taken of each eye to

obtain an accurate estimation of IOP. A comparison between pre- and post-dilation IOPs was made to ensure a sharp rise had not occurred. Post-dilation IOPs were measured at the end of participants' one-hour appointment.

4.4.4 Posterior-Segment Optical Coherence Tomography

After IOP assessment, tropicamide 1% was instilled in each imaged eye to induce pupil dilation and thereby facilitate imaging of the crystalline lens. As tropicamide takes approximately 20 minutes to reach its full effect on the pupil, OCT scans of participants' retinæ were taken at this time. PS-OCT does not require pupil dilation to obtain adequate quality images and the Spectralis OCT described in Chapter 2 was used for retinal imaging. Attempts were made to image the macula, including fovea, and peripapillary retinal nerve fibre layer (RNFL).

Participants were seated and asked to place their chin and forehead on the Spectralis' respective rests. Their head was aligned correctly by adjusting the chin rest vertically and they were asked to look at the internal fixation target consisting of a blinking blue spot of light. To focus the instrument, its joystick was maneuvered by the researcher to view the retinal cSLO image; this was then brought into sharp focus by adjusting the appropriate knob on the Spectralis. When focus was achieved and the appropriate cross-section of the retina to be imaged was correctly aligned, the automated retinal tracking system of the Spectralis OCT was initiated. Initially, line scans were taken of the macula ensuring centration on the fovea. Line scans were followed by macular cube scans. Following the macular scans, peripapillary RNFL scans were obtained. For this, participants were required to shift their gaze nasally; the internal fixation light of the Spectralis moves for this purpose. If participants had difficulty fixating on the internal blue light, the external fixation target was used.

Macular scans were analysed using the Early Treatment of Diabetic Retinopathy Study (ETDRS) grid (see figure 4.4.1); the Spectralis' viewing software defined macular thickness as the distance between Bruch's membrane and the internal limiting membrane. The peripapillary RNFL scan consisted of a circle scan surrounding the optic nerve head as shown in figure 4.4.2. The Spectralis' software automatically segmented the RNFL and calculated thickness globally as well as for six peripapillary sectors. Line scans were analysed for minimum foveal thickness as shown in figure 4.4.3 and also for foveal pit depth by averaging the thickest nasal and temporal measurements of the line scan and subtracting the minimum foveal thickness.

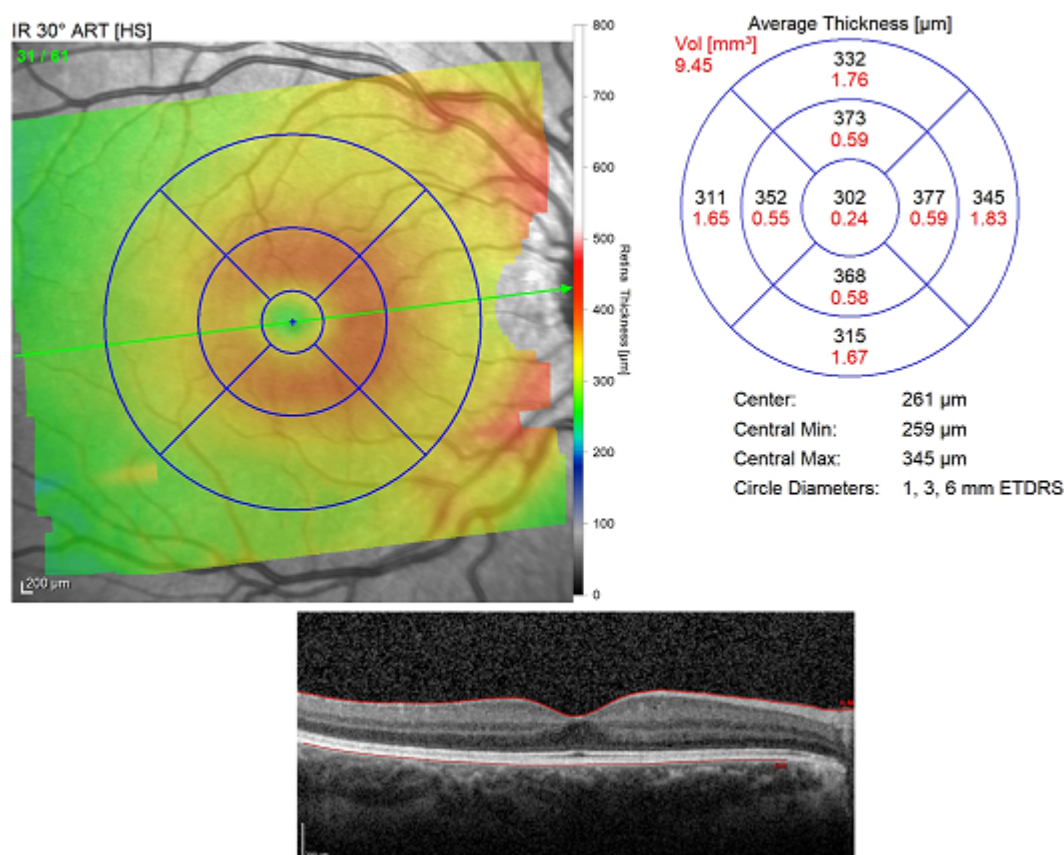


Figure 4.4.1 The ETDRS grid analysis conducted by the Spectralis OCT. Average thickness values are shown in black text while volumes are shown in red. The ETDRS grid consists of a central 1mm ring surrounded by 3 and 6mm rings which are further subdivided into superior, inferior, nasal and temporal quadrants.

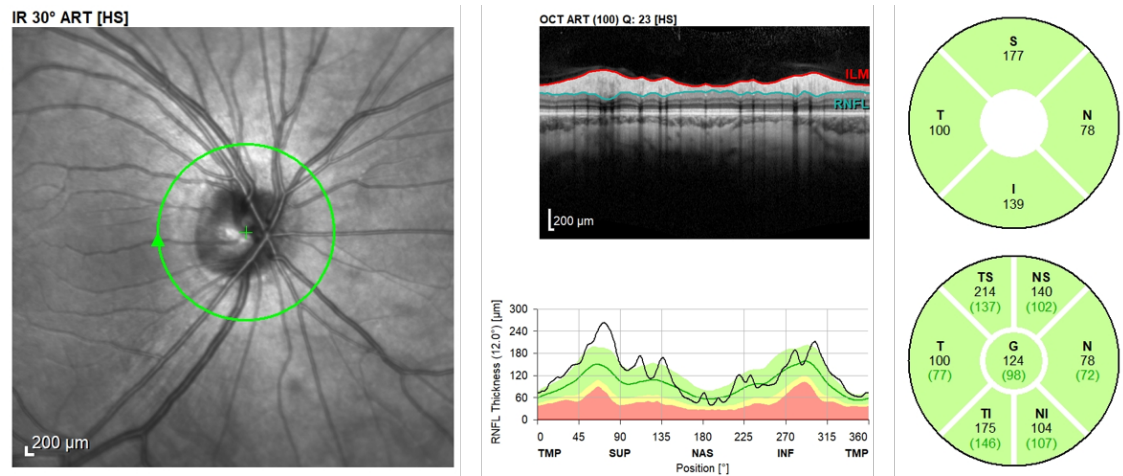


Figure 4.4.2 The RNFL analysis conducted by the Spectralis OCT. The circular grid in the bottom right hand corner of the image shows the mean thickness in each subfield (in black text) with the values from the normalised database in green.

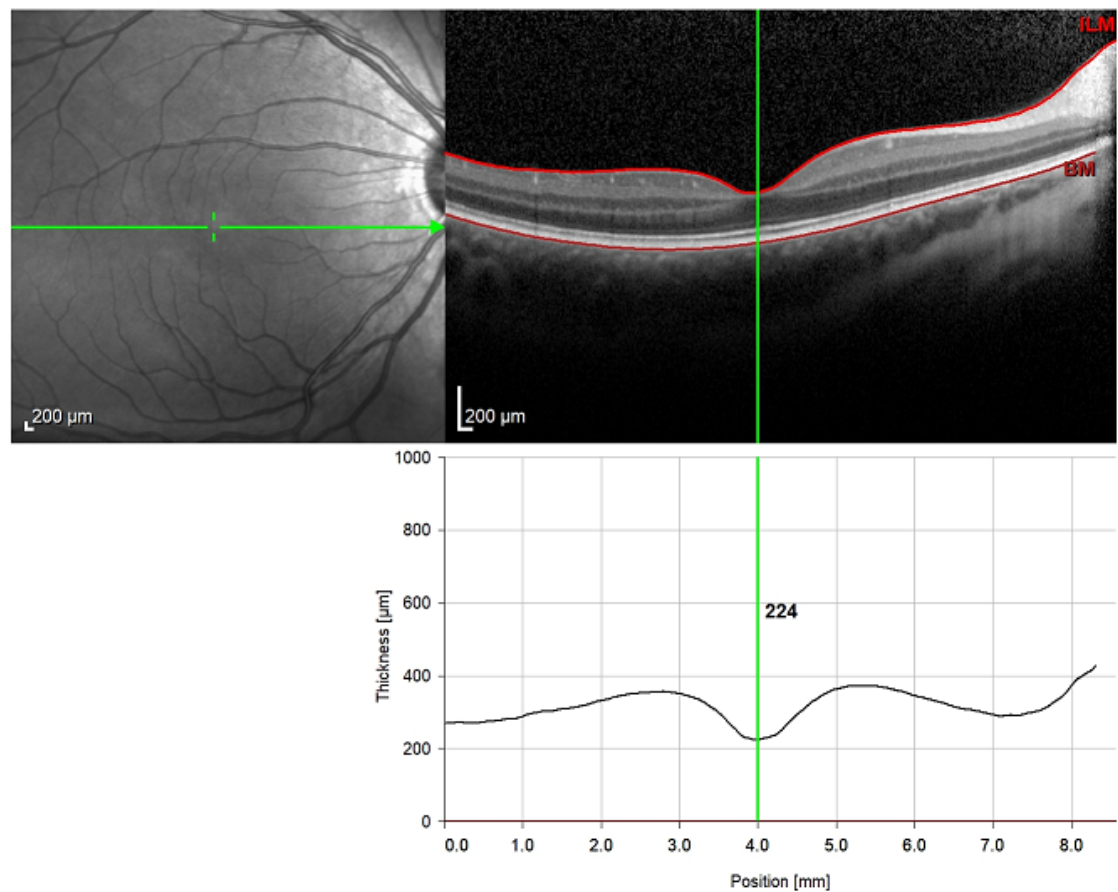


Figure 4.4.3 A Spectralis line scan through the macula. The area of minimum thickness has been selected with the green reference line showing a value of 224 μm.

4.4.5 Crystalline Lens Slit-Lamp Imaging and LOCS III Grading

After imaging with the Spectralis OCT, participants were given a short break to ensure maximum pupil dilation and to avoid fatigue. Following this, crystalline lens imaging was undertaken using the modified Nikon FS-3 slit-lamp described in Chapter 2. The same camera and slit lamp settings described in Chapter 3 were used:

3. Camera Settings:

- a. ISO sensitivity: 6400
- b. Flash Intensity: Level #9 (1/60s of LED at full brightness)
- c. Shutter Speed: 1/60s

4. Slit-Lamp Settings:

- a. For imaging the Nucleus:
 - i. Slit width: 0.2mm
 - ii. Slit height: Extended over pupillary margins
 - iii. Angle of illumination: Exactly 45 degrees to objective lenses
 - iv. Filter: None
- b. For Imaging Cortical and PSC opacities:
 - i. Slit width: Variable, usually between 3-5mm
 - ii. Slit height: Variable – enough to provide adequate retroillumination
 - iii. Angle of illumination: 3-5 degrees to objective lenses
 - iv. Filter: None

Both optic sections and retroillumination images were taken of all crystalline lenses. Participants were seated at the slit-lamp and asked to place their chin and head on the appropriate rests. The chinrest was adjusted vertically to correctly align the participant's head in the microscope. The participant was asked to look straight ahead but if they experienced difficulty doing this, the researcher used hand movements and verbal communication to keep their attention. Participants were told they would see a flashing

light when the photographs were taken. All images were captured with the room lights switched off. Multiple photographs were taken so that the best quality image could be used for grading.

LOCS III grading was attempted for all photographs. Images were graded at the same computer terminal and monitor with the settings described in Chapter 3. The transparency of LOCS III standard images was illuminated by the lightbox described in Chapter 3 and set directly beside the monitor for grading. Grades were assigned for the three types of cataract LOCS III is capable of characterising (Chylack *et al.* 1993). A detailed outline of the LOCS III grading process has been described in Chapter 3. It should be noted that if any dot or flake like opacity that has been reported in DS was seen on retroillumination, it was graded as a cortical opacity in line with the LOCS III protocol.

4.4.6 Visante Anterior Segment Imaging and Grading

Once slit-lamp photography was conducted, participants' crystalline lenses were imaged with the Visante AS-OCT. Again, participants were seated at the instrument with their head and chin placed on the Visante's respective rests and asked to look at the internal fixation target. Their eyes were then aligned by adjusting chin and forehead position using the Visante's controls. The crystalline lens was brought into focus for imaging; to ensure correct alignment, the corneal reflex was visualised. Images were captured when the corneal reflex just disappeared in order to facilitate subsequent grading of the images for opacity. B-scans of the lens at a 90-degree orientation were taken to coincide with slit-lamp images however, if participants' lids interfered with imaging due to narrow palpebral aperture, 180-degree B-scans were also acquired. B-scan orientation was also adjusted to image any other opacities seen in the lens during slit-lamp imaging. As seen in chapter 3, because of the superior imaging quality, crystalline lenses were captured in the Visante's high-resolution mode. As opposed to the 6mm imaging depth possible with low-resolution

B-scans, high-resolution scans are only capable of a 3mm imaging depth; therefore, separate B-scans of the anterior and posterior lens were acquired. B-Scans were graded for opacity using the custom software described in Section 3.4.7.1. In anticipation of dot-like opacities that have been reported in DS, these would be graded in a similar manner to cortical and PSC morphologies. In addition to PIR and PAR the total number of dot opacities would be counted as well.

Chapter 5 outlines the results and discussion for lens opacity in DS while Chapter 6 does the same for PS-OCT imaging.

Chapter 5: Cataract in Down Syndrome

5.1 Introduction

This chapter discusses the results and interpretation of the assessment of the Down Syndrome crystalline lens as outlined in the Chapter 4. Imaging of the lenses obtained using the slit-lamp and Visante AS-OCT and their grading are discussed. Comparisons are made to the crystalline lens opacities in the 50 to 60-year-old group of typically developed individuals studied in Chapter 3. Firstly, the recruitment and success rates are outlined below followed by descriptions of participants' visual acuities and measures of lens opacity with slit-lamp grading and anterior segment OCT imaging.

5.2 Results

5.2.1 Recruited Participants

In total 30 participants were recruited from the various agencies stated in section 4.2.2. Two participants were excluded from the study leaving a total cohort of 28. The first excluded participant was diagnosed with a brain tumour and the second was a wheelchair user and therefore, unable to complete any assessment or imaging. Attempts were made to image both eyes of all included participants however in two participants one eye was excluded due to the presence of pathology (corneal degenerative disease with neovascularisation and esotropia respectively). This meant that attempts were made to image 54 eyes from the 28 participants. The mean age of participants was 24.10 ± 14.20 (SD) years with a range of 6.05 to 55.36. The cohort consisted of 17 males and 11 females.

5.2.2 Visual Acuity Assessment

Monocular habitual VA was successfully measured in 51 of 54 eyes (94%). Habitual refractive correction was worn for all participants, though in a few cases, it was not possible to determine whether spectacles were worn typically. The missing measurements were from two participants: in one case, VA could not be obtained from either eye of the participant due to lack of cooperation and in the second, the participant was only able to complete VA measurement in the right eye. The distribution of VA for all measured eyes was not normal (Shapiro-Wilk, $p < 0.001$) with a median value of 0.300 ± 0.275 (IQR) logMAR. VA in measured eyes ranged from 0.050 to 0.800 logMAR. When grouped by whether VA was measured using letter or picture optotypes, the distribution containing letter VA was not normally distributed (Shapiro-Wilk, $p = 0.002$) but picture acuity was normally distributed (Shapiro-Wilk, $p = 0.219$). Participants' VA levels were compared to the typical adults aged 50 to 60-years described in chapter 3; a Mann-Whitney U test showed a significant difference between both groups ($U = 80.00$, $p < 0.001$) with worse VA in those with DS. Table 5.2.1 outlines the descriptive statistics for the DS and typical adults acting as control groups. Figures 5.2.1, 5.2.2 and 5.2.3 show the histograms and Q-Q plots for VA in the DS group.

VA Type	Mean VA (Std. Dev.)	Range (VA)	Median VA (IQR)	Shapiro- Wilk	Mean Age (Std. Dev.)
DS Letter (n = 33)	0.343 (0.205)	0.050 to 0.800	0.275 (0.250)	$p < 0.001$	22.25 (9.92)
DS Picture (n = 18)	0.424 (0.230)	0.100 to 0.800	0.400 (0.381)	$p = 0.219$	25.08 (17.67)
Total DS (n = 51)	0.371 (0.215)	0.050 to 0.800	0.300 (0.275)	$p < 0.001$	23.25 (13.08)
Controls (n = 56)	-0.053 (0.123)	-0.20 to 0.38	-0.080 (0.155)	$p < 0.001$	54.11 (3.25)

Table 5.2.1 Summary of VA distributions' mean, median, range and indicators of normality for DS and control participants

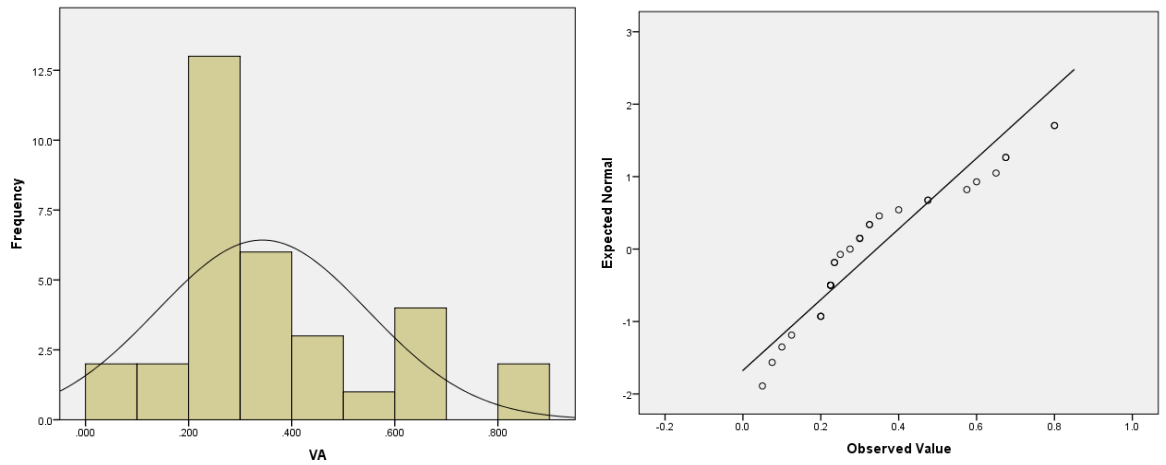


Figure 5.2.1 Histogram and Q-Q Plot of VA frequencies from all 18 DS eyes measured with letter optotypes.

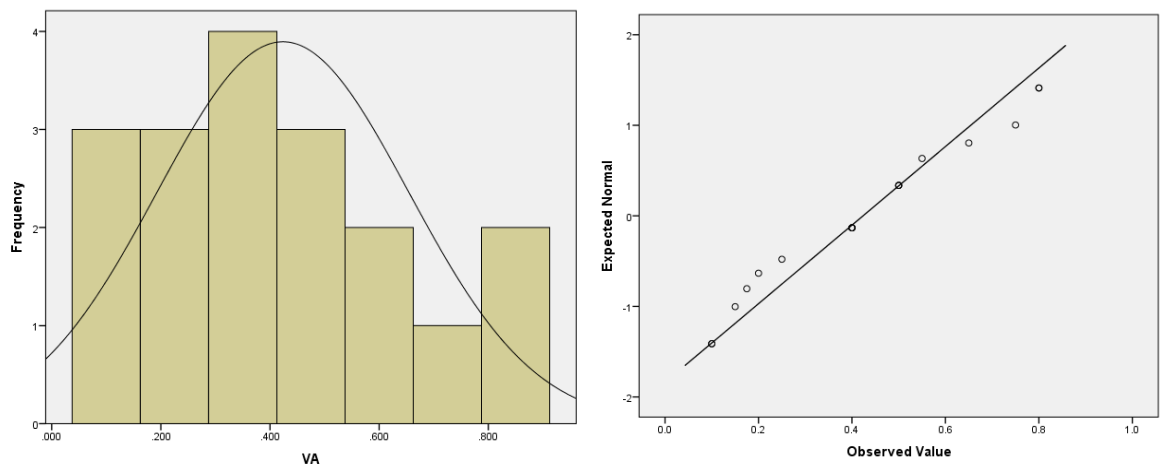


Figure 5.2.2 Histogram and Q-Q Plot of VA frequencies from all 33 DS eyes measured with picture optotypes.

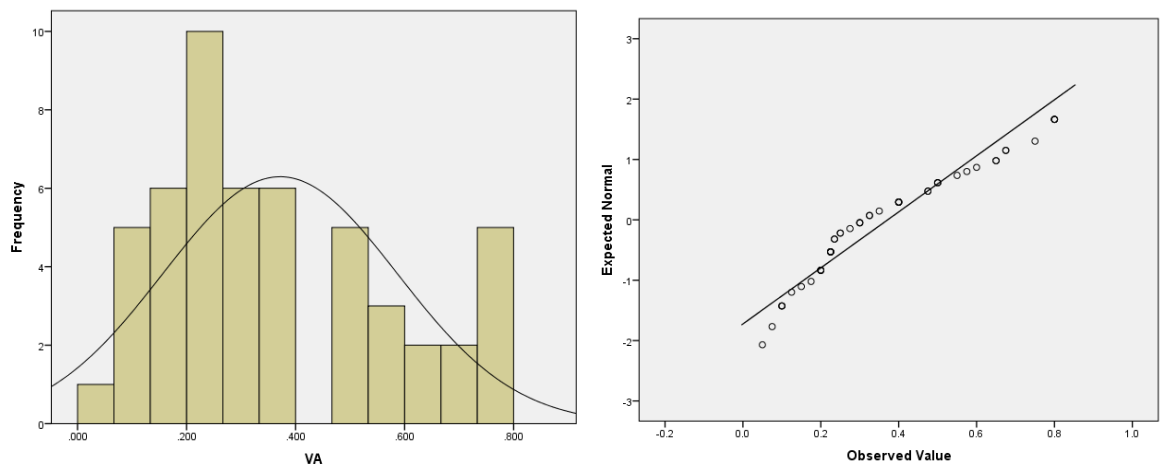


Figure 5.2.3 Histogram and Q-Q Plot of combined VA frequencies from all DS eyes measured.

Spearman rank order analysis showed a moderate correlation between habitual VA and age for all 26 DS left eyes ($\rho = 0.640$, $p < 0.001$). Linear regression also showed a relation between VA and age albeit less than the correlation between the two measures ($F_{(1, 24)} = 17.135$, $p < 0.001$, $R^2 = 0.417$). Figure 5.2.4 shows the scatterplot of the above described relationship.

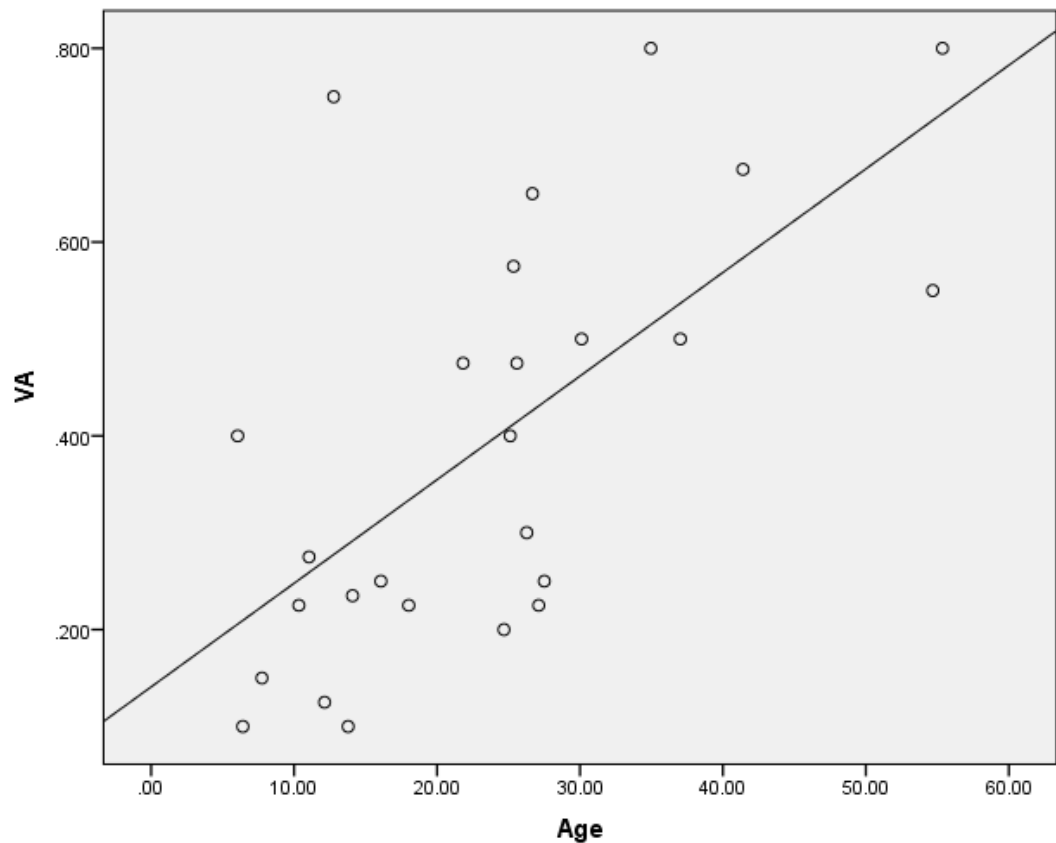


Figure 5.2.4 Scatterplot showing the significant relation between VA and age for the left eye only ($F_{(1, 24)} = 17.135$, $p < 0.001$, $R^2 = 0.417$).

5.2.3 LOCS III Grading of Crystalline Lenses in Down Syndrome

Slit-lamp imaging and subsequent LOCS III grading for at least one measure of opacity was successful in 39 of the 54 imaged eyes. The below sections outline the results for nuclear, cortical and posterior subcapsular measures of opacity.

5.2.3.1 LOCS III Nuclear Opalescence and Colour

LOCS III NO and NC scores were obtained for all 39 imaged eyes. The scores for NO were not normally distributed (Shapiro-Wilk, $p < 0.001$) and scores ranged from 0.1 to 2.2 with a median of 0.4 ± 0.4 (IQR). NC scores ranged from 0.1 to 2.5 with a median value of 0.3 ± 0.4 (IQR) and the distribution was, again, not normal (Shapiro-Wilk, $p < 0.001$). When compared, Mann-Whitney U tests showed significant differences between both DS NO and NC scores and those of the control group. NO and NC grades of opacity were higher in controls (NO: $U = 112.00$, $p < 0.001$; NC: $U = 158.00$, $p < 0.001$). Figures 5.2.5 and 5.2.6 show the histograms and Q-Q plots for NO and NC scores in the DS group. Figure 5.2.7 shows pictures of lenses with no and significant opacity. Table 5.2.2 describes the distribution of NO and NC in the DS and control groups.

LOCS III Measure		Mean (SD)	Median (IQR)	Range	Shapiro-Wilk
DS n = 39	NO	0.5 (0.5)	0.4 (0.4)	0.1 to 2.2	$p < 0.001$
	NC	0.5 (0.6)	0.3 (0.4)	0.1 to 2.5	$p < 0.001$
Controls n = 56	NO	1.8 (0.3)	1.8 (0.4)	1.2 to 2.7	$p = 0.040$
	NC	1.7 (0.5)	1.8 (0.8)	0.5 to 2.5	$p = 0.442$

Table 5.2.2 Summary of LOCS III NO and NC measures for Down Syndrome and Control participants

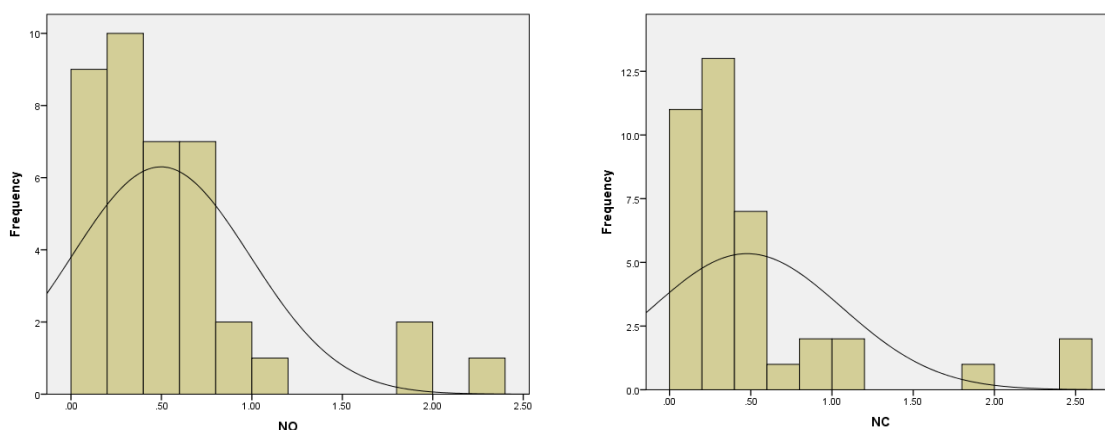


Figure 5.2.5 Histograms for total participant NO (left) and NC (right) with overlaid distribution curves.

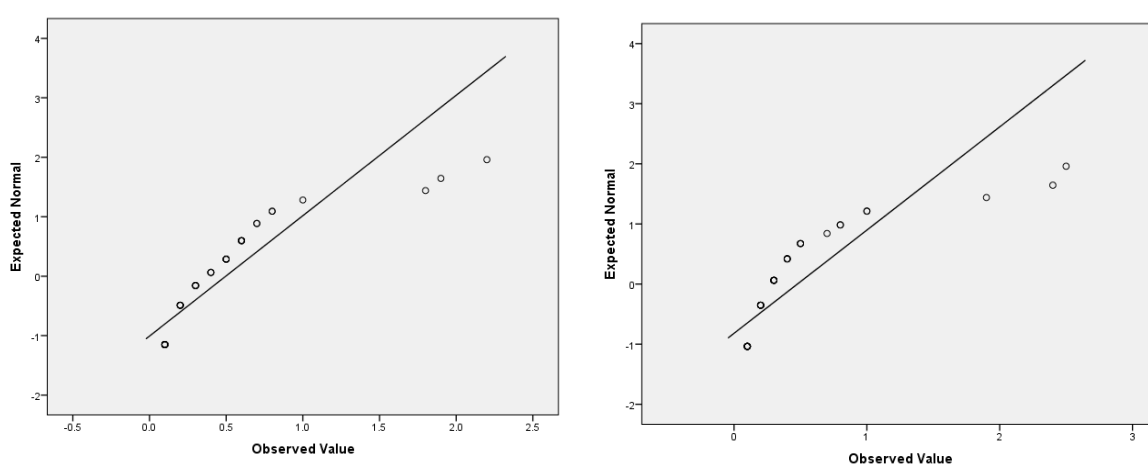


Figure 5.2.6 Q-Q plots of participant NO (left) and NC (right) values showing deviation from normality in both cases.

For the DS group, Spearman's rank order analysis showed significant correlations between both LOCS III nuclear measures and age as well as VA. Age was very strongly correlated and VA was moderately correlated; the data are summarised in table 5.2.3.

	NO		NC	
	Rho	Sig.	Rho	Sig.
DS Age	0.794	$p < 0.001$	0.858	$p < 0.001$
DS VA	0.332	$p = 0.039$	0.455	$p = 0.004$

Table 5.2.3 Summary of Spearman's rank order correlation between NO, NC and age as well as VA for participants with DS.

Linear regression was performed to compare both LOCS III nuclear measures to age and VA. Similar significant relations were found as in the above correlations however, VA was not as strongly related to either NO or NC. Table 5.2.4 summarises this data.

	NO			NC		
	F	Sig.	R ²	F	Sig.	R ²
DS Age	(1, 37) = 117.531	p < 0.001	0.761	(1, 37) = 135.566	p < 0.001	0.786
DS VA	(1, 37) = 6.075	p = 0.018	0.141	(1, 37) = 9.926	p = 0.003	0.212

Table 5.2.4 Summary of linear regression between NO, NC and age as well as VA for participants with DS.

Figures 5.2.7 and 5.2.8 show the scatterplots for the above linear relationships between NO, NC compared to Age and VA.

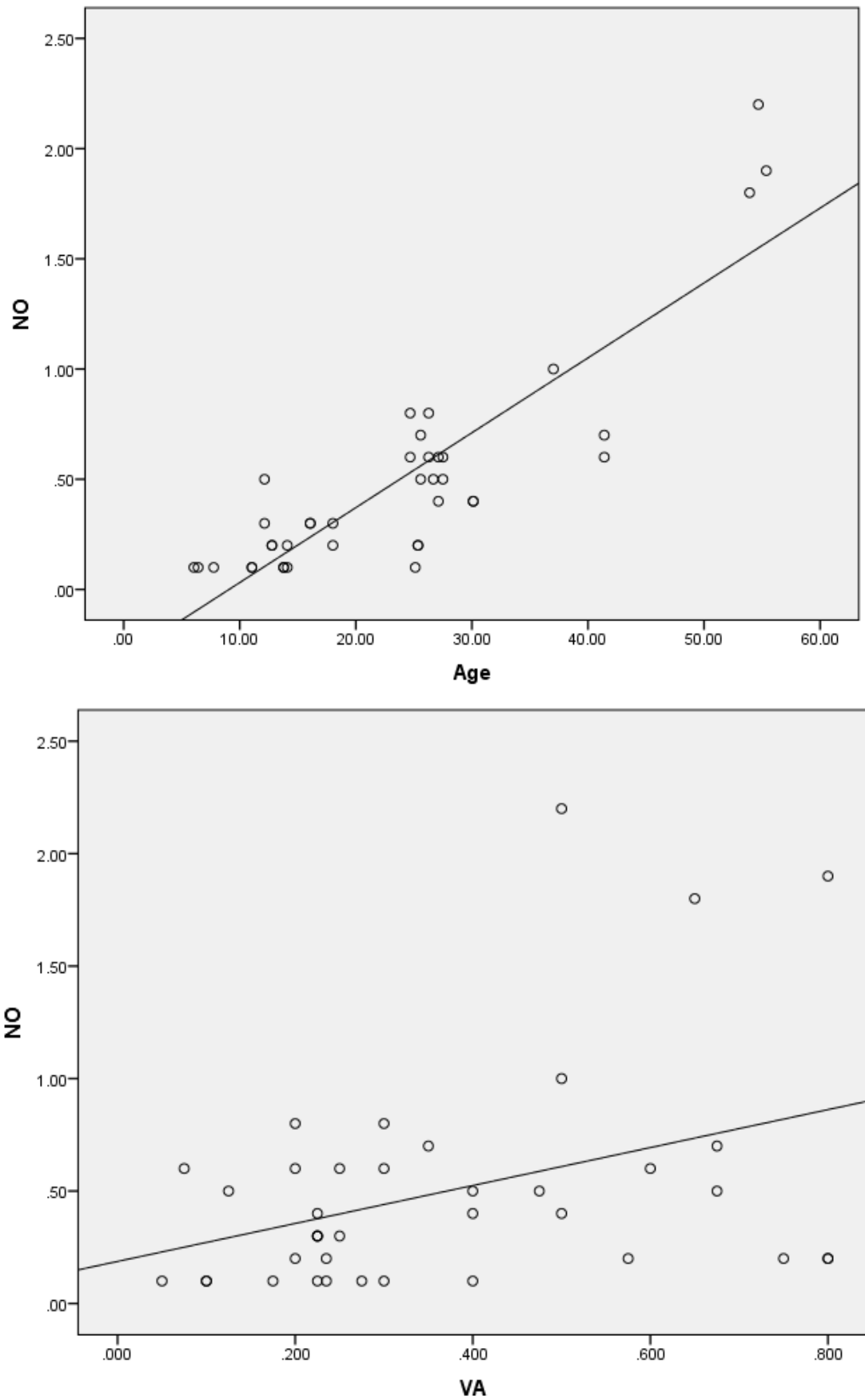


Figure 5.2.7 Scatterplots showing the significant relation between NO and Age (top) and VA (bottom).

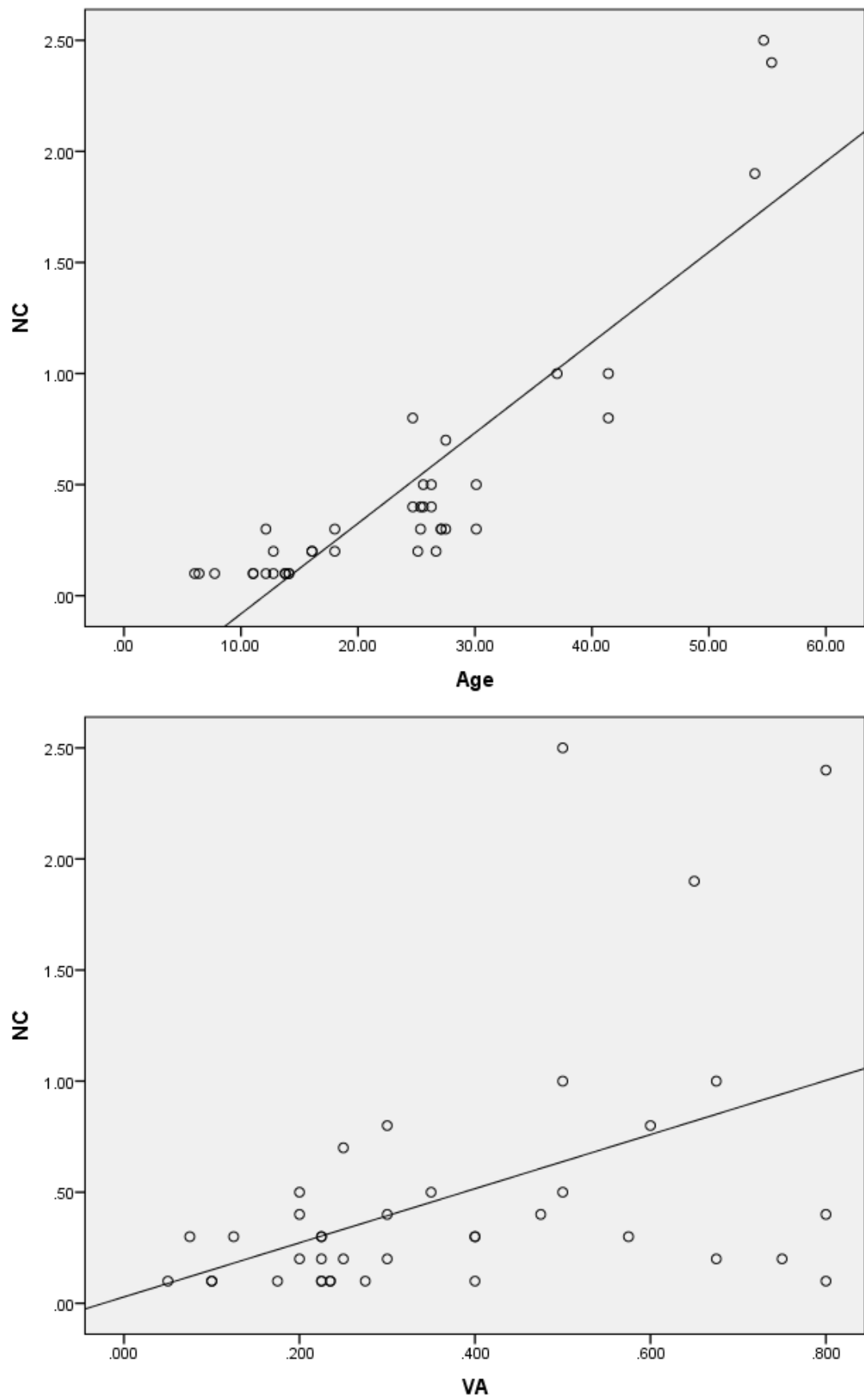


Figure 5.2.8 Scatterplots showing the significant relation between NC and Age (top) and VA (bottom).

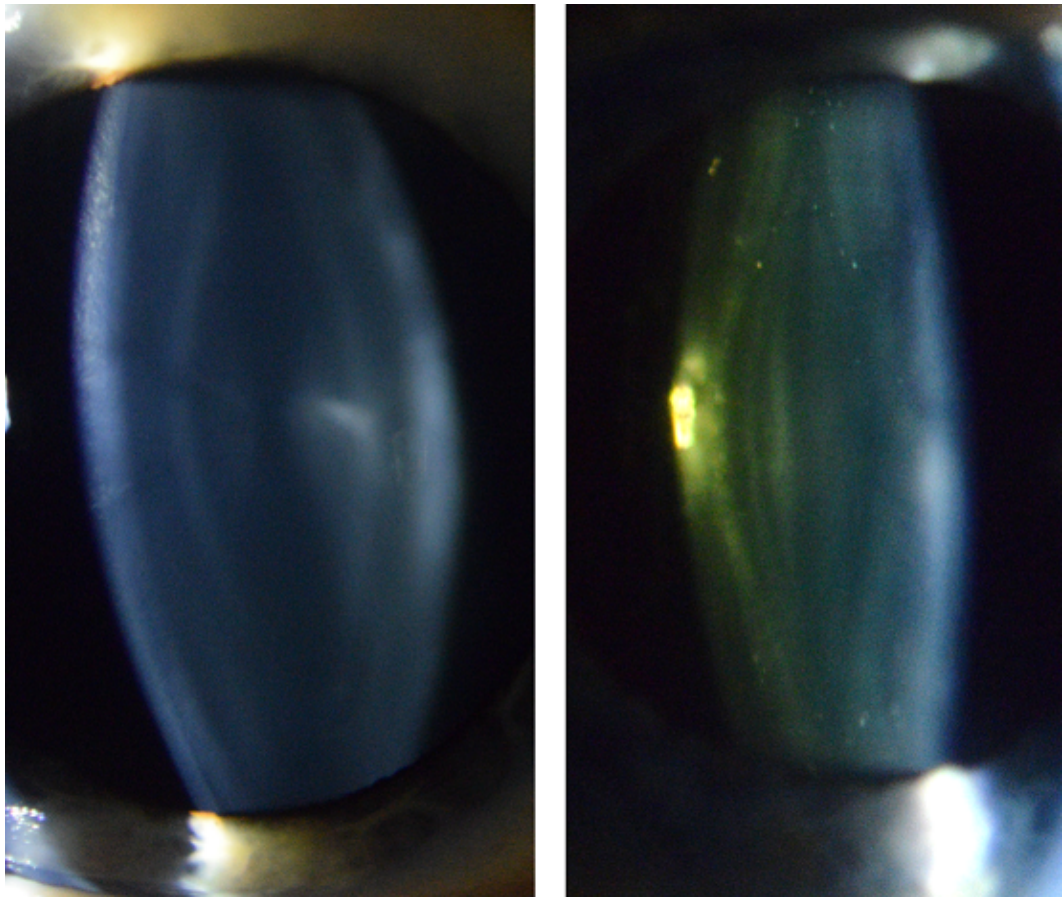


Figure 5.2.9 Optic sections of crystalline lenses showing no opacity (Left) (Participant 16 RE, NO: 0.1 and NC: 0.1) and nuclear opacity (Right) (Participant 23 LE NO:1.9, NC:2.4).

5.2.3.2 LOCS III Cortical Grading

A total of 15 DS eyes (28%) were successfully imaged and scored for LOCS III C grades. The distribution of C values was not normal (Shapiro-Wilk, $p = 0.009$) and grades ranged from 0.1 to 2.4 with a median of 0.5 ± 0.7 (IQR). Grades above 0.1 occurred in 12 (80%) of the imaged eyes. A Mann-Whitney U test showed that C grades were significantly greater in the DS group when compared to controls ($U = 115.500$, $p < 0.001$). Spearman's correlation analysis showed no association between C and either Age or VA. The same held true for linear regression, with no relation between C and the variables. Figure 5.2.10 shows the histogram and Q-Q plot for the distribution of LOCS III C grades and table 5.2.5 summarises the distribution and above-mentioned correlation and regression analyses. Figure 5.2.11 demonstrates a clear lens and one with opacity.

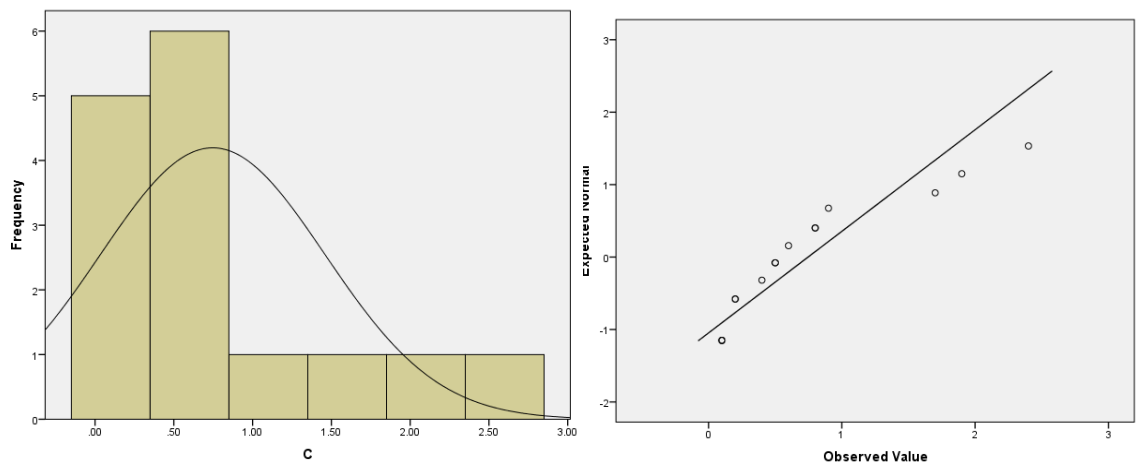


Figure 5.2.10 Histogram (left) and Q-Q (right) plots of the C distribution for all gradable images, showing skewness.

	Median (IQR)	Mean (SD)	Range	Correlation		Regression	
				Age	VA	Age	VA
C n=15	0.5 (0.7)	0.7 (0.7)	0.1 to 2.4	Not Significant	Not Significant	Not Significant	Not Significant

Table 5.2.5 Summary of descriptive statistics of C grades and analyses of correlations between it, Age and VA.

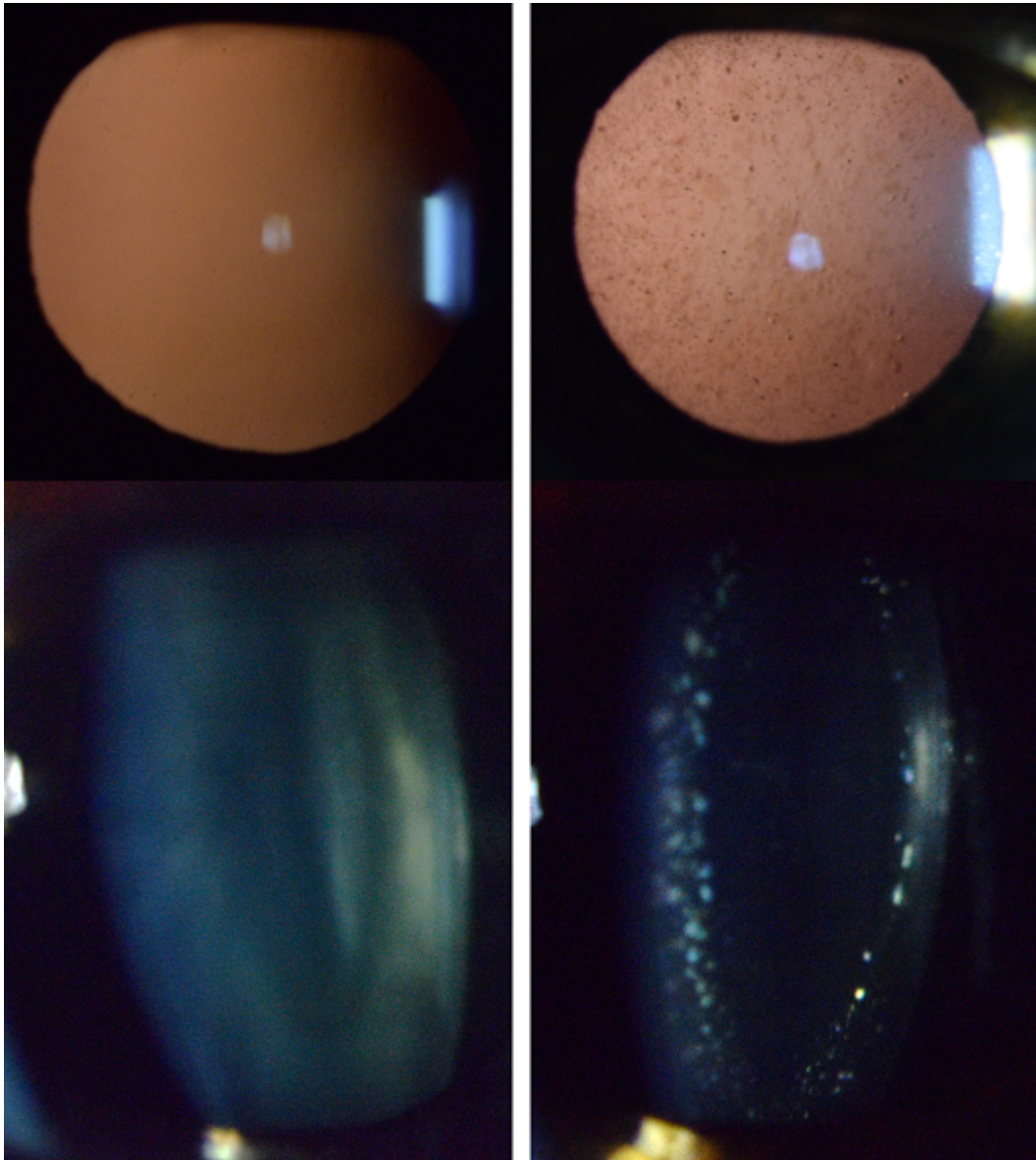


Figure 5.2.11 Retroillumination images (top) and corresponding optic sections of crystalline lenses showing no opacity (Left) (LOCS III C: 0.1) and cortical dot opacities (Right) (Participant 7 RE LOCS III C: 2.4).

5.2.3.3 LOCS III Posterior Subcapsular Grading

As with the above cortical grading of lens opacity, only 15 eyes (28%) were gradable for LOCS III P opacities. P grades above 0.1 were only present in two eyes from two separate participants. Naturally, the distribution of P grades was not normal (Shapiro-Wilk, $p < 0.001$). The P grades above 0.1 were in the eyes of the eldest and third-eldest participants aged 55.36 and 53.92 years respectively. These two eyes also had poor VAs of 0.800 and 0.650 logMAR respectively. The presence of posterior subcapsular opacification differed from controls as there was no presence of the opacities in the latter population. Figure 5.2.12 shows the histogram and Q-Q plots and table 5.2.6 summarises the distribution of LOCS P values in DS.

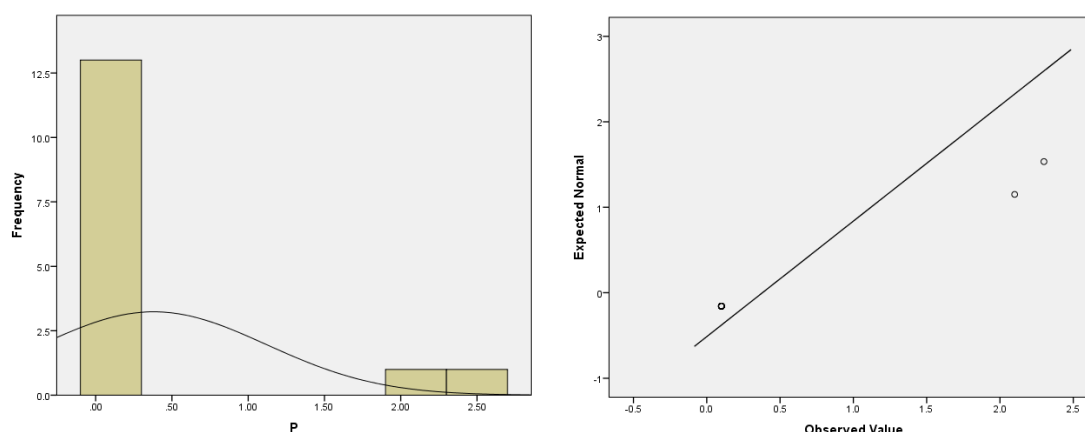


Figure 5.2.12 Histogram (left) and Q-Q (right) plots of the P distribution for all gradable images, showing skewness.

	Median	IQR	Range	Mean	Std. Dev.	Shapiro-Wilk
P (n = 15)	0.1	0.0	0.1 to 2.3	0.4	0.7	$p < 0.001$

Table 5.2.6 Summary of descriptive statistics of P grades and analysis of normality

Spearman's analyses showed a correlation between P and Age ($Rho = 0.587$, $p = 0.022$) but not VA. Linear regression analyses also showed a relation between P and Age ($F_{(1, 13)} = 21.919$, $R^2 = 0.628$, $p < 0.001$) and VA ($F_{(1, 13)} = 6.153$, $R^2 = 0.321$, $p = 0.028$). Figure 5.2.13 shows the scatterplots for the comparisons showing the outliers; once these were

removed the correlations and regressions became, expectedly, insignificant. Figure 5.2.14 shows the retroillumination images of PSC in both participants.

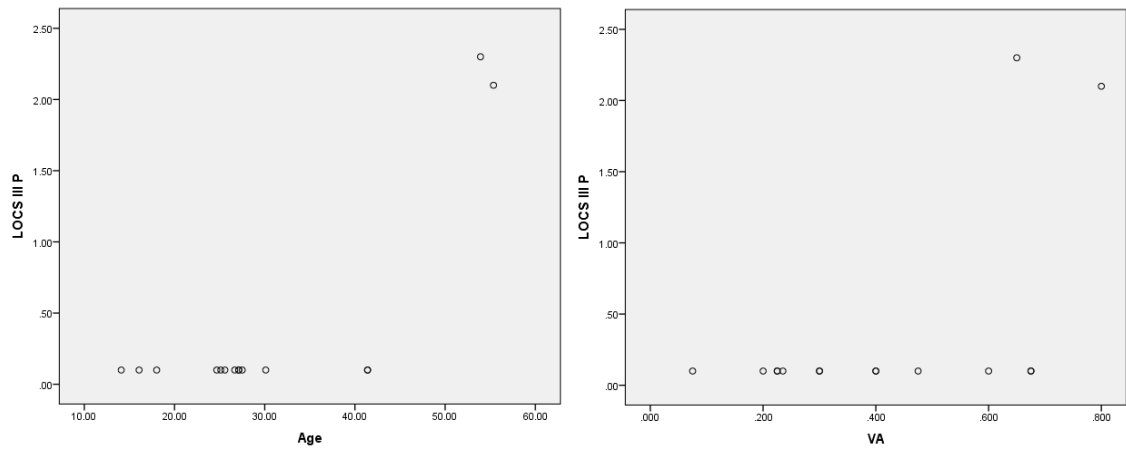


Figure 5.2.13 Scatterplots showing the relation between P and Age (left) and VA (right) and the effect of the outliers.

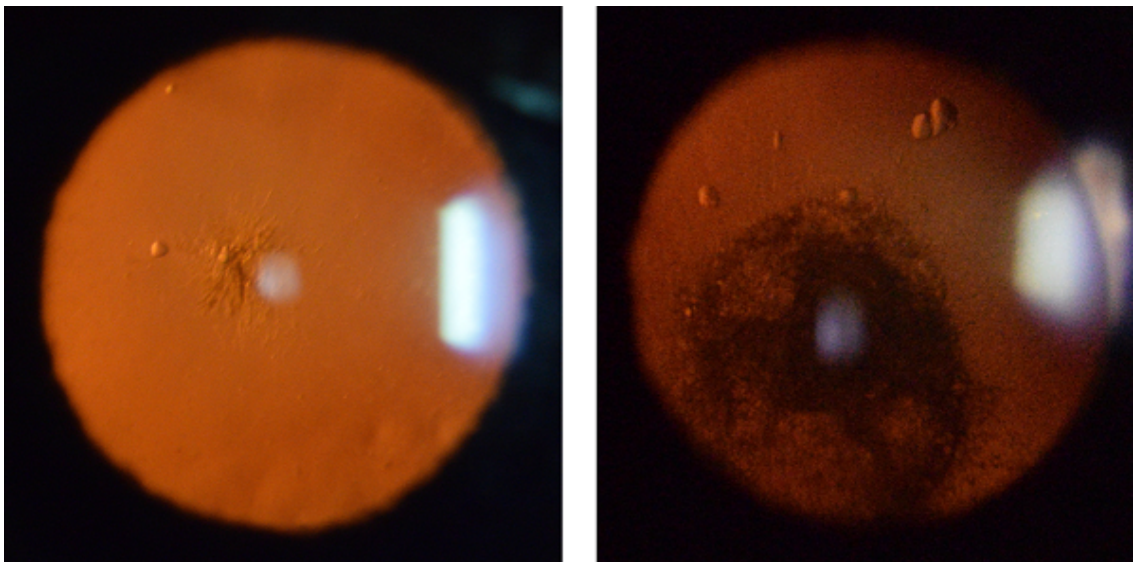


Figure 5.2.14 Retroillumination images of crystalline lenses showing PSC in the only two DS participants who presented with this morphology of cataract.

5.2.4 OCT Grading of Lens Opacity in Down Syndrome

5.2.4.1 OCT Nuclear Grading

High resolution anterior and posterior B-scans of the crystalline lens were captured in 33 (61.11%) of the 54 imaged eyes in DS. The images were graded to determine nuclear PIR. PIR values were not normally distributed (Shapiro-Wilk, $p < 0.001$) with a median of 1.188 \pm 0.70 (IQR); values ranged from 1.102 to 1.454. Figure 5.2.15 shows the histogram and Q-Q plots for the distribution.

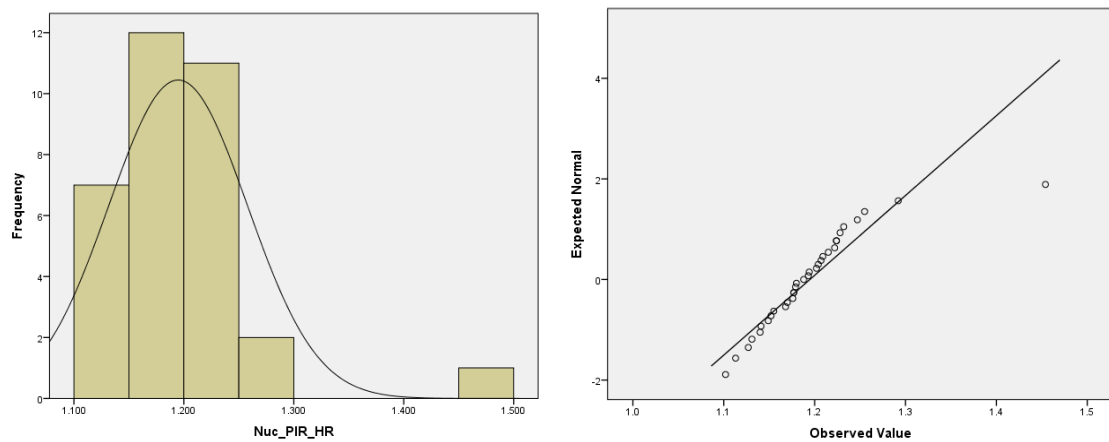


Figure 5.2.15 Histogram and Q-Q plot describing the distribution of Nuclear PIR in the DS group.

When compared to controls, a Mann-Whitney U test showed that nuclear PIR was significantly lower in those with DS ($U = 277.500$, $p < 0.001$). Spearman's correlation analyses showed significant associations between nuclear PIR and both age and VA. Linear regression also showed moderate relations between nuclear PIR and both age and VA. Table 5.2.7 summarises the correlations and regressions while figure 5.2.16 shows the scatterplots.

High-resolution PIR			
	Correlation		Linear Regression
	Rho	Sig.	
Age	0.666	$p < 0.001$	$F_{(1,31)}=34.110$, $R^2=0.524$, $p<0.001$
VA	0.578	$p < 0.001$	$F_{(1,31)}=9.238$, $R^2=0.230$, $p=0.005$

Table 5.2.7 The statistics correlation and regression analyses performed between Nuclear PIR and both Age and VA.

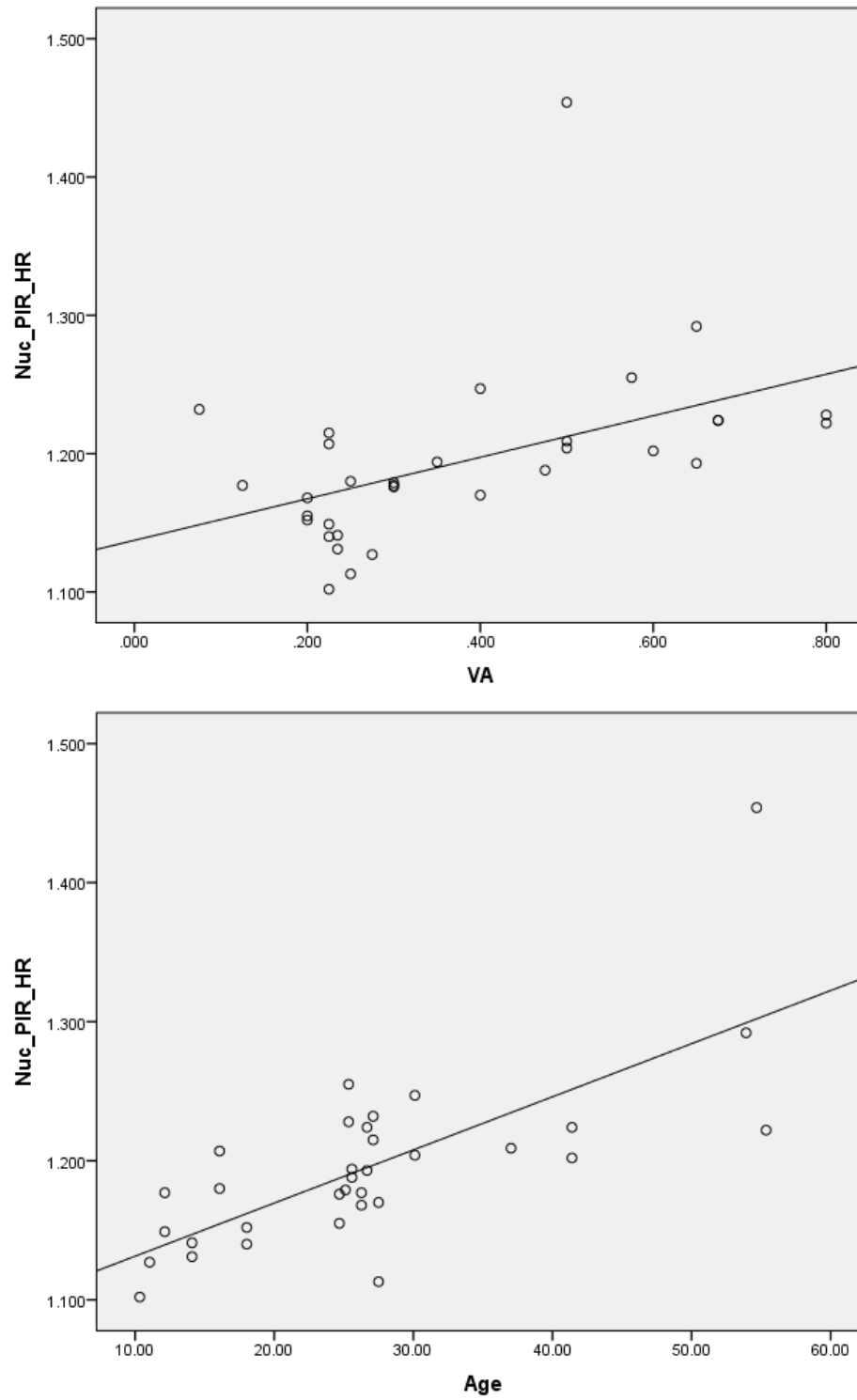


Figure 5.2.16 Scatterplots showing the relation between P and VA (top) and Age (bottom).

5.2.4.1.2 Comparison of Nuclear PIR to LOCS III Nuclear Grades

As with controls, LOCS III nuclear grades were compared to nuclear PIR values. Spearman's analysis showed significant correlations between PIR and both NO and NC, with moderate strength of association for both measures. The strength of correlations between the measures was very similar to those in the control group; the correlations for both groups are summarised in table 5.2.8.

	Group	High-Resolution PIR
LOCS III NO	DS	Rho = 0.360 p = 0.047
	Controls	Rho = 0.420 p = 0.004
LOCS III NC	DS	Rho = 0.437 p = 0.014
	Controls	Rho = 0.429 p = 0.003

Table 5.2.8 Summary of the correlations between Nuclear PIR and LOCS III grades for both DS and control groups.

Linear regression analyses were performed to compare nuclear PIR values to LOCS III NO and NC grades. Significant relations of moderate strength were found. These relations were much stronger than those found in controls and are shown in Table 5.2.9.

Figure 5.2.17 shows the scatterplots for the regressions in the DS group.

	Group	High-Resolution PIR
LOCS III NO	DS	$F_{(1,29)} = 25.932$ $R^2 = 0.467$ p < 0.001
	Controls	$F_{(1,44)} = 9.363$ p = 0.004 $R^2 = 0.175$
LOCS III NC	DS	$F_{(1,29)} = 22.715$ $R^2 = 0.460$ p < 0.001
	Controls	$F_{(1,44)} = 8.256$ p = 0.006 $R^2 = 0.158$

Table 5.2.9 Summary of the regression analyses between Nuclear PIR and LOCS III grades for both DS and control groups.

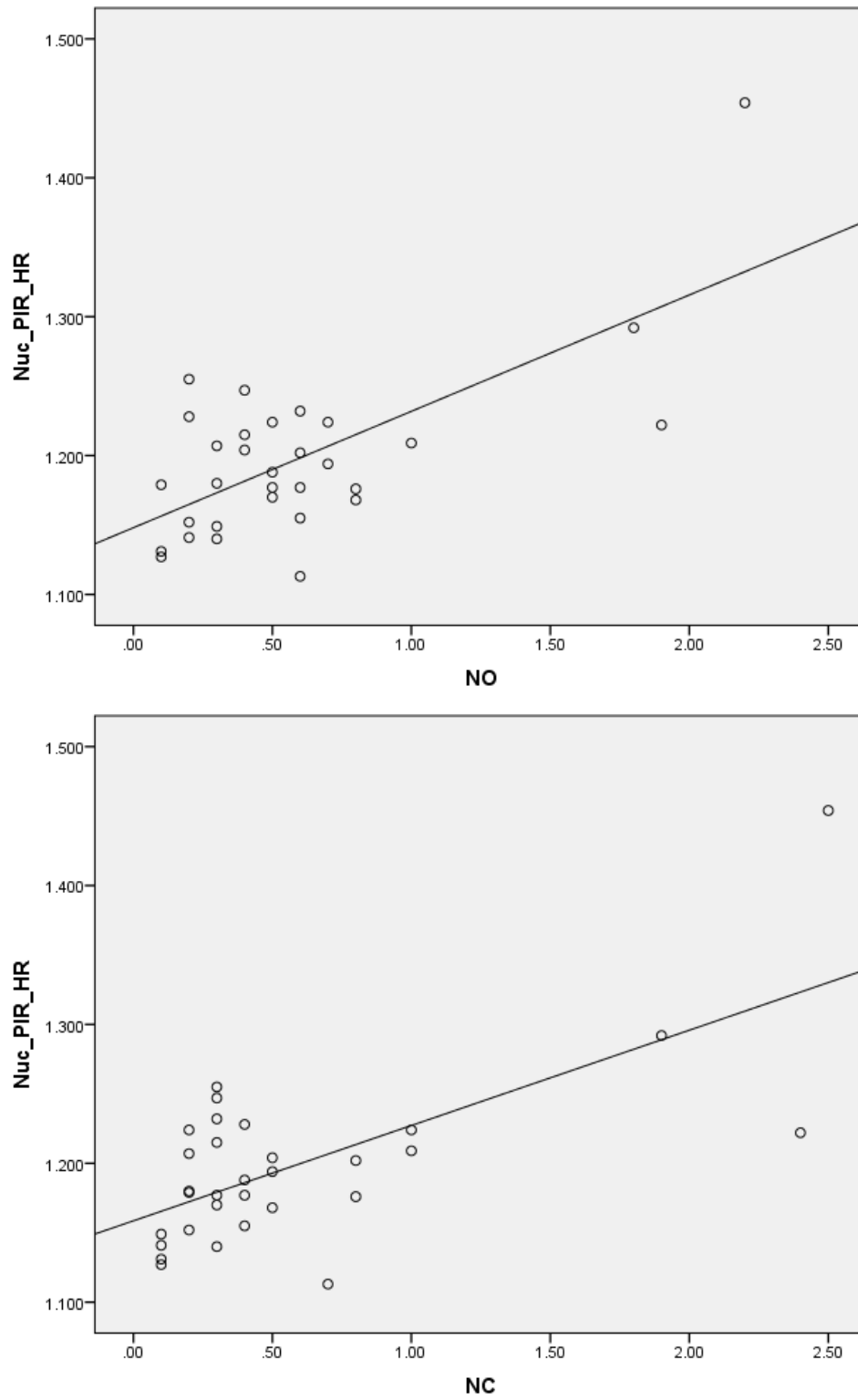


Figure 5.2.17 Scatterplots showing the relation between Nuclear PIR and LOCS III NO (top) and NC (bottom).

5.2.4.2 OCT Cortical Grading in DS

As mentioned previously, the presence of cortical lens opacities was high in the DS group. A total of 33 high-resolution AS-OCT B-scans were graded for cortical opacity. One participant showed traditional cortical cataract in both eyes and successful grading was performed for cortical dot opacities in 16 other eyes.

The participant with traditional cortical cataract was 26.67 years-old with PIRs of 1.383 and 1.456, and PARs of 0.049 and 0.148 in right and left eyes respectively. All other participants received a grade of 0.000 for cortical PIR and PAR. Naturally, there was no correlation between the presence of age-related cortical cataract and either age or VA. Comparisons were not made between this type of cataract in the DS group and that in controls as none of the control participants with cortical opacities were successfully imaged with AS-OCT.

Cortical dot opacities were graded for PIR, PAR, and number of opacities present in the cortex. Those lenses without the presence of any dot opacities were given a score of 0.000 for each measure. The distributions of dot PIR, PAR, and number of dots were not normal in any case (Shapiro-Wilk). Table 5.2.10 summarises the distribution for each measure of dot opacity and figures 5.2.18, 5.2.19 and 5.2.20 show their histograms and Q-Q plots.

Measure	Median	IQR	Range	Mean	Std. Dev.	Shapiro-Wilk
Dot PIR (n = 16)	0.000	1.299	0.000 to 1.1680	0.643	0.678	p < 0.001
Dot PAR (n = 16)	0.000	0.017	0.000 to 0.138	0.021	0.040	p < 0.001
Number of Dots (n = 16)	0.00	9.00	0 to 50	7.58	13.45	p < 0.001

Table 5.2.10 Descriptive statistics for OCT measures of cortical opacity in Down syndrome.

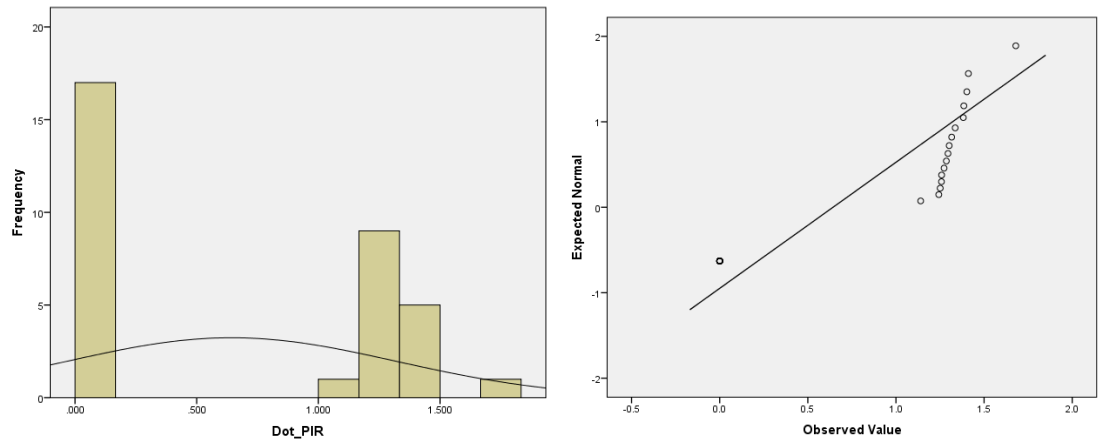


Figure 5.2.18 Histogram and Q-Q plot describing the distribution of Cortical Dot PIR in the DS group.

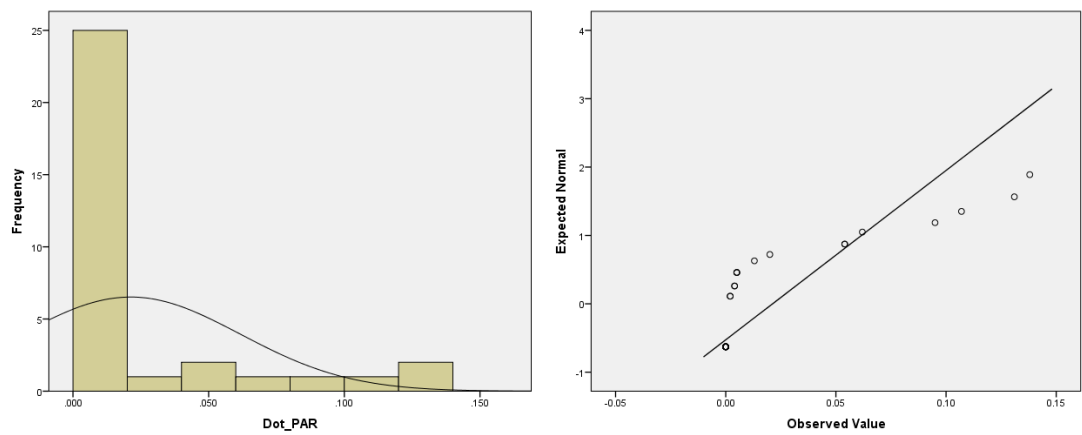


Figure 5.2.19 Histogram and Q-Q plot describing the distribution of Cortical Dot PAR in the DS group.

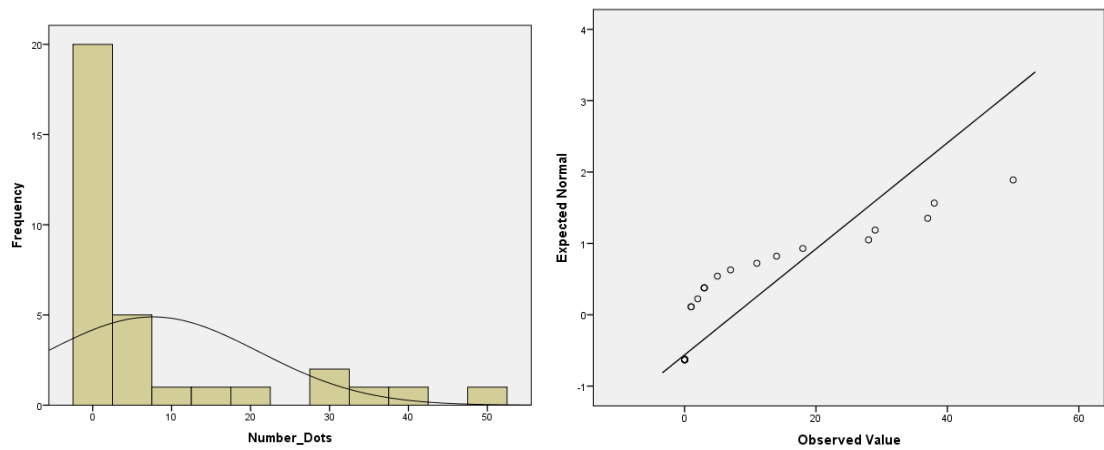


Figure 5.2.20 Histogram and Q-Q plot describing the distribution of number of cortical dots in the DS group.

Spearman's rank order analyses showed that dot PIR, PAR and total number were not associated to either participant age or VA. Naturally, linear regression analyses also did not show any relations between the measures of dot opacity and VA or age. Again, comparisons for the above analyses could not be made to controls because of the lack of any non-age-related cortical cataract in that population. Figure 5.2.21 shows OCT B-scans of age-related and dot cortical cataract in two participants with DS.

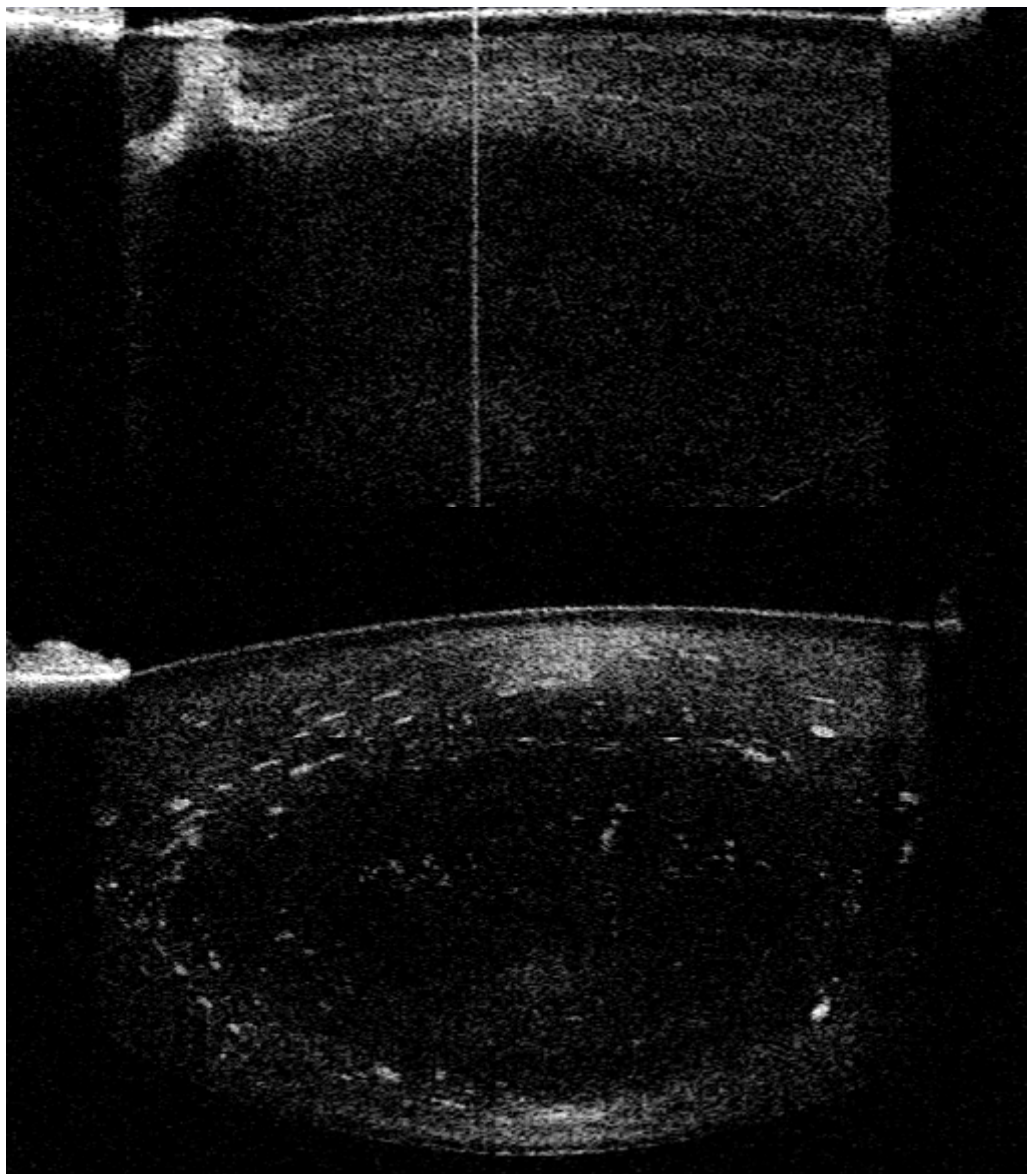


Figure 5.2.21 AS-OCT B-Scans showing age-related cortical cataract (top) and dot opacities (bottom) in two different participants with DS.

5.2.4.2.1 Comparisons of Cortical PIR Measures to LOCS III C Grades

Comparisons were made between OCT age-related and dot opacity measures of cataract, and LOCS III C scores for the DS group. Spearman's rank order analyses only showed a significant correlation between dot PAR and total number of dot opacities with LOCS III C. Linear regression analyses showed both dot PAR and total number of dots were significantly related to LOCS III C. Table 5.2.11 summarises these analyses. Scatterplots for the two significant regressions are shown in figure 5.2.22. No comparisons of the above analyses were made to cortical PIR or PAR as this was only present in one participant. Comparisons were not made in controls due to the lack of dot like cortical opacities in the distribution.

OCT Measure	LOCS III C		
	Correlation		Linear Regression
	Rho	Sig.	
Dot PIR	0.409	p = 0.146	Not Significant
Dot PAR	0.665	p = 0.009	$F_{(1,12)}=23.652, R^2=0.663, p<0.001$
Number of Dots	0.690	p = 0.006	$F_{(1,12)}=39.789, R^2=0.768, p<0.001$

Table 5.2.11 Summary of Spearman's correlation and linear regression analyses between OCT cortical measures of cataract and LOCS III C grades.

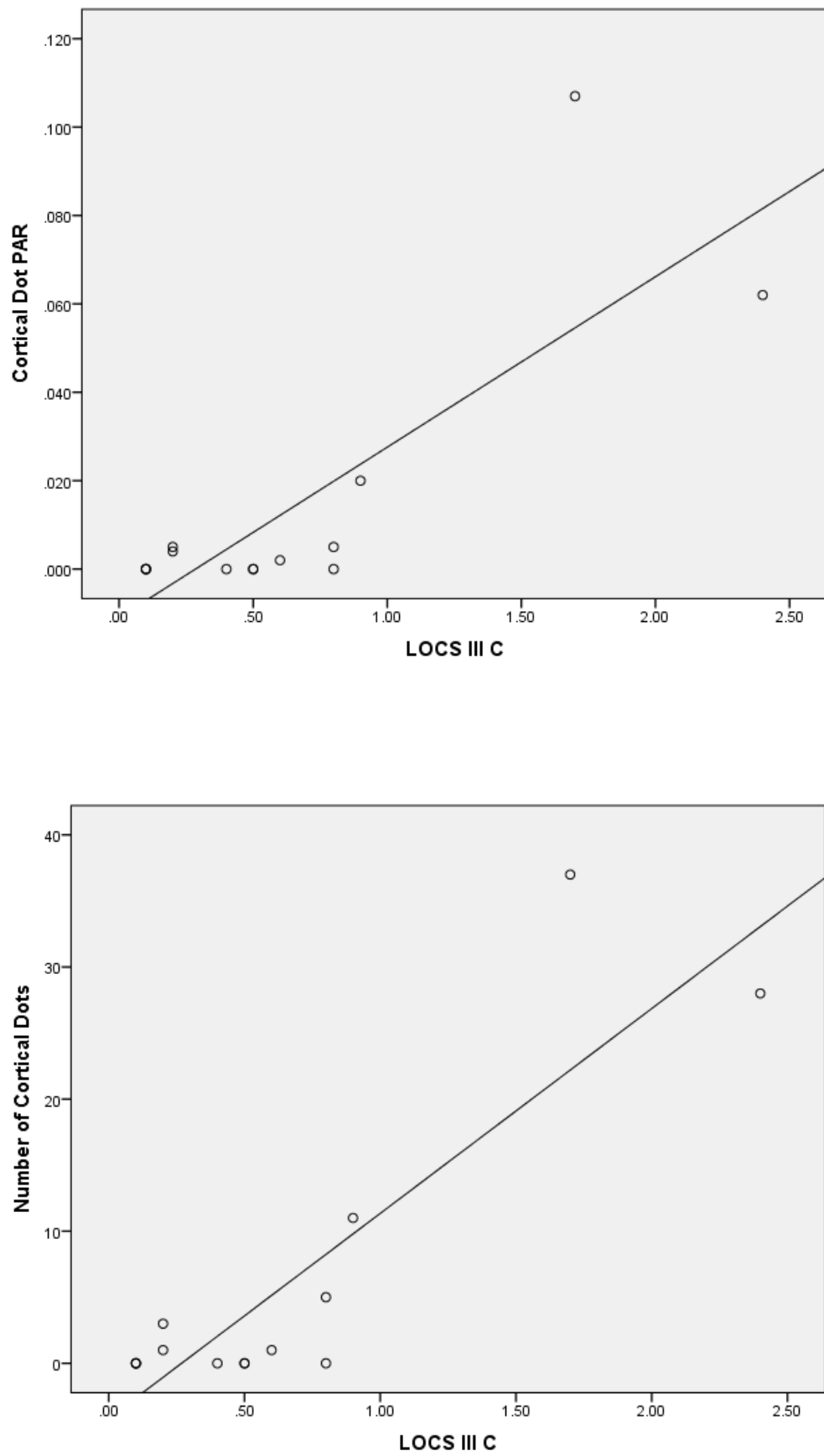


Figure 5.2.22 Scatterplots showing the relation between Cortical Dot PIR and LOCS C (top) and Number of Cortical Dots and LOCS III C (bottom).

5.2.4.3 OCT Posterior Subcapsular Grading in DS

The presence of posterior-subcapsular opacification detected with OCT in the study cohort was low. Only the same two eyes that had a LOCS III P grade over 0.1 also obtained scores above 0.000 for OCT PSC PIR and PAR. For participant 27 (RE: female 53.92 years of age), PSC PIR was 1.557 and PAR was 0.175, and for participant 23 (LE: male aged 55.36 years) PIR was 1.338 and PAR was 0.242. Figure 5.2.23 shows the OCT B-scans for both participants. Contrary to that found in the DS cohort, there was no presence of PSC in controls. Statistical analysis was not performed comparing LOCS III to OCT PSC due to the distribution of data containing outliers that influence the results as described in section 5.2.4.2.1.

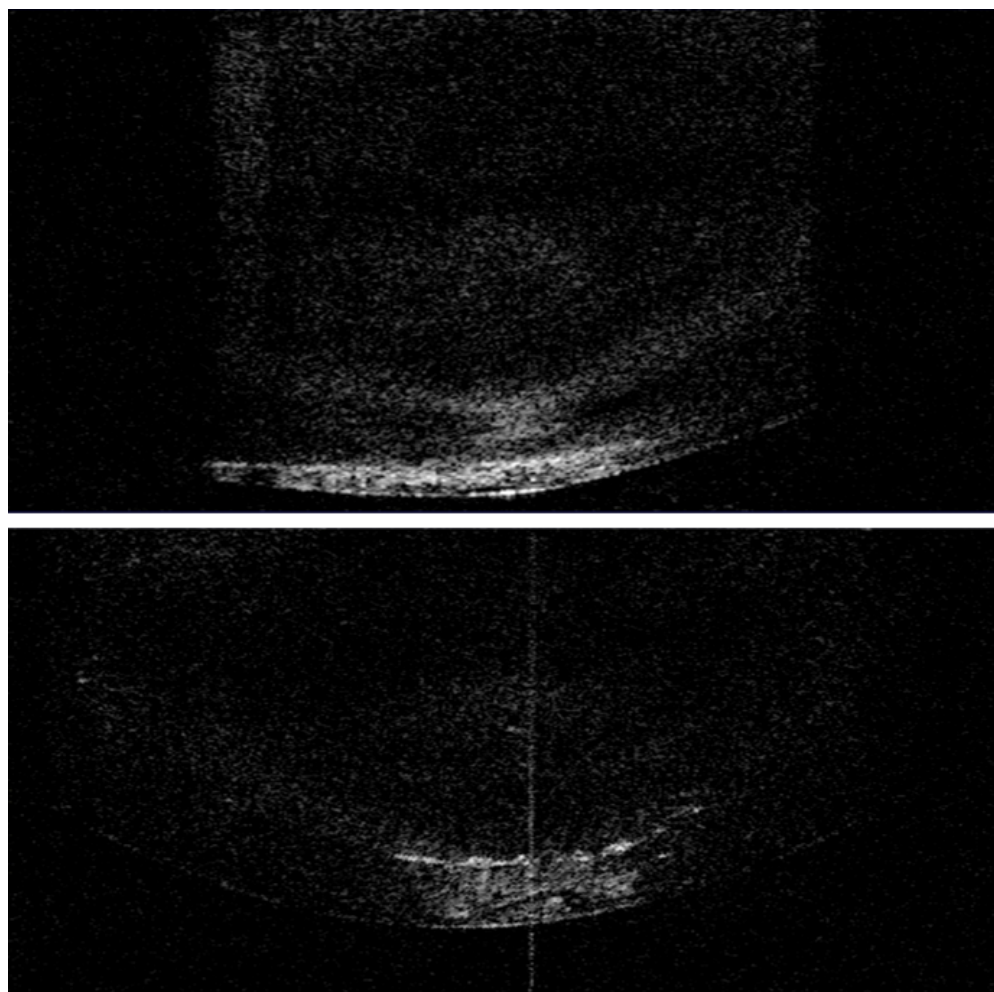


Figure 5.2.23 AS-OCT B-scans of the posterior crystalline lens showing PSC in the only two DS participants who presented with this morphology of cataract.

5.3 Discussion

5.3.1 Recruitment of Participants

This study successfully recruited its goal of 30 participants with DS however, two were excluded as explained in section 5.2.1. Overall, recruitment was difficult with over 200 potential participants directly solicited over the course of the study. Many parents and carers were initially interested in the study but became reluctant when they were informed of the need for pharmacologic pupil dilation. The study also successfully recruited subjects across a wide age range, including those at the higher end of life expectancy (Glasson *et al.* 2002; Bittles *et al.* 2007; Zigman 2013).

5.3.2 Visual Acuity

Monocular habitual VA measurement was obtained in 95% of eyes. Accounting for the intellectual disability in those with DS as summarised in chapter one, this is an excellent success rate. The VA levels of this study's cohort agree with previous research conducted in those with DS (Courage *et al.* 1994; Woodhouse *et al.* 1996; Tsiaras *et al.* 1999). Therefore, the statistically significant difference in VA found between this study's DS and control groups is acceptable. In the DS cohort, VA measures from both picture and letter optotypes were combined as research has shown that both crowded Kay picture and logMAR letter acuity is comparable (Elliott and Firth 2009). A small caveat lies in the fact that DS participants' habitual VAs were assessed in this study; while all parents and carers were asked to bring current spectacles and be aware of the participants' medical history, when participants arrived with a carer, in all but one case, they were unaware of any past medical or ophthalmic history, or if the participant was wearing current spectacles. Saying this, participants who attended day centres were seen regularly by a hospital optometrist for eye examinations.

5.3.3 Morphology of Lens Opacity in DS

5.3.3.1 Success Rates of Imaging the Lens in DS

There were mixed results regarding the successful capture of both slit lamp and AS-OCT images of the crystalline lens in those participants with DS. Slit lamp imaging of optic sections to enable nuclear LOCS III grading was quite successful, with 72.2% of eyes imaged. The success rate of retroillumination imaging for LOCS III C and P grading dropped significantly to 27.8%. This reduction is due to the careful alignment of the slit lamp illumination and axial position of the eye required to attain adequate retroillumination of the crystalline lens from the fundus. As participants with DS often did not sit still or were not able to maintain steady fixation for an adequate amount of time, the red reflex was either lost upon initiating capture of the photograph or never obtained in the first place. Imaging of the nucleus was easier in this instance because the slit lamp could be manipulated to ensure an optic section was maintained along with the movements of the participant's eyes. The discrepancy between gradable areas of the lens disappeared when acquiring AS-OCT B-scans. While the success rate of obtaining high-resolution B-scans was slightly lower than that of slit lamp imaging for LOCS III nuclear measures at 61.1%, these same images were also useable for grading every area of the crystalline lens. The lower capture rate of high-resolution OCT images compared to slit lamp optic sections was most likely a result of three factors: 1) AS-OCT imaging was conducted towards the end of the participants' appointments causing them to become tired and restless; 2) the Visante OCT was intimidating for participants as it required their eyes and face to be positioned just centimetres from the face of the instrument, with its chin and headrests in constant movement during imaging; 3) participants were required to maintain steady fixation for a few seconds while B-scans were acquired; as they had a natural tendency to look around, imaging artifacts were introduced, or central alignment of the crystalline lens was lost.

5.3.3.2 General Morphology of Lens Opacity in DS

In terms of age-related cataract that occurs in typically developed adults, the comparison between lens opacity found in DS and controls is interesting. When examining nuclear opacification, those with DS had much lower levels than their older controls. When comparing LOCS III nuclear measures between the groups, mean NO and NC values were very low in DS and the only three DS participants with grades over 1.0 were 55.4, 53.9 and 54.7 years of age; these participants were all in the same age bracket as controls and their LOCS III nuclear grades fit within the normal range of the control's distributions. Differences between DS and control groups were also seen in the correlation and regression analyses comparing LOCS III nuclear grades to age and VA. Regarding correlation, NO and NC were strongly associated with age and moderately with VA in DS, while in controls the only significant association was between NO and VA. Similarly, regression showed relations between LOCS III nuclear grades and both age and VA in DS but only between NO and VA in controls. These discrepancies are likely due to the large age spread in the DS cohort, especially with the very clear nuclei in children and young adults. Although the entire cohort of typically developed adults studied in Chapter 4 were not used as controls, the above-mentioned inconsistencies concerning correlation and regression are eliminated for VA when the entire cohort of typically developed adult participants is considered; this reinforces the idea that correlation and regression analyses were weak in controls due to their age range only spanning 10 years.

When comparing AS-OCT nuclear PIR values between DS and controls, the results were similar to those described above. Again, those with DS had significantly lower PIRs when compared to controls. The range of PIR values in DS was much greater than in controls. While correlation and regression analyses were significant between PIR and age as well as VA in DS again, as with LOCS III NO and NC, there was no relationship between these in controls. Again, this is likely due to the large spread of age in the DS cohort compared

to controls. While there was this difference between PIR, age and VA between groups the similarity between LOCS III nuclear measures and PIR correlations was very good. Also, the regression between NO, NC and PIR was slightly stronger in DS but this, again, may be due to the wide-ranging ages in the DS group. In summary, looking at both LOCS III and OCT measures of cataract, age-related nuclear lens opacification does not seem to occur at a younger age in DS.

The starkest difference between DS and controls occurred with the presence of cortical lens opacities. There were age-related cortical opacities present in three eyes from three control participants. In the DS group one participant presented with an age-related morphology of cortical cataract but many had multiple dot opacities within the cortex. As mentioned previously, the success rate of slit-lamp imaging to assess cortical opacity in DS by LOCS III analysis was very low, with gradable images in only 15 eyes. Of the graded eyes for C, 12 (80.0%) of them had scores above 0.1 and out of these, solely dot like opacities were present in 11 (73.3%) eyes. In the eye with age-related cortical cataract, there were no dot opacities visible in the retroillumination image. Interestingly, the participant with age-related cortical cataract was 26.67 years old and this explains the correlation and regression analyses showing no relation between LOCS III C and age.

Of the 33 eyes imaged with AS-OCT 18 (54.5%) had the presence of cortical opacities and of these, dot opacities were present in 16 (48.5%) eyes. The two eyes where dot opacities were not detected but cortical cataract was, belonged to participant number 5; this is the same participant who's RE was successfully graded for LOCS III C but where slit lamp retroillumination imaging was not successful in the LE. It should be noted that not all eyes imaged and graded for LOCS III C at the slit lamp were successfully imaged with AS-OCT. Despite this, the much higher image acquisition success rate in OCT highlights its potential effectiveness over the slit lamp retroillumination technique required for LOCS

III grading of non-nuclear opacities in populations of those with intellectual disability. Although there were mismatches where eyes were graded for LOCS III C but not OCT cortical measures and vice versa, based on the similar lack of correlation or regression seen in LOCS III C and OCT cortical grading, it is certain that the cortical opacities present in DS did not influence VA and were not related to age.

Through the course of acquiring images of the crystalline lens in DS, it was noted that occasionally, dot opacities were visible when viewing an optic section of the lens and sometimes, these were not visible on retroillumination. Also, due to the sparse number of dot opacities present in some participants, in some cases, the Visante OCT was not able to image them because a correctly aligned B-Scan could not be acquired while the participant maintained adequate fixation. The difference in the presence of dot opacities between LOCS III and AS-OCT images in this study could create confusion as to the actual prevalence of this specific morphology in DS however, when the researcher was photographing participants at the slit lamp, any opacities seen were noted. Therefore, a more reliable prevalence of these opacities can be determined by accounting for the eyes with dot opacities that were graded either solely with LOCS III or OCT ($n = 12$), and both LOCS III and OCT ($n = 7$). Of the eyes that were not successfully imaged with either modality, the researcher noted the presence of at least one dot opacity in seven additional eyes. Finally, accounting for the lack of cortical opacity noted in 10 eyes, it can be surmised that 26 out of 36 (72.2%) eyes showed the presence of cortical dot opacities in DS. In summary, the presence of age-related cortical cataract may occur at a younger age in DS (although this was identified in only one participant), but the presence of dot opacities in the cortex occurs at a very high rate. Furthermore, these cortical dot opacities seem to occur randomly without any link to age.

Participants with DS showed a greater presence of age-related PSC compared to controls. Although LOCS III P grading was only possible in 15 eyes, in the 33 eyes that were successfully imaged with OCT, no other PSC opacities were found. While the correlation and regression analyses showed a relation to VA and Age, this is a result of the two eyes with PSC acting as outliers. It should be noted that OCT provides benefits of imaging opacities for intensity and area; while LOCS III P grading requires a subjective interpretation of area only while disregarding darkness of the opacity, OCT imaging showed the exact location of PSC in the lens and allowed the discernment that the PSC in participant 27 was smaller in area but greater in intensity than that in participant 23. Saying this, the PSC opacities in the two participants were quite large and most likely would have had a significant effect on vision.

5.3.3.3 Morphology of Cataract in DS Compared to Previous Studies

In general, nuclear lens opacity does not seem to occur at a younger age or greater rate in those with DS but this cannot be said for age-related cortical and PSC opacification. The age-related cortical opacity occurred in a participant who was very young and while the posterior-subcapsular opacities occurred in the eldest individuals, this was in stark contrast to the absence of this type in any of the control eyes.

When compared to studies of lens opacity in DS, this study presents interesting results. The presence of lenticular opacity was seen in 77.8% of the 36 eyes that were either imaged by or seen at the slit lamp by the researcher. Previous studies have reported prevalence ranging from 4-72% (Jaeger 1980; Catalano 1990; Hestnes *et al.* 1991; Berk *et al.* 1996; daCunha and Moreira 1996; Woodhouse, Griffiths, *et al.* 2000; Kim *et al.* 2002; Liza-Sharmini *et al.* 2006; Fimiani *et al.* 2007; Krinsky-McHale *et al.* 2012; Fong *et al.* 2013; Wong and Ho 1997). Many of the studies reporting low rates of lens opacity were conducted in children and adolescents; this may account for the lower rates as some studies have

detected little cataract in those less than approximately 12 years of age (daCunha and Moreira 1996; Kim *et al.* 2002; Liza-Sharmini *et al.* 2006); the results from this study match very well with this as the lenses were clear in all imaged eyes of participants under the age of 12 years (n=5). Of the previous studies examining cataract in adults with DS, similarities do show between them and this study. Jaeger (1980) examined the eyes of 74 participants with DS aged 15 to 64 years and found 55.4% to have the presence of lens opacities. Of these opacities, the vast majority (65.8%) were describe as ‘flake-like’ opacities (Jaeger 1980); the author’s description of these matched those of the dot opacities that appeared in this study. Jaeger (1980) also found that 18.9% of the study group presented with age-related cataract at an average age of 48 years. Again, this matches well with the ages of participants in this study for age-related nuclear and PSC opacities. A study conducted by Woodhouse *et al.* (2000) on 31 DS adults with a mean age of 36.7 years, found a cataract prevalence of 22.6% however, there was no mention of morphology beyond either developmental or congenital. Woodhouse *et al.*’s (2000) study was done as part of a large ophthalmic screening where pupils were not dilated, and lens opacity was assessed with a direct ophthalmoscope; it is reasonable to assume that if these participants were examined under dilation using a slit lamp, the detection of cataract would be much higher. Another study examining the presence of lens opacity in adults with DS looked at past medical records to determine the occurrence of ophthalmic disorders in the group (Krinsky-McHale *et al.* 2012). The authors analysed 455 medical records from participants 30 to 81 years of age and found that cataract was the most common ophthalmic condition, with a prevalence of 42% (Krinsky-McHale *et al.* 2012). Krinsky-McHale *et al.* (2012) found the average age of cataract diagnosis to be 48.43 years; the authors did not make any mention of cataract morphology but based upon the fact that they were reviewing past medical records, these may have been age-related. There was an increasing prevalence of cataract with age noted by Krinsky-McHale *et al.* (2012) and, assuming these were age related opacities, this aligns with that of the nuclear opacification found in this study. Fong *et at.*

(2013) have recently conducted a study with one of the most descriptive analyses of cataract morphology in adults with DS. When examining 91 adults aged from 30 to 56 years, Fong et al. (2013) found that 72% of participants had the presence of opacities in the lens. Of those lens opacities, 50.6% were described as blue dot cataract and 45% were age-related and further broken down into 38% nuclear, 13.6% cortical and 8.5% PSC (Fong *et al.* 2013). These prevalence rates align quite well with those found in this study.

The flake-like and blue dot opacities that occur at a high prevalence in studies by Jaeger (1980), Fong et al. (2013) and others Catalano (1990), appear to be of the same morphology as the dot opacities seen in this study. Blue dot, or more appropriately cerulean, cataract is an acquired early onset lens opacity that often is first noticed in adolescence and consists of blue or white coloured opacities scattered primarily in the cortex but also in the nucleus of the crystalline lens (Armitage *et al.* 1995; Kanski and Bowling 2011). Of those whose lenses contained these opacities in this study, a few dot opacities were occasionally seen in the nucleus; this was also noticed by Jaeger (1980) in his description. In the 16 AS-OCT images that contained dot opacities, their presence in the central area of the lens was estimated by measuring the pupil margin with a calliper tool in MATLAB and then dividing this value by two. The resulting value estimated a size of approximately 4 to 4.5mm representing an undilated pupil. A box with this estimated undilated pupil size was then drawn centrally on the crystalline lens and spanning its entire anterior to posterior length; the number of dot opacities that lay inside the box were then counted. 81.3% of eyes contained centrally located dot opacities and of these, 43.5% of total dot opacities within the lens were located centrally, on average.

5.3.3.4 Morphology of Cataract in DS Compared to Beta-Amyloid Studies

As mentioned in Chapter 1, due to the close relationship between AD and DS, cataract in this population has been studied as a potential biomarker site for A β . Goldstein et al.

(2003) initially claimed that, through post-mortem immunohistochemical analysis, A β was present in lenses with a specific type of cataract located in the supranuclear area and, compared to controls, this cataract type was only present in typically developed participants with AD. The group then extended this research into lenses from those with DS (Moncaster *et al.* 2010). The authors showed that the blue dot cerulean cataract suggested to be characteristic of DS, was the same as the supranuclear cataract found in their previous study and related to A β deposition (Moncaster *et al.* 2010). The authors stated in both studies that this cerulean cataract was supranuclear and present annularly in the deep cortex (Goldstein *et al.* 2003; Moncaster *et al.* 2010). Supranuclear cataract is defined as a narrow band of opacity found at the interface between the deep cortex and nuclear interface, and may be sometimes known as lamellar or zonular (Chylack *et al.* 1983). Figure 5.3.1 shows the location of these opacities.

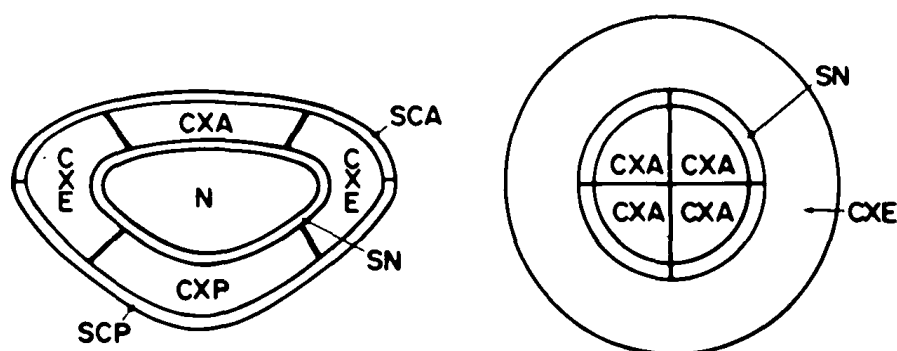


Figure 5.3.1 Cross-sectional diagrams of the crystalline lens showing the location of supranuclear (SN) opacities. Image taken from (Chylack *et al.* 1983)

The cerulean cataract found in those with DS from this study did not fit within the constraints of the supranuclear area. It was plainly visible in the OCT images that the dot opacities often progressed into the mid- and even peripheral cortex. In some cases, a few dot opacities were also present in the nucleus. While Moncaster *et al.* (2010) also claimed that the cerulean supranuclear cataract increased with age in DS, this study found no

relation between dot opacity and age in its analysis; this finding is counterintuitive in a population where prevalence and risk of AD greatly increase with age. Taking into consideration these differences, it may be possible that the relation between cerulean cataract and A β found by Goldstein et al. (2003) and Moncaster et al. (2010) may have been coincidental and a result of their very small sample sizes. This last statement is supported by subsequent studies using similar techniques as Goldstein et al. (2003) and Moncaster et al. (2010) but not finding any presence of A β in the human crystalline lens (Michael *et al.* 2014; Michael *et al.* 2013; Ho *et al.* 2014). Finally, the *in-vivo* analysis of cataract in participants with AD by Bei et al. (2015) showing no supranuclear cataract also reinforces the findings in this study.

5.4 Conclusion

This study provides a more detailed analysis of lens opacity than those that have come before. Previous studies in DS have only examined cataract qualitatively and this study, for the first time, has quantitatively graded the severity of cataract. The data produced in this study can provide a springboard for further work, but it is logical to conclude that lens opacity occurs at a very high rate in DS. Furthermore, the OCT images of lens opacity in DS have provided a unique insight into the typical location of cerulean opacity within the crystalline lens. As a result, this study has shown that cerulean cataract occurs commonly in DS, but its morphology does not appear to coincide with the description by studies linking it with A β and AD.

This study is limited by a small sample size that resulted from the reduced success rates in acquiring adequate quality images of the crystalline lens. This, coupled with the large age range present in the cohort, may have slightly weakened the undertaken statistical analyses. Saying this, the success rate of grading lens opacity was much better in AS-OCT than LOCS III; this is an exciting finding as the time domain technology of the Visante OCT

has been far surpassed by more modern Fourier domain modalities. This latter technology, especially with the newest swept-source whole eye imaging capability, will provide an excellent platform for studying opacity in the entire lens through volumetric cube scans rather than the B-scans performed in this study. Using this technology, longitudinal studies of cataract in DS are more than warranted.

Chapter 6: Posterior Segment OCT in Down Syndrome

6.1 Introduction

The following section outlines the study of retinal structure in DS using posterior segment optical coherence tomography. The same participants with DS from chapter 5 were imaged with the Spectralis PS-OCT. Imaging of the macula was performed using line and volume scans; peripapillary RNFL scans of the optic nerve head were also acquired. The methods for scan acquisition and analysis were described in Chapter 4.

6.2 B-Scans of the Macula in DS

Of the 54 eyes on which imaging was attempted, B-scans of the macula that traversed the fovea were successfully obtained in 17 eyes from 14 participants. Successful participant ages ranged from 7.75 to 54.68 years with a median of 24.68 ± 23.31 (IQR). Mean VA was 0.370 ± 0.198 (SD) logMAR with a range of 0.050 to 0.800. The age distribution was not normal while that of VA was (Shapiro-Wilk). Table 6.2.1 outlines the descriptive statistics for age and VA while figures 6.2.1 and 6.2.2 show the histograms and Q-Q plots for the measures.

Measure	Mean (SD)	Median (IQR)	Range	Shapiro-Wilk
Age (Years) (n=17)	24.86 (15.17)	24.68 (23.31)	7.75 to 54.68	p = 0.024
VA (logMAR) (n=17)	0.370 (0.198)	0.325 (0.300)	0.050 to 0.800	p = 0.503

Table 6.2.1 Descriptive statistics for age and VA in participants with DS whose eyes were successfully imaged with line scans.

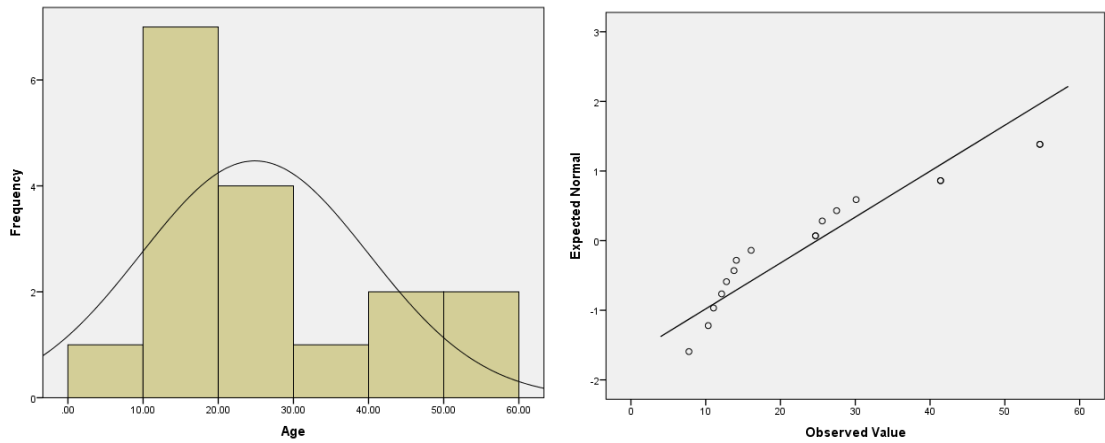


Figure 6.2.1 Histogram and Q-Q plot describing the distribution of age for those DS participants imaged with line scans.

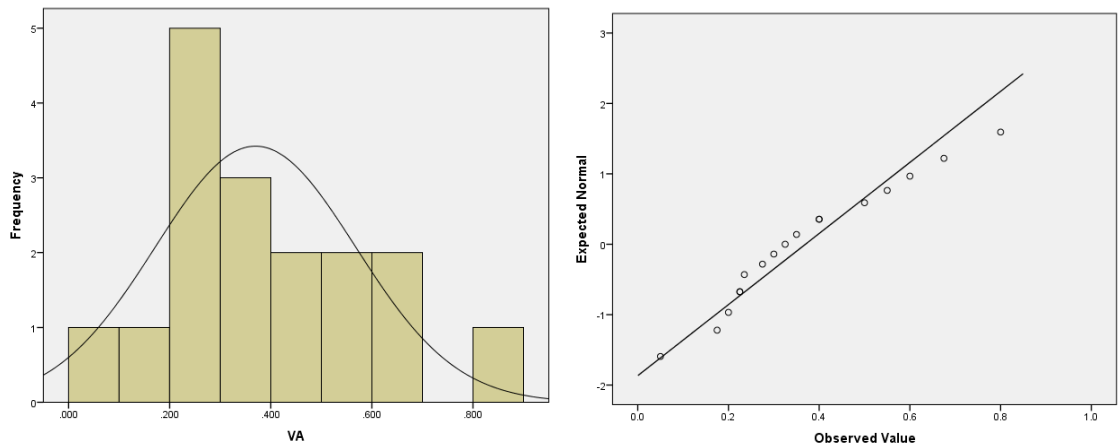


Figure 6.2.2 Histogram and Q-Q plot describing the distribution of VA for those DS participants imaged with line scans.

Data were also grouped into stratified age ranges consisting of those under 18 years and those aged 18 years and above. The distributions for VA and age are summarised for each group in tables 6.2.2 and 6.2.3.

Age Range	Mean (SD)	Median (IQR)	Range	Shapiro-Wilk
Under 18 (n=8)	12.25 (2.56)	12.45 (3.51)	7.75 to 16.07	p = 0.990
18 and Over (n=9)	36.08 (12.39)	30.11 (22.91)	24.68 to 54.68	p = 0.040

Table 6.2.2 Descriptive statistics for age in participants with DS whose eyes were successfully imaged with line scans when stratified by age.

Age Range	Mean (SD)	Median (IQR)	Range	Shapiro-Wilk
Under 18 (n=8)	0.289 (0.222)	0.230 (0.125)	0.050 to 0.800	p = 0.010
18 and Over (n=9)	0.442 (0.152)	0.400 (0.250)	0.200 to 0.675	p = 0.970

Table 6.2.3 Descriptive statistics for VA in participants with DS whose eyes were successfully imaged with line scans when stratified by age.

Macular B-scans were measured for minimum foveal thickness and foveal pit depth. Shapiro-Wilk analysis showed that both minimum thickness ($p = 0.253$) and depth ($p = 0.088$) were normally distributed. Mean minimum foveal thickness was 259 ± 20 (SD) μm with a range from 224 μm to 306 μm . Foveal pit depth ranged from 57 μm to 146 μm with a mean of $106 \pm 25\mu\text{m}$. Data for foveal thickness and pit depth were also stratified by age into groups consisting of those up to the age of 18 years and those aged 18 years and above. The descriptive data for all groups is summarised in tables 6.2.4 and 6.2.5.

Age Group (Years)	Mean (SD)	Median (IQR)	Range	Shapiro-Wilk
Under 18 (n=8)	270 (25) μm	264 (29) μm	224 to 306 μm	p = 0.489
18 and Over (n=9)	250 (8) μm	248 (9) μm	239 to 267 μm	p = 0.384
All ages (n=17)	259 (20) μm	255 (20) μm	224 to 306 μm	p = 0.253

Table 6.2.4 Descriptive statistics for minimum foveal thickness in participants with DS whose eyes were successfully imaged with line scans.

Age Group (Years)	Mean (SD)	Median (IQR)	Range	Shapiro-Wilk
Under 18 (n=8)	93 (29) μm	100 (55) μm	57 to 134 μm	p = 0.414
18 and Over (n=9)	117 (15) μm	113 (21) μm	105 to 146 μm	p = 0.009
All ages (n=17)	106 (25) μm	108 (20) μm	57 to 146 μm	p = 0.088

Table 6.2.5 Descriptive statistics for foveal pit depth in participants with DS whose eyes were successfully imaged with line scans.

Correlation analyses were performed to compare both minimum foveal thickness and pit depth to age and VA. For the comparisons between the measures and VA, where the distributions were all normal, Pearson analyses showed no association for the entire group of participants. As age was not normally distributed for all 17 eyes, a Spearman correlation was performed. A moderate association was found between age and foveal pit depth ($Rho = 0.549$, $p < 0.022$) but not minimum foveal thickness.

Linear regression was performed for the above comparisons and, again, the only significant relation was between age and foveal pit depth ($F_{(1, 15)} = 4.738$, $p = 0.046$, $R^2 = 0.240$). Figure 6.2.3 shows the scatterplot for this relation.

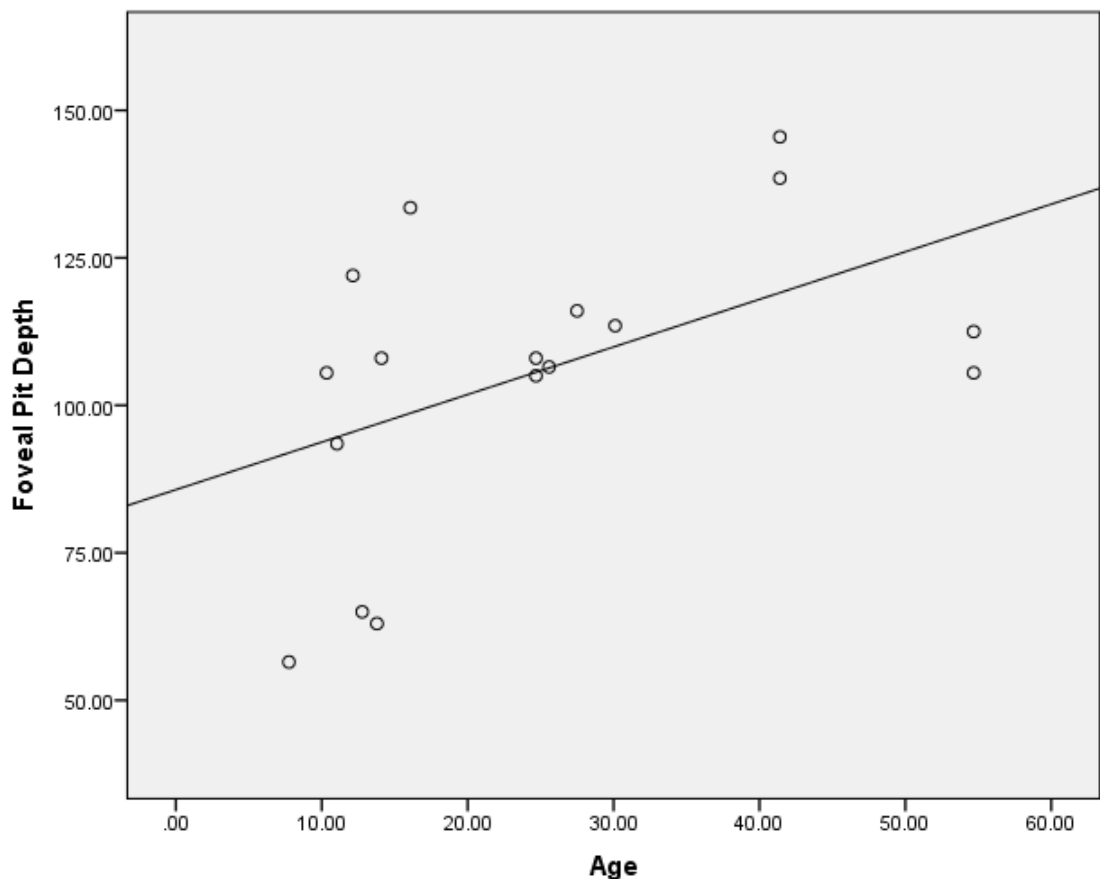


Figure 6.2.3 Scatterplot of the relationship between foveal pit depth and age.

When stratified by age, Mann-Whitney U tests showed that those aged under 18 years had significantly greater minimum foveal thickness ($U = 13.00$, $p = 0.027$) however, there was no statistically significant difference between the two groups for foveal pit depth. Correlation analyses showed no significant association for either age or VA when compared to minimum foveal thickness of foveal pit depth in those aged under 18 years. In those aged 18 years and older, VA showed a strong correlation with foveal pit depth ($Rho = 0.678$, $p = 0.045$) but not minimum foveal thickness; age was not correlated with either measure in this group. Linear regression showed a moderately strong and significant relation between VA and foveal pit depth ($F_{(1, 7)} = 10.079$, $p = 0.016$, $R^2 = 0.590$); the scatterplot is shown in figure 6.2.4.

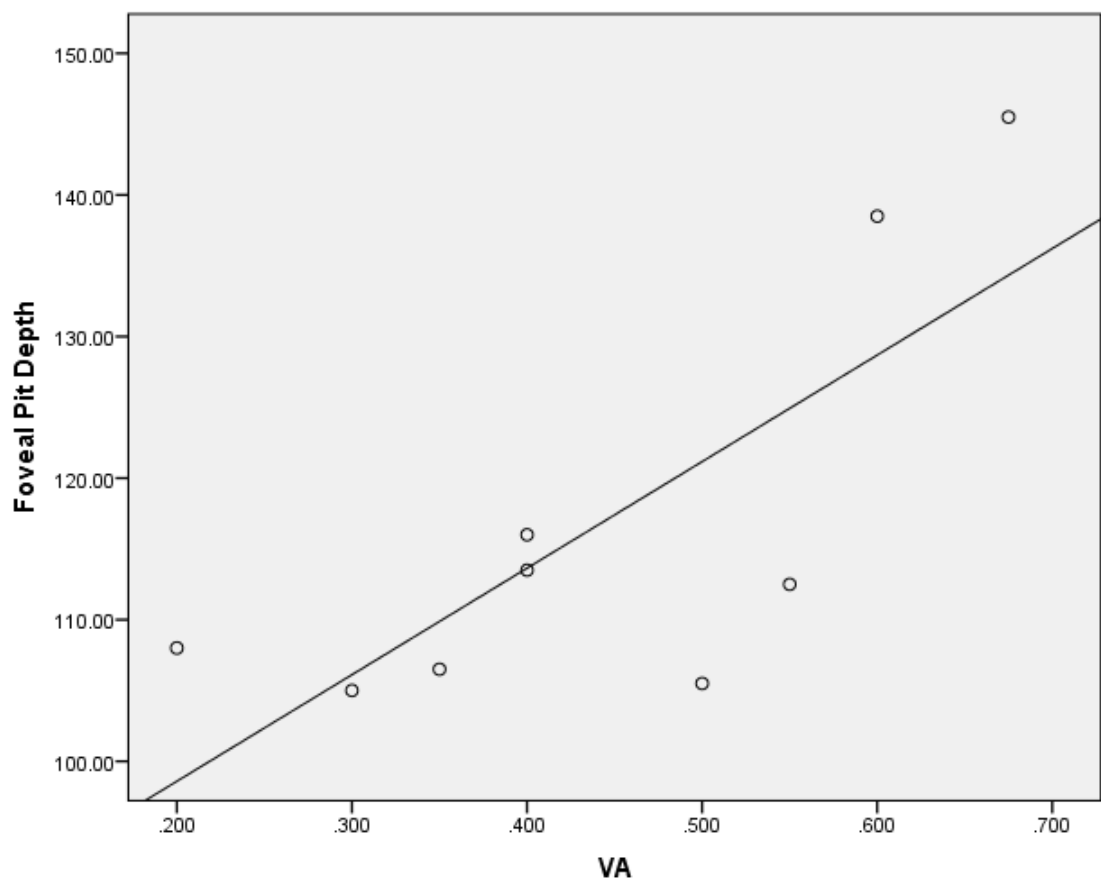


Figure 6.2.4 Scatterplot of the relationship between foveal pit depth and VA for those aged 18 years and older.

6.3 Volume Scans of the Macula in DS

Macular volume scans were successfully acquired in 6 eyes from four participants. Mean age for the group was 21.85 ± 11.52 (SD) years with a range from 10.33 to 41.40 years. VA ranged from 0.235 to 0.600 logMAR with a mean of 0.370 ± 0.143 (SD). The distributions of average macular thickness for each region of the ETDRS grid for all imaged eyes are outlined in table 6.3.1. Shapiro-Wilk testing showed that all measures of macular thickness as well as VA and age were normally distributed.

ETDRS Region	Mean (SD)	Median (IQR)	Range	Shapiro-Wilk
Central 1mm	303 (20) μm	298 (32) μm	285 to 339 μm	$p = 0.273$
Superior 3mm	371 (17) μm	369 (28) μm	353 to 400 μm	$p = 0.680$
Inferior 3mm	366 (20) μm	362 (32) μm	343 to 397 μm	$p = 0.814$
Nasal 3mm	371 (22) μm	367 (39) μm	349 to 404 μm	$p = 0.415$
Temporal 3mm	352 (20) μm	345 (29) μm	335 to 389 μm	$p = 0.117$
Superior 6mm	327 (10) μm	328 (17) μm	314 to 341 μm	$p = 0.771$
Inferior 6mm	314 (17) μm	311 (30) μm	293 to 339 μm	$p = 0.887$
Nasal 6mm	349 (13) μm	347 (24) μm	333 to 368 μm	$p = 0.847$
Temporal 6mm	307 (14) μm	305 (20) μm	289 to 331 μm	$p = 0.738$

Table 6.3.1 Summary of average retinal thickness values for each region of the macular ETDRS grid for all 6 imaged eyes.

Pearson correlation analyses showed no association between any ETDRS thickness measure and participant age or VA. Naturally, linear regression showed there was no significant relation between any ETDRS measure and either age or VA. Mann-Whitney U tests showed no significant difference between any measure when grouped by those under the age of 18 years ($n=3$) and those aged 18 years and older ($n=3$).

6.4 Retinal Nerve Fibre Layer Thickness in DS

Peripapillary RNFL scans were successfully obtained in 10 eyes from seven participants. The groups' ages ranged from 12.13 to 41.40 years with a mean of 21.27 ± 9.73 (SD) years. Mean VA was 0.292 ± 0.182 logMAR with a range from 0.050 to 0.675. Table 6.4.1 displays the descriptive statistics for all regions of RNFL thickness including tests of normality (Shapiro-Wilk); not all regions were normally distributed.

Peripapillary Region	Mean (SD)	Median (IQR)	Range	Shapiro-Wilk
Global	132 (14) μm	124 (22) μm	118 to 156 μm	$p = 0.025$
Temporal	98 (10) μm	98 (12) μm	85 to 120 μm	$p = 0.462$
Temporal-Superior	210 (30) μm	211 (49) μm	160 to 259 μm	$p = 0.988$
Temporal-Inferior	188 (16) μm	186 (23) μm	169 to 220 μm	$p = 0.354$
Nasal	87 (18) μm	81 (25) μm	65 to 120 μm	$p = 0.035$
Nasal-Superior	146 (24) μm	146 (41) μm	102 to 181 μm	$p = 0.906$
Nasal-Inferior	144 (49) μm	124 (86) μm	101 to 230 μm	$p = 0.015$

Table 6.4.1 Summary of average RNFL thickness values for each peripapillary region for all 10 eyes. P-values for normal distributions are bolded.

Depending on normalcy of the distribution, either Pearson or Spearman correlation analyses did not show any significant association between any RNFL thickness region and either age or VA. When stratified by age, there was no significant difference in RNFL thickness in any peripapillary region between those under the age of 18 years ($n=5$) and those aged 18 years and older ($n=5$) (Mann-Whitney U test).

6.5 Discussion

6.5.1 Success Rates

Successful acquisition of adequate quality PS-OCT images was very low for all three scanning modalities with only 31%, 19% and 11% of macular line, macular volume and peripapillary RNFL tomographs captured. These poor rates are most likely due to the PS-OCT imaging being conducted just after the installation of tropicamide, in a small window of time before imaging of the crystalline lens was undertaken. As crystalline lens imaging was a priority of this thesis, less emphasis was placed on acquiring PS-OCTs. The time limitation for PS-OCT is demonstrated by the decreasing success rates from line scans through to macular volume scans. While line scans could be captured very quickly if participants were able to fixate on the Spectralis' internal target, much more time was required for RNFL and especially macular cube scans, which required very steady fixation while multiple B-scans were captured.

6.5.2 Macular Thickness in DS

To date, the only published *in vivo* data examining the macula using OCT has been conducted by Laguna *et al.* (2013) and O'Brien *et al.* (2015). In the first study, the authors performed macular volume scans on five eyes from three participants with DS. Laguna *et al.* (2013) reported that retinal thickness was greater in DS when compared to age matched controls particularly at the central 1mm ETDRS subfield. The authors also reported that the gross appearance of the retinal layers of macular OCT B-scans did not appear different to a typically developed retina (Laguna *et al.*, 2013); the macular scans from this study also support this as all images of adequate quality showed a regular appearance and order of retinal layers. O'Brien *et al.* (2015) performed macular volume scans in 17 children with DS aged 6-16 years and compared thickness to age-matched controls. Macular thickness was determined to be significantly greater in all areas of the ETDRS grid apart from the

temporal areas (O'Brien *et al.* 2015). Similarly to this study, O'Brien *et al.* (2015) also found no association between macular thickness and VA in DS.

Although this study did not include age-matched controls, previous work has been conducted to determine normative values. A study conducted by Grover *et al.* (2009) performed macular volume scans on 50 adults with no retinal pathology aging in range from 20 to 84 years. The authors went on to determine normative values for each ETDRS subfield and also found no association between retinal thickness and age. Table 6.5.1 summarises the normative data collected by Grover *et al.* (2009) as well as the data from this study for retinal thickness in DS.

ETDRS Region	This Study's Mean (SD) for participants with DS	Normative Data for Mean (SD) Retinal Thickness Determined by Grover <i>et al.</i>
Central 1mm	303 (20) μm	270.2 (22.5) μm
Superior 3mm	371 (17) μm	336.0 (20.6) μm
Inferior 3mm	366 (20) μm	334.9 (16.7) μm
Nasal 3mm	371 (22) μm	335.0 (19.3) μm
Temporal 3mm	352 (20) μm	322.6 (16.5) μm
Superior 6mm	327 (10) μm	329.6 (16.4) μm
Inferior 6mm	314 (17) μm	325.4 (16.6) μm
Nasal 6mm	349 (13) μm	339.5 (16.9) μm
Temporal 6mm	307 (14) μm	320.1 (15.4) μm

Table 6.5.1 Summary of average retinal thickness values for each region of the macular ETDRS grid for all 6 imaged eyes in this study (left column) and normative data obtained by Grover *et al.* (2009) (right column).

While the data from this study show no association between retinal thickness and age, which agrees with the findings by Grover *et al.* (2009), retinal thickness in DS appears to be significantly thicker in the central and 3mm ETDRS subfields when compared to

normative values. Hence, the data from this study supports that found by Laguna *et al.* (2013) and O'Brien *et al.* (2015).

As foveal hypoplasia has been mentioned to occur in DS (Stirn Kranjc 2012), minimum foveal thickness and foveal pit depth were measured from macular B-scans through the fovea. While regression and correlation analyses showed an association between increasing foveal pit depth and worsening VA in those aged 18 years and older, which is counterintuitive, this was most likely influenced by the two outliers (see figure 6.2.4) and the small sample size. The association between foveal pit depth and increasing age was also very weak and bordering on statistical insignificance. A larger sample size is required to determine whether these relations remain with greater statistical power.

Again, because controls were not included in this study, it is difficult to determine the exact morphology of the fovea in DS and whether this is differed from that in a typically developed eye. Normative data for foveal thickness and have been determined using similar methods of measurement. Tick *et al.* (2011) measured minimum foveal thickness and foveal pit depth in 110 eyes of 57 healthy adults aged 18 to 45 years using a Spectralis PS-OCT. Using custom software, the authors determined mean foveal thickness to be 230 ± 21 (SD) μm and mean foveal pit depth to be 131 ± 22 (SD) μm (Tick *et al.* 2011). In this study, mean minimum foveal thickness was 259 ± 20 (SD) μm and mean foveal pit depth was $106 \pm 25\mu\text{m}$. Therefore, this study, even when stratified by age to account for the absence of those under 18 years in Tick *et al.*'s (2011) sample, gives evidence that those with DS appear to have thicker foveae and decreased foveal depth compared to their typically developed counterparts. Although minimum foveal thickness was significantly greater in those with DS under 18 years of age compared to participants 18 and older, the

fact that this difference disappeared between the stratified age ranges for foveal pit depth reinforces the previously mentioned point.

6.5.3 Retinal Nerve Fibre Layer Thickness in DS

There are no reports in the literature quantifying retinal thickness in a sample of those with DS. While controls were not present in this study, a normative database for RNFL thickness derived from 201 subjects of ‘Caucasian ethnicity’ aged from 18 to 78 years exists within the Spectralis’ analysis software (Heidelberg Engineering 2013). When compared to this normative database the RNFL appeared to be significantly thicker in certain quadrants. While the figures from the Spectralis’ normative database are not available, there have been studies deriving these figures in adults and children. Leung *et al.* (2010) determined normal peripapillary RNFL thickness using the Spectralis PS-OCT in 76 adults with a mean age of 48.76 ± 13.54 years while, in a separate study, Yanni *et al.* (2013) used a Spectralis PS-OCT to determine normative values in 83 children aged from five to 15 years; the data from these studies along with those from this study are outlined in table 6.5.2.

Peripapillary Region	This Study's Mean (SD) for all Participants	This Study's Mean (SD) for Adults	This Study's Mean (SD) for Children	Leung <i>et al.</i> Normative Mean (SD) for Adults	Yanni <i>et al.</i> Normative Mean (SEM) for Children
Global	132 (14)	129 (10)	135 (19)	104.5(10.1)	107.6(1.2)
Temporal	98 (10)	101 (12)	96 (8)	86.3(15.8)	76.5(1.9)
Temporal-Superior	210 (30)	207 (31)	212 (31)	144.4(18.6)	145.1(2.2)
Temporal-Inferior	188 (16)	181 (8)	196 (20)	158.7(19.1)	147.0(2.1)
Nasal	87 (18)	83 (20)	91 (18)	68.6(16.5)	84.5(1.9)
Nasal-Superior	146 (24)	153 (22)	139 (26)	110.2(22.9)	116.2(2.8)
Nasal-Inferior	144 (49)	125 (35)	162 (57)	111.7(24.1)	125.4(3.0)

Table 6.5.2 Summary of average RNFL values in μm for each peripapillary region for all participants and bracketed by age along with and normative data obtained by Leung *et al.* (2010) and Yanni *et al.* (2013).

Comparing the results from this study to those from Leung *et al.* (2010) and Yanni *et al.* (2013), strongly suggests that the RFNL layer is thicker globally and especially in the temporal-superior and nasal-superior regions in those with DS. As it has also been reported that RNFL thickness decreases with age it is interesting to note the absence of this occurrence in this study although this may be a result of the low sample size.

6.5.4 Retinal Structure in DS Compared to Studies in AD

As explained in Chapter 1, the prevalence of AD in DS is high with all individuals showing neuropathological signs by the age of 40 years. Studies of retinal structure in typically developed adults with AD using OCT have demonstrated characteristic changes that correspond with neurodegeneration (Cunha, Almeida, *et al.* 2016; Doustar *et al.* 2017; den Haan *et al.* 2017). Specifically, studies have shown strong evidence for peripapillary RNFL thinning in AD compared to aged matched controls (Paquet *et al.* 2007; Marziani *et al.* 2013; Kirbas *et al.* 2013; Cunha, Lopes, *et al.* 2016; Cunha, Almeida, *et al.* 2016; Doustar *et al.* 2017; den Haan *et al.* 2017). In a recent meta-analysis, den Haan *et al.* (2017) determined that while RNFL thinning occurred in all four peripapillary quadrants in AD, the superior and inferior quadrants were thinner than the nasal and temporal quadrants. The results from this study suggest the complete opposite occurs in the retina in DS when compared to the above-mentioned studies in AD, with a thicker RNFL compared to typically developed adults and children. A similar discrepancy is seen between the macular thickness results in this study when compared to studies of macular thickness of typically developed adults with AD. Studies have shown that macular thickness is thinner in each ETDRS subfield in typical adults with AD when compared to age-matched controls (Marziani *et al.* 2013; Cunha, Almeida, *et al.* 2016; den Haan *et al.* 2017). A meta-analysis by den Haan *et al.* (2017) determined thinning to be the highest in the outer ring, followed by the inner ring and then fovea in those with AD. Again, the results from this study suggest that the macula in DS does not follow the pattern of change seen in AD.

6.6 Conclusion

While this study is small in sample size and limited by the lack of controls, it has added valuable data to the assessment of retinal structure in DS. The results from this study mirror those of Laguna *et al.* (2013) and O'Brien *et al.* (2015) suggesting a thickened macular structure in those with DS. Also, the decreased foveal pit depth typical of the participants in this study, lends support to the presence of foveal hypoplasia occurring in this population. Finally, this is the first study to examine peripapillary RNFL thickness in DS and the data show that the features of this structure in DS does not seem related to those found in AD. Further large-scale longitudinal study of the above parameters should be conducted to detail retinal characteristics in DS.

Chapter 7: Thesis Summary and Future Work

7.1 Primary Outcomes

The primary aim of this thesis was to profile the structure of cataract that occurs in the down syndrome eye in detail. A number of steps were taken in order to accomplish this. Firstly, the modification and digitisation of a slit-lamp biomicroscope to capture high-resolution images of the eye was carried out as described in Chapter 2. The method developed in this thesis can be applied to various models of slit-lamp biomicroscopes as an inexpensive means of updating or adding features to older equipment. This is useful for, not only research labs and clinics alike, but perhaps in developing nations as well.

The second outcome of this thesis was the production of custom software to process raw OCT sensor data and subsequently segment it as a means of analysing crystalline lens opacity. A method to process .bin files from the Visante OCT has been described in Chapter 3, providing a solution for other researchers who may encounter difficulty with this. Furthermore, the application of the software to study a population of typically developed adults has demonstrated its utility in accurately analysing age-related crystalline lens opacity and shown the potential of OCT to determine the location and quantify the severity of any lens opacity; in line with this, the novel use of PIR and PAR provide an approach that will be useful in future studies of lens opacity. The agreement to LOCS III analysis and previous studies of visual function in relation to cataract further cement the use of OCT as an objective and repeatable method of assessing lens opacity.

Following on from the above outcomes, the primary aim of this thesis was achieved using the newly developed and validated method of OCT analysis to perform a detailed study of lens opacity in a population of individuals with Down syndrome. This is the first study to perform such an analysis of cataract in DS including the provision of quantitative data. Punctate dot opacities appear to be characteristic in DS and their morphology does not

coincide with previous studies linking supranuclear cataract to Alzheimer's disease. This study has also shown the superiority of OCT imaging, when compared to slit-lamp assessment, in determining location of lens opacity; it enabled the observation that dot opacities were often present centrally in the anterior and posterior cortex and, occasionally, nucleus of the crystalline lens.

As an adjunct, this thesis also examined macular and peripapillary retinal structure in DS using OCT. Findings show increased macular thickness and evidence for foveal underdevelopment, which express agreement with the few brief studies examining retinal structure in DS. The RNFL results from this study are the first to be reported in DS and do not coincide with the thinning that has been reported by previous work in typically developed adults with Alzheimer's disease.

7.2 Limitations

In terms of OCT imaging and grading of cataract, there are a few limitations of this study. The use of time-domain technology resulted in a slow acquisition time of B-scans and the requirement to capture separate anterior and posterior images of the crystalline lens at a lower resolution compared to more modern Fourier-domain technology. Furthermore, the capability of the Visante OCT to only acquire single line scans meant that only B-scans through the most significant portion of lens opacity could be captured. This means that the complete assessment of all lens opacity within the crystalline lens could not be measured. Saying this, the current methods of assessing lens opacity are limited by this same two-dimensional analysis. Finally, the manual segmentation required by the custom software opens the analysis of lens opacity to human error; although care was taken by the researcher in segmenting the images which resulted in good repeatability, this is not practical for clinical application in large cohorts.

The above limitations also affect the results for the assessment of lens opacity in Down syndrome. Contrasting with typically developed adults, the intellectual disability present in those with DS contributed to a lower success rate in image acquisition and therefore, reduced statistical power. The two-dimensional B-scans were also not able to provide exhaustive data on the severity and location of lens opacity in this population because of the limitations in OCT imaging mentioned above. Further, as this study of lens opacity in DS was cross-sectional and over a wide age range, it cannot be determined conclusively as to how lens opacity changes over time individually in those with DS.

As it was conducted as an addendum, the assessment of retinal structure in this thesis is limited by its small sample size. Due to the poor imaging success rate and lack of controls, the data only provide a preliminary view of retinal morphology in DS. Less of an emphasis was placed on successfully acquiring useable images as a countermeasure to reduce fatigue in participants and thereby increase the chances of acquiring images of the crystalline lens. The data from this portion of the study can be used to provide a small insight into the morphology of retinal structure in DS but are useful for power calculations and future study design.

7.3 Future Work

As OCT has been shown to provide a robust method of imaging and assessing lens opacity, further application and development towards this are warranted. Modern Fourier-domain modalities of OCT can be used to image the crystalline lens volumetrically; this will enable very high-resolution images showing the status of opacity throughout the entire lens. Through the continued improvement of the software, algorithms can be developed to automate the segmentation of these three-dimensional tomographs; applying this to whole-eye OCT will provide an ideal solution of examining cataract in diseased and clinical populations.

The above-mentioned improvements can then be applied to further assess the status of lens opacity in DS. By performing a longitudinal study, a detailed understanding of how the crystalline lens changes in DS can be attained. This will be useful in understanding whether the punctate lenticular opacities seen in DS occur randomly or are associated with other cognitive or disease processes. These longitudinal studies would ideally be conducted in cohorts of those with DS who are seen regularly within the Hospital Eye Service; this would significantly increase imaging success rates, as participants would not have to undergo a battery of assessments in one sitting. Also, as this thesis was concerned with the morphological assessment of cataract in DS, an emphasis was not placed on the functional assessment of vision. Further studies examining cataract in DS with OCT imaging along with the assessment of contrast sensitivity would be useful.

Finally, the results of this thesis show that a detailed assessment of retinal structure using OCT is warranted in DS. A larger study with the inclusion of typically developed controls and those with diagnosed AD would provide valuable information as to whether the retina exhibits similar changes to those in AD, or if this is not the case as suggested by the data in this study.

References

- Al-Hemidan, A.I., Al-Hazzaa, S.A., Chavis, P. and Al-Hussein, H. (1999). Optic disc elevation in Down syndrome. *Ophthalmic genetics* **20**:45–51.
- Albert, M.S., DeKosky, S.T., Dickson, D., Dubois, B., Feldman, H.H., Fox, N.C., Gamst, A., *et al.* (2011). The diagnosis of mild cognitive impairment due to Alzheimer's disease: Recommendations from the National Institute on Aging-Alzheimer's Association workgroups on diagnostic guidelines for Alzheimer's disease. *Alzheimer's and Dementia* **7**:270–279.
- Alexander, M., Ding, Y., Foskett, N., Petri, H., Wandel, C. and Khwaja, O. (2016). Population prevalence of Down's syndrome in the United Kingdom. *Journal of Intellectual Disability Research* **60**:874–878.
- Andley, U.P. (2007). Crystallins in the eye: Function and pathology. *Progress in retinal and eye research* **26**:78–98.
- Anwar, A.J., Walker, J.D. and Frier, B.M. (1998). Type 1 diabetes mellitus and Down's syndrome: Prevalence, management and diabetic complications. *Diabetic Medicine* **15**:160–163.
- Armitage, M.M., Kivlin, J.D. and Ferrell, R.E. (1995). A progressive early onset cataract gene maps to human chromosome 17q24. *Nature Genetics* **9**:37–40.
- Augusteyn, R.C. (2010). On the growth and internal structure of the human lens. *Experimental eye research* **90**:643–654.
- Bailey, I.L., Bullimore, M.A., Raasch, T.W. and Taylor, H.R. (1991). Clinical grading and the effects of scaling. *Investigative ophthalmology & visual science* **32**:422–432.
- Bailey, I.L. and Lovie-Kitchin, J.E. (2013). Visual acuity testing. From the laboratory to the clinic. *Vision Research* **90**:2–9.
- Beacher, F. and Murphy, D.G.M. (2006). Neuroimaging studies of individuals with Down syndrome. In: Prasher, V. P. (ed.) *Down Syndrome and Alzheimer's Disease Biological Correlates*. Oxford: Radcliffe Publishing Ltd, pp. 157–175.
- Bei, L., Shui, Y.B., Bai, F., Nelson, S.K., Van Stavern, G.P. and Beebe, D.C. (2015). A test of lens opacity as an indicator of preclinical Alzheimer Disease. *Experimental Eye Research* **140**:117–123.

- Bell, R., Rankin, J. and Donaldson, L.J. (2003). Down's syndrome: occurrence and outcome in the north of England, 1985-99. *Paediatr Perinat Epidemiol* **17**:33–39.
- Van den Berg, T.J.T.P., Franssen, L., Kruijt, B. and Coppens, J.E. (2013). History of ocular straylight measurement: A review. *Zeitschrift für Medizinische Physik* **23**:6–20.
- Van Den Berg, T.J.T.P., Van Rijn, L.J. (René, Michael, R., Heine, C., Coeckelbergh, T., Nischler, C., Wilhelm, H., *et al.* (2007). Straylight Effects with Aging and Lens Extraction. *American Journal of Ophthalmology* **144**.
- Berk, A.T., Saatci, A.O., Ercal, M.D., Tunc, M. and Ergin, M. (1996). Ocular findings in 55 patients with Down's syndrome. *Ophthalmic genetics* **17**:15–19.
- Bertram, L. and Tanzi, R.E. (2008). Thirty years of Alzheimer's disease genetics: the implications of systematic meta-analyses. *Nature Reviews Neuroscience* **9**:768–778.
- Bittles, A.H., Bower, C., Hussain, R. and Glasson, E.J. (2007). The four ages of Down syndrome. *European Journal of Public Health* **17**:221–225.
- Blennow, K., Hampel, H., Weiner, M. and Zetterberg, H. (2010). Cerebrospinal fluid and plasma biomarkers in Alzheimer disease. *Nature Reviews Neurology* **6**:131–144.
- Bron, A.J., Wolff, E., Tripathi, R.C. and Tripathi, B.J. (1997). *Wolff's Anatomy of the Eye and Orbit*. 8th ed. London: Chapman & Hall Medical.
- Bull, M.J. (2011). Clinical Report-Health Supervision for Children With Down Syndrome. *Pediatrics* **128**:393–406.
- Burdick, D., Soreghan, B., Kwon, M., Kosmoski, J., Knauer, M., Henschen, A., Yates, J., *et al.* (1992). Assembly and Aggregation Properties of Synthetic Alzheimers a4/Beta Amyloid Peptide Analogs. *Journal of Biological Chemistry* **267**:546–554.
- Caputo, A.R., Wagner, R.S., Reynolds, D.R., Guo, S. and Goel, A.K. (1989). Down Syndrome - Clinical Review of Ocular Features. *Clinical pediatrics* **28**:355–358.
- Carl Zeiss Meditec *Visante Model 1000 System Software Version 3.0 User Manual*.
- Castane, M., Boada-Rovira, M. and Hernandez-Ruiz, I. (2004). [Eye conditions as features of Down's syndrome in patients over 40 years of age]. *Rev Neurol* **39**:1017–1021.
- Catalano, R.A. (1990). Down syndrome. *Survey of ophthalmology* **34**:385–398.
- Catalano, R.A. and Simon, J.W. (1990). Optic Disk Elevation in Downs-Syndrome. *American Journal of Ophthalmology* **110**:28–32.

- Chan, T.C.Y., Li, E.Y.M. and Yau, J.C.Y. (2014). Application of anterior segment optical coherence tomography to identify eyes with posterior polar cataract at high risk for posterior capsule rupture. *Journal of Cataract and Refractive Surgery* **40**:2076–2081.
- Chapman, R.S. and Hesketh, L.J. (2000). Behavioral phenotype of individuals with down syndrome. *Mental Retardation and Developmental Disabilities Research Reviews* **6**:84–95.
- Chua, B.E., Mitchell, P. and Cumming, R.G. (2004). Effects of cataract type and location on visual function: The Blue Mountains Eye Study. *Eye* **18**:765–772.
- Chylack, L.T., Lee, M.R., Tung, W.H. and Cheng, H.M. (1983). Classification of Human Senile Cataractous Change by the American Cooperative Cataract Research Group (Ccrgr) Method .1. Instrumentation and Technique. *Investigative ophthalmology & visual science* **24**:424–431.
- Chylack, L.T., Leske, M.C., McCarthy, D., Khu, P., Kashiwagi, T. and Sperduto, R. (1989). Lens Opacities Classification System-Ii (Locs-Ii). *Archives of Ophthalmology* **107**:991–997.
- Chylack, L.T., Leske, M.C., Sperduto, R., Khu, P. and McCarthy, D. (1988). Lens Opacities Classification-System. *Archives of Ophthalmology* **106**:330–334.
- Chylack, L.T., Wolfe, J.K., Singer, D.M., Leske, M.C., Bullimore, M.A., Bailey, I.L., Friend, J., *et al.* (1993). The Lens Opacities Classification System III. *Archives of Ophthalmology* **111**:831–836.
- Cicinelli, M.V., Rabiolo, A., Sacconi, R., Carnevali, A., Querques, L., Bandello, F. and Querques, G. (2017). Optical coherence tomography angiography in dry age-related macular degeneration. *Survey of Ophthalmology* **63**:236–244.
- Contestabile, A., Benfenati, F. and Gasparini, L. (2010). Communication breaks-Down: From neurodevelopment defects to cognitive disabilities in Down syndrome. *Progress in Neurobiology* **91**:1–22.
- Courage, M.L., Adams, R.J. and Hall, E.J. (1997). Contrast sensitivity in infants and children with Down syndrome. *Vision research* **37**:1545–1555.
- Courage, M.L., Adams, R.J., Reyno, S. and Kwa, P.G. (1994). Visual-Acuity in Infants and Children with Down-Syndrome. *Developmental medicine and child neurology* **36**:586–593.

Cregg, M., Woodhouse, J.M., Pakeman, V.H., Saunders, K.J., Gunter, H.L., Parker, M., Fraser, W.I., *et al.* (2001). Accommodation and refractive error in children with Down syndrome: Cross-sectional and longitudinal studies. *Investigative ophthalmology & visual science* **42**:55–63.

Cregg, M., Woodhouse, J.M., Stewart, R.E., Pakeman, V.H., Bromham, N.R., Gunter, H.L., Trojanowska, L., *et al.* (2003). Development of refractive error and strabismus in children with Down syndrome. *Investigative ophthalmology & visual science* **44**:1023–1030.

Cullen, J.F. and Butler, H.G. (1963). Mongolism (Down's Syndrome) and Keratoconus. *The British journal of ophthalmology* **47**:321–330.

Cunha, L.P., Almeida, A.L.M., Costa-Cunha, L.V.F., Costa, C.F. and Monteiro, M.L.R. (2016). The role of optical coherence tomography in Alzheimer's disease. *International Journal of Retina and Vitreous* **2**:24.

Cunha, L.P., Lopes, L.C., Costa-Cunha, L.V.F., Costa, C.F., Pires, L.A., Almeida, A.L.M. and Monteiro, M.L.R. (2016). Macular Thickness Measurements with Frequency Domain-OCT for Quantification of Retinal Neural Loss and its Correlation with Cognitive Impairment in Alzheimer's Disease Mori, K. (ed.). *PLOS ONE* **11**:e0153830.

daCunha, R.P. and Moreira, J.B.D. (1996). Ocular findings in Down's syndrome. *American Journal of Ophthalmology* **122**:236–244.

Dentchev, T., Milam, A.H., Lee, V.M.-Y., Trojanowski, J.Q. and Dunaief, J.L. (2003). Amyloid-beta is found in drusen from some age-related macular degeneration retinas, but not in drusen from normal retinas. *Molecular vision* **9**:184–90.

Devlin, L. and Morrison, P.J. (2004). Accuracy of the clinical diagnosis of Down syndrome. *The Ulster medical journal* **73**:4–12.

Doustar, J., Torbati, T., Black, K.L., Koronyo, Y. and Koronyo-Hamaoui, M. (2017). Optical Coherence Tomography in Alzheimer's Disease and Other Neurodegenerative Diseases. *Frontiers in Neurology* **8**:701.

Doyle, L., Little, J.A. and Saunders, K.J. (2013). Repeatability of OCT lens thickness measures with age and accommodation. *Optometry and Vision Science* **90**:1396–1405.

Doyle, L., Saunders, K.J. and Little, J.-A. (2016). Trying to see, failing to focus: near visual impairment in Down syndrome. *Scientific Reports* **6**:20444.

- Doyle, S.J., Bullock, J., Gray, C., Spencer, A. and Cunningham, C. (1998). Emmetropisation, axial length, and corneal topography in teenagers with Down's syndrome. *British Journal of Ophthalmology* **82**:793–796.
- Drexler, W. (2004). Ultrahigh-resolution optical coherence tomography. *Journal of Biomedical Optics* **9**:47.
- Drexler, W. and Fujimoto, J.G. (2008). *Optical Coherence Tomography : Technology and Applications*. Springer.
- Drexler, W. and Fujimoto, J.G. (2008). State-of-the-art retinal optical coherence tomography. *Progress in Retinal and Eye Research* **27**:45–88.
- Drexler, W., Liu, M., Kumar, A., Kamali, T., Unterhuber, A. and Leitgeb, R.A. (2014). Optical coherence tomography today: speed, contrast, and multimodality. *Journal of Biomedical Optics* **19**:71412.
- Elliott, D. (2007). *Clinical Procedures in Primary Eye Care*.
- Elliott, D.B. (1993). Evaluating visual function in cataract. *Optometry and vision science : official publication of the American Academy of Optometry* **70**:896–902.
- Elliott, D.B. and Situ, P. (1998). Visual acuity versus letter contrast sensitivity in early cataract. *Vision Research* **38**:2047–2052.
- Elliott, D.B., Yang, K.C.H. and Whitaker, D. (1995). Visual acuity changes throughout adulthood in normal, healthy eyes: seeing beyond 6/6. *Optometry and vision science* **72**:186–191.
- Elliott, M.C. and Firth, A.Y. (2009). The logMAR Kay picture test and the logMAR acuity test: A comparative study. *Eye* **23**:85–88.
- Esbensen, A.J. (2010). *Health Conditions Associated with Aging and End of Life of Adults with down Syndrome*.
- Esmacelpour, M., Považay, B., Hermann, B., Hofer, B., Kajic, V., Kapoor, K., Sheen, N.J.L., *et al.* (2010). Three-dimensional 1060-nm OCT: Choroidal thickness maps in normal subjects and improved posterior segment visualization in cataract patients. *Investigative Ophthalmology and Visual Science* **51**:5260–5266.
- Evereklioglu, C., Yilmaz, K. and Bekir, N.A. (2002). Decreased central corneal thickness in children with Down syndrome. *Journal of Pediatric Ophthalmology & Strabismus* **39**:274–277.

- Fercher, A.F., Mendedoht, K. and Werner, W. (1988). Eye-length measurement by interferometry with partially coherent light. *Optics Letters* **13**:186.
- Ferris, F.L. 3rd and Bailey, I. (1996). Standardizing the Measurement of Visual Acuity for Clinical Research Studies: Guidelines from the Eye Care Technology Forum. *Ophthalmology* **103**:181–182.
- Filippello, M., Cascone, G., Zagami, A. and Scimone, G. (1997). Impression cytology in Down's syndrome. *British Journal of Ophthalmology* **81**:683–685.
- Fimiani, F., Iovine, A., Carelli, R., Pansini, M., Sebastio, G. and Magli, A. (2007). Incidence of ocular pathologies in Italian children with Down syndrome. *European journal of ophthalmology* **17**:817–822.
- Fong, A.H.C., Shum, J., Ng, A.L.K., Li, K.K.W., McGhee, S. and Wong, D. (2013). Prevalence of ocular abnormalities in adults with Down syndrome in Hong Kong. *British Journal of Ophthalmology* **97**:423–428.
- Forrester, M.B. and Merz, R.D. (2002). Epidemiology of Down syndrome (trisomy 21), Hawaii, 1986–97. *Teratology* **65**:207–212.
- Franssen, L., Coppens, J.E. and Van Den Berg, T.J.T.P. (2006). Compensation comparison method for assessment of retinal straylight. *Investigative Ophthalmology and Visual Science* **47**:768–776.
- Frederikse, P.H., Garland, D., Zigler, S., Piatigorsky, J., Frederikse, P.H., Garland, D., Zigler, J.S., *et al.* (1996). Cell Biology and Metabolism : Oxidative Stress Increases Production of β -Amyloid Precursor Protein and β -Amyloid (A) in Mammalian Lenses , and A Has Toxic Effects on Lens Epithelial Cells Oxidative Stress Increases Production of β - Amyloid Precursor Prote. *The Journal of Biological Chemistry* **271**:10169–10174.
- Freeman, S.B., Taft, L.F., Dooley, K.J., Allran, K., Sherman, S.L., Hassold, T.J., Khoury, M.J., *et al.* (1998). Population-based study of congenital heart defects in Down syndrome. *American Journal of Medical Genetics* **80**:213–217.
- Frisoni, G.B.G.B.G., Fox, N.C.N.N.C.N., Jack, C.C.R.C.R.C., Scheltens, P. and Thompson, P.M.P.M. (2010). The clinical use of structural MRI in Alzheimer disease. *Nature Reviews, Neurol* **6**:67–77.

- Fujimoto, J. and Swanson, E. (2016). The development, commercialization, and impact of optical coherence tomography. *Investigative Ophthalmology and Visual Science* **57**:OCT1-OCT13.
- Gabriele, M.L., Wollstein, G., Ishikawa, H., Xu, J., Kim, J., Kagemann, L., Folio, L.S., *et al.* (2010). Three dimensional optical coherence tomography imaging: Advantages and advances. *Progress in Retinal and Eye Research* **29**:556–579.
- Gao, S.S., Jia, Y., Zhang, M., Su, J.P., Liu, G., Hwang, T.S., Bailey, S.T., *et al.* (2016). Optical coherence tomography angiography. *Investigative Ophthalmology and Visual Science* **57**:OCT27-OCT36.
- Genin, E., Hannequin, D., Wallon, D., Slegers, K., Hiltunen, M., Combarros, O., Bullido, M.J., *et al.* (2011). APOE and Alzheimer disease: a major gene with semi-dominant inheritance. *Molecular Psychiatry* **16**:903–907.
- Gholami, S., Reus, N.J. and Berg, T.J.T.P. Van Den (2017). Changes in Intraocular Straylight and Visual Acuity with Age in Cataracts of Different Morphologies. *Journal of Ophthalmology* **2017**.
- Glasson, E.J., Sullivan, S.G., Hussain, R., Petterson, B. a, Montgomery, P.D. and Bittles, a H. (2002). The changing survival profile of people with Down's syndrome: implications for genetic counselling. *Clinical genetics* **62**:390–393.
- Goldstein, L.E., Muffat, J.A., Cherny, R.A., Moir, R.D., Ericsson, M.H., Huang, X., Mavros, C., *et al.* (2003). Cytosolic β -amyloid deposition and supranuclear cataracts in lenses from people with Alzheimer's disease. *Lancet* **361**:1258–1265.
- Grieco, J., Pulsifer, M., Seligsohn, K., Skotko, B. and Schwartz, A. (2015). Down syndrome: Cognitive and behavioral functioning across the lifespan. *American Journal of Medical Genetics, Part C: Seminars in Medical Genetics* **169**:135–149.
- Grover, S., Murthy, R.K., Brar, V.S. and Chalam, K. V. (2009). Normative Data for Macular Thickness by High-Definition Spectral-Domain Optical Coherence Tomography (Spectralis). *American Journal of Ophthalmology* **148**:266–271.
- Grulkowski, I., Manzanera, S., Cwiklinski, L., Sobczuk, F., Karnowski, K. and Artal, P. (2018). Swept source optical coherence tomography and tunable lens technology for comprehensive imaging and biometry of the whole eye. *Optica* **5**:52.

- Guo, L., Salt, T.E., Luong, V., Wood, N., Cheung, W., Maass, A., Ferrari, G., *et al.* (2007). Targeting amyloid-beta in glaucoma treatment. *Proceedings of the National Academy of Sciences of the United States of America* **104**:13444–13449.
- den Haan, J., Verbraak, F.D., Visser, P.J. and Bouwman, F.H. (2017). Retinal thickness in Alzheimer's disease: A systematic review and meta-analysis. *Alzheimer's and Dementia: Diagnosis, Assessment and Disease Monitoring* **6**:162–170.
- Haass, C., Schlossmacher, M.G., Hung, A.Y., Vigo-Pelfrey, C., Mellon, A., Ostaszewski, B.L., Lieberburg, I., *et al.* (1992). Amyloid β -peptide is produced by cultured cells during normal metabolism. *Nature* **359**:322–325.
- Hall, N.F., Lempert, P., Shier, R.P., Zakir, R. and Phillips, D. (1999). Grading nuclear cataract: Reproducibility and validity of a new method. *British Journal of Ophthalmology* **83**:1159–1163.
- Hardy, J. and Selkoe, D.J. (2002). The Amyloid Hypothesis of Alzheimer's Disease: Progress and Problems on the Road to Therapeutics. *Science* **297**:353–356.
- Hartley, D., Blumenthal, T., Carrillo, M., DiPaolo, G., Esralew, L., Gardiner, K., Granholm, A.C., *et al.* (2015). Down syndrome and Alzheimer's disease: Common pathways, common goals. *Alzheimer's and Dementia* **11**:700–709.
- Haugen, O.H. and Hovding, G. (2001). Strabismus and binocular function in children with Down syndrome. A population-based, longitudinal study. *Acta Ophthalmologica Scandinavica* **79**:133–139.
- Haugen, O.H., Hovding, G. and Eide, G.E. (2001). Biometric measurements of the eyes in teenagers and young adults with Down syndrome. *Acta Ophthalmologica Scandinavica* **79**:616–625.
- Haugen, O.H., Hovding, G. and Lundstrom, I. (2001). Refractive development in children with Down's syndrome: a population based, longitudinal study. *British Journal of Ophthalmology* **85**:714–719.
- Hayasaka, Y. and Hayasaka, S. (2004). Bilateral congenital macular coloboma in a boy with Down syndrome. *European journal of ophthalmology* **14**:565–567.
- Head, E., Lott, I.T., Wilcock, D.M. and Lemere, C.A. (2016). Aging in Down Syndrome and the Development of Alzheimer's Disease Neuropathology. *Current Alzheimer research* **13**:18–29.

- Heidelberg Engineering (2013). SPECTRALIS OCT User Manual.
- Hestnes, A., Sand, T. and Fostad, K. (1991). Ocular Findings in Downs-Syndrome. *Journal of mental deficiency research* **35**:194–203.
- Ho, C.Y., Troncoso, J.C., Knox, D., Stark, W. and Eberhart, C.G. (2014). Beta-amyloid, phospho-tau and alpha-synuclein deposits similar to those in the brain are not identified in the eyes of Alzheimer's and Parkinson's disease patients. *Brain Pathology* **24**:25–32.
- Huang, D., Swanson, E.A., Lin, C.P., Schuman, J.S., Stinson, W.G., Chang, W., Hee, M.R., *et al.* (1991). Optical coherence tomography. *Science* **254**:1178–81.
- Isas, J.M., Luibl, V., Johnson, L. V., Kaye, R., Wetzel, R., Glabe, C.G., Langen, R., *et al.* (2010). Soluble and mature amyloid fibrils in drusen deposits. *Investigative Ophthalmology and Visual Science* **51**:1304–1310.
- Ito, Y., Shimazawa, M., Tsuruma, K., Mayama, C., Ishii, K., Onoe, H., Aihara, M., *et al.* (2012). Induction of amyloid- β (1-42) in the retina and optic nerve head of chronic ocular hypertensive monkeys. *Molecular vision* **18**:2647–57.
- Izatt, J.A., Hee, M.R., Swanson, E.A., Lin, C.P., Huang, D., Schuman, J.S., Puliafito, C.A., *et al.* (1994). Micrometer-Scale Resolution Imaging of the Anterior Eye In Vivo With Optical Coherence Tomography. *Archives of Ophthalmology* **112**:1584.
- Jaeger, E.A. (1980). Ocular findings in Down's syndrome. *Transactions of the American Ophthalmological Society* **78**:808–845.
- Jarrett, J.T., Berger, E.P. and Lansbury, P.T. (1993). The carboxy terminus of the beta amyloid protein is critical for the seeding of amyloid formation: implications for the pathogenesis of Alzheimer's disease. *Biochemistry* **32**:4693–7.
- Jarrold, C., Nadel, L. and Vicari, S. (2009). Memory and neuropsychology in Down syndrome. *Down Syndrome: Research & Practice* **12**:196–201.
- John, F.M., Bromham, N.R., Woodhouse, J.M. and Candy, T.R. (2004). Spatial vision deficits in infants and children with Down syndrome. *Investigative ophthalmology & visual science* **45**:1566–1572.
- Johnson, Z., Lillis, D., Delany, V., Hayes, C. and Dack, P. (1996). The epidemiology of Down syndrome in four counties in Ireland 1981-1990. *Journal of public health medicine* **18**:78–86.

- Kahn, H.A., Leibowitz, H.M., Ganley, J.P., Kini, M.M., Colton, T., Nickerson, R.S. and Dawber, T.R. (1977). The Framingham Eye Study. I. Outline and major prevalence findings. *American Journal of Epidemiology* **106**:17–32.
- Kallen, B., Mastroiacovo, P. and Robert, E. (1996). Major congenital malformations in Down syndrome. *Am J Med Genet* **65**:160–166.
- Kanski, J.J. and Bowling, B. (2011). *Clinical Ophthalmology: A Systematic Approach: Expert Consult*. Edinburgh ;New York : Elsevier/Saunders.
- Kao, C.-Y., Richdale, K., Sinnott, L.T., Grillott, L.E. and Bailey, M.D. (2011). Semiautomatic extraction algorithm for images of the ciliary muscle. *Optometry and vision science : official publication of the American Academy of Optometry* **88**:275–289.
- Karbassi, M., Khu, P.M., Singer, D.M. and Chylack, L.T. (1993). Evaluation of Lens Opacities Classification-System-Iii Applied at the Slitlamp. *Optometry and Vision Science* **70**:923–928.
- Karran, E., Mercken, M. and Strooper, B. De (2011). The amyloid cascade hypothesis for Alzheimer's disease: an appraisal for the development of therapeutics. *Nature Reviews Drug Discovery* **10**:698–712.
- Kerbage, C., Sadowsky, C.H., Tariot, P.N., Agronin, M., Alva, G., Turner, F.D., Nilan, D., et al. (2014). Detection of Amyloid beta Signature in the Lens and Its Correlation in the Brain to Aid in the Diagnosis of Alzheimer's Disease. *American Journal of Alzheimers Disease and Other Dementias* **30**:738–745.
- Kiernan, D.F., Mieler, W.F. and Hariprasad, S.M. (2010). Spectral-Domain Optical Coherence Tomography: A Comparison of Modern High-Resolution Retinal Imaging Systems. *American Journal of Ophthalmology* **149**:18–31.e2.
- Kim, J.H., Hwang, J.M., Kim, H.J. and Yu, Y.S. (2002). Characteristic ocular findings in Asian children with Down syndrome. *Eye* **16**:710–714.
- Kim, U. and Hwang, J.-M. (2009). Refractive errors and strabismus in Asian patients with Down syndrome. *Eye* **23**:1560–1564.
- Kim, Y.N., Park, J.H. and Tchah, H. (2016). Quantitative Analysis of Lens Nuclear Density Using Optical Coherence Tomography (OCT) with a Liquid Optics Interface: Correlation between OCT Images and LOCS III Grading. *Journal of Ophthalmology*:3025413.

- Kirbas, S., Turkyilmaz, K., Anlar, O., Tufekci, A. and Durmus, M. (2013). Retinal Nerve Fiber Layer Thickness in Patients With Alzheimer Disease. *Journal of Neuro-Ophthalmology* **33**:58–61.
- Kirwan, J., Venter, L., Stulting, A. and Murdoch, I. (2003). LOCS III examination at the slit lamp, do settings matter? *Ophthalmic Epidemiology*:259–266.
- Kjersem, B. and Krohn, J. (2013). Transillumination imaging of intraocular tumours. *Journal of Visual Communication in Medicine* **36**:26–30.
- Klaver, C.C.W., Wolfs, R.C.W., Vingerling, J.R., Hofman, A. and de Jong, P. (1998). Age-specific prevalence and causes of blindness and visual impairment in an older population - The Rotterdam Study. *Archives of Ophthalmology* **116**:653–658.
- Klein, B.E.K., Klein, R. and Linton, K.L.P. (1992). Prevalence of Age-Related Lens Opacities in a Population - the Beaver Dam Eye Study. *Ophthalmology* **99**:546–552.
- Klein, B.E.K., Klein, R., Linton, K.L.P., Magli, Y.L. and Neider, M.W. (1990). Assessment of Cataracts from Photographs in the Beaver Dam Eye Study. *Ophthalmology* **97**:1428–1433.
- Koo, E., Chang, J.R., Agron, E., Clemons, T.E., Sperduto, R.D., Ferris III, F.L., Chew, E.Y., *et al.* (2013). Ten-Year Incidence Rates of Age-Related Cataract in the Age-Related Eye Disease Study (AREDS): AREDS Report No. 33. *Ophthalmic epidemiology* **20**:71–81.
- Koronyo-Hamaoui, M., Koronyo, Y., Ljubimov, A. V., Miller, C.A., Ko, M.H.K., Black, K.L., Schwartz, M., *et al.* (2011). Identification of amyloid plaques in retinas from Alzheimer's patients and noninvasive in vivo optical imaging of retinal plaques in a mouse model. *NeuroImage* **54**:S204–S217.
- Krinsky-McHale, S.J., Jenkins, E.C., Zigman, W.B. and Silverman, W. (2012). Ophthalmic disorders in adults with down syndrome. *Current gerontology and geriatrics research* **2012**:974253.
- Krinsky-McHale, S.J., Silverman, W., Gordon, J., Devenny, D.A., Oley, N. and Abramov, I. (2014). Vision Deficits in Adults with Down Syndrome. *Journal of Applied Research in Intellectual Disabilities* **27**:247–263.
- Krivchenia, E., Huether, C.A., Edmonds, L.D., May, D.S. and Guckenberger, S. (1993). Comparative epidemiology of Down syndrome in two United States populations, 1970–1989. *American Journal of Epidemiology* **137**:815–828.

- Krohn, J. and Kjersem, B. (2012). A modified digital slit lamp camera system for transillumination photography of intraocular tumours. *British Journal of Ophthalmology* **96**:475–477.
- Kusters, M.A.A., Verstegen, R.H.J., Gemen, E.F.A. and de Vries, E. (2009). Intrinsic defect of the immune system in children with Down syndrome: a review. *Clinical and experimental immunology* **156**:189–193.
- Kymionis, G.D., Diakonis, V.F., Liakopoulos, D.A., Tsoulnaras, K.I., Klados, N.E. and Pallikaris, I.G. (2014). Anterior segment optical coherence tomography for demonstrating posterior capsular rent in posterior polar cataract. *Clinical Ophthalmology* **8**:215–217.
- Laguna, A., Barallobre, M.-J., Marchena, M.-Á., Mateus, C., Ramírez, E., Martínez-Cue, C., Delabar, J.M., *et al.* (2013). Triplication of DYRK1A causes retinal structural and functional alterations in Down syndrome. *Human molecular genetics* **22**:2775–2784.
- Lai, F.M., Woo, B.H., Tan, K.H., Huang, J., Lee, S.T., Tan, B.Y., Tan, B.H., *et al.* (2002). Birth prevalence of Down syndrome in Singapore from 1993 to 1998. *Singapore medical journal* **43**:70–76.
- Lee, N.-C., Chien, Y.-H. and Hwu, W.-L. (2017). A Review of Biomarkers for Alzheimer's Disease in Down Syndrome. *Neurology and Therapy* **6**:69–81.
- Leger, F., Fernagut, P.-O., Canron, M.-H., Léoni, S., Vital, C., Tison, F., Bezard, E., *et al.* (2011). Protein Aggregation in the Aging Retina. *Journal of Neuropathology & Experimental Neurology* **70**:63–68.
- Lehman, B.M., Berntsen, D.A., Bailey, M.D. and Zadnik, K. (2009). Validation of OCT-based Crystalline Lens Thickness Measurements in Children. *Optometry and vision science : official publication of the American Academy of Optometry* **86**:181.
- Lehmann, M., Koedam, E.L.G.E., Barnes, J., Bartlett, J.W., Ryan, N.S., Pijnenburg, Y.A.L., Barkhof, F., *et al.* (2012). Posterior cerebral atrophy in the absence of medial temporal lobe atrophy in pathologically-confirmed Alzheimer's disease. *Neurobiology of Aging* **33**:627.e1-627.e12.
- Leinenbach, A., Pannee, J., Dülffer, T., Huber, A., Bittner, T., Andreasson, U., Gobom, J., *et al.* (2014). Mass spectrometry-based candidate reference measurement procedure for quantification of amyloid-?? in Cerebrospinal fluid. *Clinical Chemistry* **60**:987–994.

- Leske, M.C., Chylack, L.T., He, Q.M., Wu, S.Y., Schoenfeld, E., Friend, J. and Wolfe, J. (1997). Incidence and progression of cortical and posterior subcapsular opacities - The longitudinal study of cataract. *Ophthalmology* **104**:1987–1993.
- Leung, C.K. shun, Ye, C., Weinreb, R.N., Cheung, C.Y.L., Qiu, Q., Liu, S., Xu, G., *et al.* (2010). Retinal Nerve Fiber Layer Imaging with Spectral-Domain Optical Coherence Tomography. A Study on Diagnostic Agreement with Heidelberg Retinal Tomograph. *Ophthalmology* **117**:267–274.
- Little, J.-A., Woodhouse, J.M., Lauritzen, J.S. and Saunders, K.J. (2007). The impact of optical factors on resolution acuity in children with down syndrome. *Investigative ophthalmology & visual science* **48**:3995–4001.
- Little, J.-A., Woodhouse, J.M., Lauritzen, J.S. and Saunders, K.J. (2009). Vernier Acuity in Down Syndrome. *Investigative ophthalmology & visual science* **50**:567–572.
- Little, J.-A., Woodhouse, J.M. and Saunders, K.J. (2009). Corneal Power and Astigmatism in Down Syndrome. *Optometry and Vision Science* **86**:748–754.
- Liu, B., Rasool, S., Yang, Z., Glabe, C.G., Schreiber, S.S., Ge, J. and Tan, Z. (2009). Amyloid-peptide vaccinations reduce {beta}-amyloid plaques but exacerbate vascular deposition and inflammation in the retina of Alzheimer's transgenic mice. *The American journal of pathology* **175**:2099–110.
- Liza-Sharmini, A.T., Azlan, Z.N. and Zilfalil, B.A. (2006). Ocular findings in Malaysian children with Down syndrome. *SMJ Singapore Medical Journal* **47**:14–19.
- Ljubic, A., Trajkovski, V. and Stankovic, B. (2011). Strabismus, refractive errors and nystagmus in children and young adults with Down syndrome. *Ophthalmic genetics* **32**:204–211.
- Loane, M., Morris, J.K., Addor, M.C., Arriola, L., Budd, J., Doray, B., Garne, E., *et al.* (2013). Twenty-year trends in the prevalence of Down syndrome and other trisomies in Europe: impact of maternal age and prenatal screening. *European journal of human genetics : EJHG* **21**:27–33.
- Lovie-Kitchin, J.E. (1989). Validity and reliability of visual acuity measurements. *Ophthalmic and Physiological Optics* **9**:458–458.
- Lowe, R.F. (1949). The eyes in mongolism. *The British journal of ophthalmology* **33**:131–174.

- Mainster, M.A. and Turner, P.L. (2012). Glare's causes, consequences, and clinical challenges after a century of ophthalmic study. *American Journal of Ophthalmology* **153**:587–593.
- Malt, E.A., Dahl, R.C., Haugsand, T.M., Ulvestad, I.H., Emilsen, N.M., Hansen, B., Cardenas, Y.E.G., *et al.* (2013). Health and disease in adults with Down syndrome. *Tidsskrift for den Norske lægeforening: tidsskrift for praktisk medicin, ny række* **133**:290–294.
- Mäntyjärvi, M. and Laitinen, T. (2001). Normal values for the Pelli-Robson contrast sensitivity test. *J Cataract Refract Surg* **27**:261–6.
- Marder, L., Tulloh, R. and Pascall, E. (2015). Cardiac problems in Down syndrome. *Paediatrics and Child Health* **25**:23–29.
- Marziani, E., Pomati, S., Ramolfo, P., Cigada, M., Giani, A., Mariani, C. and Staurenghi, G. (2013). Evaluation of Retinal Nerve Fiber Layer and Ganglion Cell Layer Thickness in Alzheimer's Disease Using Spectral-Domain Optical Coherence Tomography. *Investigative Ophthalmology & Visual Science* **54**:5953.
- McCarty, C.A., Mukesh, B.N., Fu, C.L. and Taylor, H.R. (1999). The epidemiology of cataract in Australia. *American Journal of Ophthalmology* **128**:446–465.
- McKhann, G.M., Knopman, D.S., Chertkow, H., Hyman, B.T., Jack, C.R., Kawas, C.H., Klunk, W.E., *et al.* (2011). The diagnosis of dementia due to Alzheimer's disease: Recommendations from the National Institute on Aging-Alzheimer's Association workgroups on diagnostic guidelines for Alzheimer's disease. *Alzheimer's and Dementia* **7**:263–269.
- McKinnon, S.J., Lehman, D.M., Kerrigan-Baumrind, L.A., Merges, C.A., Pease, M.E., Kerrigan, D.F., Ransom, N.L., *et al.* (2002). Caspase activation and amyloid precursor protein cleavage in rat ocular hypertension. *Investigative Ophthalmology and Visual Science* **43**:1077–1087.
- Mehra, V. and Minassian, D.C. (1988). A Rapid Method of Grading Cataract in Epidemiological-Studies and Eye Surveys. *British Journal of Ophthalmology* **72**:801–803.
- Métneki, J. and Czeizel, A.E. (2005). Increasing total prevalence rate of cases with Down syndrome in Hungary. *European journal of epidemiology* **20**:525–535.

- Van Der Meulen, I.J.E., Gjertsen, J., Kruijt, B., Witmer, J.P., Rulo, A., Schlingemann, R.O. and Van Den Berg, T.J.T.P. (2012). Straylight measurements as an indication for cataract surgery. *Journal of Cataract and Refractive Surgery* **38**:840–848.
- Michael, R. and Bron, A.J. (2011). The ageing lens and cataract: a model of normal and pathological ageing. *Philos Trans R Soc Lond B Biol Sci* **366**:1278–1292.
- Michael, R., Otto, C., Lenferink, A., Gelpi, E., Montenegro, G.A., Rosandić, J., Tresserra, F., *et al.* (2014). Absence of amyloid-beta in lenses of Alzheimer patients: A confocal Raman microspectroscopic study. *Experimental Eye Research* **119**:44–53.
- Michael, R., Van Rijn, L.J., Van Den Berg, T.J.T.P., Barraquer, R.I., Grabner, G., Wilhelm, H., Coeckelbergh, T., *et al.* (2009). Association of lens opacities, intraocular straylight, contrast sensitivity and visual acuity in European drivers. *Acta Ophthalmologica* **87**:666–671.
- Michael, R., Rosandić, J., Montenegro, G.A., Lobato, E., Tresserra, F., Barraquer, R.I. and Vrensen, G.F.J.M. (2013). Absence of beta-amyloid in cortical cataracts of donors with and without Alzheimer's disease. *Experimental Eye Research* **106**:5–13.
- Mitchell, P., Cumming, R.G., Attebo, K. and Panchapakesan, J. (1997). Prevalence of Cataract in Australia: The Blue Mountains Eye Study. *Ophthalmology* **104**:581–588.
- Moncaster, J.A., Pineda, R., Moir, R.D., Lu, S., Burton, M.A., Ghosh, J.G., Ericsson, M., *et al.* (2010). Alzheimer's disease amyloid- β links lens and brain pathology in down syndrome. *PLoS ONE* **5**.
- Nadel, L. (2003). Down's syndrome: a genetic disorder in biobehavioral perspective. *Genes, Brain and Behavior* **2**:156–166.
- NICE (2016). *Dementia Diagnosis and Assessment - NICE Pathways* [Online]. Available at: <https://pathways.nice.org.uk/pathways/dementia/dementia-diagnosis-and-assessment#content=view-node%3Anodes-diagnosis-of-subtype> [Accessed: 21 May 2017].
- Ning, A., Cui, J., To, E., Ashe, K.H. and Matsubara, J. (2008). Amyloid- β Deposits Lead to Retinal Degeneration in a Mouse Model of Alzheimer Disease. *Investigative Ophthalmology & Visual Science* **49**:5136.
- Nischler, C., Michael, R., Wintersteller, C., Marvan, P., Emesz, M., Van Rijn, L.J., Van Den Berg, T.J.T.P., *et al.* (2010). Cataract and pseudophakia in elderly European drivers. *European Journal of Ophthalmology* **20**:892–901.

- Normando, E.M., Coxon, K.M., Guo, L. and Cordeiro, M.F. (2009). Focus on: Amyloid β . *Experimental Eye Research* **89**:446–447.
- O'Brien, S., Wang, J., Smith, H.A., Donaldson, D.L., Haider, K.M., Roberts, G.J., Sprunger, D.T., *et al.* (2015). Macular structural characteristics in children with Down syndrome. *Graefes Archive for Clinical and Experimental Ophthalmology* **253**:2317–2323.
- Olsen, C.L., Cross, P.K., Gensburg, L.J. and Hughes, J.P. (1996). The effects of prenatal diagnosis, population ageing, and changing fertility rates on the live birth prevalence of Down syndrome in New York State, 1983–1992. *Prenatal diagnosis* **16**:991–1002.
- Paquet, C., Boissonnot, M., Roger, F., Dighiero, P., Gil, R. and Hugon, J. (2007). Abnormal retinal thickness in patients with mild cognitive impairment and Alzheimer's disease. *Neuroscience Letters* **420**:97–99.
- Patterson, T., Rapsey, C.M. and Glue, P. (2013). Systematic review of cognitive development across childhood in Down syndrome: Implications for treatment interventions. *Journal of Intellectual Disability Research* **57**:306–318.
- Paz Filgueira, C., Sánchez, R.F., Issolio, L.A. and Colombo, E.M. (2016). Straylight and Visual Quality on Early Nuclear and Posterior Subcapsular Cataracts. *Current Eye Research* **41**:1209–1215.
- Perez, S.E., Lumayag, S., Kovacs, B., Mufson, E.J. and Xu, S. (2009). β -Amyloid Deposition and Functional Impairment in the Retina of the APP^{swe}/PS1 Δ E9 Transgenic Mouse Model of Alzheimer's Disease. *Investigative Ophthalmology & Visual Science* **50**:793.
- Považay, B., Hermann, B., Unterhuber, A., Hofer, B., Sattmann, H., Zeiler, F., Morgan, J.E., *et al.* (2007). Three-dimensional optical coherence tomography at 1050 nm versus 800 nm in retinal pathologies: enhanced performance and choroidal penetration in cataract patients. *Journal of Biomedical Optics* **12**:41211.
- Prasher, V.P. (2006). *Down Syndrome and Alzheimer's Disease : Biological Correlates*. Radcliffe.
- Prasher, V.P., Sachdeva, N. and Tarrant, N. (2015). Diagnosing dementia in adults with Down's syndrome. *Neurodegenerative disease management* **5**:249–56.
- Prince, M., Bryce, R., Albanese, E., Wimo, A., Ribeiro, W. and Ferri, C.P. (2013). The global prevalence of dementia: A systematic review and metaanalysis. *Alzheimer's and Dementia* **9**:63–75.

- Rahmani, B., Tielsch, J.M., Katz, J., Gottsch, J., Quigley, H., Javitt, J. and Sommer, A. (1996). The cause-specific prevalence of visual impairment in an urban population - The Baltimore Eye Survey. *Ophthalmology* **103**:1721–1726.
- Reidy, A., Minassian, D.C., Vafidis, G., Joseph, J., Farrow, S., Wu, J., Desai, P., *et al.* (1998). Prevalence of serious eye disease and visual impairment in a north London population: population based, cross sectional study. *BMJ* **316**:1643–1646.
- Remington, L.A. (2012). *Clinical Anatomy and Physiology of the Visual System*. 3rd ed. St. Louis, Missouri: Butterworth-Heinemann.
- Richdale, K., Bullimore, M.A. and Zadnik, K. (2008). Lens thickness with age and accommodation by optical coherence tomography. *Ophthalmic and Physiological Optics* **28**:441–447.
- Richdale, K., Sinnott, L.T., Bullimore, M.A., Wassenaar, P.A., Schmalbrock, P., Kao, C.Y., Patz, S., *et al.* (2013). Quantification of age-related and per diopter accommodative changes of the lens and ciliary muscle in the emmetropic human eye. *Investigative Ophthalmology and Visual Science* **54**:1095–1105.
- Richman, J., Spaeth, G.L. and Wirostko, B. (2013). Contrast sensitivity basics and a critique of currently available tests. *Journal of Cataract and Refractive Surgery* **39**:1100–1106.
- Roizen, N.J. and Patterson, D. (2003). Down's syndrome. *Lancet* **361**:1281–1289.
- Roth, G.M., Sun, B., Greensite, F.S., Lott, I.T. and Dietrich, R.B. (1996). Premature aging in persons with Down syndrome: MR findings. *American Journal of Neuroradiology* **17**:1283–1289.
- Scheltens, P., Blennow, K., Breteler, M.M.B., de Strooper, B., Frisoni, G.B., Salloway, S. and Van der Flier, W.M. (2016). Alzheimer's disease. *Lancet* **388**:505–517.
- Selikowitz, M. (2008). *Down Syndrome: The Facts*. Third Edit. NY, USA: Oxford University Press.
- Selikowitz, M. (1992). Health-Problems and Health Checks in School-Aged Children with Down-Syndrome. *Journal of paediatrics and child health* **28**:383–386.
- Seubert, P., Vigo-Pelfrey, C., Esch, F., Lee, M., Dovey, H., Davis, D., Sinha, S., *et al.* (1992). Isolation and quantification of soluble Alzheimer's β -peptide from biological fluids. *Nature* **359**:325–327.

- Shapiro, M.B. and France, T.D. (1985). The Ocular Features of Downs-Syndrome. *American Journal of Ophthalmology* **99**:659–663.
- Sharma, K.K. and Santhoshkumar, P. (2009). Lens aging: Effects of crystallins. *Biochimica Et Biophysica Acta-General Subjects* **1790**:1095–1108.
- Sherk, M.C. and Williams, T.D. (1979). Disk Vascularity in Downs-Syndrome. *American Journal of Optometry and Physiological Optics* **56**:509–511.
- Shoji, M., Golde, T., Ghiso, J., Cheung, T., Estus, S., Shaffer, L., Cai, X.-D., *et al.* (1992). Production of the Alzheimer amyloid beta protein by normal proteolytic processing. *Science* **258**:126.
- Silverman, W. (2007). Down syndrome: Cognitive phenotype. *Mental Retardation and Developmental Disabilities Research Reviews* **13**:228–236.
- Sparrow, J.M., Bron, A.J., Brown, N.A.P., Ayliffe, W. and Hill, A.R. (1986). The Oxford Clinical Cataract Classification and Grading System. *International ophthalmology* **9**:207–225.
- Sparrow, N.A., Frost, N.A., Pantelides, E.P. and Laidlaw, D.A. (2000). Decimalization of The Oxford Clinical Cataract Classification and Grading System. *Ophthalmic epidemiology* **7**:49–60.
- Sperling, R.A., Aisen, P.S., Beckett, L.A., Bennett, D.A., Craft, S., Fagan, A.M., Iwatsubo, T., *et al.* (2011). Toward defining the preclinical stages of Alzheimer's disease: Recommendations from the National Institute on Aging-Alzheimer's Association workgroups on diagnostic guidelines for Alzheimer's disease. *Alzheimer's and Dementia* **7**:280–292.
- Stewart, R.E., Woodhouse, J.M. and Trojanowska, L.D. (2005). In focus: the use of bifocal spectacles with children with Down's syndrome. *Ophthalmic and Physiological Optics* **25**:514–522.
- Stirn Kranjc, B. (2012). Ocular abnormalities and systemic disease in Down syndrome. *Strabismus* **20**:74–77.
- Stoll, C., Dott, B., Alembik, Y. and Roth, M.-P. (2015). Associated congenital anomalies among cases with Down syndrome. *European Journal of Medical Genetics* **58**:674–680.
- De Strooper, B. and Annaert, W. (2000). Proteolytic processing and cell biological functions of the amyloid precursor protein. *Journal of cell science* **113**:1857–1870.

- Sullivan, S.G., Hussain, R., Glasson, E.J. and Bittles, A.H. (2007). The profile and incidence of cancer in Down syndrome. *Journal of Intellectual Disability Research* **51**:228–231.
- Swanson, E. a, Izatt, J. a, Hee, M.R., Huang, D., Lin, C.P., Schuman, J.S., Puliafito, C. a, *et al.* (1993). In vivo retinal imaging by optical coherence tomography. *Optics Letters* **18**:1864–1866.
- Tagliabue, G., Tessandori, R., Caramaschi, F., Fabiano, S., Maghini, A., Tittarelli, A., Vergani, D., *et al.* (2007). Descriptive epidemiology of selected birth defects, areas of Lombardy, Italy, 1999. *Population health metrics* **5**:4.
- Tan, A.C.S., Wang, J.J., Lamoureux, E.L., Wong, W., Mitchell, P., Li, J., Tan, A.G., *et al.* (2011). Cataract Prevalence Varies Substantially with Assessment Systems: Comparison of Clinical and Photographic Grading in a Population-Based Study. *Ophthalmic epidemiology* **18**:164–170.
- Taylor, H.R. and West, S.K. (1989). The Clinical Grading of Lens Opacities. *Australian and New Zealand Journal of Ophthalmology* **17**:81–86.
- Tholozan, F.M.D. and Quinlan, R.A. (2007). Lens cells: More than meets the eye. *The international journal of biochemistry & cell biology* **39**:1754–1759.
- Thylefors, B., Chylack, L.T., Konyama, K., Sasaki, K., Sperduto, R., Taylor, H.R., West, S., *et al.* (2002). A simplified cataract grading system. *Ophthalmic epidemiology* **9**:83–95.
- Tick, S., Rossant, F., Ghorbel, I., Gaudric, A., Sahel, J.A., Chaumet-Riffaud, P. and Paques, M. (2011). Foveal shape and structure in a normal population. *Investigative Ophthalmology and Visual Science* **52**:5105–5110.
- Tsiaras, W.G., Pueschel, S., Keller, C., Curran, R. and Giesswein, S. (1999). Amblyopia and visual acuity in children with Down's syndrome. *British Journal of Ophthalmology* **83**:1112–1114.
- Tyan, S., Shih, A.Y., Walsh, J.J., Maruyama, H., Sarsoza, F., Ku, L., Eggert, S., *et al.* (2012). Molecular and Cellular Neuroscience Amyloid precursor protein (APP) regulates synaptic structure and function. *Molecular and Cellular Neuroscience* **51**:43–52.
- van Velthoven, M.E.J., van der Linden, M.H., de Smet, M.D., Faber, D.J. and Verbraak, F.D. (2006). Influence of cataract on optical coherence tomography image quality and retinal thickness. *The British journal of ophthalmology* **90**:1259–62.

- Vicari, S., Bellucci, S. and Carlesimo, G.A. (2005). Visual and spatial long-term memory: differential pattern of impairments in Williams and Down syndromes. *Developmental Medicine & Child Neurology* **47**:305–311.
- Vincent, A.L., Weiser, B.A., Cupryn, M., Stein, R.M., Abdoell, M. and Levin, A. V (2005). Computerized corneal topography in a paediatric population with Down syndrome. *Clinical and Experimental Ophthalmology* **33**:47–52.
- Wagner, R.S., Caputo, A.R. and Reynolds, R.D. (1990). Nystagmus in Downs-Syndrome. *Ophthalmology* **97**:1439–1444.
- Walsh, D.M. and Selkoe, D.J. (2007). A β oligomers - A decade of discovery. *Journal of Neurochemistry* **101**:1172–1184.
- Wang, R.K., Jacques, S.L., Ma, Z., Hurst, S., Hanson, S.R. and Gruber, A. (2007). Three dimensional optical angiography. *Optics Express* **15**:4083.
- Webb, R.L. and Murphy, M.P. (2012). β -Secretases, alzheimers disease, and down syndrome. *Current Gerontology and Geriatrics Research* **2012**.
- West, S.K., Munoz, B., Schein, O.D., Duncan, D.D. and Rubin, G.S. (1998). Racial differences in lens opacities: The Salisbury Eye Evaluation (SEE) Project. *American Journal of Epidemiology* **148**:1033–1039.
- West, S.K., Rosenthal, F., Newland, H.S. and Taylor, H.R. (1988). Use of Photographic Techniques to Grade Nuclear Cataracts. *Investigative ophthalmology & visual science* **29**:73–77.
- Williams, E.A., McGuone, D., Frosch, M.P., Hyman, B.T., Laver, N. and Stemmer-Rachamimov, A. (2017). Absence of Alzheimer Disease Neuropathologic Changes in Eyes of Subjects With Alzheimer Disease. *Journal of Neuropathology & Experimental Neurology* **76**:376–383.
- Williams, E.J., McCormic, Aq and Tischler, B. (1973). Retinal Vessels in Downs-Syndrome. *Archives of Ophthalmology* **89**:269–271.
- Wisniewski, K.E., Dalton, A.J., McLachlan, D.R.C., Wen, G.Y. and Wisniewski, H.M. (1985). Alzheimer's disease in Down's syndrome: Clinicopathologic studies. *NEUROLOGY* **35**:957–961.
- Wong, A.L., Leung, C.K.-S., Weinreb, R.N., Cheng, A.K.C., Cheung, C.Y.L., Lam, P.T.-H., Pang, C.P., *et al.* (2009). Quantitative assessment of lens opacities with anterior segment optical coherence tomography. *British Journal of Ophthalmology* **93**:61–65.

- Wong, V. and Ho, D. (1997). Ocular abnormalities in Down syndrome: An analysis of 140 Chinese children. *Pediatric neurology* **16**:311–314.
- Woodhouse, J.M., Clegg, M., Gunter, H.L., Sanders, D.P., Saunders, K.J., Pakeman, V.H., Parker, M., *et al.* (2000). The effect of age, size of target, and cognitive factors on accommodative responses of children with Down syndrome. *Investigative ophthalmology & visual science* **41**:2479–2485.
- Woodhouse, J.M., Griffiths, C. and Gedling, A. (2000). The prevalence of ocular defects and the provision of eye care in adults with learning disabilities living in the community. *Ophthalmic and Physiological Optics* **20**:79–89.
- Woodhouse, J.M., Hodge, S.J. and Earlam, R.A. (1994). Facial characteristics in children with Down's syndrome and spectacle fitting. *Ophthalmic and Physiological Optics* **14**:25–31.
- Woodhouse, J.M., Meades, J.S., Leat, S.J. and Saunders, K.J. (1993). Reduced Accommodation in Children with Down-Syndrome. *Investigative ophthalmology & visual science* **34**:2382–2387.
- Woodhouse, J.M., Pakeman, V.H., Clegg, M., Saunders, K.J., Parker, M., Fraser, W.I., Sastry, P., *et al.* (1997). Refractive errors in young children with Down syndrome. *Optometry and Vision Science* **74**:844–851.
- Woodhouse, J.M., Pakeman, V.H., Saunders, K.J., Parker, M., Fraser, W.I., Lobo, S. and Sastry, P. (1996). Visual acuity and accommodation in infants and young children with Down's syndrome. *Journal of Intellectual Disability Research* **40**:49–55.
- Wormstone, I.M., Collison, D.J., Hansom, S.P. and Duncan, G. (2006). A focus on the human lens in vitro. *Environmental Toxicology and Pharmacology* **21**:215–221.
- Wu, J. and Morris, J.K. (2013). The population prevalence of Down's syndrome in England and Wales in 2011. *European journal of human genetics : EJHG* **21**:1016–1019.
- Yamaguchi, K. and Tamai, M. (1990). Congenital Macular Coloboma in Down-Syndrome. *Annals of Ophthalmology* **22**:222–223.
- Yang, L., Rieves, D. and Ganley, C. (2012). Brain Amyloid Imaging — FDA Approval of Florbetapir F18 Injection. *New England Journal of Medicine* **367**:885–887.
- Yang, Q., Rasmussen, S.A. and Friedman, J.M. (2002). Mortality associated with Down's syndrome in the USA from 1983 to 1997: A population-based study. *Lancet* **359**:1019–1025.

- Yanni, S.E., Wang, J., Cheng, C.S., Locke, K.I., Wen, Y., Birch, D.G. and Birch, E.E. (2013). Normative reference ranges for the retinal nerve fiber layer, macula, and retinal layer thicknesses in children. *American Journal of Ophthalmology* **155**.
- Yurdakul, N.S., Ugurlu, S. and Maden, A. (2006). Strabismus in Down syndrome. *Journal of Pediatric Ophthalmology & Strabismus* **43**:27–30.
- Zana, M., Janka, Z. and Kálmán, J. (2007). Oxidative stress: A bridge between Down's syndrome and Alzheimer's disease. *Neurobiology of Aging* **28**:648–676.
- Zigman, W.B. (2013). Atypical aging in down syndrome. *Developmental Disabilities Research Reviews* **18**:51–67.

Appendix A-1

The code used to program the Arduino. Comments are preceded by '//'.

```
#include <LiquidCrystal.h>

LiquidCrystal lcd( 9, 8, 4, 5, 6, 7 );

const int ledPin = 3;    // set output pin for the LED
const int upButton = 12; // input for up button to increase flash intensity
const int downButton = 11; //input for down button to decrease flash intensity
const int eN1 = 14; // set output pin for EN1 of H-bridge
const int eN2 = 15; // set output pin for EN2 of H-bridge
const int shutterRel = 2; // set pin to connect to second optocoupler in order for camera
shutter release
const int pMos = 13; // set pin 13 as the output for photoMOS - this will set the
buckblock LED to zero brightness if the arduino fails and control the post-flash
brightness
int channel = 1;
int buttonUpState = 0;
int buttonDownState = 0;
int prevBtnUp = LOW;
int prevBtnDwn = LOW;
unsigned long lastBtnUp = 0;
unsigned long lastBtnDwn = 0;
int transInt = 5;
int flashIntensity = 1;
int flashState = 0;
int prevFlash = HIGH;
int shutState = 0;
int prevShut = HIGH;
unsigned long lastFlash = 0;
unsigned long lastShut = 0;
boolean hShoeSignal = false; // this is for the DoWhile loop. This will wait for the
hotshoe signal from the DSLR

void setup() {
  // the following portion of the code runs once when the Arduino is powered on or
  reset:
  // declare the ledPin as an OUTPUT:
  pinMode(ledPin, OUTPUT);
  digitalWrite(ledPin, HIGH);
  // declare eN1 and eN2 as outputs
  pinMode(eN1, OUTPUT);
  digitalWrite(eN1, LOW);
  pinMode(eN2, OUTPUT);
  digitalWrite(eN2, HIGH);
  delay(100);
  digitalWrite(eN2, LOW);
  // declare pin 10 as an INPUT with internal pullup resistor on to connect to flash hot
  shoe
  pinMode(10, INPUT_PULLUP);
```

```

// declare the buttonPin as an input
pinMode(upButton, INPUT);
digitalWrite(upButton, LOW);
pinMode(downButton, INPUT);
digitalWrite(downButton, LOW);
// declare A2 as a digital input with internal pullup resistor on to connect to joystick
button on slit lamp
pinMode(16, INPUT_PULLUP);
// declare shutterRel as an output and set to low
pinMode(shutterRel, OUTPUT);
digitalWrite(shutterRel, LOW);
// declare pMos as an output and set to high
pinMode(pMos, OUTPUT);
digitalWrite(pMos, HIGH);
// Display text on LCD
lcd.begin(16, 2);
lcd.clear();
lcd.setCursor(0, 0);
lcd.print("Set Flash Level");
lcd.setCursor(0, 1);
lcd.print("Press Up/Down:");
}

```

```

void loop() {
  // The following is the main code that runs repeatedly:

  // The below is the settings for the buttons to set the desired level of flash intensity
  which will be the channel variable
  buttonUpState = digitalRead(upButton);
  buttonDownState = digitalRead(downButton);

  if (buttonUpState == HIGH && prevBtnUp == LOW)
  {
    if (millis() - lastBtnUp > transInt)
    {
      channel++;
      if (channel > 9)
      {
        channel = 9;
      }
      lastBtnUp = millis();
    }
  }
  prevBtnUp = buttonUpState;

  if (buttonDownState == HIGH && prevBtnDwn == LOW)
  {
    if (millis() - lastBtnDwn > transInt)
    {
      channel--;
      if (channel < 1)
      {

```

```

    channel = 1;
  }
  lastBtnDwn = millis();
}
}
prevBtnDwn = buttonDownState;

// Below will display the current 'Flash Level' on the LCD and assign a value for
flashIntensity based on channel level
lcd.setCursor(15,1);
lcd.print(channel);
switch (channel) {
  case 1: // if channel is 1
    flashIntensity = 1335;
    break;
  case 2:
    flashIntensity = 1779;
    break;
  case 3:
    flashIntensity = 2373;
    break;
  case 4:
    flashIntensity = 3164;
    break;
  case 5:
    flashIntensity = 4219;
    break;
  case 6:
    flashIntensity = 5265;
    break;
  case 7:
    flashIntensity = 7500;
    break;
  case 8:
    flashIntensity = 10000;
    break;
  case 9:
    flashIntensity = 16000;
    break;
}
delay(10);

//The below will wait for the trigger signal from the slit lamp joystick and then trigger
the camera shutter. The do/while statement will wait for the hot shoe signal and then
trigger the solenoid/flash

shutState = digitalRead(16);
if (shutState == LOW && prevShut == HIGH)
{
  if (millis() - lastShut > transInt)
  {
    digitalWrite(eN1, HIGH);

```

```

delay(100);
digitalWrite(eN1, LOW);
delay(500);
digitalWrite(shutterRel, HIGH);
do
{
    flashState = digitalRead(10);
    if (flashState == LOW && prevFlash == HIGH)
    {
        if (millis() - lastFlash > transInt)
        {
            digitalWrite(ledPin, LOW);
            delayMicroseconds(flashIntensity);
            digitalWrite(pMos, LOW);
            delayMicroseconds((16000 - (flashIntensity)));
            digitalWrite(ledPin, HIGH);
            digitalWrite(pMos, HIGH);
            lastFlash = millis();
            hShoeSignal = true;
        }
    }
    prevFlash = flashState;
} while (hShoeSignal == false);
delay(500);
digitalWrite(shutterRel, LOW);
digitalWrite(eN2, HIGH);
delay(100);
digitalWrite(eN2, LOW);
lastShut = millis();
}
}
prevShut = shutState;
hShoeSignal = false;
}

```

Appendix A-2



Ulster University
Cromore Road
Coleraine
County Londonderry
BT52 1SA
Northern Ireland
T: +44 (0)28 7012 3047
F: +44 (0)28 7012 4172
E: optometry@ulster.ac.uk
ulster.ac.uk/optometry

RESEARCH PARTICIPANT INFORMATION SHEET

Project title: Comparative study of two ocular imaging modalities in an older adult population.

Dear Sir/Madam,

Thank you for taking the time to consider participating in this research study. This information leaflet is designed to help you understand what is involved and what will be asked of you before you decide to take part or not. Please read the following information. I will be happy to answer any queries you have relating to the study.

What is the purpose of this study?

The human eye contains a natural lens called the crystalline lens. It is a transparent, focusing component within the eye. As we get older, the lens can lose its transparency. If the loss of transparency becomes substantial, this is called a cataract. Cataracts are fairly common and tend to occur as we enter seventh or eighth decade (but this can be sooner).

Much research has gone into photographing the human lens in order to understand how its structure changes with time. Most methods require a detailed image of the lens to be captured by special photography using a Slit-Lamp Biomicroscope. This is a non-contact and quick technique to perform.

In this study, we would like to compare the above method of photographing the lens with a new method that uses infrared rather than visible light to image the eye. This instrument is called the Visante Anterior Segment Optical Coherence Tomographer (AS-OCT).

Why have I been chosen?

You have been chosen because you are an adult who has not had cataract surgery. You can still take part in the study if you wear glasses.

School of
Biomedical Sciences -
Optometry Clinic

Do I have to take part?

No, participation is voluntary and reading this leaflet will help you decide if you are happy to be included as a participant. If you wish to take part, I will give you a consent form to sign. You may opt out of the study at any stage of the process.

What will happen to me if I take part?

You will receive copies of the signed consent form and information leaflet for your own reference. The study itself will require you to attend the Vision Science Research Laboratory at the University of Ulster, Coleraine on one occasion at a time convenient for you. Your visit should not last more than 1 hour (this includes a break whilst the eye drops take effect).

This study includes:

- A few questions relating to eye health. This is only to check you are eligible for the study.
- A measurement of your vision involving reading letters on a chart while wearing your current glasses (if you normally wear them).
- An intraocular pressure (IOP) measurement for both eyes. This is a measure of the internal pressure of the eye. It involves using a device called a non-contact tonometer held in front of the eye. A small amount of air is released onto the front surface of the eye which is used to calculate pressure.

Following these preliminary measures, one drop of Tropicamide Hydrochloride 1% will be instilled into both eyes. There will then be a 20-minute break to allow the drops to take full effect. This drug is routinely used in optometric practice to widen the pupil - this improves the view of internal eye structures.

Once the eye drops take effect, we will capture images of the lenses in both of your eyes using the two above mentioned instruments. Both techniques require you to put your chin on a rest and to keep still. You will be asked to look at a target while the images are captured. It should only take a few minutes in total to do this.

Finally, we will recheck the Intraocular pressure in both eyes.

Are there any risks/side effects associated with this study?

All methods used in this study are non-invasive and quick to perform.

Tropicamide Hydrochloride 1% is commonly used in optometric practice to dilate pupils however, you may experience mild ocular discomfort lasting a few seconds following instillation. Your near vision may be a little blurred and you may experience sensitivity to bright light for up to 4 hours after the drops are put in. There is a small risk of induced angle closure (which may cause the pressure in your eye to increase) when using mydriatic drugs; this is extremely rare and will be minimized by conducting all necessary preliminary tests and monitoring IOP.

What if something goes wrong?

It is unlikely that something will go wrong during this study however, procedures are in place should any adverse events occur. The University has insurance cover for staff and students who carry out research involving people. The University knows about this research project and has approved it. Further details on the complaints procedure can be found in the University's "Research Ethics and Governance" webpage, Internet address:

<http://research.ulster.ac.uk/rg/0208ResearchVolunteerComplaintsProcedure.pdf>

Any complaint should be made, in the first instance, to the Chief Investigator (Dr Julie-Anne Little). Any complaint you make will be treated seriously and reported to the appropriate authority.

Will my taking part in this study be confidential?

All personal data will be stored electronically and password protected. The data will be anonymized for confidentiality and any written material will be kept in a locked filing cabinet.

Data will only be used for the purposes of evaluating the aims of the study. Research data will be kept for 24 months after the end of the data collection period.

What will happen to the results of the study?

The results and information gained from this study may contribute to scientific knowledge and also be valuable in further lens studies.

Who is organising and funding the research?

The research is organised by Dr Julie-Anne Little, Optometrist and Senior Lecturer and Professor Kathryn Saunders, Optometry and Vision Science.

Who has reviewed this study?

The School of Biomedical Sciences Research Ethics Filter Committee.

Contact Details

Further information can be obtained from:

Dr Julie Anne Little
Senior Lecturer in Optometry
School of Biomedical Sciences
Ja.little@ulster.ac.uk
Tel: 02870124374

Mr Aman Mahil
Optometrist, PhD Student
School of Biomedical Sciences
mahil-ad@email.ulster.ac.uk
Tel: 02870123718

Thank you for your time,

Aman Mahil



Ulster University
 Cromore Road
 Coleraine
 County Londonderry
 BT52 1SA
 Northern Ireland
 T: +44 (0)28 7012 3047
 F: +44 (0)28 7012 4172
 E: optometry@ulster.ac.uk
ulster.ac.uk/optometry

Participant Consent Form

Title of Project:

Comparative study of two ocular imaging modalities in an older adult population.

Chief Investigator: Dr Julie-Anne Little

Please initial

- I confirm that I have been given and have read and understood the Information sheet for the above study and have asked and received answers to any questions raised []
- I understand that my participation is voluntary and that I am free to withdraw at any time without giving a reason and without my rights being affected in any way []
- I understand that the researchers will hold all information and data collected securely and in confidence and that all efforts will be made to ensure that I cannot be identified as a participant in the study (except as might be required by law) and I give my permission for the researchers to hold relevant personal data []
- I give consent for a letter of information to be written to my GP to inform them of any abnormalities detected during the study []
- I understand the procedures that will be undertaken []
- I agree to take part in the above study []

Name of Subject	Signature	Date
Name of person taking consent	Signature	Date
Name of researcher	Signature	Date

School of
 Biomedical Sciences -
 Optometry Clinic

Appendix A-3



Office for Research Ethics Committees Northern Ireland (ORECNI)

Customer Care & Performance Directorate
Unit 4, Lissue Industrial Estate West
Rathdown Walk
Moir Road
Lisburn
BT28 2RF
Tel: 028 95361400
www.orecni.hscni.net
HSC REC A

13 October 2016

Dr Julie-Anne Little
Senior Lecturer in Optometry
Biomedical Sciences Research Institute
Room G159, Ulster University
Cromore Road
Coleraine, BT52 1SA

Dear Dr Little

Study title:	Characterising cataract and investigating retinal structure in the Down syndrome eye.
REC reference:	16/NI/0200
Protocol number:	N/A
IRAS project ID:	191505

Thank you for your letter of 12 October 2016, responding to the Committee's request for further information on the above research and submitting revised documentation.

The further information has been considered on behalf of the Committee by the Chair of the HSC REC A September 2016 Full Committee meeting

We plan to publish your research summary wording for the above study on the HRA website, together with your contact details. Publication will be no earlier than three months from the date of this opinion letter. Should you wish to provide a substitute contact point, require further information, or wish to make a request to postpone publication, please contact the REC Manager, Kathryn Taylor, RECA@hscni.net.

Confirmation of ethical opinion

On behalf of the Committee, I am pleased to confirm a **favourable ethical opinion** for the above research on the basis described in the application form, protocol and supporting documentation as revised, subject to the conditions specified below.

Conditions of the favourable opinion

The REC favourable opinion is subject to the following conditions being met prior to the start of the study.

Management permission must be obtained from each host organisation prior to the start of the study

Providing Support to Health and Social Care



at the site concerned.

Management permission should be sought from all NHS organisations involved in the study in accordance with NHS research governance arrangements. Each NHS organisation must confirm through the signing of agreements and/or other documents that it has given permission for the research to proceed (except where explicitly specified otherwise).

Guidance on applying for NHS permission for research is available in the Integrated Research Application System, www.hra.nhs.uk or at <http://www.rdforum.nhs.uk>.

Where a NHS organisation's role in the study is limited to identifying and referring potential participants to research sites ("participant identification centre"), guidance should be sought from the R&D office on the information it requires to give permission for this activity.

For non-NHS sites, site management permission should be obtained in accordance with the procedures of the relevant host organisation.

Sponsors are not required to notify the Committee of management permissions from host organisations

Registration of Clinical Trials

All clinical trials (defined as the first four categories on the IRAS filter page) must be registered on a publicly accessible database within 6 weeks of recruitment of the first participant (for medical device studies, within the timeline determined by the current registration and publication trees).

There is no requirement to separately notify the REC but you should do so at the earliest opportunity e.g. when submitting an amendment. We will audit the registration details as part of the annual progress reporting process.

To ensure transparency in research, we strongly recommend that all research is registered but for non-clinical trials this is not currently mandatory.

If a sponsor wishes to contest the need for registration they should contact Catherine Blewett (catherineblewett@nhs.net), the HRA does not, however, expect exceptions to be made. Guidance on where to register is provided within IRAS.

It is the responsibility of the sponsor to ensure that all the conditions are complied with before the start of the study or its initiation at a particular site (as applicable).

Ethical review of research sites

NHS sites

The favourable opinion applies to all NHS sites taking part in the study, subject to management permission being obtained from the NHS/HSC R&D office prior to the start of the study (see "Conditions of the favourable opinion" below).

Non-NHS sites

I am pleased to confirm that the favourable opinion applies to the following research site(s), subject to site management permission being obtained prior to the start of the study at the site (see under 'Conditions of the favourable opinion below').

<i>Research site</i>	<i>Principal Investigator / Local Collaborator</i>
Optometry Clinic and Vision Science Research Laboratory, Ulster University	Dr Julie-Anne Little

Approved documents

The final list of documents reviewed and approved by the Committee is as follows:

Document	Version	Date
Evidence of Sponsor insurance or indemnity (non NHS Sponsors only) [Sponsorship and Indemnity Letter]	1	29 August 2016
IRAS Checklist XML [Checklist_07092016]		07 September 2016
IRAS Checklist XML [Checklist_12102016]		12 October 2016
Letter from funder [Sponsorship and Indemnity Letter]	1	29 August 2016
Letter from sponsor [Sponsorship and Indemnity Letter]	1	29 August 2016
Other [Northern Health and Social Care Trust Participant Identification Centre Acceptance Letter]	1	19 August 2016
Other [Details of Case History]	1	12 October 2016
Other [Distress Protocol]	1	12 October 2016
Other [General Optical Council Standards of Practice]	1	01 April 2016
Other [Ulster University Policy for the Protection of Children and Vulnerable Adults]	1	01 September 2015
Other [College of Optometrists Tropicamide Information Sheet]	1	12 October 2016
Other [Applicant's Response to the Research Ethics Committee Comments]	1	12 October 2016
Participant consent form [Consent Form for Parents and Carers]	2	12 October 2016
Participant consent form [Consent form for Participants]	2	12 October 2016
Participant consent form [Assent Form for Parents and Carers of Adults who are Unable to Consent]	1	12 October 2016
Participant consent form [Assent Form for Younger Participants]	1	12 October 2016
Participant information sheet (PIS) [Simplified PIS]	1	30 June 2016
Participant information sheet (PIS) [PIS for Parents and Carers]	2	12 October 2016
Participant information sheet (PIS) [PIS for Participants]	2	12 October 2016
Participant information sheet (PIS) [PIS for Parents and Carers of Adults Who are Unable to Consent]	1	12 October 2016
REC Application Form [REC_Form_07092016]		07 September 2016
Referee's report or other scientific critique report [School of Biomedical Sciences Research Ethics Committee Report]	1	22 June 2016
Referee's report or other scientific critique report [Response to Research Ethics Filter Committee Report]	1	30 June 2016
Referee's report or other scientific critique report [Peer Review by Dr Julie McClelland]	1	18 July 2016
Referee's report or other scientific critique report [Peer Review by Dr Lesley Doyle]	1	21 July 2016
Research protocol or project proposal [Protocol]	2	12 October 2016
Summary CV for Chief Investigator (CI) [Dr Julie-Anne Little CV]	1	30 June 2016
Summary CV for student [Aman Mahil CV]	1	30 June 2016
Summary CV for supervisor (student research) [Prof Kathryn Saunders CV]	1	30 June 2016

Statement of compliance

The Committee is constituted in accordance with the Governance Arrangements for Research Ethics Committees and complies fully with the Standard Operating Procedures for Research Ethics Committees in the UK.

After ethical review

Reporting requirements

The attached document "*After ethical review – guidance for researchers*" gives detailed guidance on

reporting requirements for studies with a favourable opinion, including:

- Notifying substantial amendments
- Adding new sites and investigators
- Notification of serious breaches of the protocol
- Progress and safety reports
- Notifying the end of the study

The HRA website also provides guidance on these topics, which is updated in the light of changes in reporting requirements or procedures.

User Feedback

The Health Research Authority is continually striving to provide a high quality service to all applicants and sponsors. You are invited to give your view of the service you have received and the application procedure. If you wish to make your views known please use the feedback form available on the HRA website: <http://www.hra.nhs.uk/about-the-hra/governance/quality-assurance/>

HRA Training

We are pleased to welcome researchers and R&D staff at our training days – see details at <http://www.hra.nhs.uk/hra-training/>

16/NI/0200	Please quote this number on all correspondence
------------	--

With the Committee's best wishes for the success of this project.

Yours sincerely



pp Dr Alastair Walker
Vice-Chair – Chair of HSC REC A September 2016 Full REC Meeting
Email: RECA@hscni.net

Enclosures: "After ethical review – guidance for researchers"

Copy to: Nick Curry, Ulster University



www.northerntrust.hscni.net

Governance Department

19th August 2016

Dr Julie-Anne Little
Senior Lecturer in Optometry
Ulster University
Room G159
School of Biomedical Sciences
Coleraine
BT52 1SA

Dear Dr Little,

Study title: Investigating cataract and retinal structure in Down syndrome

HSC Trust reference: NT16-0533-08 (Please quote this number in all future correspondence)

Thank you for submitting the required documentation for your study to the Northern Health & Social Care Trust to be involved as a Participant Identification Centre.

Governance checks have been undertaken in accordance with the requirements under the Research Governance Framework for Health and Social Care, and relevant legislation. I am pleased to confirm that following completion of these checks approval for the study to go ahead within the Northern Health & Social Care Trust is now granted.

I wish you every success with your project.

Yours sincerely,

Dr Desmond Rooney
Head of NHSCT Research & Development

Cc Mr Aman-Deep S Mahill, UU
Professor Kathryn J Saunders, UU
Mr Nick Curry, UU

Research & Development Office, Bush Road, Bush Road, Antrim. BT41 2QB
Telephone Number: 02894 424751

Northern Health and Social Care Trust
 @NHSCTrust

*To deliver excellent integrated services
in partnership with our community*

COMPASSION



C

OPENNESS



O

RESPECT



R

EXCELLENCE



E



Ulster University
Crumore Road
Coleraine
County Londonderry
BT52 1SA
Northern Ireland
T: +44 (0)28 7012 3047
F: +44 (0)28 7012 4172
E: optometry@ulster.ac.uk
ulster.ac.uk/optometry

PARTICIPANT INFORMATION SHEET FOR PARENTS/GUARDIANS

Project title: Characterising cataract and investigating retinal structure in Down syndrome.

Dear Sir or Madam:

Your son/daughter (or person you care for) is invited to take part in a research study. This leaflet provides information outlining the study and what it involves. Please read it carefully before deciding to volunteer the person you care for and the researchers will be happy to address any concerns or questions you may have.

What is the purpose of this study?

The human eye contains a natural lens called the crystalline lens. It is a clear, focusing component within the eye. As we get older, the lens can become cloudy. This is called a cataract and cataracts stop us seeing as well as we should. Cataracts are fairly common in older people, but rare in children and younger adults.

Some research on individuals with Down syndrome has shown that cataract occurs more often and at a younger age. However, it is not known whether the cataracts that people with Down syndrome get are the same type as those that we see in older people, or if they are different. If we knew this, it might make eye care professionals better at finding and treating cataract in people with Down syndrome.

In this study, we would like to take photos of the lenses inside the eyes of people with Down syndrome. We will use two special cameras, one that is connected to a microscope and the other which uses near-infrared light to view structures inside the eye. Both cameras have been designed to be safe for taking pictures inside the eye. Nothing touches the eye with either of these techniques.

There is also a second aspect to this study that will examine the structure of the retina in Down syndrome. The retina is a layer of cells at the back of the eye. It is responsible for converting the light that enters our eye into signals that can be processed by our brain. This in turn, allows us to see.

We would also like to use the same infra-red camera to take a photograph of the retina. We know that people with Down syndrome need glasses more often than other people. Even when they wear their glasses they don't always see perfectly. We want to know if this is because the retina is different in Down syndrome. If it is, it could help explain why people with Down syndrome don't always see as well as they should. Not much research has been done before to study retinal structure in Down Syndrome and if there are differences, this may help us better understand how and why vision can be reduced in Down syndrome and to look for ways of improving or maximising vision.

Why has the person I care for been chosen?

The person you care for has been chosen as he/she has Down syndrome and has not had cataract surgery. It is your and the person you care for's decision whether they take part in the study or not. If you and the person you care for decide to participate in the study you will be given this information sheet to keep. We would like to see the person you care for whether they wear glasses or not.

What will happen to the person I care for if he/she takes part?

You will receive copies of the signed consent form and this information leaflet for you to keep. The study itself will require you and the person you care for to attend our Optometry Clinic at Ulster University, Coleraine on one occasion at a time convenient for you. The visit will last approximately one hour (this includes a break for eye drops that to take effect). **If the person you care for does wear glasses, please bring them with you.**

This study includes:

- A few questions relating to the eye and general health of the person you care for.
- A measurement of the person's vision.
- An intraocular pressure (IOP) measurement for both eyes. This is a measure of the internal pressure of the eye.

Following these preliminary measures, an eye drop will be put into both eyes (tropicamide 1%). There will then be a 20-minute break to allow the drops to take full effect. This eye drop is routinely used in hospitals and optometry practices to widen the pupil; this improves the view inside the eye and will help us take the best photos we can.

After the break, we will take pictures of the lenses and retinas in both of the person you care for's eyes. This will require them to put their chin on a rest and keep still for a few seconds at a time. They will be asked to look at a picture while the images are taken. It should only take a few minutes in total to do this. We have worked a lot with children and young adults with Down syndrome, so we are used to getting the most from brief periods of cooperation. Finally, the pressure in both eyes will be rechecked.

We would be happy to arrange transportation to the optometry clinic for you and the person you care for if you need it. **Due to the eye drops, we will give the person you care for a free pair of sunglasses at the end of the session.**

What are the possible risks/side effects to the person you care for by their taking part in this study?

All methods used in this study are non-invasive and quick to perform.

Tropicamide 1% is commonly used in optometric practice to dilate pupils however, it can cause mild discomfort lasting a few seconds following instillation. Near vision may be a little blurred after the drops, and bright lights can be a little uncomfortable for up to 6 hours afterwards. **There is a small risk of increased eye pressure; this is extremely rare and will be minimized by conducting all necessary preliminary tests and monitoring eye pressure.**

What if something goes wrong?

It is unlikely that something will go wrong during this study however, procedures are in place should any adverse event occur. An information sheet outlining the symptoms of increased eye pressure and what to do if the person you care for experiences them will be given to you at the end of the research session; Emergency contact details will also be on this sheet. The University has insurance cover for staff and students who carry out research involving people. Both the University and the Northern Health & Social Care Trust know about this research project and have approved it.

Any complaint should be made, in the first instance, to the lead researcher (Dr Julie-Anne Little). Any complaint you make will be treated seriously and reported to the appropriate authority.

Will the person you care for's participation in this study be kept confidential?

All personal data will be stored electronically and password protected. The data will be anonymized for confidentiality and any written material will be kept in a locked filing cabinet.

Data will only be used for the purposes of evaluating the aims of the study. Any details of the personal data collected in this study will not be disclosed to anyone other than the research team.

What will happen to the results of the study?

The results and information gained from this study may contribute to scientific knowledge and also be valuable in further studies of vision and disease in Down syndrome.

Who is organising and funding the research?

The research is organised by Dr Julie-Anne Little, Optometrist & Senior Lecturer and Professor Kathryn Saunders. It is funded by the Department of Employment and Learning.

What do I do now?

If you and the person you care for would like to take part, please sign the consent form and contact Mr Aman Mahil to arrange an appointment to attend Ulster University's Optometry Clinic. You or the person you care for are free to withdraw from the study at any time without reason, as participation in this study is voluntary.

Contact details

Further information can be obtained from:

Dr Julie-Anne Little
Senior Lecturer in Optometry
School of Biomedical Sciences
ja.little@ulster.ac.uk
Tel: 028 70124374

Mr Aman Mahil
Optometrist, PhD Student
School of Biomedical Sciences
mahil-ad@email.ulster.ac.uk
Tel: 028 70123718

Thank you for your time and consideration.



Ulster University
Cromore Road
Coleraine
County Londonderry
BT52 1SA
Northern Ireland
T: +44 (0)28 7012 3047
F: +44 (0)28 7012 4172
E: optometry@ulster.ac.uk
ulster.ac.uk/optometry

Parent/Guardian Assent Form

Title of Project: Characterising cataract and investigating retinal structure in Down syndrome.

Chief Investigator: Dr Julie-Anne Little

Please initial

- I confirm that I have been given and have read and understood the Information sheet for the above study and have asked and received answers to any questions raised. []
- I understand that participation is voluntary and that I and/or the person I care for are free to withdraw at any time without giving a reason and without our rights being affected in any way. []
- I understand that the researchers will hold all information and data collected securely and in confidence and that all efforts will be made to ensure that the person I care for cannot be identified as a participant in the study (except as might be required by law) and I give my assent for the researchers to hold the person I care for's relevant personal data. []
- I give assent for a letter of information to be written to the person's GP to inform them of any abnormalities detected during the study. []
- I understand the procedures that will be undertaken on the person I care for. []
- I assent to the person I care for taking part in the above study. []
- I understand the researcher may use an anonymous photograph of the eye of the person I care for in a scientific publication or presentation. I agree to the use of these images for this purpose. []
- I understand that should I withdraw the person I care for from the study, that any collected data will be retained. []

Name of participant

Name of person giving assent

Signature

Date

Name of researcher

Signature

Date



Ulster University
 Cromore Road
 Coleraine
 County Londonderry
 BT52 1SA
 Northern Ireland
 T: +44 (0)28 7012 3047
 F: +44 (0)28 7012 4172
 E: optometry@ulster.ac.uk
ulster.ac.uk/optometry

PARTICIPANT INFORMATION SHEET

Project title: Studying the eyes of people with Down Syndrome.

Hi,

We're Aman, Julie-Anne and Kathryn from Ulster University and we want to know more about how people with Down Syndrome see. You can read this sheet about what we're doing and ask us questions whenever you like.

Inside of our eyes, there is a lens that helps to focus light. Sometimes this lens gets cloudy and stops us from seeing things clearly. In this study, we would like to take pictures of your eyes using special cameras to see what your lens looks like.

We would also like to use these special cameras to take pictures of the back of your eye. This part of the eye is called the retina and it is important in helping us see. We would like to find out what your retina looks like and what it looks like in other people with Down syndrome's eyes too.

The cameras that we use to take the pictures will never touch your eyes or make you feel uncomfortable.

We are asking you to take part in our study because you have Down Syndrome. You don't have to take part in our study if you don't want to.

If you would like for us to take pictures of your eyes, we will bring you to Ulster University in Coleraine for an appointment. You can come with your Mum, Dad or your carers. **If you wear glasses, please bring them with you.**

At your appointment we will:

- First ask you some questions about your eyes.
- We will check the pressure in your eyes.
- Next, we will put some drops into your eyes. These drops will make it easier for us to take the photos of your eyes. Sometimes the drops make things look a little blurry and also make lights seem brighter, but don't worry, this is normal and will stop in a few hours.
- Once the drops have started to work, we will take pictures of your eyes.
- When we are done taking the pictures, we check the pressure of your eyes again.
- Remember, if you don't feel comfortable at any time, you can tell us to stop. You can also ask us questions whenever you want.
- Your appointment will take around one hour.

We will help you get to the university and you will also get a free pair of sunglasses if you take part in our study.

We will make sure not to share any of your pictures with anyone else except the research team and they will also be given a special code. That way nobody will be able to know that the pictures are of your eyes. We also keep everything locked in a cabinet.

If you would like us to take pictures of your eyes, please call Aman to set a time to come to Ulster University's Optometry Clinic. You don't have to take part if you don't want to and you can ask as many questions as you like.

Thank you for reading this letter.

Julie-Anne
Tel: 028 70124374

Aman
Tel: 028 70123718



Participant Consent Form

Ulster University
Cromore Road
Coleraine
County Londonderry
BT52 1SA
Northern Ireland
T: +44 (0)28 7012 3047
F: +44 (0)28 7012 4172
E: optometry@ulster.ac.uk
ulster.ac.uk/optometry

Title of Project: Studying the eyes of people with Down Syndrome.

Chief Investigator: Dr Julie-Anne Little

If you would like to be in the study, please:

- write your name in the space below
- sign your name and write the date at the bottom of the page

Please remember, if you don't want to be in the study, you don't have to sign this form.

I, _____ [Print your name], am happy to be in this research study.

By saying yes to taking part in the study, I am saying that:

- ✓ I know what the study is about
- ✓ I know what I will happen during my visit
- ✓ I have been allowed to ask questions and they have been answered
- ✓ I know that I don't have to be in the study if I don't want to
- ✓ I know that I can ask to stop taking part in the study at any time
- ✓ I am happy for the pictures of my eyes to be used in papers and posters and know that they will not have my name or personal details on them.
- ✓ I am happy for a letter to be written to my GP if the researcher thinks a doctor needs to examine me
- ✓ I know that the researchers won't tell anyone what any of my details are and will keep them safe

Signature [Sign here]

Date [Write the date here]

Researcher Name

Researcher Name

Date

School of
Biomedical Sciences -
Optometry Clinic

Appendix A-4



Gwasanaeth Moeseg Ymchwil
Research Ethics Service



Wales REC 3
Sixth Floor, Churchill House
17 Churchill Way
Cardiff CF10 2TW

Telephone : 029 2037 6829
Fax : 029 2037 6824
E-mail : corinne.scott@wales.nhs.uk
Website : www.hra.nhs.uk
Fax:

29 July 2016

Dr J Margaret Woodhouse
Senior Lecturer
School of Optometry and Vision Sciences
Cardiff University,
Maindy Road
Cardiff CF24 4LU

Dear Dr Woodhouse

Study title: Visual Development and Visual Defects in Children with Down's Syndrome
REC reference: 08/MRE09/46
Protocol number: SPON 536-08
Amendment number: 5
Amendment date: 07 July 2016
IRAS project ID: 3389

The above amendment was reviewed at the meeting of the Sub-Committee held on 29 July 2016.

The members of the Committee taking part in the review gave a favourable ethical opinion of the amendment on the basis described in the notice of amendment form and supporting documentation.

Approved documents

The documents reviewed and approved at the meeting were:

Document	Version	Date
Copies of advertisement materials for research participants [Poster/leaflet to recruit control participants]	1	13 June 2016
Notice of Substantial Amendment (non-CTIMP)	5	07 July 2016
Other [Aman-Deep Mahil CV]		08 June 2016
Participant information sheet (PIS) [Parent/legal Guardian information sheet and consent form (children with DS; slit-lam and OCT imaging)]	Main study 3.3, June 2016	
Research protocol or project proposal	4, June 2016	

Membership of the Committee

The members of the Committee who took part in the review are listed on the attached sheet.

All investigators and research collaborators in the NHS should notify the R&D office for the relevant NHS care organisation of this amendment and check whether it affects R&D approval of the research.

Statement of compliance

The Committee is constituted in accordance with the Governance Arrangements for Research Ethics Committees and complies fully with the Standard Operating Procedures for Research Ethics Committees in the UK.

We are pleased to welcome researchers and R & D staff at our NRES committee members' training days – see details at <http://www.hra.nhs.uk/hra-training/>

08/MRE09/46:	Please quote this number on all correspondence
--------------	--

Yours sincerely



Dr. Corinne Scott
Senior Ethics Service Manager
Health and Care Research Wales

pp Mrs. Monika Hare
Vice Chair

Email: corinne.scott@wales.nhs.uk

Enclosures: List of names and professions of members who took part in the review

Wales REC 3

Attendance at Sub-Committee of the REC meeting on 29 July 2016

Committee Members:

Name	Profession	Present	Notes
Mrs Monika Hare	Vice Chair / Lay member	Yes	Chaired meeting
Dr Richard Walker	Alternate Vice Chair / Lay Plus member	Yes	
Dr Pete Wall	Chair / Clinical Physiologist	Yes	

Also in attendance:

Name	Position (or reason for attending)
Dr Corinne Scott	Senior Ethics Service Manager

School of Optometry and Vision Sciences
Ysgol Optometreg a Gwyddorau'r Golwg



College of Biomedical and Life Sciences
Cardiff University
Maindy Road
Cardiff
CF24 4HQ
Wales UK

Tel Ffôn +44(0)29 2087 4374
Fax Ffacs +44(0)29 2087 4859
<http://www.cardiff.ac.uk/optom/>

Prifysgol Caerdydd
Heol Maindy
Caerdydd
CF24 4HQ
Cymru, Y Deyrnas Gyfunol

PARTICIPANT INFORMATION SHEET

Visual development and visual deficits in children with Down's syndrome

We would like to invite you and your child to take part in our study. Before you decide, you need to understand why the research is being done and what it would involve for your child. Please take time to read the following information carefully.

Who are we?

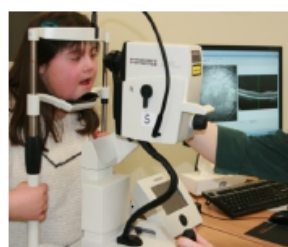
At the Down's Syndrome Vision Research Unit, we have been studying visual development in children with Down's syndrome since 1992. Children with Down's syndrome are at much greater risk of eye and vision disorders than are typically developing children. For example, older children with Down's syndrome have eyes which are a different shape to typical eyes.



Why are we asking you to enrol your child in the study?

Children with Down's syndrome are at much greater risk of eye and vision disorders than are typically developing children. Even when children wear glasses to correct long or short-sight, or even if they do not need glasses, children with Down's syndrome may have some visual difficulties. It is, therefore, very important that we understand the ways in which children's eyes develop and how we can best help them make the most of their vision.

What will we do?



The study will involve taking pictures of the natural lens and also the back of your child's eyes. To do this we will use cameras that are attached to microscopes which are routinely used to view the internal and external eye during eye examinations.

Your child simply needs to place his/her chin and forehead on rests and fixate on a target while we take the photographs.

In order to obtain good quality images, an eye drop will be used to dilate the pupil. The drop can cause glare/sensitivity to light for up to six hours afterwards, so your child will be given a pair of sunglasses to help with this.

We would also like to record the usual clinical measures we make during a normal eye examination, of spectacle prescription and detail vision, as well as your child's age.

Parent/legal guardian information sheet
June 2016

Main study version 3.2

What are the disadvantages and risks of my child taking part?

There are no potential risks in taking part as the researchers are all clinicians with experience in examining the eyes of children. However, this study is not suitable for individuals with epilepsy due to health and safety issues that arise from the use of flashing lights. It is not anticipated that participation will cause distress in any way.



Will my child's information be confidential?

The information about you and your child remains completely confidential. The researchers will be using the results for their PhD and postdoctoral studies. When we write dissertation/reports, and when we publish research results (in journals or in talks etc.) we do not identify your child in any way. We do like to use photographs of the children as often as possible for teaching purposes, such as lectures and posters, but we always ask for your permission first, and of course, send you a copy of the photograph.

Will I know the results of the research?

If you indicate on the consent form that you would like to hear about the results, we will keep your contact details, and will send a report to you in due course.

Do I have to enrol my child?

Children who join our study are extremely valuable to us and we appreciate all of the effort that parents put in to take part. Children who cannot co-operate are just as valuable, because measuring the success rate of the instruments is important information. But joining the study is voluntary, and you have the right to refuse. In any case, we respect your decision and it will not affect the standards of eye care your child will get in our clinic.

What happens if I want to withdraw my child from the study?

You are free to withdraw at any time, without giving a reason. However, any published results that included your child's data will be impossible to modify or discard. Nonetheless, if you decide to withdraw your child, we promise not to use his/her past and future results in any further studies that take place after the date on which we are informed of your decision.

If you are happy for your child to join the study, please sign the form overleaf

J. Margaret Woodhouse

Flors Vinuela-Navarro

Aman-Deep Mahil

Tel: +44 (0)29 2087 6522

Email: woodhouse@cf.ac.uk

<http://www.cardiff.ac.uk/optom/DownsSyndromeGroup/Home.html>

The work of the Down's Syndrome Vision Research Unit has been funded over the years by:
The Down's Syndrome Association, Mencap with the Community Fund, Mencap City Foundation,
PPP Foundation, National Eye Research Centre, Welsh Assembly Government

Parent/legal guardian information sheet
June 2016

Main study version 3.2

